

---

Electronic Thesis and Dissertation Repository

---

4-23-2021 10:30 AM

# Integrated Modelling of Wastewater Treatment and Sewer Processes - Interactions of Fluid Flow, Mass Transfer, and Biochemical Reactions

Ahmed Khalil, *The University of Western Ontario*

Supervisor: DeGroot, Christopher T., *The University of Western Ontario*

Co-Supervisor: Straatman, Anthony G., *The University of Western Ontario*

A thesis submitted in partial fulfillment of the requirements for the Doctor of Philosophy degree in Mechanical and Materials Engineering

© Ahmed Khalil 2021

Follow this and additional works at: <https://ir.lib.uwo.ca/etd>



Part of the [Environmental Engineering Commons](#), and the [Other Mechanical Engineering Commons](#)

---

## Recommended Citation

Khalil, Ahmed, "Integrated Modelling of Wastewater Treatment and Sewer Processes - Interactions of Fluid Flow, Mass Transfer, and Biochemical Reactions" (2021). *Electronic Thesis and Dissertation Repository*. 7730.

<https://ir.lib.uwo.ca/etd/7730>

This Dissertation/Thesis is brought to you for free and open access by Scholarship@Western. It has been accepted for inclusion in Electronic Thesis and Dissertation Repository by an authorized administrator of Scholarship@Western. For more information, please contact [wlsadmin@uwo.ca](mailto:wlsadmin@uwo.ca).

## Abstract

Numerical modelling of wastewater management systems is crucial for investigating alternative designs and developing strategies for operation and control that improve the performance of the treatment stage (such as improving the aeration systems in activated sludge systems). Modelling can also help operators to mitigate common problems that arise from unwanted biochemical conversions in the sewer networks (such as the production of sulfide and methane). Therefore, this work focuses on two major areas related to modelling wastewater management systems. First, it seeks to develop more accurate models for aeration systems in activated sludge reactors. Second, it seeks to studying the mathematical formulation and sensitivity/uncertainty related to input parameters for biochemical models of sewer system. Based on the uncertainty analysis of the sewer models, an improved biochemical model for the biological oxidation of sulfide using nitrate dosing is developed. This allows for the investigation of different dosing strategies and to propose optimized experimental plans for lab-scale experiments.

A CFD model integrated with the population balance model (PBM) was developed to simulate the aeration of a bubble column of clean water operating in a homogeneous flow regime. This study aims at investigating the influence of the liquid phase flow field on the evolution of the bubble size distribution (BSD) from a fine pore air diffuser to the free surface of the water. Moreover, the local oxygen mass transfer rate is calculated based on the bubbles' relative velocity and interfacial area, which is deduced from the modelled BSD, between the air bubbles and water. The model is validated by experimental data obtained from literature. The validation is based on the BSD and the values of the oxygen mass transfer coefficient ( $K_{La}$ ). A comparison between different PBM closure models for the bubble breakup and coalescence rates is conducted to determine the proper closure models for this flow regime. The study shows the influence of the flow field, especially near the free surface of water, on the BSD and  $K_{La}$ . Moreover, a comparison is conducted with the simulation results of the constant bubble size (CBS) approximation to show the inaccuracy that accompanies this approximation. The results show that the widely used constant bubble

size approximation can predict the global gas holdup reasonably, but poor matching with the oxygen mass transfer is obtained.

Uncertainty analysis of the Wastewater Aerobic/Anaerobic Transformation in Sewers (WATS) biochemical model is conducted. The analysis is concerned with the uncertainty of the biochemical model parameters and its mathematical form. The WATS model is implemented in 1-D (CSTR-in-series) and CFD frameworks. The 1-D model is used to study the uncertainty/sensitivity analysis by the Monte Carlo technique, and standardized regression coefficients (SRC) are determined to quantify the importance of the different biochemical model parameters. The CFD model is used to study the influence of two assumptions that are used in the 1-D model; homogenization of the reactions that occur in the biofilm and neglecting the non-uniform distribution of the particulate matters due to settling of solids. It is concluded that the 1-D model approximations are reasonable in the case of simple pressure mains.

Modelling of a lab-scale experiment, intended to replicate the behaviour of a sewer pipe, is conducted to determine the optimal nitrate dosing strategy in the system. The WATS model is extended to include the biological oxidation of sulfide by nitrate dosing. The experiment is modelled as a series-of-CSTRs. The developed model is calibrated and validated using experimental data collected from the system. A dosing strategy is developed to be used in the planning of experiments.

## Keywords

Computational fluid dynamics, bubble column, population balance model, bubble size distribution, gas-liquid mass transfer, sewers, uncertainty/sensitivity analysis, WATS model, standardized regression coefficient method, sulfide formation, nitrate dosing.

## Summary for Lay Audience

Wastewater management systems, which involve the collection system (sewer networks) and wastewater treatment plants, are critical for the protection of human health and the environment. Mathematical modelling of wastewater management systems is useful for predicting their performance. Through modelling, the design of different processes can be made more efficient or their performance can be improved. The biological and chemical conversions that happen in these systems can be beneficial, such as the reactions that occur in activated sludge reactors, which help to degrade waste organic material before it is discharged to the environment. On the other hand, these conversions could be harmful to humans and environment, for example to formation of sulfide and methane in sewer systems. Therefore, mathematical modelling is crucial to study the different sections of the wastewater management system and is more efficient than conducting expensive and time-consuming experiments and measurement campaigns in full-scale utilities. However, the most common mathematical models in this field rely on approximations that are necessary to simplify the complexity of the real world. These approximations could carry high uncertainty that may affect the accuracy of the model predictions which could subsequently result in wasted resources or substandard designs. Therefore, more sophisticated mathematical models such as computational fluid dynamics (CFD) could be used either directly in the design and operation process or indirectly by verifying the more simplified models.

This doctoral thesis is divided into two parts. The first part is concerned with a common approximation used in modelling the aeration of the biological treatment reactors where either the oxygen transfer rate from air bubbles is assumed to be homogeneous (uniform) throughout the reactor or a non-uniform distribution is considered but with the assumption of all the bubbles have the same size. This approximation is studied, and an alternative model based on CFD framework integrated with a statistical model is proposed. The study shows that the simplified models cannot address the strong influence of the water flow field and the evolution of the bubble size on the oxygen mass transfer rate. In the second part, uncertainty/sensitivity analysis is conducted on the widely used WATS biochemical model for the reactions in sewer systems. The biochemical model is also implemented in a CFD framework to study the approximations of the 1-D models. The studied assumptions are the homogenization of the reactions that occur in the biofilm only and neglecting the settling of

particulate matter. It is concluded from this investigation that the 1-D model can predict the biological and chemical conversion satisfactorily and the approximations are valid to be used in the case of simple pressure mains. Therefore, the 1-D framework is used to implement the WATS model that was extended to include one of the most common control strategies for sulfide levels in the sewer system, which involves nitrate dosing to stimulate a certain population of microorganisms that exist in the biofilm to oxidize the produced sulfide biologically. The developed model is used to determine the optimal dosing strategy that will be followed in a lab-scale experiment.

## Co-Authorship Statement

This doctoral thesis is prepared as an integrated-article thesis according to the regulations stipulated by the School of Graduate and Postdoctoral Studies (SGPS) at the University of Western Ontario. The thesis includes co-authored articles where the contribution of each author is stated below.

### **Chapter 2: Effects of flow velocity and bubble size distribution on oxygen mass transfer in bubble column reactors – A critical evaluation of the CFD-PBM model**

Ahmed Khalil conducted the numerical simulations, analysed the results, and contributed to writing the paper; Diego Rosso participated in the research design and contributed to writing the paper; Christopher DeGroot directed the research and contributed to writing the paper.

**Status:** Under review at Water Environment Research

### **Chapter 3: Uncertainty analysis of rising sewer models with respect to input parameters and model structure using Monte Carlo simulations and computational fluid dynamics**

The numerical simulations were conducted by Ahmed Khalil with guidance from Christopher DeGroot, Damien Batstone and Domenico Santoro. The literature survey and data analysis were completed by Ahmed Khalil. The research design was proposed collaboratively by Ahmed Khalil, Christopher DeGroot, Domenico Santoro and Damien Batstone. The first draft was prepared by Ahmed Khalil and was edited by Christopher DeGroot, Damien Batstone and Domenico Santoro.

**Status:** accepted at Water Science and Technology

### **Chapter 4: Numerical study of the nitrate dosing in lab-scale experiment of sewer system**

Ahmed Khalil conducted the numerical simulations and the tracer test of the system. Bassem Haroun and Nouha Klai conducted the experimental analysis. Christopher DeGroot and Domenico Santoro were involved in the conception and design of the study. The first

manuscript was prepared by Ahmed Khalil and reviewed by Christopher DeGroot, Domenico Santoro and Bassem Haroun.

**Status:** In preparation for submission to Water Science and Technology

## Acknowledgments

First of all, I would like to express sincere gratitude to my supervisor, Prof. Christopher DeGroot, for his continuous support and guidance throughout my Ph.D. I have learned a lot from him about mathematical modelling and how to be a better researcher. I enjoyed working with him. I would like also to acknowledge my advisory committee members, Prof. Anthony Straatman, Prof. Kamran Siddiqui and Prof. Martha Dagnew, for their guidance towards the success of my work.

I would like to thank Dr. Domenico Santoro (USP Technologies) for his support and guidance. It was my pleasure to work with him during the multiple industrial internships provided by Trojan technologies and USP Technologies.

I would like also to thank Prof. Diego Rosso (University of California, Irvine) and Prof. Damien Batstone (University of Queensland) for their insightful discussion about my work. Their recommendations to improve my research were very helpful to me.

I also thank my family for their endless support and advice during this journey. A special thanks to my beloved wife Faten for her support and patience through all these years. I really appreciate the support I received from my brothers Atef, Farouk and Gameel.

I would also like to thank my colleagues in our research group. Special thanks to Dr. Mahmoud Elhalwagy and Dr. Ahmed Shawky for their support and insightful discussions that I really enjoyed.



# Table of Contents

Abstract .....	ii
Summary for Lay Audience .....	iv
Co-Authorship Statement.....	vi
Acknowledgments.....	viii
Table of Contents .....	ix
List of Tables .....	xiii
List of Figures .....	xiv
List of Appendices .....	xix
List of Abbreviation.....	xx
Nomenclature .....	xxiii
Chapter 1 .....	1
1 Introduction and Literature Review .....	1
1.1 Background .....	1
1.2 Modelling of Wastewater Management Systems .....	9
1.2.1 Complete modelling.....	9
1.2.2 Hydrodynamics and mixing models in the sewer network and WWTPs .	12
1.2.3 Aeration modelling .....	16
1.2.4 Biochemical model in wastewater management system.....	18
1.3 Uncertainty of the biochemical models .....	23
1.4 Objectives of the Thesis.....	30
1.5 Thesis organization .....	31
1.6 References.....	33
Chapter 2.....	42

2	Effects of flow velocity and bubble size distribution on oxygen mass transfer in bubble column reactors – A critical evaluation of the CFD-PBM model.....	42
2.1	Introduction.....	42
2.2	Problem Description .....	47
2.2.1	Validation Data .....	47
2.2.2	Numerical Model .....	49
2.3	Governing Equations .....	50
2.3.1	Euler-Euler Two-Fluid Model .....	50
2.3.2	Interfacial Force Models .....	54
2.3.3	Population Balance Model.....	56
2.3.4	Coalescence Model .....	58
2.3.5	Breakup Models .....	59
2.3.6	Boundary and Initial Conditions.....	60
2.4	Results and Discussion .....	60
2.4.1	Grid Independence Test .....	60
2.4.2	8 L·min <sup>-1</sup> Flow Rate.....	62
2.4.3	2 L·min <sup>-1</sup> Flow Rate.....	75
2.4.4	Gas Holdup .....	77
2.4.5	Oxygen Mass Transfer Rate.....	79
2.5	Conclusions.....	83
2.6	References.....	85
Chapter 3	.....	92
3	Uncertainty analysis of rising sewer models with respect to input parameters and model structure using Monte Carlo simulations and computational fluid dynamics...	92
3.1	Introduction.....	92
3.2	Materials and Methods.....	96
3.2.1	Measurement data .....	96

3.2.2	Biochemical model .....	97
3.2.3	CSTR-in-series process model.....	99
3.2.4	Calibration and uncertainty/sensitivity analysis .....	99
3.2.5	Distributed parameter CFD model.....	103
3.3	Results and Discussion .....	107
3.3.1	Monte Carlo Simulations .....	107
3.3.2	Uncertainty/Sensitivity Analysis .....	107
3.3.3	CFD Model Results.....	115
3.4	Conclusions.....	120
3.5	References.....	122
Chapter 4	.....	126
4	Numerical study of the nitrate dosing in lab-scale experiment of sewer system .....	126
4.1	Introduction.....	126
4.2	Material and methods.....	130
4.2.1	Experiment setup .....	130
4.2.2	Developing biofilm and nitrate dosing .....	131
4.2.3	System hydrodynamics .....	132
4.2.4	Data for the mathematical model calibration/validation.....	132
4.2.5	Biochemical mathematical model.....	132
4.3	Results and Discussion .....	136
4.3.1	Numerical model calibration/validation without nitrate dosing .....	137
4.3.2	Numerical model calibration for nitrate dosing .....	140
4.3.3	Nitrate dosing rate and location study .....	142
4.3.4	Dosing in the 1 <sup>st</sup> reactor .....	142
4.3.5	Dosing in the 2 <sup>nd</sup> reactor .....	144
4.3.6	Dosing in the 3 <sup>rd</sup> reactor.....	144

4.3.7	Dosing in the 4 <sup>th</sup> reactor.....	147
4.3.8	HRT versus nitrate concentration .....	147
4.4	Conclusions.....	150
4.5	References.....	151
Chapter 5	.....	155
5	Summary and recommendations for future work.....	155
5.1	Summary .....	155
5.2	Recommendations for future work .....	157
Appendices	.....	160
Curriculum Vitae	.....	167

## List of Tables

Table 3-1: Model parameters default values and variation range .....	102
Table 3-2: Standardized regression coefficients for linear models of soluble COD, VFA, and total sulfide with the determination coefficients (R <sup>2</sup> ) for each model. The values in bold are those with the most significant effects on the model outputs .....	114
Table 4-1: Kinetics added to the WATS model.....	133
Table 4-2: Mathematical model process definitions.....	135
Table 4-3: Mathematical model state variable definitions.....	135

## List of Figures

Figure 1-1: COD fractionation in wastewater (Metcalf & Eddy, 2003) .....	4
Figure 1-2: Solids fractionation in wastewater (Metcalf & Eddy, 2003) .....	5
Figure 1-3: Wastewater management system .....	8
Figure 1-4: Complete modelling of biological treatment in aeration tank.....	12
Figure 1-5: Compartmentalization of CFD domain and connectivity between compartments .....	16
Figure 1-6: Key biological, chemical and physical processes in gravity sewers.....	21
Figure 2-1: Experimental bubble column setup (adapted from Amaral et al., 2018) with bubble size measurement locations denoted by dashed lines .....	48
Figure 2-2: Illustration of the bubble column computational domain, where the blue colour (bottom rectangle) indicates space occupied by water and the red colour (top rectangle) indicates space occupied by air, in the initial condition .....	50
Figure 2-3: Time-averaged velocity profiles for the water phase on the coarse, medium, and fine meshes at 1.2 m above the air diffuser .....	61
Figure 2-4: Instantaneous velocity vector field for the water phase on the coarse grid (left) and fine grid (right).....	62
Figure 2-5: Instantaneous contour plot of the air volume fraction for the gas flow rate of 8 $\text{L} \cdot \text{min}^{-1}$ .....	64
Figure 2-6: Cumulative BSD (top) and BSD (bottom) for the validation of 8 $\text{L} \cdot \text{min}^{-1}$ simulation.....	65
Figure 2-7: Time-averaged air velocity at 1.2 m above the air diffuser using three different volume fractions at the inlet; 0.5, 0.8, and 0.9.....	67

Figure 2-8: Cumulative BSD (top) and BSD (bottom) for the boundary conditions tested with different values of air volume fraction at the diffuser .....	68
Figure 2-9: Cumulative BSD (top) and BSD (bottom) for different numbers of bubble size classes .....	70
Figure 2-10: Cumulative BSD (top) and BSD (bottom) using different bubble breakup model .....	71
Figure 2-11: Cumulative BSD (top) and BSD (bottom) for simulation employing the bubble coalescence due to turbulence and different rising velocity .....	73
Figure 2-12: Air volume fraction contours from the simulation adopting Ishii and Zuber's drag model .....	74
Figure 2-13: Cumulative BSD for the simulation using Ishii's and Zuber's drag model .....	75
Figure 2-14: Cumulative BSD (top) and BSD (bottom) for gas flow rate of $2 \text{ L} \cdot \text{min}^{-1}$ .....	76
Figure 2-15: Instantaneous contours of air volume fraction for the gas flow rate of $2 \text{ L} \cdot \text{min}^{-1}$ .....	77
Figure 2-16: Gas holdup vs gas flow rate for the simulation adopting Schiller-Naumann's and Ishii-Zuber's drag models in comparison to experimental data .....	78
Figure 2-17: Profiles of averaged (a) $K_{La}$ ; (b) interfacial area density, $a$ ; (c) $K_L$ ; (d) Sauter diameter; (e) air volume fraction; and (f) air relative velocity along the bubble column height for air flow rate of $8 \text{ L} \cdot \text{min}^{-1}$ .....	81
Figure 2-18: Profiles of averaged (a) $K_{La}$ ; (b) interfacial area density, $a$ ; (c) $K_L$ ; (d) Sauter diameter; (e) air volume fraction; and (f) air relative velocity along the bubble column height for air flow rate of $2 \text{ L} \cdot \text{min}^{-1}$ .....	82
Figure 2-19: Global oxygen mass transfer measurement against CFD-BPM simulation.....	83
Figure 3-1: Key processes in the WATS model implemented in the current study .....	98

Figure 3-2: Model uncertainties for (a) soluble COD, (b) VFA, (c) total sulfide, represented using mean, 10th and 90th percentiles, and upper and lower band values from the Monte Carlo simulations .....	108
Figure 3-3: Graphical representation of the sensitivity of the predicted time-series of soluble COD concentration at the outlet for selected model parameters .....	110
Figure 3-4: Graphical representation of the sensitivity of the predicted time-series of VFA concentration at the outlet for selected model parameters.....	110
Figure 3-5: Graphical representation of the sensitivity of the predicted time-series of total sulfide concentration at the outlet for selected model parameters .....	111
Figure 3-6: Histogram for the time-averaged Monte Carlo output compared with the fitted linear multivariate model for soluble COD .....	112
Figure 3-7: Histogram for the time-averaged Monte Carlo output compared with the fitted linear multivariate model for VFA .....	113
Figure 3-8: Histogram for the time-averaged Monte Carlo output compared with the fitted linear multivariate model for total sulfide .....	113
Figure 3-9: Plots of mass-weighted average at pipe outlet of the CFD model vs 1-D model of soluble COD concentration at the outlet.....	116
Figure 3-10: Plots of mass-weighted average at pipe outlet of the CFD model vs 1-D model of VFA concentration at the outlet.....	116
Figure 3-11: Plots of mass-weighted average at pipe outlet of the CFD model vs 1-D model of total sulfide concentration at the outlet.....	117
Figure 3-12: Contour plots of the concentrations of (a) total COD (mgCOD/L), (b) soluble COD (mgCOD/L), and (c) total sulfide (mgS/L) for a cross-section of the pipe halfway between the inlet and outlet .....	118
Figure 3-13: Plot of the radial concentration profiles of particulate COD at different locations along the length of the sewer pipe .....	120



Figure 4-1: Schematic of the lab-scale system .....	131
Figure 4-2: Mathematical model biochemical processes included .....	134
Figure 4-3: Cumulative residence time distribution (F(t)) of the tracer test against the numerical model results .....	136
Figure 4-4: Model calibration: average concentration measurements at the effluent (blue columns) and model predictions effluent of each reactor in the system for sulfide, sulfate, soluble COD and VFA (R1-R4) .....	138
Figure 4-5: Calibrated sulfide production: measurement and model prediction of sulfide concentration at the system effluent .....	138
Figure 4-6: Model validation: average concentration measurements at the effluent and model predictions effluent of each reactor in the system for sulfide, sulfate, soluble COD and VFA .....	139
Figure 4-7: Validated sulfide production: measurement and model prediction of sulfide concentration at the system effluent .....	140
Figure 4-8: Calibrated profile of sulfide oxidation: measurement and model prediction of sulfide concentration at the system effluent.....	141
Figure 4-9: Calibrated profile of nitrate reduction: measurement and model prediction of nitrate concentration at the system effluent .....	141
Figure 4-10: Sulfide (top) and nitrate (bottom) concentrations in the effluent of the reactors (R1-R4) when dosing in R1 .....	143
Figure 4-11: Sulfide (top) and nitrate (bottom) concentrations in the effluent of the reactors (R1-R4) when dosing in R2 .....	145
Figure 4-12: Sulfide (top) and nitrate (bottom) concentrations in the effluent of the reactors (R1-R4) when dosing in R3 .....	146

Figure 4-13: Sulfide (top) and nitrate (bottom) concentrations in the effluent of the reactors (R1-R4) when dosing in R4 .....	148
Figure 4-14: Effective nitrate dosing to achieve 0.5 mgS/L sulfide in the effluent.....	149
Figure 4-15: Effective nitrate dosing to achieve 0.5 mgNO <sub>3</sub> -N/L sulfide in the effluent ....	149

## List of Appendices

Appendix A: Supplementary information for Chapter 3 .....	160
---	-----

## List of Abbreviation

<b>AD</b>	Anaerobic digester
<b>ADM</b>	Anaerobic digestion model
<b>ANOVA</b>	Analysis of variance
<b>ASM</b>	Activated sludge model
<b>BOD</b>	Biological oxygen demand
<b>BSD</b>	Bubble size distribution
<b>CBS</b>	Constant bubble size
<b>CFD</b>	Computational fluid dynamics
<b>CM</b>	Class method
<b>COD</b>	Chemical oxygen demand
<b>CSTR</b>	Continuously Stirred-Tank Reactor
<b>EE</b>	Elementary effects
<b>FAST</b>	Fourier amplitude sensitivity testing
<b>HRT</b>	Hydraulic retention time
<b>IF</b>	Interactions between the factors
<b>IWA</b>	International water association
<b>OAT</b>	One model factor at a time
<b>ODE</b>	Ordinary differential equation
<b>WWTP</b>	Wastewater treatment plant

<b>WRRF</b>	Water resource recovery facility
<b>TKE</b>	Turbulent kinetic energy
<b>TS</b>	Total solids
<b>TOC</b>	Total organic solids
<b>VOCs</b>	Volatile organic carbon
<b>rbCOD</b>	Readily biodegradable chemical oxygen demand
<b>VFA</b>	Volatile fatty acids
<b>TSS</b>	Total suspended solids
<b>TDS</b>	Total dissolved solids
<b>VSS</b>	Volatile suspended solids
<b>OTE</b>	Oxygen transfer efficiency
<b>SRT</b>	Solids retention time
<b>RTD</b>	Residence time distribution
<b>PBM</b>	Population balance model
<b>PAOs</b>	Phosphorus accumulating organisms
<b>MA</b>	Methanogenic archaea
<b>SRB</b>	Sulfate reducing bacteria
<b>WATS</b>	Wastewater aerobic/anaerobic transformation in sewers
<b>SRC</b>	Standardized regression coefficient
<b>MC</b>	Monte Carlo simulation

<b>LHS</b>	Latin hypercube sampling
<b>NR-SOB</b>	Nitrate reducing- sulfide oxidizing bacteria
<b>hNRB</b>	Heterotrophic nitrate reducing bacteria
<b>TN</b>	Total nitrogen
<b>SN</b>	Soluble nitrogen
<b><math>\alpha</math>-factor</b>	Wastewater correction factor, the ratio of process water to clean water standard OTE

## Nomenclature

$Pe$	Peclet number
$J$	Number of the tanks-in-series
$m_{O_2}^o$	Oxygen mass transfer rate, $kg/s$
$K_L a$	Volumetric mass transfer coefficient of the liquid side, $s^{-1}$
$V_{\text{tank}}$	Tank volume, $m^3$
$K_L$	Oxygen mass transfer coefficient of the liquid side, $m/s$
$a$	Air bubble specific interfacial area, $m^2/m^3$
$x_i$	Model factor $i$ (chapter 1 and 3)
$y$	Model output (chapter 1 and 3)
$b_i$	Coefficient of term $i$ in linear model equation (chapter 1 and 3)
$V ( )$	Variance operator
$E ( )$	Expectancy operator
$S_i$	First order effect index of factor $i$ in the extended FAST method
$S_{Ti}$	Total effect index of factor $i$ in the extended FAST method
$t$	Time, $s$
$\overline{U}_k$	Averaged velocity vector of phase $k$ , $m/s$
$\overline{R}_k^{eff}$	Viscous and Reynolds turbulent stresses, $m^2/s^2$
$\overline{p}$	Mean common static pressure, $Pa$
$g$	Gravitational acceleration, $m/s^2$
$\overline{F}_k$	Sum of all interfacial forces between phases, $N$

$\overline{F}_D$	Drag force, $N$
$\overline{F}_{VM}$	Virtual mass force, $N$
$\overline{F}_L$	Lift force, $N$
$d_{32}$	Sauter bubble diameter, $m$
$d_i$	Bubble size of class $i$ , $m$
$f_i$	Normalized volume fraction of gas bubble class $i$
$k$	Turbulent kinetic energy (TKE), $m^2/s^2$
$P$	Production rate of TKE, $m^2/s^3$
$d_g$	Gas phase equivalent diameter, $m$
$C_{\varepsilon 1}$	Turbulence model constant
$C_{\varepsilon 2}$	Turbulence model constant
$C_P$	Turbulence model constant
$C_D$	Drag coefficient
Re	Reynolds number based on bubbles equivalent diameter
$\overline{U}_r$	Relative velocity between the gas and liquid phase, $m/s$
$Eu$	Eötvös (or, equivalently, Bond) number
$C_L$	Lift force coefficient
$C_{VM}$	Virtual mass force coefficient
$n_i$	Number of bubbles of class $i$
$B_{iC}$	Birth rate of bubbles of class $i$ due to coalescence, $s^{-1}$
$D_{iC}$	Death rate of bubbles of class $i$ due to coalescence, $s^{-1}$



$B_{iB}$	Birth rate of bubbles of class $i$ due to breakup, $s^{-1}$
$D_{iB}$	Death rate of bubbles of class $i$ due to breakup, $s^{-1}$
$v_i$	Bubble volume in bubble class $i$ , $m^3$
$a(v, v')$	coalescence rate between the bubble class $v$ and size $v'$
$b(v)$	Breakup rate of the bubble class of size $v$
$m(v)$	Number of daughter bubble produced by the breakup of a bubble of size $v$
$p(v, v')$	probability density function for the generation of bubble of size $v$ out of the breakup of bubble of size $v'$
$D_L$	Oxygen diffusion coefficient in water, $m^2/s$
$\overline{v_i}$	Mean velocity vector, $m/s$ (chapter 3)
$S_{\phi_k}$	Source term of scalar $\phi_k$
$v_s$	Reference settling velocity, $m/s$ (chapter 3)
$v_o$	Solids settling velocity, $m/s$ (chapter 3)
$X_{\min}$	Non-settleable solids concentration, $kg/m^3$
$X_s$	Solids concentration, $kg/m^3$
$r_h, r_p$	Constants for solids settling velocity function

### **Greek symbol**

$\alpha_k$	Volume fraction of phase $k$
$\beta$	Standard regression coefficient
$\varepsilon_l$	Dissipation rate of the turbulent kinetic energy in liquid phase, $m^2/s^3$
$\phi_k$	Source term induced by bubbles motion in TKE equation, $m^2/s^3$ (chapter 2)

$\phi_\varepsilon$	Source term induced by bubbles motion in dissipation rate of TKE equation, $m^2/s^4$
$\phi_k$	Scalar variable representing the concentration of species $k$ (chapter 3)
$\nu^t$	Turbulence viscosity, $m^2/s$
$\sigma_k$	Turbulence model constant
$\sigma_\varepsilon$	Turbulence model constant
$\rho_k$	Density of phase $k$ , $kg/m^3$
$\tau$	Mean residence time, $s$
$\overline{\omega_b}$	Vorticity of continuous phase, $s^{-1}$
$\Gamma_k$	Diffusivity of scalar $k$
$\mu$	Dynamic viscosity, $Pa.s$

### Subscripts

$g$	gas phase
$l$	liquid phase
$a$	dispersed phase (chapter 2)
$b$	continuous phase (chapter 2)

## Chapter 1

### 1 Introduction and Literature Review

#### 1.1 Background

Effective wastewater management systems are imperative for modern cities all over the world. With the continuously growing population and accelerated urbanization, the demand for water resources is rising and, subsequently, the produced wastewater from households and industry is increasing every day. Direct disposal of wastewater to the environment with inadequate treatment carries a brutal danger to both human health and ecosystems. Wastewater contains pathogenic microorganisms such that discharging the wastewater to freshwater resources results in spreading of waterborne diseases. Moreover, oxidation of the carbonaceous organic compounds in wastewater by the dissolved oxygen in receiving water has a detrimental impact on the marine life. In addition, nutrients in wastewater could stimulate the growth of aquatic plants and microorganisms.

The economic growth of the developing countries is contingent on the pollution control which is a key factor of the improvement of the agricultural and industrial productivity. The United Nations (UN) adopted 17 Sustainable Development Goals (SDGs) (UNHCR, 2017) that include clean water and sanitation goal (SGD 6). SGD 6 is for ensuring the availability and sustainability of the water and sanitation management systems. It is stated that discharging the wastewater without treatment or reuse is an existential threat of human being. Indeed, untreated wastewater is a critical source of deadly pathogens in food and water. In addition, discharging wastewater without reuse dissipates a huge amount of water, nutrients, energy and materials that can be recovered.

Governments enforce stringent regulations on the treatment of wastewater prior to discharge to the environment. These regulations set the removal objectives of the treatment process. The primary objectives include the removal of the wastewater constituents that have an immediate and long-term impact on human health and environment such as pathogenic organisms, suspended solids and biodegradable organics,

in addition to nutrients such as phosphorous and nitrogen. Furthermore, the allowable concentration of these constituents in the discharged wastewater have been reduced significantly over the years in light of more recent research into the environmental harm caused by wastewater pollutants. Therefore, the degree of the wastewater treatment that is required by the regulations has become more stringent.

In developed countries, the concept of wastewater treatment is being extended beyond its traditional scope of simply removing pollutants and pathogens prior to returning water to the environment or reusing. The goal of such systems includes the recovery of some wasted resources along with reducing the cost and improving the efficiency. Therefore, renaming of Wastewater Treatment Plants (WWTP) to Water Resource Recovery Facilities (WRRF) is advocated by different water quality associations (Coats and Wilson, 2017). The recovery of resources such as energy, in the form of biogas, chemicals (e.g. phosphate), valuable materials (e.g. cellulose fibres, bioplastic, etc.), is active research in the academic community (Loosdrecht and Brdjanovic, 2014).

Wastewater produced from residential and industrial sources has a complex composition of organic and inorganic dissolved and suspended matter in addition to microorganisms. In order to properly design and control wastewater management systems, the quality of the wastewater should be adequately described. Wastewater quality is characterised based on physical properties and the chemical and biological constituents (Metcalf & Eddy, 2003). The physical properties of wastewater include density, temperature, conductivity, color, odor and turbidity along with the solids content that is composed of suspended and dissolved solids. Moreover, the typical chemical parameters of wastewater comprise pH level, alkalinity, Total Solids (TS), Biological Oxygen Demand (BOD), Chemical Oxygen Demand (COD), Total Organic Carbon (TOC), nitrogen and phosphorus concentrations. The biological characteristics of the wastewater that describe the microorganism population are essential due to the important role of bacteria and other microorganisms in degradation and stabilization of the organic matter.

Organic matter, generally composed of a combination of carbohydrates, proteins, fats, oils and grease, is a major concern because of its influence on the environment. The

constituents of organic matter cannot be distinguished separately, therefore techniques have been developed to measure aggregate organic constituents in wastewater that have the same characteristics. Moreover, other advanced methods are used for measuring some organic components individually, e.g. Volatile Organic Compounds (VOCs). Most common analyses used to quantify the aggregate organic constituents of wastewater are BOD, COD and TOC (Metcalf & Eddy, 2003). Measuring BOD is the most widely used method to estimate the organic pollution that is based on quantifying the dissolved oxygen consumption in wastewater sample seeded with population of bacteria over a period of five days ( $BOD_5$ ).  $BOD_5$  indicates the amount of the biodegradable organic matter in wastewater. However, this test has a number of limitations that include the long time needed to complete the test, the fact that only biodegradable matter can be determined, and that the sample needs to be pretreated in the case of high toxicity wastewater. COD is another measure that takes much less time, around 2-3 hours, and does not need pretreatment of the sample. In this method, organic matter is chemically oxidized using dichromate in strong acid solution and heating. However, in order to assess the treatability of the wastewater, fractionation of the measured COD is required. The fractionation is based on the biodegradability of the soluble and particulate COD. The fractionation of COD is required to be more detailed for the mathematical modelling of the biochemical conversions in wastewater, since these models include many additional wastewater constituents (Makinia and Zaborowska, 2020). The last common method to measure the organic matter is the TOC measure where total organic carbon concentration is determined by oxidizing the organic carbon to carbon dioxide using ultraviolet radiation, heat and oxygen, and chemical oxidant. TOC is commonly recommended to be used in the control system since a relationship with the BOD of a specific wastewater could be established and it needs 5 to 10 minutes to complete the test (Metcalf & Eddy, 2003). Measurements of wastewater organic loading is routinely conducted at different sections of the wastewater management system.

Fractionation of the organic matter in wastewater is essential to determine the portion that can be removed by the biological treatment and the mechanisms of the biodegradation. Moreover, it is imperative for mathematical modelling of the biochemical conversion rates (Makinia and Zaborowska, 2020). COD measurement comprises the biodegradable

and non-biodegradable constituent concentrations in wastewater. These constituents are in soluble and particulate form. Typical fractionation of the COD is depicted in Fig (1-1). While the soluble non-biodegradable constituents leave the sewer system and treatment plant without any change, the particulate non-biodegradable constituents accumulate in the biosolids. Microorganisms in the wastewater system can easily utilize readily biodegradable substrates (rbCOD), which are typically soluble matters. rbCOD is further fractionated into Volatile Fatty Acids (VFAs) and more complex COD that can be fermented to VFAs. However, particulate and colloidal COD needs more biodegradation by extracellular enzymes that are produced by the microorganism so that it can be absorbed through the microorganisms' cell wall. Therefore, the biodegradation of the particulate COD is slower than the soluble fraction. The biodegradability of organic matters in wastewater is determined by the biodegradable fraction in the total COD. For untreated municipal wastewater, the ratio of BOD/COD determines the biodegradability of pollutants in the wastewater hence better treatability by the biological means. While the ratio BOD/COD varies from 0.3 to 0.8, untreated wastewater water with BOD/COD greater than 0.5 is considered easily biologically treatable (Metcalf & Eddy, 2003).

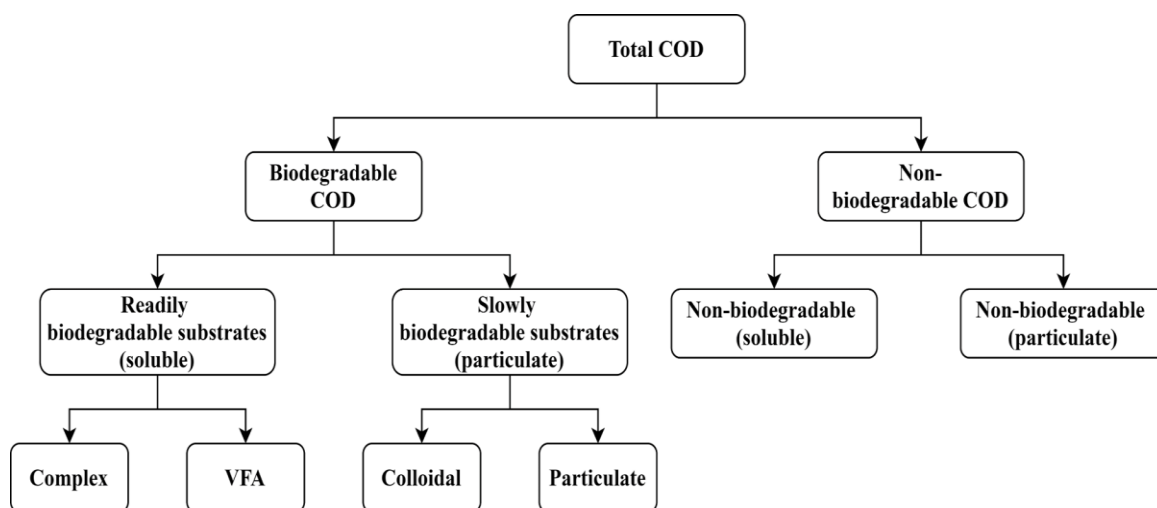


**Figure 1-1: COD fractionation in wastewater (Metcalf & Eddy, 2003)**

Solids concentration is the most important parameter that is used to characterize wastewater. TS is fractionated into total suspended solids (TSS) and total dissolved solids (TDS) (Fig 1-2). The concentration of the TSS is typically measured by filtering a sample of the wastewater through a filter paper (the most commonly accepted pore size is 1.2  $\mu\text{m}$ ) and measuring the weight of the retained solids after drying at 105°C. Solids that can escape from the filter with the filtrate is considered to be dissolved and colloidal solids. The organic portion of solids is volatile. This portion is measured as fraction of BOD, organic nitrogen and organic phosphorus. On the other hand, the inorganic solids are considered fixed solids. the ratio of the volatile suspended solids (VSS) to TSS in raw wastewater is typically 0.6-0.8 (Metcalf & Eddy, 2003).

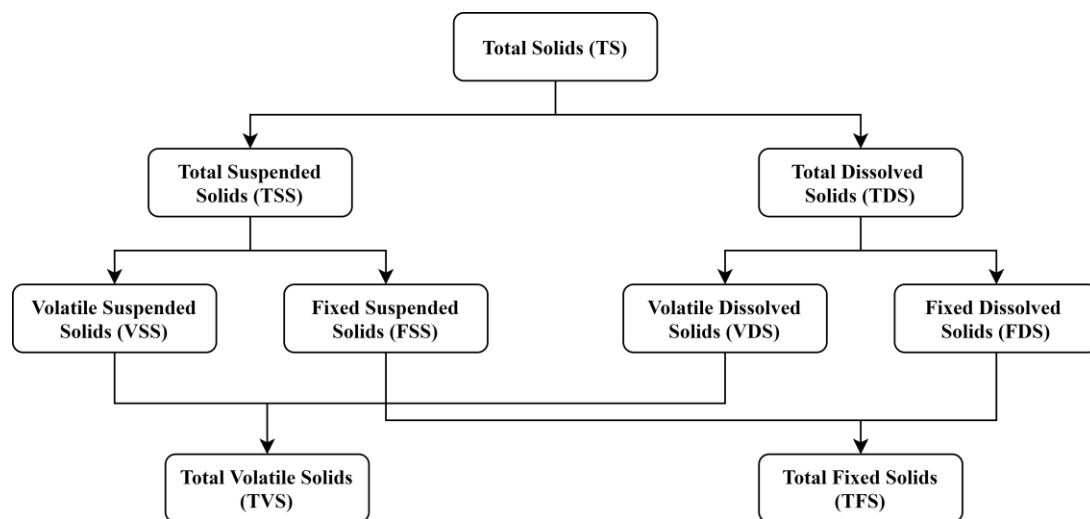


**Figure 1-2: Solids fractionation in wastewater (Metcalf & Eddy, 2003)**

Management system of wastewater starts with the collection (sewer) system which collects transports municipal and industrial wastewater (Fig. 1-3). Sewer networks may be designed to collect and transport sanitary wastewater and stormwater separately (separated sewers) or together (combined sewers). Combined sewers act as sanitary sewers only during dry-weather periods. However, overflow structures, e.g. detention tanks, are included for wet-weather periods, since the flow rate may be up to 100-1000

times the average of the dry-weather conditions (Hvitved-Jacobsen and Nielsen, 2013). For the last 50 -100 years, separate sewers have been widely used to control the levels of contamination of the discharged flow to receiving water bodies during wet-weather periods. Variability over day and night of wastewater flow rate and hence the residence time in the sewer system relies on the type of the sewer system and behaviour of the community. Sanitary and stormwater sewers are different in terms of the hydraulics and composition. Stormwater sewer design is largely concerned with the hydraulics and solids transportation with minor attention to the chemical and biological reactions. On the other hand, for sanitary sewers, the chemical and biological conversions are of high importance to consider during the design and operation. Most of the sewer systems are designed to transport wastewater and stormwater by gravity where the flow is characterized as open-channel flow. Therefore, the sewer pipes are partially filled and oxygen diffusion from the sewer atmosphere to the wastewater occurs. However, some segments of the sewer network involve pumping stations and pressurized pipes, mainly due to changes in elevation. In these segments, pipes are fully filled and dissolved oxygen is depleted by the biochemical reactions in a short distance at the beginning of the pipe. The type of the sewage and the transport method determine the change in the wastewater constituents and flow rate that is delivered to the wastewater treatment facility.

The WWTP is the next element in the wastewater management system, where residential and industrial wastewater is treated before being disposed to the environment or reused. The main objectives of wastewater treatment are: (1) removal of suspended solids; (2) removal of the organic biodegradable substrate that may cause oxygen depletion in the receiving water; and (3) inactivation of pathogens (Qasim, 2017). National legislation on the quality of discharged water defines the standard composition that the treatment should achieve. Treatment of wastewater includes several physical, chemical and biological processes to accomplish the targeted composition of the discharged treated wastewater. In general, the soluble and solids pollutants are removed over several processes that could be grouped into stages based on the nature of the processes in each stage. Conventionally, these stages are named as primary, secondary and tertiary stages (Metcalf & Eddy, 2003).



The preliminary stage involves physical processes such as screening to remove large floating objects that might clog pipes and to remove grit, which includes sand, seeds, and other solids that are generally heavier than organic matter. After grit removal, the sewage still contains organic and inorganic suspended minute particles that could be removed by a sedimentation tank in the primary stage. The secondary stage includes biological and chemical processes that remove the soluble, colloidal and particulate biodegradable organic matters, and further remove suspended solids. The biological removal of organic matter is based on selectively stimulating the active microorganisms in the system to consume the organic matter as food for producing new cells and for energy. This is achieved by providing oxygen, through an aeration system, to the microorganisms and maintaining favorable conditions, temperature and pH level, for their activities. The aeration system provides oxygen, as an electron acceptor, to the wastewater to support the aerobic activities of the obligate aerobic microorganisms that require oxygen for producing energy. The new bacteria tissue can be removed from the wastewater by further solids settling by gravity in the secondary settling tanks. The secondary stage objective is extended to include the removal of nutrients, i.e. nitrogen and phosphorus, from the wastewater. This requires stimulating other microorganisms' activities that only happen in the absence of oxygen (anaerobic conditions), e.g. fermentation, and activities that utilize nitrate as electron acceptor (anoxic conditions) that is produced in the aerobic condition. This is achieved by using different connected compartments for each condition, as shown in Fig. 1-3, which represents a typical advanced biological treatment to remove nutrients. Additionally, tertiary stage might be required for the reuse of the wastewater. Typically, tertiary stage includes filtration of the secondary effluent to remove any residual suspended solids and more disinfection of the discharged wastewater (Metcalf & Eddy, 2003). Moreover, the tertiary stage includes disinfection process to kill the pathogenic bacteria and reduce the odors. The disinfection is performed either by injecting chlorine to the effluent of the secondary settling tank or by more advanced methods using ultraviolet light or ozone.

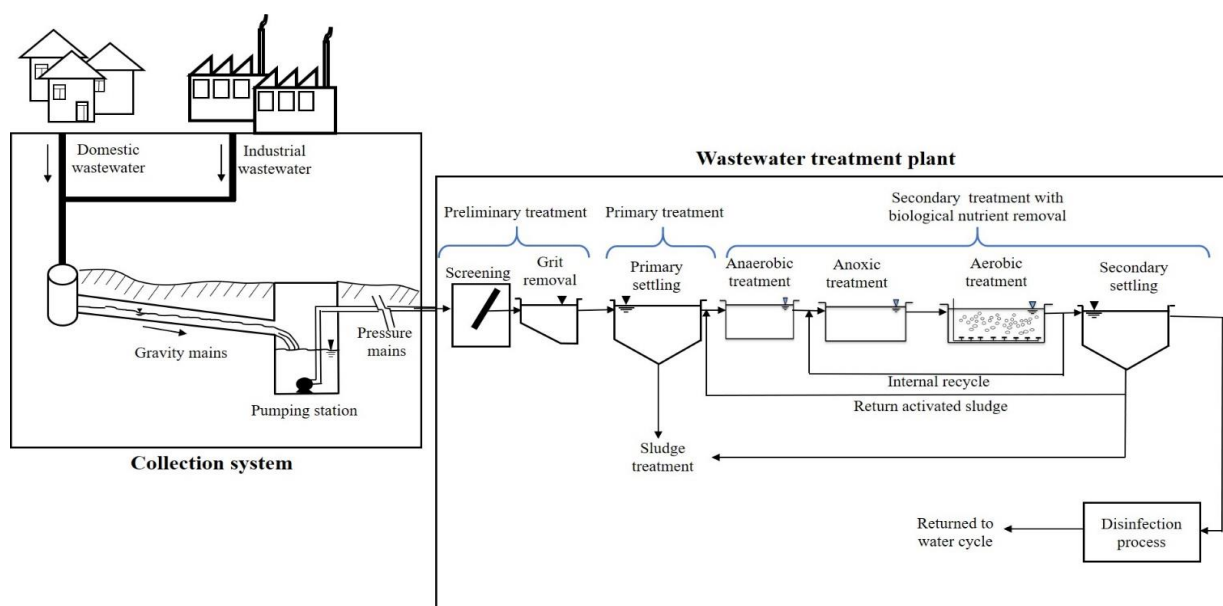


**Figure 1-3: Wastewater management system**

Shifting wastewater treatment towards resource recovery necessitates energy utilization optimization. It is estimated that the energy used for wastewater treatment and water delivery is about 2% of the total energy consumption all over the world. Moreover, this energy represents approximately 20% of the energy used by municipalities (Pasini, 2019). Specific energy required for biological wastewater treatment varies between 0.2 to 2 kWh per cubic meter of wastewater treated. The energy consumption in the biological treatment depends on the characteristics of the influent wastewater, permissible pollutants in the effluent, and technologies installed and capacity of treatment plant (Singh et al., 2016; Gude, 2015). Aeration of the aerobic reactors consumes the majority of the energy utilized in the wastewater treatment process. It was reported that 45 to 75% of the energy consumed in the treatment plant is through the aeration in the secondary stage (Rosso et al., 2011). Therefore, studying aeration systems and the factors affecting oxygen mass transfer in wastewater is important to efforts toward reducing the aeration energy requirement.

Aeration systems are assessed based on the Oxygen Transfer Efficiency (OTE), which describes the percentage of the oxygen transferred from the air bubbles into the liquid

phase of the reactor as compared to the oxygen supplied. Factors influence the OTE could be categorized into environmental conditions (e.g. atmospheric temperature and pressure), process conditions (e.g. concentration of surface active agents such as surfactants, process design, solids concentration as function of Solids Retention Time (SRT) and air diffuser fouling) and reactor design parameters, (e.g. diffusers density and arrangement, reactor configuration and water height in the reactor) (Baquero-Rodríguez et al., 2018).

In general, design, operation and control of wastewater management systems requires a comprehensive understanding of the hydrodynamics, biological and chemical reactions and physical processes take place in the flow of the wastewater. Conducting experiments requires building expensive pilot-scale setups that are both expensive and time-consuming. Another alternative is to develop conceptual mathematical models that can describe the hydrodynamics and the biological and chemical conversions along with lab-scale experimental measurements. Moreover, the ease of constructing such models allows more flexibility at developing and examining many alternative designs and control strategies.

## 1.2 Modelling of Wastewater Management Systems

Mathematical models play a crucial role in the design and control of wastewater management systems. Both engineering consulting firms and the academic community are pursuing the development of the mathematical models not only to provide more accurate predictions for the carbonaceous substrate, nutrients and sulfur conversions, but also for resource recovery, energy consumption, and gases emission that contribute to greenhouse gases thus global warming (Lizarralde et al., 2015). Modelling part of the system or the whole system depends on the purpose of the modelling project and the capability of the available data and resources.

### 1.2.1 Complete modelling

Complete modelling of a wastewater management system involves modelling of the hydrodynamics, biochemical conversions of wastewater constituents and mass transfer processes along with other physical processes in all sections of the wastewater

management system (Makinia and Zaborowska, 2020). Modelling the hydrodynamics of the wastewater treatment reactors or the sewer pipes provides critical information pertaining the mixing between the constituents of the wastewater and retention time of the wastewater in specified sections. In addition, flow characteristics have a profound influence on the other physical processes, such as the increase in mass transfer that arises due to turbulence in the flow (Teuber, 2020). On the other hand, biochemical conversion models describe the conversion rates of the wastewater constituents due to biological and chemical reactions, thereby the rate of change of concentrations with respect to time. Moreover, mass transfer models simulate the diffusion of some species from the gas phase to the liquid phase and the gas stripping from the liquid phase to the gas phase. For instance, mass transfer is essential for modelling the dissolved oxygen levels that are available for microorganisms in the biological treatment reactors. Another important example is the stripping of hydrogen sulfide in sewer systems (Teuber, 2020). Considering a complete model of a wastewater treatment system is a challenging task that requires coding of multiple interconnected models which would require high computational power to solve. Therefore, approximations are usually made by neglecting or simplifying the effects of some aspects of the complete model to reduce the complexity of the model and its computational cost. Some of these approximations are justified, yet more investigation is needed to study the influence of these approximations on the accuracy of the models.

Interaction between the different sub-models contained within the complete model is crucial to assess the approximations that may be assumed during conceptual development of a model for a certain section of the wastewater management system (Makinia and Zaborowska, 2020). Hydrodynamics of the wastewater flow is characterized as a turbulent multiphase flow that contains solid and gas phases in the liquid water phase. The significance of these phases relies on their volume fractions in the liquid phase, their effect on the properties of the liquid phase, and their role in the biological and chemical conversions. For instance, comprehensive modelling of the aeration tank in the secondary stage of the biological wastewater treatment, including nutrient removal, is depicted in Fig. 1-4. The model could be divided into two sub-models that are hydrodynamic and biochemical sub-models. It is also essential to model the oxygen mass transfer from the

gas phase to the liquid phase, yet this process is interrelated with both the hydrodynamic and biochemical sub-models. For the hydrodynamics modelling, the reactor geometry and influent liquid phase flow rate profile are the main inputs to the sub-model. However, the influence of the concentration of solids, e.g. biomass, particulate substrate, etc., that are derived from the biochemical model should be considered to determine the rheological properties of the liquid medium. Moreover, the aeration system configuration and air flow rate profile are required. The interphase forces between the phases in the hydrodynamic sub-model determine the volume fraction distribution of the phases and the turbulence levels. The gas phase has a particular importance as discussed in chapter 2. The flow field of the gas phase determines the distribution of the dissolved oxygen concentration in the reactor.

Along with velocity field, the volume fraction distribution and bubble size distribution are necessary for the accurate prediction of the oxygen mass transfer rate. This rate is used as a source term for dissolved oxygen state variable in the biochemical sub-models that are to be described in section 1.2.4. Furthermore, the pH level and the temperature of the fluid have an influence on the biokinetics that are commonly accounted for as a correction factor of the biokinetic rates. The biochemical sub-model is responsible for predicting the rate of change of each wastewater constituent concentration with respect to time. The biochemical sub-model assumes homogeneity of the different constituents, hence the microorganisms are assumed to be in contact with the same concentrations at all the locations of the compartments that are defined based on the hydrodynamic models, which will be discussed in section 1.2.2. With all of these model interdependencies, it is the work of the wastewater process modeller to determine which interactions are important and those which can be neglected. It is the goal of this work to further elucidate.

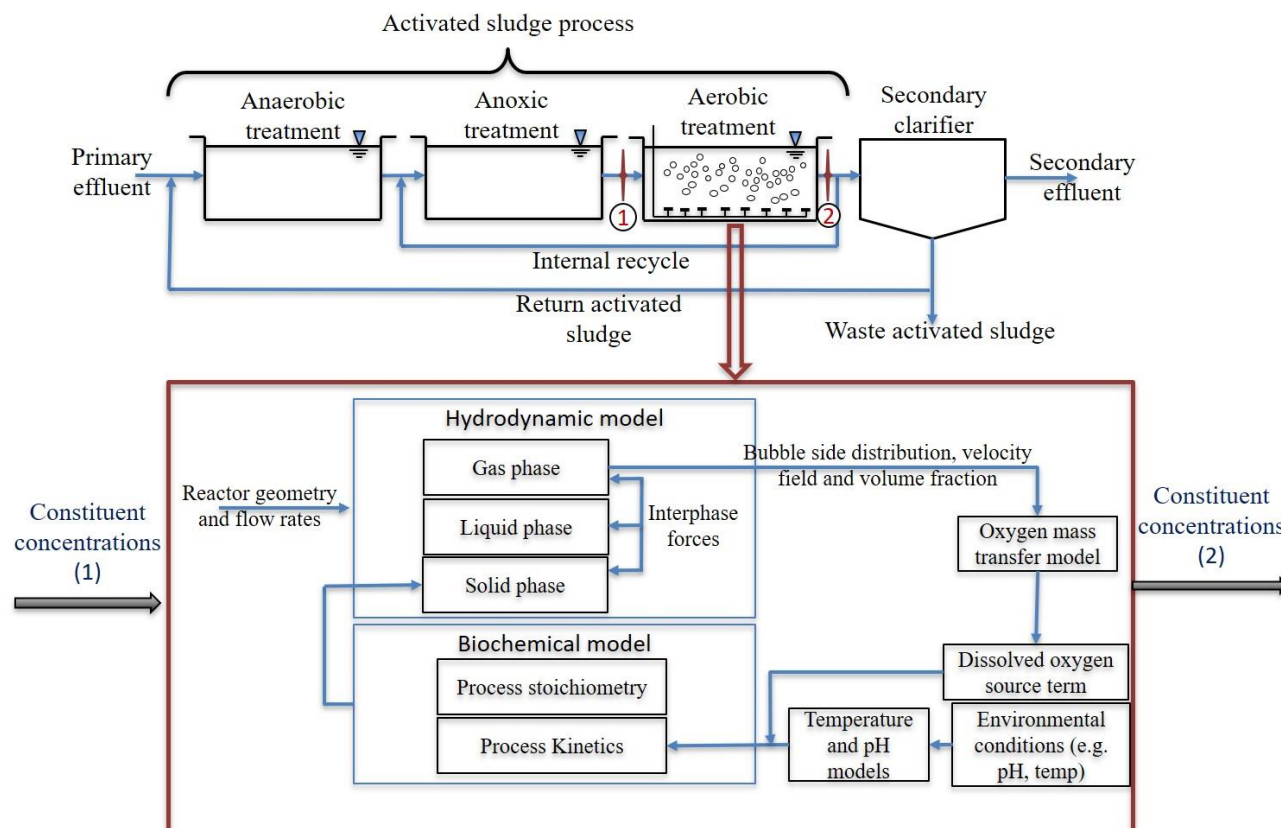


**Figure 1-4: Complete modelling of biological treatment in aeration tank**

### 1.2.2 Hydrodynamics and mixing models in the sewer network and WWTPs

Flow in wastewater management systems varies from simple pipe flow in sewer network to more complex flows in the different types of activated sludge reactors with and without aerators. Therefore, wastewater management systems involve various kinds of hydrodynamic configuration that can be bracketed from two ideal configurations; plug flow and completely mixed tank (Metcalf & Eddy, 2003). The plug flow configuration could be characterized as a pipe flow where all the flow particles exiting the reactor have the exact residence time. On the other hand, a completely mixed tank or Continuously Stirred-Tank Reactor (CSTR) is characterized by all constituents of the liquid phase being completely homogeneous all the times. A series of CSTRs is commonly used for

modelling reactors that have a flow regime existing between the ideal plug flow and CSTR.

The objective of a hydrodynamic model is to approach the real flow behaviour in the reactor where the Residence Time Distribution (RTD) deviates from the ideal configurations of completely mixed reactor and plug flow. This deviation could be a result of number of factors such as the geometry and the aspect ratio of the reactor, insufficient input mixing power, non-streamlined inlet and outlet, the fluctuations of the inlet velocity and the temperature and density difference between the inflow and the content of the system (Metcalf & Eddy, 2003).

Modelling the hydrodynamics of the different elements of the wastewater management system could be conducted using simplified systemic process models or using Computational Fluid Dynamics (CFD) which is more detailed modelling. Another approach that was introduced is the compartmental model, which is intended to capture the flow better than a systemic process model at a computational cost much less than CFD (Rigopoulos and Jones, 2003; Qiao et al., 2013).

Systemic process models are robust and simple models that are used extensively in modelling chemical reactors. These models represent the reactor either as a plug flow with axial dispersion, namely the Axial Dispersion Model (ADM), or as a series of CSTRs. AD model is characterized by two parameters which are the axial dispersion number, which is simply the reciprocal of the Peclet number ( $Pe$ ), and the mean residence time ( $\tau$ ). Series of CSTR models are characterized by the number of the tanks-in-series ( $J$ ) and the mean residence time. However, the series of CSTR model suffers from a drawback that arises in the case of flow rate variation, hence the number of CSTRs that represents the system is not constant for the dynamic simulations. Therefore, Potier et al. (2005) introduced the concept of perfectly mixed cells with back-mixing thereby the number of the CSTR is constant with varying back-mixing coefficient that is calculated based on the flow rate. The two models of the systemic approach are equivalent. An equivalence relation between the parameters of the two models ( $Pe = 2J + 1$ ) could be used in most of the cases (Le Moullec et al., 2008).

Conventionally, the parameters of these two models are estimated using a tracer test that is conducted on the real reactor or using CFD simulation. Although this approach is simple in terms of the computational power and time needed, it has a limited applicability and cannot be used for extrapolation under different operation conditions. Moreover, it does not give sufficient details regarding the hydrodynamics in the reactor and needs many approximations to model localized reactions such in case of reactions happening in the biofilm.

CFD is a numerical method that is used to simulate the flow of the fluids, as well as mass and heat transfer. CFD has been widely used in different engineering applications where the flow field is a key element of the design that requires optimization. The application of CFD has witnessed an enormous development to improve the solution accuracy and to reduce the computational power required of the simulation. Moreover, great developments in the available computing power (e.g. super computers, computational clusters, and servers) widen the applications of CFD in engineering fields by reducing the total simulation runtime. In addition, CFD can tackle the flow of various fluids in complex geometries that may include more than one phase. The ability of CFD to be integrated with chemical and biological models makes it an attractive tool to be used instead of the classical approaches, when greater detail is required. The concept underlying CFD is to discretize the flow domain flow into a number of non-overlapping computational cells. Each cell could be considered as a CSTR that is connected with the neighbour cells through the cell faces. The transport of wastewater constituents between cells is computed based on advection and diffusion. Advection is a result of transport due to the flow field, while diffusion results from both molecular and turbulent diffusion. The chemical and biological conversion rates can also be included for all the constituents of the wastewater. The conversion rates are computed at each computational cell based on the value of the local constituent concentrations (Karpinska and Bridgeman, 2016; Le Moullec et al., 2010a; Sánchez et al., 2018; Glover et al., 2006; Lei and Ni, 2014). This feature makes CFD an outstanding approach to model the reactors where highly localized biochemical reactions take place such as the reactions happen in attached biofilms. The capability of CFD to model the flow field of interacting phases in the system adds another advantage of the ability to model the solids separation processes and aeration



systems. CFD is also able to effectively identify dead zones that exist due to inadequate design and can be used to identify alternative designs based on detailed study of the flow field (Karpinska and Bridgeman, 2016).

Compartmental models are another approach in which the reactor geometry is divided into a number of functional compartments (Fig. 1-5). The basis of dividing the reactor geometry is that the physio-chemical properties are homogenous within each compartment, where compartments are derived using CFD or general knowledge of the process (Le Moullec et al., 2010b). CFD investigations of the liquid flow field without reactions is conducted on the reactor geometry prior to the compartmentalization of the domain. The connectivity and the shape of the compartments are determined based on the analysis of the turbulence characteristics, which includes the turbulent kinetic energy and turbulence dissipation rate, and air volume fraction distribution in the domain. The connectivity and flux between these compartments are determined using the CFD simulation results. It is worth mentioning that the turbulent dispersion between the compartments is crucial to model the transport of different species in the compartmental model. While the flow rates between the compartments are directly determined using the liquid flow field of the CFD study, the turbulent dispersion is more challenging to be quantified. Le Moullec et al. (2008) and Le Moullec et al. (2010b) made an analogy with Potier's systemic model (Potier et al., 2005) to determine the turbulent dispersion as a back-mixing flow. However it was claimed that the compartmental model has a much lower computational expense, but the compartmental model is very dependent upon the computationally-intensive CFD results and the determination of the back mixing flow that represents the turbulent dispersion is based on a strong approximation as explained in (Le Moullec et al., 2010b). Furthermore, there are no clear guidelines for the partitioning of the domain, especially, for the reactors with more complex geometry and aeration system.

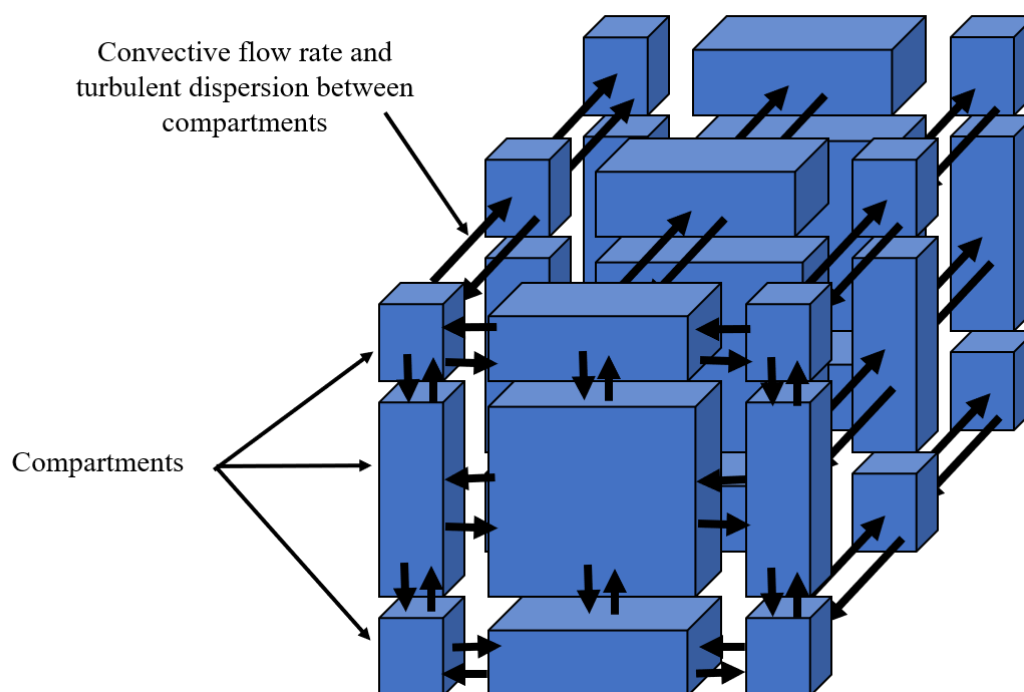


**Figure 1-5: Compartmentalization of CFD domain and connectivity between compartments**

Although the flow in the sewer systems is rather simple since most of the sewer network system segments are simple straight pipes, the flow turbulence in some segments is important in terms of gases emission (Teuber, 2020). Commonly the sewer system is modelled using the CSTR-in-series concept. However, this necessitates to apply several approximations associated with the biochemical model that is used that may have a significant effect on the accuracy of the simulations. Moreover, turbulence is not considered in the mass transfer calculations.

### 1.2.3 Aeration modelling

As illustrated above, aeration is a major part of the wastewater treatment process that needs accurate modelling to optimize the energy consumption. Modelling of the aeration is commonly based on the assumption of completely mixed reactor. The oxygen mass

transfer rate is computed using two-film theory where the two films are assumed along the interface between the air and liquid phase. However, it was proved that the mass transfer resistance from the liquid side is predominant. Therefore, the resistance from the gas side is commonly ignored (Kulkarni, 2007). Oxygen mass transfer rate,  $m_{O_2}^o$ , in clean water in tank of volume  $V_{\text{tank}}$  is expressed as the multiplication of the volumetric mass transfer coefficient of the liquid side,  $K_L a$ , and the difference between saturation concentration of dissolved oxygen and the concentration of the dissolved oxygen in the bulk liquid phase (Eq. 1.1).

$$m_{O_2}^o = K_L a (C^* - C) V_{\text{tank}} \quad (1.1)$$

The coefficient  $K_L a$  is defined as the mass transfer coefficient of the liquid side,  $K_L$ , multiplied by the specific interfacial area,  $a$ , (ratio between interfacial air-liquid area to reactor volume) since the interfacial area between air and liquid phase is difficult to measure. Yet, measuring the mass transfer coefficient in the process water is difficult due to the utilization rate by the microorganisms in the bioreactor. Therefore, a lumped factor is used to account for the difference between oxygen mass transfer in the clean water and process water ( $\alpha$ -factor). Historically, the  $\alpha$ -factor is assumed to be constant in process models knowing the  $K_L a$  of clean water from measurement in clean water or data from the air diffuser manufacturer. However, this results in misleading calculation of oxygen transfer rate (Jiang et al., 2017). In fact,  $\alpha$ -factor is dynamic because of the temporal change of a number of parameters such as SRT and the concentration of organic matter in the reactor (Leu et al., 2009). Therefore, more effort has been done in order to improve the modelling of  $\alpha$ -factor by introducing empirical correlation between the  $\alpha$ -factor and the main parameters that have significant influence (Sánchez et al., 2018; Lei and Ni, 2014). However, using the empirical approach to study the aeration performance in bioreactors offers a limited understanding of the mechanisms of the oxygen mass transfer. Several studies have been published to understand and optimize the aeration using more mechanistic approach. Studies such as the work of Amaral et al. (2018) that

showed the inaccuracy of the assumption uniform  $K_L a$  at all the levels of the reactor. The separation between the mass transfer coefficient  $K_L$  and air-liquid specific interfacial area was proposed, where the interfacial area might be assumed as a constant using mean diameter of the bubbles or modeled using statistical models such as Population Balance Model (PBM) (Amaral, 2019). Moreover, adopting CFD to model the distribution of the gas phase through the bioreactor and compute the  $K_L$  based on the flow field has been conducted for more accurate presentation of the dead zone (Le Moullec et al., 2010a; Jiang et al., 2017). Furthermore, integration between PBM and CFD could be powerful to optimize the performance and design of aeration system in the future (Amaral et al., 2019).

#### 1.2.4 Biochemical model in wastewater management system

Several models of the biochemical reactions and physical processes have been developed based on the experimental data obtained from measurement campaigns in existing facilities of wastewater management, pilot-scale reactors, and lab-scale reactors. These models are widely used in the industry for designing new facilities, improving existing ones, and controlling the different processes in the system. The objective of these models is adjusted based on the part of the system that is modelled. For instance, the objective of WWTP models could be to determine the efficiency of the WWTP to remove the different pollutants from the received wastewater before disposing it to the water bodies. On the other hand, for the sewer system, the objective may be to determine the conversion of the different species on the way to the WWTP, along with the prediction of the formation of harmful species such as sulfide or methane. Moreover, other differences related to the concentration of the biomass, solids, and soluble substrate determine the importance and the form of the models for the biochemical processes involved.

##### 1.2.4.1 Biochemical modelling of biological wastewater treatment

Modelling of biochemical processes in biological treatment of wastewater has become essential part of the design and operation process since the project launched by International Water Association (IWA) to develop mathematical models of the activated sludge process (Henze et al. 2000). Activated Sludge Model (ASM) series have been

developed to model the removal of carbon, nitrogen and phosphorus from wastewater in activated sludge processes. While Activated Sludge Model No. 1 (ASM1) described in Henze et al. (1987) is to model nitrification and denitrification processes, other extensions of this model have been introduced in ASM2 and ASM2d (Henze et al., 1999; Gujer et al., 1995) to include the capability of predicting the biological phosphorus uptake. This is implemented by describing the internal storage compounds of Phosphorus Accumulating Organisms (PAOs). However, since ASM1 was the most common model used in industrial and academic projects, ASM3 (Gujer et al., 1999) was introduced to resolve several deficits that have been appeared. On the other hand, biochemical mathematical models have been introduced as well for the anaerobic digester by IWA anaerobic digestion modelling task group (Batstone et al., 2002).

Along with the biochemical processes that are mediated by the microorganisms, several processes take place during the biological treatment. These processes are commonly referred to as physico-chemical processes that comprise gas-liquid mass transfer, chemical precipitation and aquatic dissociation/association reactions (Lizarralde et al., 2015). Physico-chemical processes are commonly neglected while modelling the biological wastewater treatment using the standard IWA ASM series due to the complexity of implementing these reactions and the weak benefits gained (Batstone et al., 2012). However, for complete modelling of the WWTP that comprises the IWA ASM-series for activated sludge processes and the ADM for the anaerobic digester, the implementation of the physico-chemical models in the IWA models is essential (Batstone et al., 2012). While the alkalinity is considered sufficient for the IWA models to monitor the drop in the pH level, integration with AD modelling necessitates mechanistic modelling of pH levels. Therefore, Flores-Alsina et al. (2015) have implemented the dynamic calculation of the pH level for ASM-series in the physico-chemical framework. Nevertheless, for the modelling of the advanced wastewater biological treatment to remove the phosphorus using chemical dosing, the physic-chemical processes (Hauduc et al., 2015) are influential to the model prediction.

#### 1.2.4.2 Biochemical modelling of the collection system

The transformations of different wastewater constituents in sewers could be relatively high due to the long residence time from the source to the treatment facilities (Hvitved-Jacobsen et al., 2013). In-sewer biological and chemical conversions include the aerobic, anaerobic, and anoxic microbial growth and respiration processes using biodegradable organic matter and nutrients. Since the concentration of the nitrate in wastewater is typically low, the anoxic processes are not of importance if no treatment is applied using nitrate injection. Thus, processes in the sewer systems are either aerobic or anaerobic. For the gravity mains, oxygen mass transfer across the free surface of the flow occurs providing oxygen for the microorganisms in the liquid phase. Anaerobic conditions in the gravity mains could exist locally in the biofilm developed on the pipe walls. In pressure mains anaerobic conditions prevail since the sewer pipe is full of sewage flow with no source of oxygen, if there is no oxygen injected.

Although carbon and nutrient concentrations in sewer are not the limiting condition for the suspended biomass growth, the biomass kinetics is slow with respect to the average Hydraulic Retention Time (HRT) in the sewer systems. The biofilm developed on the sewer pipe walls and sediments at the bottom of the sewer pipe represent the proper environment for anaerobic biomass to grow (Fig. 1-6). Consequently, biomass accumulation in the biofilm and sediments is the main location of the production and of main species commonly observed in the sewer flow, e.g. methane by Methanogenic Archaea (MA) and sulfide by Sulfate Reducing Bacteria (SRB) ((Hvitved-Jacobsen et al., 2013; Liu et al., 2015). The main limitation to the biomass growth in the biofilm comes from the diffusion rate of the different substrate to the deep layer of the biofilm. Hydrogen sulfide production by the suspended solids is insignificant if compared with the contribution of the anaerobic bacteria in the biofilm (Gutierrez et al., 2009). Sulfide production in the biofilm depends on the dominance of the anaerobic conditions with the molecular diffusivity of the limiting substrates in the biofilm. That can be illustrated clearly in the biofilm measurement reported in (Mohanakrishnan et al., 2009).

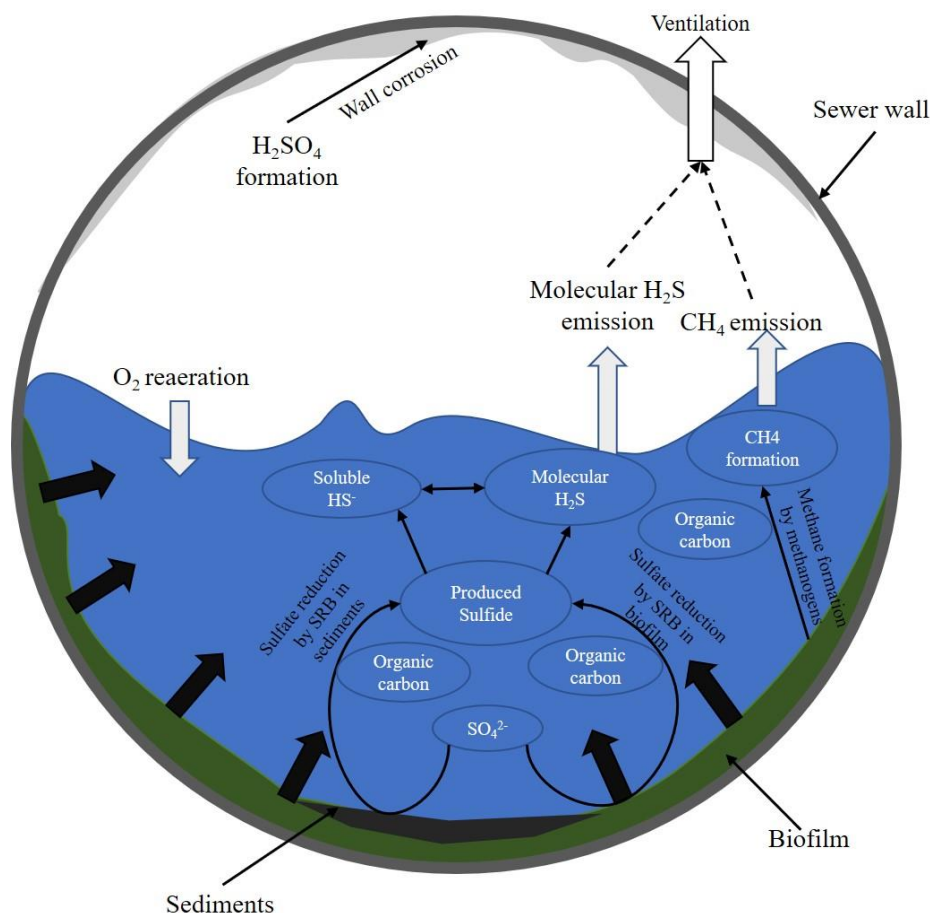


**Figure 1-6: Key biological, chemical and physical processes in gravity sewers**

The most common issues that arise in sewer systems is due to anaerobic processes. The formation of VOC, sulfide, and methane represent threats to the environment and health of humans. In addition, the further oxidation of hydrogen sulfide on the inner walls of the sewer pipes leads to corrosion of the pipes, which leads to expensive maintenance costs. Several strategies have been developed to overcome the problems of the formation and emission of these species. These strategies include addition of chemicals, such as metals salts, to promote the precipitation of the sulfide and injecting oxygen or nitrate to oxidize sulfide formed. Furthermore, different commercial alkalis are used to prevent the presence of the molecular form of the hydrogen sulfide, preventing mass transfer across the liquid-gas interface (Mora et al., 2016; Mohanakrishnan et al., 2009).

First attempts to model the in-sewer biochemical processes were concerned with the predicting sulfide production rate (Pomeroy and Parkhurst, 1978; Boon, 1975). These studies proposed empirical models for the prediction of the concentration of sulfide in sewer system based on the concentration of the organic matter, flow conditions, and the characteristics of the sewer pipes. However, these empirical models do not provide information regarding the sulfide formation mechanisms. Moreover, well controlled experiments are conducted to obtain these empirical models and cannot be used for the variation of the wastewater characteristics. Therefore, more conceptual models have been developed in the literature that are based on IWA activated sludge models.

Widely used biochemical models of the sewer system are stemmed from activated sludge models, ASM-series, and anaerobic digestion models. However, large differences exist between the modelling of the in-sewer processes and activated sludge processes. For instance, the main objective of the activated sludge models is to evaluate the removal efficiency of organic carbon, phosphorus, and nitrogen from wastewater. On the other hand, for sewer systems, the conversion of the soluble substrate and biomass production is of interest along with the prediction of the production rate of VOC, sulfide, and methane. Moreover, the conditions for the biomass growth are different; active biomass in activated sludge system is mainly exists in dense sludge flocs that comprise biodegradable and nonbiodegradable particulate COD with high concentration of active biomass. Substrate limited growth conditions prevail in the activated sludge system, while low concentrations of biomass exist in high concentration of substrate in sewer systems. Although the conversions occur in the biofilm are either neglected or inadequately considered in the activated sludge models, since it is insignificant if compared with the conversions in the bulk phase, the role of the biofilm in the sewer systems is crucial and requires special attention. Thus, using the accumulated experience of the activated sludge modelling to build a sewer system model is an effective method (Hvitved-Jacobsen et al., 2013).

Mathematical modelling of the biochemical processes in the sewer system has witnessed a huge development since the work published by Bjerre et al. (1998) that is based on ASM No.1 with addition of two other types of hydrolysis. Hvitved-Jacobsen et al. (1999)



further developed the model for the pressure mains by adding the anaerobic processes and the sulfate reduction process. The Wastewater Aerobic/Anaerobic Transformations in Sewers (WATS) model was introduced in the work of Hvitved-Jacobsen et al. (2000) where a more detailed model of the carbon and sulfur cycles were included. The integration between the carbon and sulfur cycle was implemented in the work of Tanaka et al. (2000). However, the emission of hydrogen sulfide to the gas phase was considered in the model by Yongsiri et al. (2003) in order to complete the cycle of sulfur in the in-sewer processes. The SeweX model that was developed in the work of Sharma et al. (2008a) and Sharma et al. (2008b) was based on WATS model. This model was further extended in (Guisasola et al., 2009) to predict the formation of methane by MA in the biofilm, hence the competition with SRB was considered. In addition, a model to predict the development of the biofilm was developed (Jiang et al., 2009).

Since sulfide production control is widely achieved by oxygen or nitrate injection as one of the strategies used for the prevention of sulfide emission, several studies have been conducted to model sulfide oxidation (Mora et al., 2016; Mora et al., 2015). Oxidation of produced hydrogen sulfide may occur either chemically or biologically by the sulfide-oxidizing bacteria. However, it was reported that the aerobic and anoxic oxidation of sulfide is biological (Nielsen et al., 2006).

### 1.3 Uncertainty of the biochemical models

Model-based design, operation, and development of control strategies for wastewater management systems is prone to the risk of not meeting the regulatory standards due to the uncertainty of the modelling. Moreover, the uncertainty of the model could affect the cost management of the control and chemical dosing systems which is essential for the wastewater management industry. Flores-Alsina et al. (2008) demonstrated the influence of the uncertainty of model parameters on decision making for control strategies of wastewater management systems. Especially for integrated models of wastewater management systems, the complexity of the integration of the models of catchments, sewers and WWTPs makes decision making more difficult (Benedetti et al., 2008). Therefore, special attention has been drawn to the uncertainty analysis of the model-based design and management of the wastewater management systems.

The main sources of uncertainty of the models are categorized into three classes (McKay et al., 1999) which are (i) input or subjective uncertainty; (ii) structural uncertainty; and (iii) stochastic uncertainty. Input or subjective uncertainty comprises the uncertainty of the model parameters and input variables (Freni et al., 2009). This kind of uncertainty arises from the approximations and assumptions pertaining to wastewater characterization, flow profile, and model parameters. The fact that the model parameter default values are defined as ranges, rather than unique values, calibration is required to specify the true values for a given problem. This gives rise to the identifiability problem of the model parameters, which is a result of inadequate data points or unsuitable data used in the calibration process (Freni et al., 2009). This problem reduces the confidence in the calibrated set of parameters. Moreover, the model input variables have natural variation, while the model parameters are assumed constant, which could be another cause of the input uncertainty. The common methods used in uncertainty analysis of complex systems are summarized in the work of (Helton and Davis, 2003) where the relation and the differences between the uncertainty and sensitivity analysis is clarified.

Model parameters and input variables are commonly referred to as “model factors” in the uncertainty and sensitivity analysis literature, thereby it will be used consistently herein. Structural uncertainty is the uncertainty related to the approximations of the mathematical form used. This uncertainty originates from the imperfect representation of reality by making approximation of the physical real system to facilitate the mathematical model. For instance, the misuse of the hydrodynamics and mixing models to simulate the flow in the system could be one of the reasons of the structural uncertainty. Stochastic uncertainty could be included in the model itself as a random failure events of some components of the system.

Sensitivity and uncertainty analysis are an essential task for implementing mechanistic models so that the behaviour of the models with respect to various sources of uncertainty can be identified (Sin et al., 2009). Uncertainty and sensitivity analysis are widely performed conjointly since their definitions are closely related. Uncertainty analysis is conducted to study the uncertainty of the model output due to the propagation of the model factors uncertainty. On the other hand, sensitivity analysis is used to quantify the

characteristics of the model factors and determine the influence of each factor on the model output. Another definition of the sensitivity analysis is related to the uncertainty analysis as analysis of variance problem (ANOVA) (Sin et al., 2011), where the variance in the model output is decomposed and attributed to each of the model factors thereby the weight of each factor in the output variance could be quantified. In other words, the uncertainty analysis provides the probability distribution of the model outputs that corresponds to the uncertainty in the model input. The mean and the variance could be derived from this distribution to indicate the most likely and variability of the model outputs. On the other hand, the sensitivity analysis identifies and prioritizes the sources of the uncertainty.

Uncertainty analysis framing defines the sources of the uncertainty that are to be considered in the study and quantification method of the uncertainty. For instance, Sin et al., (2009) conducted uncertainty analysis for WWTP design problem under different model framings (uncertainty of the biochemical model parameter and influent characterization, hydraulics and mass transfer and combined all together). It was demonstrated the effect of the uncertainty on the design output under these proposed framings, concluding that the uncertainty of the different framings is almost additive if combined together.

Various sensitivity analysis methods have been developed for studying the mathematical models of the environmental fields. The common objectives of the sensitivity analysis are summarized as: factors prioritisation, factors fixing, factors mapping, and variance cutting. Where the factors prioritization and fixing are to rank the influence of the input factors on the model output and identify the non-influential factors, respectively. By identifying the non-influential inputs, their values could be fixed at the default, therefore, reducing the space of calibration. Inputs priorization reveals the inputs that should be well studied to reduce the variance in the model output. Factors mapping identifies the factors that lead the output to certain regions, and variance cutting is to identify a set of factors with minimum number that should be fixed to achieve a certain low level of model output variance (Neumann, 2012). According to Cosenza et al. (2013), the sensitivity analysis methods are classified into three groups: (i) local methods; (ii) global methods; and (iii) screening methods. Selection of the method to conduct the sensitivity

analysis is commonly based on the objectives of the study, the model complexity, the computational cost, the relation between the model factors and the output, and the correlation between the factors. However, not all of these factors are known prior to the study, especially the relation between the factors which is commonly unclear. The methods adopted in the literature vary in the number of simulations that should be performed. This is an essential factor for the complex environmental models that are highly nonlinear and stiff and have a huge number of parameters. Moreover, the dependence between the parameters and the form of the model are key factors to choose the method for the sensitivity analysis.

Local methods are exemplified in the differential analysis (derivative-based method) where the sensitivity of the model output is evaluated at a specific location of the factors space due to infinitesimal change of one model factor at a time (OAT). This method is based on computing the partial derivative of the model output with respect to a certain model factor with the other factor values are fixed at most probable values (mean values). Cosenza et al. (2013) have demonstrated the false conclusion that may be extracted of the study using this method due to the model non-linearity and abundant interaction between the model factors. Several studies have implemented the derivative-based method to conduct the sensitivity analysis of the environmental models (Neumann, 2012). Among the various sensitivity methods used in the literature to study the behaviour of complex model, differential analysis is widely used for the applications of the wastewater management since it requires low computational cost. Differential analysis is inherently local in terms of parameter values and requires differentiation of the whole system of equations which is tedious process and prone to error either in the derivation of the equations or the implementation.

Global methods are implemented over the entire space of the possible values of the model factors, thereby a large number of simulations may be required to cover the input space. Global sensitivity analysis methods typically require Monte Carlo simulations to be conducted. Widely used global methods in the literature include global Morris screening (Morris, 1991; Campolongo et al., 2007), regression-based methods, e.g. Standardised Regression Coefficients (SRC) (Saltelli et al., 2008), and variance-based methods, e.g.

Fourier Amplitude Sensitivity Testing (FAST), extended FAST and relevant method of Sobol indices methods (Sobol, 2001; Saltelli et al., 1999). These methods define a number of sensitivity measures for each model factor that are used to evaluate the study objectives.

Morris screening method is based on computing multiple Elementary Effects (EEs) where EE of factor  $i$  is defined as the change in the model outputs after applying perturbation to the model factor  $i$ . The mathematical form of the EE is described in Eq. 1.2 of the influence of factor  $x_i$  of  $k$  model factors on the model output  $y$ .

$$EE_i(x_i) = \frac{y(x_1, \dots, x_{i-1}, x_i + \Delta, x_{i+1}, \dots, x_k) - y(x_1, \dots, x_{i-1}, x_i, x_{i+1}, \dots, x_k)}{\Delta} \quad (1.2)$$

While the form of Eq. 1.2 is similar to the numerical approximation of the partial derivative of the model output with respect to the model factor  $x_i$ , the perturbation  $\Delta$  is not infinitesimal and defined based on the number of levels of the factor space sampling. In order to explore the global effect of each factor,  $r$  replicates of the  $EE_i$  are computed over the factor space. The mean and standard deviation of the  $r$  replicates for each factor are defined as sensitivity measures. The application of this method on the environmental system is reported in Ruano et al. (2011) and Vezzaro et al. (2011).

Another approach is adopting the Monte Carlo (MC) technique to perform the uncertainty and sensitivity analysis. The main advantage of MC technique is no need for the manipulation or modification of the original model. In the MC technique, a number of possible sampling procedures are used to form a sampling space of the model factors (Helton and Davis, 2003). Evaluation of the model output using the all the vectors in the sampling space is the next step. A variety of sensitivity analysis procedures are available to determine the weight of the model input using the MC simulations output. The MC approach is a method reduce the time required for the calibration of the biological model as suggested by Sin et al. (2008). The SRC method is adopted to quantify the influence of each factor on the model output by implementing a regression process of the MC simulations output to a multivariate linear model (Eq. 1.3) and the coefficients  $b_i$  are

obtained. Coefficients  $b_i$  are normalized using the standard deviation  $\sigma$  of the MC simulation outputs  $y$  and model factors  $x_i$  to obtain the standardized slopes  $\beta_i$ .

$$y = \sum b_i \cdot x_i + a \quad (1.3)$$

$$\beta_i = b_i \cdot \frac{\sigma_{x_i}}{\sigma_y} \quad (1.4)$$

$|\beta_i|$  values are used for the ranking of the model factors where the sign of  $\beta_i$  indicates the direction of influence of the specified factor on the model results. For the case of  $\sum \beta_i = 1$ , the model could be considered as a linear model thereby the factors prioritization and determining the non-influential factors could be performed (Saltelli et al., 2004). However, for the nonlinear models, only factor prioritization could be reliably obtained (Cosenza et al., 2013). Since this method investigates the first order effect, it does not explore the interactions between the model factors. Moreover, it is proposed by (Saltelli et al., 2004) that the SRCs could be considered valid sensitivity measures only when the coefficient of determination  $R^2$  of the regression process is greater than 0.7.

Variance-based methods are based on variance decomposition theorems that indicate that the model output variance can be decomposed into conditional variances Eq. 1.5. In Eq. 1.5, the  $V$  and  $E$  stand for variance and expectancy operators, respectively, whereas the subscript  $i$  and  $-i$  indicate that the operation is evaluated over the factor  $i$  and all the factors except factor  $i$ , respectively.

$$V(y) = V_i(E_{-i}(y | x_i)) + E_i(V_{-i}(y | x_i)) \quad (1.5)$$

These methods have the advantage that they do not require the linearity or the monotonicity of the examined model. Extended Fourier Amplitude Sensitivity Test (FAST) method (Saltelli et al., 1999) is widely used recently due to its capability of evaluation the interactions between the factors (IF). It results from combining the FAST method (Cukier et al., 1973) with Sobol' variance method (Sobol, 2001). For each factor  $x_i$  two measures are defined: first order effect index ( $S_i$ ) and total effect index ( $S_{Ti}$ ). The

value of the  $S_i$  (defined in Eq.1.6) indicates the importance of the corresponding factor  $x_i$  on the model output.

$$S_i = \frac{V_{x_i}(E_{x_{-i}}(y | x_i))}{V(y)} \quad (1.6)$$

It is worth mentioning that for linear models and orthogonal factors,  $S_i$  is equivalent to the  $\beta_i$  squared of the SRC method ( $S_i = (\beta_i)^2$ ). However, the low value of  $S_i$  does not imply that the factor  $x_i$  is non-influential factor. It is necessary to evaluate  $S_{Ti}$  for all factors since the high value of  $S_{Ti}$  indicates that the corresponding factor  $x_i$  could have an indirect influence on the model output through the interaction with the other factors (Sobol, 2001). The  $S_{Ti}$  is defined as:

$$S_{Ti} = 1 - \frac{V_{x_{-i}}(E_{x_i}(y | x_{-i}))}{V(y)} \quad (1.7)$$

Several comparisons between the global methods have been carried out in the literature (Cosenza et al., 2013; Confalonieri et al., 2010; Neumann, 2012; Sun et al., 2012) to determine to assess the performance of these models. It can be concluded from these studies that all the global methods have a similar performance in terms of ranking the influential factors. However, for highly non-linear models, (Neumann, 2012) stated that the methods define first order measure only, e.g. regression-based methods, cannot be reliably adopted. On the other hand, Sun et al. (2012) proposed using two-step procedure for models with too high number of factors. The first step is to screen the factors using a local method, then a global method should be conducted. However, the study of Cosenza et al. (2013) showed that Extended FAST method and SRC give similar results regarding the factor prioritization, knowing that that SRC was used out of its recommended range ( $R^2 < 0.7$ ), whereas discrepancy was observed in the results of global Morris screening method. It was proposed to conduct sensitivity analysis adopting multiple methods simultaneously for the sack of robustness of the study.

## 1.4 Objectives of the Thesis

The overall goal of this work is to develop detailed models of some challenging sections of the wastewater management systems using CFD framework. CFD is a robust computational method to simulate the hydrodynamics of single phase and multiphase flow, spatial distribution of different species and mass transfer. Therefore, the approximations of common models could be examined. To achieve this overall goal, the following specific objectives have been identified:

- i. To develop a CFD-PBM model to capture the BSD evolution correctly and investigate the common approximations of modelling the aeration system in activated sludge system,
- ii. To develop a CFD model integrated with the biochemical reactions of sewer systems, but with more accurate description of the heterogeneous reactions to examine the approximations of the 1-D models, and
- iii. To use the most efficient model from the previous objective to simulate the performance of a lab-scale experiment to develop a nitrate dosing plan to study the different strategies of nitrate dosing.

The primary motivation of this work is to use the high capabilities of CFD analysis to simulate the different processes involved in the wastewater management system. However, using CFD models in such systems might be unaffordable nowadays due to the high computational cost. Therefore, CFD could be more useful to examine the conventional models used in the industry. Two applications are chosen herein where CFD could play an important role in determining the inaccuracy. The first application, described in objective (i), is to investigate the influence of the constant bubble assumption or uniform  $K_La$  throughout the reactor. To reach this goal, a validated CFD-PBM model is adopted that can capture the BSD and oxygen mass transfer parameters. CFD-PBM, which has been witnessed recently a great progress, is studied and a comparison between different closure models of bubble coalescence and breakup is presented. The second application is described in objective (ii) and (iii), where the effect of neglecting the solids settling and homogenization of heterogeneous reactions is the main concern. CFD model is developed to integrate the biochemical reactions with



hydrodynamics simulation. However, uncertainty/sensitivity analysis of the WATS biochemical model is conducted. Then, the conclusions of objective (ii) are used to determine how to model the performance of a lab-scale experiment and propose a nitrate dosing strategy. However, since this experiment is intended to be used to study sulfide biological oxidation by nitrate, the WATS model is extended to include the relevant reactions.

## 1.5 Thesis organization

Thesis is organized into three articles that are discussing two knowledge gaps in the modelling and physics of the aeration of the activated sludge systems and the modelling the biochemical conversions in the sewer network.

- *Chapter 2:* A CFD-PBM model is developed and validated using experimental data from literature. The validation is based on the measurement of BSD at different levels and  $K_La$  in a bubble column reactor. A comparison between different closure models of bubbles coalescence and breakup is conducted. A detailed analysis of the effect of the BSD and the flow field on the local  $K_La$  is conducted. The validity of the constant bubble size approximation is analyzed and discussed.
- *Chapter 3:* Uncertainty/sensitivity analysis of the WATS biochemical model implemented in 1-D CSTRs-in-series form is conducted to determine the influential parameters in the biochemical model. A CFD model is integrated with the WATS model to simultaneously simulate the hydrodynamics and the biochemical reactions in the sewer. The CFD model is developed to consider the settling of particulate matters and the heterogeneity of the biofilm reactions. A novel method of implementing the surface reactions in ANSYS FLUENT (CFD commercial software) is developed and verified. The verified CFD model is used to examine the accuracy of the results of the 1-D model where the effect of neglecting the particulate setting and the homogenization of the biofilm reactions are evaluated.
- *Chapter 4:* Based on the conclusion in chapter 3, a lab-scale experiment is modelled using The WATS model in the form of CSTRs-in-series. However, the

goal of this chapter is to evaluate different strategies of nitrate dosing in the lab-scale experiment. Therefore, the WATS model is extended to include the biological oxidation of sulfide in anoxic conditions. The developed model is calibrated and validated using measurement data from the experiment. Then, the different strategies are tested, and recommendations are proposed for efficient nitrate dosing in the system.

- *Chapter 5:* summary of the present study and main contribution is reported along with recommendations for future work.

## 1.6 References

- A. A. Kulkarni, “Mass Transfer in Bubble Column Reactors: Effect of Bubble Size Distribution,” *Ind. Eng. Chem. Res.*, vol. 46, no. 7, pp. 2205–2211, 2007.
- Amaral, A. (2019). *Towards a detailed understanding of oxygen transfer in wastewater treatment: the effect of bubble size distribution* (Doctoral dissertation, Ghent University).
- Amaral, A., Bellandi, G., Rehman, U., Neves, R., Amerlinck, Y., & Nopens, I. (2018). Towards improved accuracy in modeling aeration efficiency through understanding bubble size distribution dynamics. *Water research*, 131, 346-355.
- Amaral, A., Gillot, S., Garrido-Baserba, M., Filali, A., Karpinska, A. M., Plósz, B. G., ... & Rosso, D. (2019). Modelling gas–liquid mass transfer in wastewater treatment: when current knowledge needs to encounter engineering practice and vice versa. *Water science and technology*, 80(4), 607-619.
- Baquero-Rodríguez, G. A., Lara-Borrero, J. A., Nolasco, D., & Rosso, D. (2018). A Critical Review of the Factors Affecting Modeling Oxygen Transfer by Fine-Pore Diffusers in Activated Sludge: Baquero-Rodríguez et al. *Water Environment Research*, 90(5), 431-441.
- Batstone, D. J., Keller, J., Angelidaki, I., Kalyuzhnyi, S. V., Pavlostathis, S. G., Rozzi, A., ... & Vavilin, V. A. (2002). The IWA anaerobic digestion model no 1 (ADM1). *Water Science and technology*, 45(10), 65-73.
- Batstone, D. J., Amerlinck, Y., Ekama, G., Goel, R., Grau, P., Johnson, B., ... & Voleke, E. (2012). Towards a generalized physicochemical framework. *Water Science and Technology*, 66(6), 1147-1161.
- Benedetti, L., Bixio, D., Claeys, F., & Vanrolleghem, P. A. (2008). Tools to support a model-based methodology for emission/immission and benefit/cost/risk analysis of

- wastewater systems that considers uncertainty. *Environmental Modelling & Software*, 23(8), 1082-1091.
- Boon, A. G. (1975). Formation of sulphide in rising main sewers and its prevention by injection of oxygen. *Prog. Wat. Tech.*
- Bjerre, H. L., Hvitved-Jacobsen, T., Teichgräber, B., & Schlegel, S. (1998). Modeling of aerobic wastewater transformations under sewer conditions in the Emscher River, Germany. *Water environment research*, 70(6), 1151-1160.
- Campolongo, F., Cariboni, J., & Saltelli, A. (2007). An effective screening design for sensitivity analysis of large models. *Environmental modelling & software*, 22(10), 1509-1518.
- Chen, L., Tian, Y., Cao, C., Zhang, S., & Zhang, S. (2012). Sensitivity and uncertainty analyses of an extended ASM3-SMP model describing membrane bioreactor operation. *Journal of membrane science*, 389, 99-109.
- Coats, E. R., & Wilson, P. I. (2017). Toward nucleating the concept of the water resource recovery facility (WRRF): perspective from the principal actors. *Environmental science & technology*, 51(8), 4158-4164.
- Cosenza, A., Mannina, G., Vanrolleghem, P. A., & Neumann, M. B. (2013). Global sensitivity analysis in wastewater applications: A comprehensive comparison of different methods. *Environmental modelling & software*, 49, 40-52.
- Cukier, R. I., Fortuin, C. M., Shuler, K. E., Petschek, A. G., & Schaibly, J. H. (1973). Study of the sensitivity of coupled reaction systems to uncertainties in rate coefficients. I Theory. *The Journal of chemical physics*, 59(8), 3873-3878.
- Flores-Alsina, X., Rodríguez-Roda, I., Sin, G., & Gernaey, K. V. (2008). Multi-criteria evaluation of wastewater treatment plant control strategies under uncertainty. *Water research*, 42(17), 4485-4497.
- Flores-Alsina, X., Mbamba, C. K., Solon, K., Vrecko, D., Tait, S., Batstone, D. J., &

- Gernaey, K. V. (2015). A plant-wide aqueous phase chemistry module describing pH variations and ion speciation/pairing in wastewater treatment process models. *Water Research*, 85, 255-265.
- Freni, G., Mannina, G., & Viviani, G. (2009). Identifiability analysis for receiving water body quality modelling. *Environmental Modelling & Software*, 24(1), 54-62.
- Glover, G. C., Printemps, C., Essemiani, K., & Meinhold, J. (2006). Modelling of wastewater treatment plants—how far shall we go with sophisticated modelling tools?. *Water science and Technology*, 53(3), 79-89.
- Guisasola, A., Sharma, K. R., Keller, J., & Yuan, Z. (2009). Development of a model for assessing methane formation in rising main sewers. *Water Research*, 43(11), 2874-2884.
- Gujer, W., Henze, M., Mino, T., Matsuo, T., Wentzel, M. C., & Marais, G. V. R. (1995). The activated sludge model No. 2: biological phosphorus removal. *Water science and technology*, 31(2), 1-11.
- Gujer, W., Henze, M., Mino, T., & Van Loosdrecht, M. (1999). Activated sludge model no. 3. *Water science and technology*, 39(1), 183-193.
- Gutierrez, O., Park, D., Sharma, K. R., & Yuan, Z. (2009). Effects of long-term pH elevation on the sulfate-reducing and methanogenic activities of anaerobic sewer biofilms. *Water research*, 43(9), 2549-2557.
- Hauduc, H., Takács, I., Smith, S., Szabó, A., Murthy, S., Daigger, G. T., & Spérandio, M. (2015). A dynamic physicochemical model for chemical phosphorus removal. *water research*, 73, 157-170.
- Helton, J. C., & Davis, F. J. (2003). Latin hypercube sampling and the propagation of uncertainty in analyses of complex systems. *Reliability Engineering & System Safety*, 81(1), 23-69.
- Henze, M., Grady, C. P. L., Gujer, W., Marais, G. V. R., & Matsuo, T. Activated Sludge

Model No. 1 Scientific and Technical Report London: IAWPRC, 1987. *N, 1*, 37.

Henze, M., Gujer, W., Mino, T., Matsuo, T., Wentzel, M. C., Marais, G. V. R., & Van Loosdrecht, M. C. (1999). Activated sludge model no. 2d, ASM2d. *Water science and technology*, 39(1), 165-182.

Henze, M., Gujer, W., Mino, T., & van Loosdrecht, M. C. (2000). *Activated sludge models ASM1, ASM2, ASM2d and ASM3*. IWA publishing.

Hvitved-Jacobsen, T., Vollertsen, J., & Tanaka, N. (1999). Wastewater quality changes during transport in sewers—an integrated aerobic and anaerobic model concept for carbon and sulfur microbial transformations. *Water science and technology*, 39(2), 233-249.

Hvitved-Jacobsen, T., Vollertsen, J., & Tanaka, N. (2000). An integrated aerobic/anaerobic approach for prediction of sulfide formation in sewers. *Water science and technology*, 41(6), 107-115.

Hvitved-Jacobsen, T., Vollertsen, J., & Nielsen, A. H. (2013). *Sewer processes: microbial and chemical process engineering of sewer networks*. CRC press.

Jiang, F., Leung, D. H. W., Li, S., Chen, G. H., Okabe, S., & van Loosdrecht, M. C. (2009). A biofilm model for prediction of pollutant transformation in sewers. *water research*, 43(13), 3187-3198.

Jiang, L. M., Garrido-Baserba, M., Nolasco, D., Al-Omari, A., DeClippeleir, H., Murthy, S., & Rosso, D. (2017). Modelling oxygen transfer using dynamic alpha factors. *Water research*, 124, 139-148.

Karpinska, A. M., & Bridgeman, J. (2016). CFD-aided modelling of activated sludge systems—A critical review. *Water research*, 88, 861-879.

Le Moullec, Y., Potier, O., Gentric, C., & Leclerc, J. P. (2008a). A general correlation to predict axial dispersion coefficients in aerated channel reactors. *Water research*, 42(6-7), 1767-1777.

- Le Moullec, Y., Potier, O., Gentric, C., & Leclerc, J. P. (2008b). Flow field and residence time distribution simulation of a cross-flow gas-liquid wastewater treatment reactor using CFD. *Chemical Engineering Science*, 63(9), 2436-2449.
- Le Moullec, Y., Gentric, C., Potier, O., & Leclerc, J. P. (2010). Comparison of systemic, compartmental and CFD modelling approaches: application to the simulation of a biological reactor of wastewater treatment. *Chemical engineering science*, 65(1), 343-350.
- Le Moullec, Y., Gentric, C., Potier, O., & Leclerc, J. P. (2010). CFD simulation of the hydrodynamics and reactions in an activated sludge channel reactor of wastewater treatment. *Chemical Engineering Science*, 65(1), 492-498.
- Lei, L., & Ni, J. (2014). Three-dimensional three-phase model for simulation of hydrodynamics, oxygen mass transfer, carbon oxidation, nitrification and denitrification in an oxidation ditch. *Water research*, 53, 200-214.
- Leu, S. Y., Rosso, D., Larson, L. E., & Stenstrom, M. K. (2009). Real-Time Aeration Efficiency Monitoring in the Activated Sludge Process and Methods to Reduce Energy Consumption and Operating Costs. *Water Environment Research*, 81(12), 2471-2481.
- Liu, Y., Ni, B. J., Ganigué, R., Werner, U., Sharma, K. R., & Yuan, Z. (2015). Sulfide and methane production in sewer sediments. *Water Research*, 70, 350-359.
- Lizarralde, I., Fernández-Arévalo, T., Brouckaert, C., Vanrolleghem, P., Ikumi, D. S., Ekama, G. A., ... & Grau, P. (2015). A new general methodology for incorporating physico-chemical transformations into multi-phase wastewater treatment process models. *Water Research*, 74, 239-256.
- Makinia, J., & Zaborowska, E. (2020). *Mathematical modelling and computer simulation of activated sludge systems*. IWA publishing.
- McKay, M. D., Morrison, J. D., & Upton, S. C. (1999). Evaluating prediction uncertainty in simulation models. *Computer Physics Communications*, 117(1-2), 44-51.

- Metcalf, W. (2003). Metcalf and Eddy wastewater engineering: treatment and reuse. *Wastewater Engineering: Treatment and Reuse*. McGraw Hill, New York, NY. [https://doi.org/10.1016/0309-1708\(80\)90067-6](https://doi.org/10.1016/0309-1708(80)90067-6).
- Neumann, M. B. (2012). Comparison of sensitivity analysis methods for pollutant degradation modelling: A case study from drinking water treatment. *Science of the total environment*, 433, 530-537.
- Mohanakrishnan, J., Gutierrez, O., Sharma, K. R., Guisasola, A., Werner, U., Meyer, R. L., ... & Yuan, Z. (2009). Impact of nitrate addition on biofilm properties and activities in rising main sewers. *Water research*, 43(17), 4225-4237.
- Mora, M., Fernández, M., Gómez, J. M., Cantero, D., Lafuente, J., Gamisans, X., & Gabriel, D. (2015). Kinetic and stoichiometric characterization of anoxic sulfide oxidation by SO-NR mixed cultures from anoxic biotrickling filters. *Applied microbiology and biotechnology*, 99(1), 77-87.
- Mora, M., López, L. R., Lafuente, J., Pérez, J., Kleerebezem, R., van Loosdrecht, M. C., ... & Gabriel, D. (2016). Respirometric characterization of aerobic sulfide, thiosulfate and elemental sulfur oxidation by S-oxidizing biomass. *Water research*, 89, 282-292.
- Morris, M. D. (1991). Factorial sampling plans for preliminary computational experiments. *Technometrics*, 33(2), 161-174.
- Nielsen, A. H., Hvitved-Jacobsen, T., & Vollertsen, J. (2005). Kinetics and stoichiometry of sulfide oxidation by sewer biofilms. *Water Research*, 39(17), 4119-4125.
- Nielsen, A. H., Vollertsen, J., & Hvitved-Jacobsen, T. (2006). Kinetics and stoichiometry of aerobic sulfide oxidation in wastewater from sewers—Effects of pH and temperature. *Water environment research*, 78(3), 275-283.
- Pasini, F. (2019). *Energy optimization of secondary treatment in WRRFs via off-gas and respirometric measurements* (Doctoral dissertation, University of California, Irvine).



- Pomeroy, R. D., & Parkhurst, J. D. (1978, January). The forecasting of sulfide build-up rates in sewers. In *Eighth International Conference on Water Pollution Research* (pp. 621-628). Pergamon.
- Potier, O., Leclerc, J. P., & Pons, M. N. (2005). Influence of geometrical and operational parameters on the axial dispersion in an aerated channel reactor. *Water Research*, 39(18), 4454-4462.
- Qasim, S. R. (2017). *Wastewater treatment plants: planning, design, and operation*. Routledge.
- Qiao, Z., Wang, Z., Zhang, C., Yuan, S., Zhu, Y., Wang, J., & Wang, S. (2013). PVAm-PIP/PS composite membrane with high performance for CO<sub>2</sub>/N<sub>2</sub> separation. *AIChE Journal*, 59(1), 215-228.
- Rigopoulos, S., & Jones, A. (2003). A hybrid CFD—reaction engineering framework for multiphase reactor modelling: basic concept and application to bubble column reactors. *Chemical Engineering Science*, 58(14), 3077-3089.
- Ruano, M. V., Ribes, J., Ferrer, J., & Sin, G. (2011). Application of the Morris method for screening the influential parameters of fuzzy controllers applied to wastewater treatment plants. *Water Science and Technology*, 63(10), 2199-2206.
- Rosso, D., Iranpour, R., & Stenstrom, M. K. (2005). Fifteen years of offgas transfer efficiency measurements on fine-pore aerators: Key role of sludge age and normalized air flux. *Water environment research*, 77(3), 266-273.
- Rosso, D., Lothman, S. E., Jeung, M. K., Pitt, P., Gellner, W. J., Stone, A. L., & Howard, D. (2011). Oxygen transfer and uptake, nutrient removal, and energy footprint of parallel full-scale IFAS and activated sludge processes. *Water research*, 45(18), 5987-5996.
- Saltelli, A., Ratto, M., Andres, T., Campolongo, F., Cariboni, J., Gatelli, D., ... & Tarantola, S. (2008). *Global sensitivity analysis: the primer*. John Wiley & Sons.

- Saltelli, A., Tarantola, S., & Chan, K. S. (1999). A quantitative model-independent method for global sensitivity analysis of model output. *Technometrics*, 41(1), 39-56.
- Saltelli, A., Tarantola, S., Campolongo, F., & Ratto, M. (2004). *Sensitivity analysis in practice: a guide to assessing scientific models* (Vol. 1). New York: Wiley.
- Sánchez, F., Rey, H., Viedma, A., Nicolás-Pérez, F., Kaiser, A. S., & Martínez, M. (2018). CFD simulation of fluid dynamic and biokinetic processes within activated sludge reactors under intermittent aeration regime. *Water research*, 139, 47-57.
- Sharma, K. R., Yuan, Z., de Haas, D., Hamilton, G., Corrie, S., & Keller, J. (2008a). Dynamics and dynamic modelling of H<sub>2</sub>S production in sewer systems. *Water Research*, 42(10-11), 2527-2538.
- Sharma, K., de Haas, D. W., Corrie, S., O'Halloran, K., Keller, J., & Yuan, Z. (2008b). Predicting hydrogen sulfide formation in sewers: a new model. *Water*, 35(2), 132-137.
- Sin, G., De Pauw, D. J., Weijers, S., & Vanrolleghem, P. A. (2008). An efficient approach to automate the manual trial and error calibration of activated sludge models. *Biotechnology and bioengineering*, 100(3), 516-528.
- Sin, G., Gernaey, K. V., Neumann, M. B., van Loosdrecht, M. C., & Gujer, W. (2009). Uncertainty analysis in WWTP model applications: a critical discussion using an example from design. *Water Research*, 43(11), 2894-2906.
- Sin, G., Gernaey, K. V., Neumann, M. B., van Loosdrecht, M. C., & Gujer, W. (2011). Global sensitivity analysis in wastewater treatment plant model applications: prioritizing sources of uncertainty. *Water research*, 45(2), 639-651.
- Singh, P., Kansal, A., & Carliell-Marquet, C. (2016). Energy and carbon footprints of sewage treatment methods. *Journal of environmental management*, 165, 22-30.
- Sobol, I. M. (2001). Global sensitivity indices for nonlinear mathematical models and

their Monte Carlo estimates. *Mathematics and computers in simulation*, 55(1-3), 271-280.

Sun, X. Y., Newham, L. T., Croke, B. F., & Norton, J. P. (2012). Three complementary methods for sensitivity analysis of a water quality model. *Environmental Modelling & Software*, 37, 19-29.

Tanaka, N., Hvitved-Jacobsen, T., & Horie, T. (2000). Transformations of carbon and sulfur wastewater components under aerobic–anaerobic transient conditions in sewer systems. *Water environment research*, 72(6), 651-664.

Teuber, K. (2020). A three-dimensional two-phase model for flow, transport and mass transfer processes in sewers. (Doctoral dissertation, Technische Universität Berlin).

UN High Commissioner for Refugees (UNHCR), The Sustainable Development Goals and Addressing Statelessness, March 2017, available at: <https://www.refworld.org/docid/58b6e3364.html> [accessed 8 March 2021]

V. G. Gude, “Energy storage for desalination processes powered by renewable energy and waste heat sources,” *Appl. Energy*, vol. 137, pp. 877–898, 2015.

van Loosdrecht, M. C., & Brdjanovic, D. (2014). Anticipating the next century of wastewater treatment. *Science*, 344(6191), 1452-1453.

Vezzaro, L., Eriksson, E., Ledin, A., & Mikkelsen, P. S. (2011). Modelling the fate of organic micropollutants in stormwater ponds. *Science of the Total Environment*, 409(13), 2597-2606.

Yongsiri, C., Hvitved-Jacobsen, T., Vollertsen, J., & Tanaka, N. (2003). Introducing the emission process of hydrogen sulfide to a sewer process model (WATS). *Water Science and Technology*, 47(4), 85-92.

## Chapter 2

### 2 Effects of flow velocity and bubble size distribution on oxygen mass transfer in bubble column reactors – A critical evaluation of the CFD-PBM model

Computational fluid dynamics (CFD) is used to simulate a bubble column reactor operating in the bubbly (homogenous) regime. The Euler-Euler two-fluid model, integrated with the population balance model (PBM), is adopted to compute the flow and bubble size distribution (BSD). The CFD-PBM model is validated against published experimental data for BSD, global gas holdup, and oxygen mass transfer coefficient. The sensitivity of the model with respect to the specification of boundary conditions and the bubble coalescence/breakup models is assessed. The coalescence model of Prince and Blanch (1990) provides the best results, while the output is shown to be insensitive to the breakup model. The CFD-PBM study demonstrates the importance of considering the BSD in order to correctly model mass transfer. Results show that the constant bubble size approximation results in a large error in the oxygen mass transfer coefficient, while giving acceptable results for gas holdup.

#### 2.1 Introduction

Bubble columns are multiphase reactors that are widely used in numerous industrial processes. For example, bubble columns are involved in many biochemical and petrochemical applications, as well as biochemical processes such as biological wastewater treatment (Kantarci et al., 2005). The widespread use of bubble columns in industrial applications is due to their simple operation and control, low cost, high capacity, and good heat and mass transfer characteristics between phases (Bhole et al., 2008). The operation of bubble columns is simple because the gas phase is sparged by a gas distributor maintained at the bottom of the reactor. Rising bubbles push the liquid phase in the lateral and axial directions creating circulation in the continuous phase, thereby improving the mixing. There are various types of gas distributors used in industrial applications. However, fine bubbling is favoured because it achieves high interfacial area, which facilitates more efficient mass transfer between phases and

minimises stripping of the liquid phase as vapour (Hasanen et al., 2006). Fine-bubble diffusers such as perforated flexible membrane, porous rigid ceramic, jets, mechanical turbines, and perforated cap diffusers are the most commonly used in industrial applications (Terashima et al., 2016). Due to their energy efficiency, fine-bubble diffusers made of perforated membranes and porous ceramics are the most common technology of choice in biological wastewater treatment (Tchobanoglous et al., 2014; Rosso, 2019).

Many experimental studies (*inter alia*: Zlokarnik, 1980; Amaral et al., 2018; Darmana et al., 2007; Krishna and Ellenberger, 1996; Pjontek et al., 2014; and Rzehak et al., 2017) and numerical analyses (Chen et al., 2005; Deen et al., 2001; Liang et al., 2016; Rzehak et al., 2017; and Yang, et al., 2017) have been conducted to understand and improve the performance of bubble columns by making efficient use of the limited volume available (Jakobsen, Lindborg and Dorao, 2005). These studies focused on the influence of several parameters such as column dimensions, gas sparger type and position, the properties of liquid phase, gas superficial velocity, water composition, and operating temperature and pressure. The quantification of the influence of these parameters is based on local and global gas holdup, heat and mass transfer rates, bubble characteristics, and flow regime. The key to understanding bubble column performance when operating in batch mode is to precisely predict the behaviour of the gas phase motion and the bubble size evolution along the bubble column. While overall heat and mass transfer rates can be measured for the volume, understanding the local hydrodynamics, including bubble size distribution, is required to predict these rates *a priori* or within an integrated multiphysics CFD simulation. However, limited understanding of the complex interactions between the phases and the heat and mass transfer processes hinders the optimization and scale-up of such reactors.

Computational fluid dynamics (CFD) is a promising numerical approach that can be used to calculate and optimize the performance of bubble columns. In recent years, there have been significant developments made in CFD techniques used for simulating multiphase flows, resulting in improved accuracy and stability of solutions. Many works in the literature have attempted to study the hydrodynamics of bubble columns using various

numerical approaches available, namely the Euler-Lagrange framework (Delnoij et al., 1997; Sokolichin et al., 1997) and the two-fluid model in the Euler-Euler framework (Gemello et al., 2018; Zhang et al., 2006; and Liang et al., 2016). The Euler-Lagrange method treats the fluid phase as a continuum in the Eulerian framework while the dispersed phase is tracked by solving Newton's second law of motion on the trajectory of the individual bubbles in the domain. This approach is very computationally expensive when applied to modelling high gas flow rates since it tracks the large number of bubbles individually. Hence, this model is only applicable for limited low flow rates of the dispersed phase and a limited number of bubbles within the domain. The more commonly used model is the Eulerian (or two-fluid) model, which solves a set of continuity and momentum equations for each phase in the Eulerian framework. It assumes that the immiscible phases are interpenetrating continua. The momentum and continuity equations are derived by conditional ensemble or volume averaging of single-phase forms of the fundamental conservation equations for each phase (Ishii and Hibiki, 2011; Marschall, 2011 and Rusche, 2002).

The averaging process required for the Eulerian model leads to the loss of the interfacial boundary between the different phases in the system. In practice this corresponds to modelling the two phases as separate continua, with no explicit interface, which interact only through interfacial transfer terms that capture their interaction. Generally, the complexity of multiphase flows arises from these interactions between the different phases within the system. Modelling these interactions is a complex process and can result in substantial errors in numerical simulations if not handled correctly, as will be shown in this study.

Many closure models for the interfacial forces and turbulence interactions have been developed in the literature. The interfacial forces include drag (Ishii and Zuber, 1979; Grace, 1976; Naumann and Schiller, 1935; Tomiyama, 1998; Tomiyama and Kataoka, 1998; Zhang and VanderHeyden, 2002), virtual mass (Rafique et al., 2004), turbulent dispersion (Burns et al., 2004; Gosman et al., 1992; Lopez De Bertodano, 1998; Lucas et al., 2007), and lift and wall forces (Drew and Lahey, 1987; Lucas et al., 2007; Lucas and Tomiyama, 2011; Tomiyama, 1998; Tomiyama et al., 2002; Žun, 1980). Lubchenko et al.

(2018) reviewed the wall lubrication superficial force that is commonly used in the literature to capture the gas volume fraction profile near the wall. Experimental data and direct numerical simulation (DNS) results were used to propose a new understanding of this force that is different from what is reported in the literature. As all the forces are modelled, instead of being resolved directly due to the loss of the interfacial boundaries between the phases in the Eulerian model, various models were developed either by experimental observation or by the analytical solution of a simplified problem. Including all known interfacial forces might improve the ability of a simulation to approach the real physics of the problem, yet not all forces show considerable influence on the results and only offer additional computational cost and solution instability. Therefore, one must consider carefully which forces to include and how they should be modelled.

Despite the significant influence of the bubble size distribution (BSD) in bubble column systems (Amaral, 2019), many studies published in the literature assumed a constant size throughout the whole domain. Amaral (2019) emphasized the significance of studying the variation of BSD on the mass transfer process, showing the possibility of numerically modelling the evolution of the BSD in bubble column reactor. The uniform bubble size assumption used in these studies is based on experimental observation (Gemello et al., 2018; Zhang et al., 2006; Masood and Delgado, 2014; Simonnet et al. 2008), empirical correlation (Chen et al., 2005), or assumed without justification. In most cases, this assumption is unrealistic and disregards the fact that the interaction between the bubbles and the continuous phase leads to coalescence and breakage of the bubbles as they rise. Consequently, the BSD should be considered to vary throughout the domain as a function of the hydrodynamics of the continuous phase. The BSD plays a critical role in computing interfacial forces and their direction.

Several works in the literature (Chen et al., 2005; Vik et al., 2018; Wang et al., 2005; Yang et al., 2017) are concerned with studying the evolution of the BSD in the domain by integrating the population balance model (PBM) in the CFD simulation. PBM is a statistical model that was formulated by Hulburt and Katz (1964) and has been subsequently integrated into various CFD frameworks. Several methods have been developed for the coupled solution of PBM with CFD (Hounslow et al, 1988; Kumar and

Ramkrishna, 1996; Marchisio and Fox, 2005). Methods developed by Marchisio and Fox (2005) and Randolph (2012) are based on solving transport equations for the moments of the BSD in the CFD domain, then reconstructing the BSD using the solved moments. These methods were developed to reduce the computational cost of employing the PBM model within CFD simulations. The Class Method (CM) developed by Kumar and Ramkrishna (1996) has the advantage of directly representing the BSD by a discrete set of size classes. A conventional conservation equation is formulated for each bubble class with source terms that represent the coalescence, breakup, and growth of bubbles. The mechanisms of bubble breakup and coalescence are strongly influenced by the hydrodynamics of the surrounding continuous phase. These mechanisms have been studied and numerous mechanistic models were proposed in the literature (Lehr et al., 2002; Luo and Svendsen, 1996; Wang et al., 2006; Prince and Blanch, 1990).

It is critical to employ interfacial force models that take into account the size of bubbles, whether they are modelled using moment- or class-based methods. The reason behind this is the challenging prediction of the gas holdup radial profiles. Even if the gas holdup profiles are well-predicted and match with experimental data, the constant bubble size assumption would still result in inaccurate prediction of any subsequent calculations of mass and heat transfer between the gas bubbles and the continuous liquid phase since the interfacial area plays a key role in determining such rates (Shah et al., 1982). Moreover, the correct prediction of the bubble size distribution with accurate gas holdup profile would imply that the physics of bubble dynamics in the bubble column reactor is correctly modelled and the other field quantities are also correctly predicted. In addition, the models' error can be traced. For instance, the sign conversion of the lateral lift force of the model proposed by Tomiyama et al. (1995), which is based on the bubble size, depicts the importance of simulating the BSD. Therefore, if improvement in gas holdup profile prediction is achieved with this lateral force model using the bubble size evaluated by PBM, we hypothesize that this would imply that the mathematical model is highly likely to reflect the true physics of the bubble plume dynamics.

The representation of the computational domain for bubble columns as a 2D or 3D space is an active argument in the literature and several studies have been conducted to



compare the 2D and 3D simulations (Chen et al., 2005; Krishna et al., 2000). The simplification of the domain to 2D is primarily to reduce the computational cost and improve the stability of the solution. However, it is agreed that the 2D axisymmetric domain is not appropriate for this kind of simulation (Chen et al., 2005; Krishna et al., 2000). It was explained by Chen et al. (2005) that using a 2D axisymmetric model does not capture the meandering movement of the bubble plume in the bubble column, thus inaccurate results are obtained. In this case, the authors recommended the use of 3D simulations. On the other hand, it has been shown that a 2D planar approach can be considered as a good compromise between accuracy and computational cost (Jakobsen et al., 1997).

In the present work, multiphase CFD simulations of air flow in a bubble column operating at low gas flow rates (2 and 8 L·min<sup>-1</sup>) are conducted utilizing OpenFOAM® (Weller et al., 1998) while using a 2D planar approximation of the system. Experimental data from Amaral et al. (2018) are used for validation and evaluation of the examined models. The PBM class method is adopted in the CFD simulations to capture the evolution of the bubble size distribution in the bubble column. Different model parameters are examined to illustrate the sensitivity of the results to each parameter. The oxygen transfer coefficient and gas holdup are computed and compared against measurement data to investigate the influence of the flow field on the performance of the bubble column. Moreover, the results of the global gas holdup and oxygen mass transfer are used to assess the inaccuracy of the constant bubble size assumption.

## 2.2 Problem Description

### 2.2.1 Validation Data

Experimental data from Amaral et al. (2018) is used for validation and discussion. A lab-scale bubble column reactor with dimensions of 380 mm in diameter and height of 1600 mm was used in this work. It should be noted that this reactor is too shallow to observe an increase in bubble size due to the hydrostatic pressure gradient, yet provides an excellent means of evaluating interfacial force, coalescence, and breakup models. The bubble column was built from transparent material in order to allow the authors to

measure the bubble size distribution using a high-speed camera. A flexible membrane air diffuser with an inner diameter of 30 cm, as shown in Fig. 2-1, was mounted for sparging air from the bottom of the bubble column filled with tap water. The reported measurement data includes the bubble size distribution at 5 and 120 cm above the air diffuser, global gas holdup, and global volumetric oxygen mass transfer coefficient. The measurements were taken at air flow rates ranging from 2 to 8 L·min<sup>-1</sup> which indicates the bubbly (homogeneous) flow regime is dominant. BSD measurements were taken at different levels in the bubble column illustrated in Fig. 2-1 using dashed lines. The dimensions of the bubble column and the locations of the measurements in the work of Amaral et al. (2018) are used to set up the current numerical simulations and for post-processing the results.

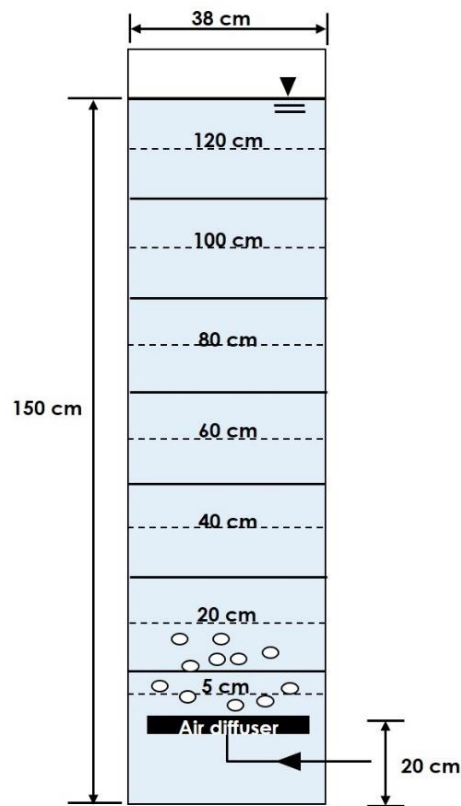


**Figure 2-1: Experimental bubble column setup (adapted from Amaral et al., 2018) with bubble size measurement locations denoted by dashed lines**

### 2.2.2 Numerical Model

A 2D planar CFD model is developed to simulate the two-phase flow field in the bubble column (see Fig. 2-1) using the OpenFOAM open source CFD code (Weller et al., 1998). In the experimental setup, the air sparger was mounted 20 cm above the bottom of the column. In order to reduce the computational cost of the CFD model, the space below the air diffuser is disregarded since it is presumed to have minimal influence on the flow fields above the air diffuser. The CFD domain is shown Fig. 2-2 where the total height of the domain is 140 cm with an initial water level of 130 cm above the air diffuser. The standard properties of air and water at 20°C are used for the model, assuming both phases are incompressible (since the hydrostatic pressure difference is too small to substantially change the gas density). Since the rising bubble plume in the bubble column exhibits dynamic behaviour, a transient simulation setup is used to control the solution stability and capture the dynamics of the bubbles. The time step size is dynamically controlled to ensure the Courant number remains below 0.5 throughout the domain. Volume fractions and the velocities of the air and water phases are sampled during the simulations to calculate the time-averaged quantities for post-processing.

The two-fluid multiphase model that is implemented in OpenFOAM is used in the current study. OpenFOAM is an open-source software package that has been developed over many years and contains many different solvers for different types of flows. In this study, the “reactingTwoPhaseEulerFoam” solver is adopted since the PBM is already integrated. The interfacial forces are modelled using the models presented in the following section.

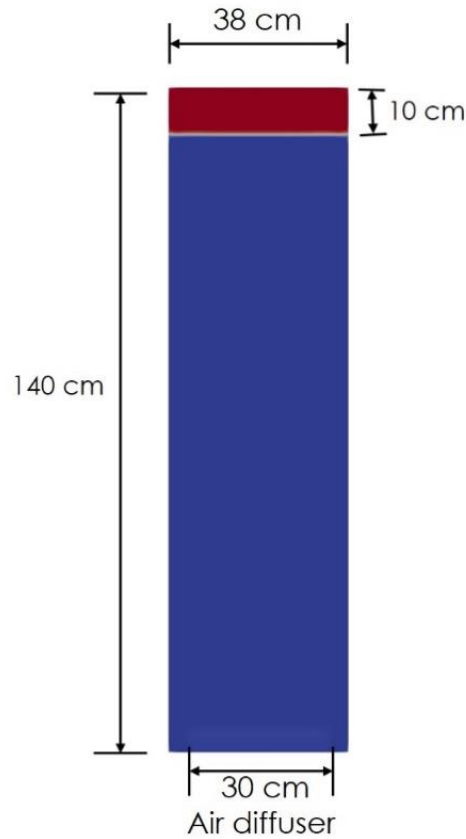


**Figure 2-2: Illustration of the bubble column computational domain, where the blue colour (bottom rectangle) indicates space occupied by water and the red colour (top rectangle) indicates space occupied by air, in the initial condition**

## 2.3 Governing Equations

### 2.3.1 Euler-Euler Two-Fluid Model

The governing equations of the two-fluid model are derived by conditional averaging of the single-liquid conservation equations. The basis of the conditional average is to multiply the single-phase flow equations by indicator functions, then ensemble average (or volume average) the result. Details regarding the conditional averaging process and derivation of the governing equations are reported in the work of Marschall (2011) and

Rusche (2002). For incompressible flow, the averaged continuity equation for phase  $k$  reads:

$$\frac{\partial \alpha_k}{\partial t} + \nabla \cdot (\alpha_k \overline{U_k}) = 0 \quad (2.1)$$

Here,  $\overline{U}$  is the averaged velocity and  $\alpha$  is the volume fraction (not to be confused with the  $\alpha$  factor describing the ratio of oxygen transfer in wastewater to clean water). The averaged momentum equations for phase  $k$  are given by:

$$\frac{\partial \alpha_k \overline{U_k}}{\partial t} + \nabla \cdot (\alpha_k \overline{U_k} \overline{U_k}) + \nabla \cdot (\alpha_k \overline{R_k^{eff}}) = -\frac{\alpha_k}{\rho_k} \nabla \overline{p} + \alpha_k g + \frac{\sum \overline{F_k}}{\rho_k} \quad (2.2)$$

where  $\overline{R_k^{eff}}$  represents the viscous and Reynolds turbulent stresses that are closed by the turbulence model,  $\overline{p}$  is the mean common static pressure between the phases,  $g$  is the gravitational acceleration,  $\rho_k$  is the density of the pertaining phase, and  $\sum \overline{F_k}$  is the sum of all interfacial forces between the two fluids, which needs to be modelled. The interfacial forces included in the current study are drag ( $\overline{F_D}$ ), virtual mass ( $\overline{F_{VM}}$ ), and lift forces ( $\overline{F_L}$ ), such that the total force is given as:

$$\sum \overline{F_k} = \overline{F_D} + \overline{F_{VM}} + \overline{F_L} \quad (2.3)$$

In order to model the free surface in the bubble column, the solver must be able to model the phase inversion where the dispersed gas phase becomes the continuous phase. A blending function for the interfacial forces is required to improve the solution stability and distinguish the continuous phase (Rusche, 2002). Thus, a representative diameter should be assigned for both phases in the system. For the CFD-PBM model, the Sauter diameter computed by the PBM is used as the bubble diameter for the gas phase while a constant value is given to the liquid phase. The Sauter diameter defined in the OpenFOAM solver is given as (Askari et al., 2019):

$$d_{32} = \frac{\sum_i f_i}{\sum_i \frac{f_i}{d_i}} \quad (2.4)$$

where  $f_i$  is the normalized volume fraction of gas bubble class  $i$  with bubble size of  $d_i$ . Further discussion is provided in section (2.3.3), which deals with the PBM. On the other hand, in the case of constant bubble size simulations, bubble sizes in the range from 1.25 to 1.75 mm (based on the gas flow rate) is defined as the average bubble size observed in the experimental data. The interfacial force models described below are represented in such a form that the continuous phase and the diameter of the dispersed phase are known.

Turbulence in bubble column reactors is generally induced by the shear stress and the bubbles' movement. The relative movement of the bubbles generates velocity fluctuations in the wake region of the bubbles. A significant source of turbulence in a bubble column with quiescent liquid is the turbulence induced by the rising bubbles in the liquid. It is observed by Mudde et al. (1997) that strong fluctuations in the liquid velocity field are present due to the motion of the rising bubbles even at low flow rates of the gas phase. Therefore, it is essential to incorporate the effect of the gas flow on the liquid phase turbulence. Turbulence generated by the mean shear follows the classic hypothesis of the energy cascade, which assumes that energy transfers from the large scale to the smaller scale until it dissipates at the Kolmogorov scale. On the other hand, the turbulence generated by bubbles follows an inverse cascade hypothesis where the turbulence is generated at the length and time scales associated with the bubble dimension and rising velocity (Jakobsen et al., 1997). The turbulence source in the liquid phase is related to the drag work of the bubbles and the relative velocity of the bubbles (Svendsen et al., 1992). Although there are two phases in the system, such that turbulence could be modelled for both phases, solving the turbulence model for the gas (dispersed) phase would not have influence on the results in most of the domain and would only contribute to additional computational cost (Oey et al., 2003). Therefore, turbulence in the gas phase is not considered and only turbulence for the liquid phase is modelled.

Several models have been developed to calculate the turbulent kinetic energy and dissipation rate either directly or indirectly. A widely used model in the literature is the model developed by Sato et al. (1980), where the turbulence induced by the bubble is accounted for by adding an additional turbulent viscosity to the original one. This model does not directly give a solution for the turbulent kinetic energy and the dissipation rate. More direct methods to model bubble-induced turbulence have been proposed. In these models, e.g. Politano et al. (2003) and Troshko and Hassan (2001), the bubble-induced turbulence is modelled by adding a source term to the turbulent kinetic energy and dissipation rate equations. Following the same method to add a source term to the turbulent kinetic energy and dissipation rate that is associated with the bubble motion, the model proposed by Lahey (2005) is used in the current work. Closure for the Reynolds turbulent stresses in the liquid phase momentum equations is obtained using the standard  $k - \varepsilon$  turbulence model with source terms to account for the influence of the bubbles' motion in the liquid phase as:

$$\frac{\partial}{\partial t}(\alpha_l k_l) + \nabla \cdot (\alpha_l k_l \overline{U_l}) = \nabla \cdot (\alpha_l \frac{v_l^t}{\sigma_k} \nabla k_l) + \alpha_l (P_l - \varepsilon_l) + \alpha_l \phi_k \quad (2.5)$$

$$\frac{\partial}{\partial t}(\alpha_l \varepsilon_l) + \nabla \cdot (\alpha_l \varepsilon_l \overline{U_l}) = \nabla \cdot (\alpha_l \frac{v_l^t}{\sigma_\varepsilon} \nabla \varepsilon_l) + \alpha_l C_{\varepsilon 1} \frac{P_l \varepsilon_l}{k_l} - \alpha_l C_{\varepsilon 2} \frac{\varepsilon_l^2}{k_l} + \alpha_l \phi_\varepsilon \quad (2.6)$$

where  $P_l$  is the production rate of the turbulent kinetic energy,  $k$ , and  $\varepsilon$  is the dissipation rate of the turbulent kinetic energy.  $\sigma_k$ ,  $\sigma_\varepsilon$ ,  $C_{\varepsilon 1}$  and  $C_{\varepsilon 2}$  are model constants. The subscripts  $l$  and  $g$  refer to the liquid and gas phase, respectively. The source terms associated with the turbulence induced by bubble motion are defined as:

$$\phi_k = \frac{k_l}{C_{\varepsilon 2} \varepsilon_l} \phi_\varepsilon \quad (2.7)$$

$$\phi_k = C_p (1 + C_D^{4/3}) \alpha_g \frac{|\overline{U_r^3}|}{d_g} \quad (2.8)$$

Here,  $C_p$  is a model constant,  $C_D$  is the drag coefficient,  $U_r$  is the relative velocity between the phases, and  $d_g$  is the diameter of the gas phase (Sauter diameter in case of using PBM).

The interfacial force in the momentum equations must be specified by closure models, as discussed in the next section.

### 2.3.2 Interfacial Force Models

The drag force is based on the dispersed phase equivalent diameter ( $d_a$ ) and is described by:

$$\overline{F_D} = \frac{3}{4} \alpha_a C_D \frac{\rho_b}{d_a} \left| \overline{U_b} - \overline{U_a} \right| (\overline{U_b} - \overline{U_a}) \quad (2.9)$$

where the drag coefficient ( $C_D$ ) is a function of the bubble Reynolds number as:

$$\text{Re} = \frac{d_a \left| \overline{U_r} \right|}{\nu_b} \quad (2.10)$$

where  $\overline{U_r}$  is mean relative velocity and  $\nu_b$  is the kinematic viscosity of the continuous phase. Two models are used for the drag coefficient calculation in the current study in an attempt to match the global gas holdup with the experimental data. The swarm correction factor that accounts for the interaction between the bubbles (Gemello et al., 2018) is not considered as the gas flow rate is low in this case, resulting in a low density of bubbles, such that little interaction between the bubbles is expected. The first drag model used is the model proposed by Naumann and Schiller (1935), which reads:

$$C_D = \begin{cases} \frac{24}{\text{Re}} (1 + 0.15 \text{Re}^{0.687}) & \text{Re} \leq 1000 \\ 0.44 & \text{Re} > 1000 \end{cases} \quad (2.11)$$

Another model that has good performance over a wide range of air flow rates has been suggested by Ishii and Zuber (1979) and is given by:



$$C_D = \max(C_{D,sphere}, \min(C_{D,ellipse}, C_{D,cap})) \quad (2.12)$$

where the drag coefficient for the different bubble shapes (spheres, ellipses, spherical caps) are defined as:

$$\begin{aligned} C_{D,sphere} &= \frac{24}{\text{Re}} (1 + 0.1 \text{Re}^{0.75}) \\ C_{D,ellipse} &= \frac{2}{3} \sqrt{Eo} \\ C_{D,cap} &= \frac{8}{3} \end{aligned} \quad (2.13)$$

Here,  $Eo$  is the Eötvös (or, equivalently, Bond) number which represents the dimensionless ratio of gravitational forces (i.e. buoyancy) vs. surface tension forces.

The lift force is a net force resulting from numerous interacting transverse forces perpendicular to the bubble rising direction. This force can be explained as a result of the asymmetric pressure distribution around the bubble (Rafique et al., 2004). The influence of the lift force was investigated by Deen et al. (2001) and Zhang et al. (2006). It was illustrated in these studies that the lift force controls the spreading of the bubble plume. Therefore, the ratio of the lift force to the drag force plays a critical role in the prediction of the gas and liquid velocity profiles. In other words, lower lift force results in less spreading of the bubble plume and steeper velocity profiles. The widely used formula for the lift force is:

$$\overline{F_L} = \alpha_a \rho_b C_L (\overline{U_b} - \overline{U_a}) \times \overline{\omega_b} \quad (2.14)$$

$$\overline{\omega_b} = \nabla \times \overline{U_b} \quad (2.15)$$

Where  $\overline{\omega_b}$  is the averaged vorticity of the continuous phase and  $C_L$  is the lift force coefficient and is modelled following the work of Tomiyama (1998):

$$C_L = \begin{cases} \min \begin{cases} 0.288 \tanh(0.121 \text{Re}) \\ 0.00105 Eo^3 - 0.0159 Eo^2 - 0.0204 Eo + 0.474 \end{cases} & Eo < 4 \\ 0.00105 Eo^3 - 0.0159 Eo^2 - 0.0204 Eo + 0.474 & 4 \leq Eo \leq 10 \\ -0.29 & Eo > 10 \end{cases} \quad (2.16)$$

The virtual mass force is the force induced by accelerating bubbles in the liquid phase where some surrounding the liquid phase are accelerated with the bubbles. The most common formulation for the virtual mass is derived in the work of Auton et al. (1988) as:

$$F_{VM} = C_{VM} \alpha_a \rho_b \left( \frac{D_a \overline{U}_a}{Dt} - \frac{D_b \overline{U}_b}{Dt} \right) \quad (2.17)$$

The virtual mass coefficient is  $C_{VM} = 0.5$ .

### 2.3.3 Population Balance Model

The population balance equation (PBE) is integrated with the two-phase CFD model in OpenFOAM in order to simulate the BSD evolution along with the flow field of the phases involved in the bubble column reactor (Bannari et al. 2008). Here we adopt the class method (CM), wherein the BSD is represented as a finite number of discrete bubble size classes. A conservation equation for each bubble class is solved in the computational domain. The conservation equation for the ‘ $i$ ’ bubble class can be written as:

$$\frac{\partial}{\partial t} (\rho_g n_i) + \nabla \cdot (\rho_g \overline{U}_g n_i) = \rho_g (B_{iC} - D_{iC} + B_{iB} - D_{iB}) \quad (2.18)$$

where  $n_i$  represents bubble number density for bubble class  $i$  in each of the computational cells.  $B_{iC}, D_{iC}, B_{iB}$  and  $D_{iB}$  are the source terms for the bubble class that represent the birth and death rates due to coalescence and the birth and death rates due to breakup, respectively. The birth and death rates for the bubble class can be represented as:

$$B_{iC} = \frac{1}{2} \int_0^v a(v-v', v') n(v-v') n(v') dv' \quad (2.19)$$

$$D_{iC} = n(v) \int_0^{+\infty} a(v, v') n(v') dv' \quad (2.20)$$

$$B_{iB} = \int_v^{+\infty} m(v') b(v') p(v, v') n(v') dv' \quad (2.21)$$

$$D_{iB} = b(v) n(v) \quad (2.22)$$

$n(v')$  is the bubble density of bubble class of size  $v'$ ;  $a(v-v', v')$  is the coalescence rate between the bubble class  $v-v'$  and size  $v'$ ;  $b(v')$  is the breakup rate of the bubble class of size  $v'$ ;  $m(v')$  is the number of daughter bubble produced by the breakup of a bubble of size  $v'$ , and  $p(v, v')$  is the probability density function for the generation of bubble of size  $v$  out of the breakup of bubble of size  $v'$ . The transport equations solved for each of the bubble classes are expressed in terms of normalized bubble class volume fraction,  $f_i$ , which is defined as:

$$f_i = \frac{\alpha_i}{\alpha_g} \quad (2.23)$$

Thus,

$$\sum f_i = 1 \quad (2.24)$$

The bubble class volume fraction can be computed as:

$$n_i v_i = \alpha_i \quad (2.25)$$

So,

$$\sum \alpha_i = \alpha_g \quad (2.26)$$

That brings Equation (2.18) to the final form for the incompressible gas phase:

$$\frac{\partial}{\partial t}(\alpha_g f_i) + \nabla \cdot (\alpha_g \bar{U}_g f_i) = v_i (B_{f_i,C} - D_{f_i,C} + B_{f_i,B} - D_{f_i,B}) \quad (2.27)$$

In order to solve the integro-differential final form of the bubble class conservation equations, discretization in the bubble size, spatial, and temporal coordinates is performed. For interested readers, more details are presented in the work of Bannari et al. (2008).

To solve the PBE, closure models for the coalescence and breakup rates are required. There are various models in the literature that use probability theory, mechanistic models, and experimental observation (Lehr et al., 2002a; Luo and Svendsen, 1996a; Prince and Blanch, 1990). Wang et al. (2005b) reviewed these models and proposed a comprehensive model that includes most of the sources of the bubble breakup and coalescence.

### 2.3.4 Coalescence Model

In the current study, the coalescence model suggested by Prince and Blanch (1990) is adopted. In this model, the bubble coalescence process is suggested to occur in three steps starting with the collision between two bubbles, trapping a small amount of liquid phase in form of thin film, then the thinning of this film takes place as the liquid drains. Finally, rupture of the film occurs, and the coalescence is complete. The influence of organic molecules on the probability of the film breakage, which is relevant for wastewater aeration applications, is not included in the coalescence model. The coalescence rate is formulated as a product of the collision rate between the bubbles and coalescence efficiency (probability) that represents the ratio of the period of time that the bubbles remain in contact to the time required for the film thinning and coalescence. Three causes for collision are considered in this model: collision due to buoyancy, laminar shear, and turbulence. The overall bubble coalescence rate is assumed to be the cumulative rate of the coalescence rates due to the relative rising velocity of bubbles with different sizes due to buoyancy, the collision of bubbles as a result of the random movement driven by turbulence, and relative motion of bubbles because of laminar shear.

The implementation of this model in OpenFOAM enables the selection of the sources of the collisions to be considered. Later, a comparison will be presented to assess the differences between including the coalescence due to rising velocity alone and with the coalescence rate due to turbulence.

### 2.3.5 Breakup Models

Although breakup rate of small bubbles in the range of the bubbly flow regime may not be significant, it plays critical role in determining the correct BSD as reported in Liao et al. (2015). Herein, the breakup reduces the fraction of larger bubbles produced by coalescence. Two different breakup models are used in the current study for comparison: the model proposed by Luo and Svendsen (1996a) and the one proposed by Lehr et al. (2002a). Both models are widely used in the literature and derive the breakup rate as the product of the frequency of the collision of turbulent eddies, which is the frequency of arriving eddies to a bubble, and the probability of breakage to occur due to this collision. The collision frequency is derived by analogy to the kinetic gas theory, assuming isotropic turbulence. Again, it is noted that the influence of various contaminants that will be present in wastewater are not included in the breakup model. The probability for breakage to occur is the main difference between the two models. In Luo's model, the breakup probability, or efficiency, of a bubble of size  $\nu$  into smaller daughter bubbles of size  $f_{B\nu}\nu$  is equivalent to the probability for the bombarding eddy of size  $\lambda$  to have a kinetic energy that is greater than or equal to the increase in the surface energy of the resulting daughter bubbles due to the increase of the interfacial surface area. However, the increase in the surface energy is a function of the breakage volume fraction,  $f_{B\nu}$ , which is assumed to be stochastic variable. The breakage volume fraction comes out directly from the solution of the model. On the other hand, for the Lehr's model, the breakage probability is derived from a force balance between the inertial force of the hitting eddy and the interfacial force of the bubble surface assuming the bubble nearly takes cylindrical form immediately before the breakage.

### 2.3.6 Boundary and Initial Conditions

The bubble size distribution at the diffuser (the inlet to the domain) is critical for the accuracy of the simulation. Therefore, the experimental measurements taken at 5 cm above the air diffuser, as reported by Amaral et al. (2018), are used as the initial and inlet boundary conditions under the implicit assumption that no change occurs to the bubble size distribution in the 5 cm above the air diffuser. The implementation and calculation of the volume fraction of each of the bubble classes is verified against the experimental data before starting each simulation. A sensitivity study for the prescribed air phase velocity and volume fraction at the inlet is undertaken herein to remove the error that might come up from defining approximated values. Three different air volume fractions are assumed with the corresponding air velocity to guarantee the same flow rate is obtained. The boundary conditions imposed on the lateral walls are no-slip conditions for the velocity profiles. At the top of the bubble column, the pressure is specified to atmospheric pressure. The air diffuser is described as an inlet boundary condition with no flow for the liquid phase, while the velocity and volume fraction of the gas phase are varied to study their effect, as presented herein.

## 2.4 Results and Discussion

### 2.4.1 Grid Independence Test

In order to minimize the influence of the spatial discretization error on the numerical simulation results, a grid independence study is conducted to ensure that the results are not significantly dependent on the mesh refinement level. A simulation case has been setup to first check using three different grids with three different resolutions. The ratio between the grid sizes is based on the outline recommended in Celik et al. (2008) with size reduction ratio of 1.3 between any two consecutive grids. The number of computational cells in the coarse, medium, and fine grids is 23520, 52920, and 85575, respectively. The time-averaged water velocity profiles at 1.2 m above the air diffuser are compared for the three cases to judge the influence of the grid refinement. The grid with medium resolution is used in the current study since further refinement showed no improvement of the simulation results. Figure 2-3 shows a comparison between the time-

averaged velocity profile of the water phase at 1.2 m above the air diffuser using the three different grids. The comparison in Fig. 2-3 shows that, for the medium and fine grids, two peaks in the velocity of the water phase near the walls are captured, while the coarse grid shows a flat profile. To study this effect, the water phase velocity vectors are plotted on the domain in Fig. 2-4. The figure depicts the impact of air pushing the water which results in a number of circulation areas near the walls. Moreover, the waving of the free surface due to the drag between the two phases is clear on the fine grid vector field while it is lost when using the coarse mesh with underestimated vortices near the free surface. Thus, the downward flow stream of the water phase at the column centre, which results from the strong circulation, could not be captured by the coarse mesh, resulting in the flat profile that is obtained. The effect of the coarse grid on the simulation results can be explained as the drag force computed using the coarse grid being less than that obtained by the fine mesh. This conclusion is drawn from the similarity between the solution obtained by the coarse mesh and that obtained by using Ishii and Zuber's drag model presented in the following sections. Therefore, the grid resolution is crucial for the simulation of the two-phase in bubble columns and should be carefully examined prior to conducting simulations.

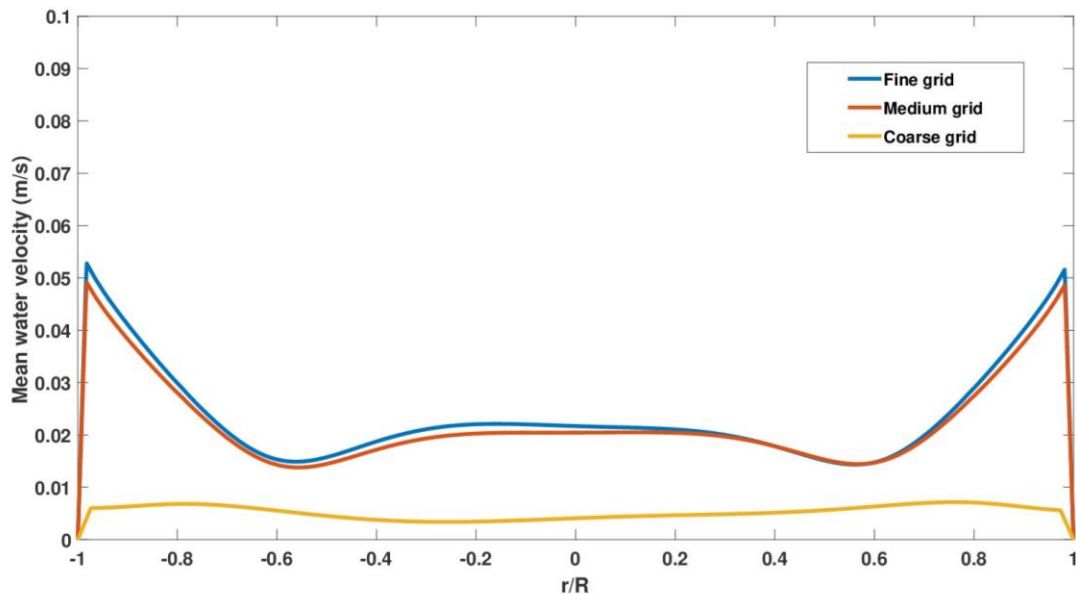


**Figure 2-3: Time-averaged velocity profiles for the water phase on the coarse, medium, and fine meshes at 1.2 m above the air diffuser**

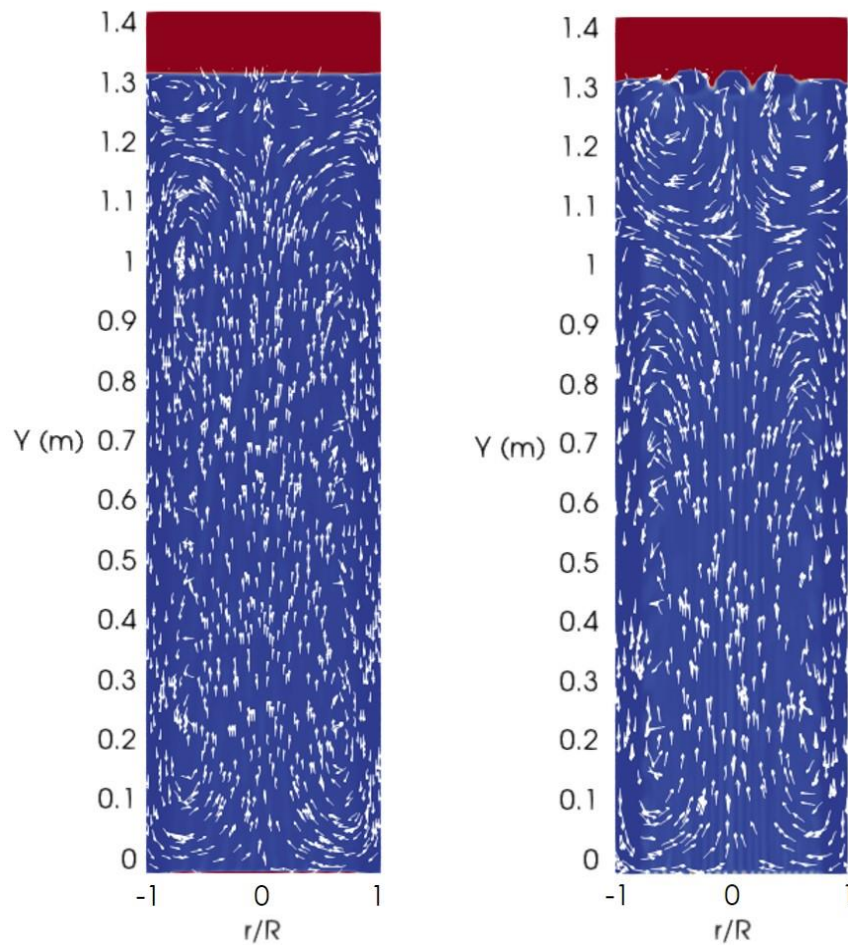


**Figure 2-4: Instantaneous velocity vector field for the water phase on the coarse grid (left) and fine grid (right)**

## 2.4.2 8 L·min<sup>-1</sup> Flow Rate

The study of the model parameters is conducted using the air flow rate of 8 L·min<sup>-1</sup> in comparison to the experimental results in the literature. This is because this flow rate is closer to the flow rates that would be expected in full-scale aeration tanks and the evolution of the BSD is more pronounced.

### 2.4.2.1 Validation Case

A base simulation is set up for validation and studying the effects of the simulation parameters on the results. In the base setup, the interfacial forces considered are:

- Drag force using the Schiller-Naumann model;



- Lift force using the Tomiyama model;
- Virtual mass force with coefficient set to 0.5.

The BSD is discretized into 32 classes for the class method of solving the PBE. The PBM coalescence model of Prince and Blanch is adopted while using Lehr's model for breakup rate. An air phase volume fraction of 0.9 is specified at the inlet, defined as the surface of the diffuser with the corresponding velocity to achieve a flow rate of  $8 \text{ L} \cdot \text{min}^{-1}$ . Several preliminary trial simulations were conducted to determine this setup for the simulation such that it matched well with the experimental data; sensitivity to different models and parameters is assessed below.

Figure 2-5 shows the contours of volume fraction for the air phase in the computational domain. Since the air diffuser diameter is almost the same as the bubble column, the bubble plume occupies most of the cross-sectional area of the column. Moreover, it is observed for the low gas flow rate (homogeneous regime) that the volume fraction profile is flat and almost uniform (Gemello et al., 2018). This is explained as the average bubble diameters in the homogeneous regime is relatively small, hence the magnitude of the lift force is low and pushes the bubbles toward the walls. This is also implemented in the lift force model where the lift force sign is determined by the bubble size (Tomiyama, 1998).

The validation of the CFD-PBM model is based on the cumulative BSD from the experimental data of Amaral et al. (2018). The BSD is extracted from the cumulative BSD for further clarification of the behaviour of the breakup and coalescence models. Figure 2-6 compares the cumulative BSD and BSD results from the simulation and the experimental data. The BSD of the simulation at time zero is also plotted against the measured BSD at 5 cm above the air diffuser. These are used to verify the assigned volume fractions of the BSD classes and for validation of the assumption that the BSD does not change from the inlet to the 5 cm plane. From the figure, excellent agreement with the measured data is obtained. The BSD shows the bubble evolution from the level of 5 cm to 120 cm above the air diffuser. It is clear that the average bubble size is moved from 0.75 mm to 1.75 mm and the profile is distributed over the bubble size range 0-4 mm. The numerical model fully captures the bubble size evolution along the column

height. However, various model parameters should be studied to understand their influence on the overall performance of the model.

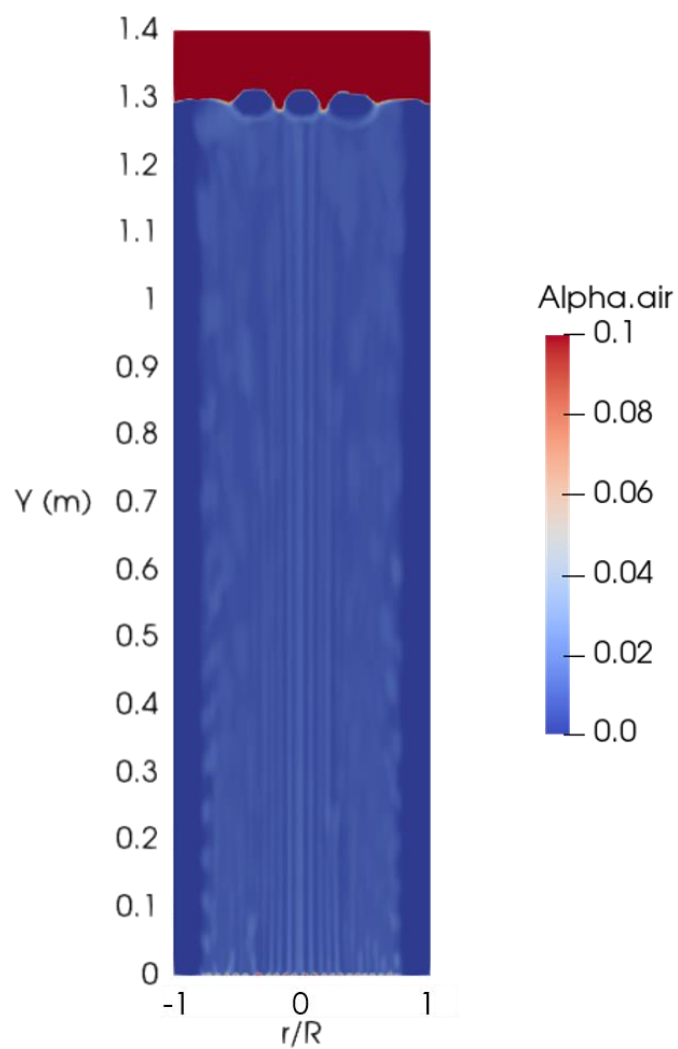


**Figure 2-5: Instantaneous contour plot of the air volume fraction for the gas flow rate of  $8 \text{ L} \cdot \text{min}^{-1}$**

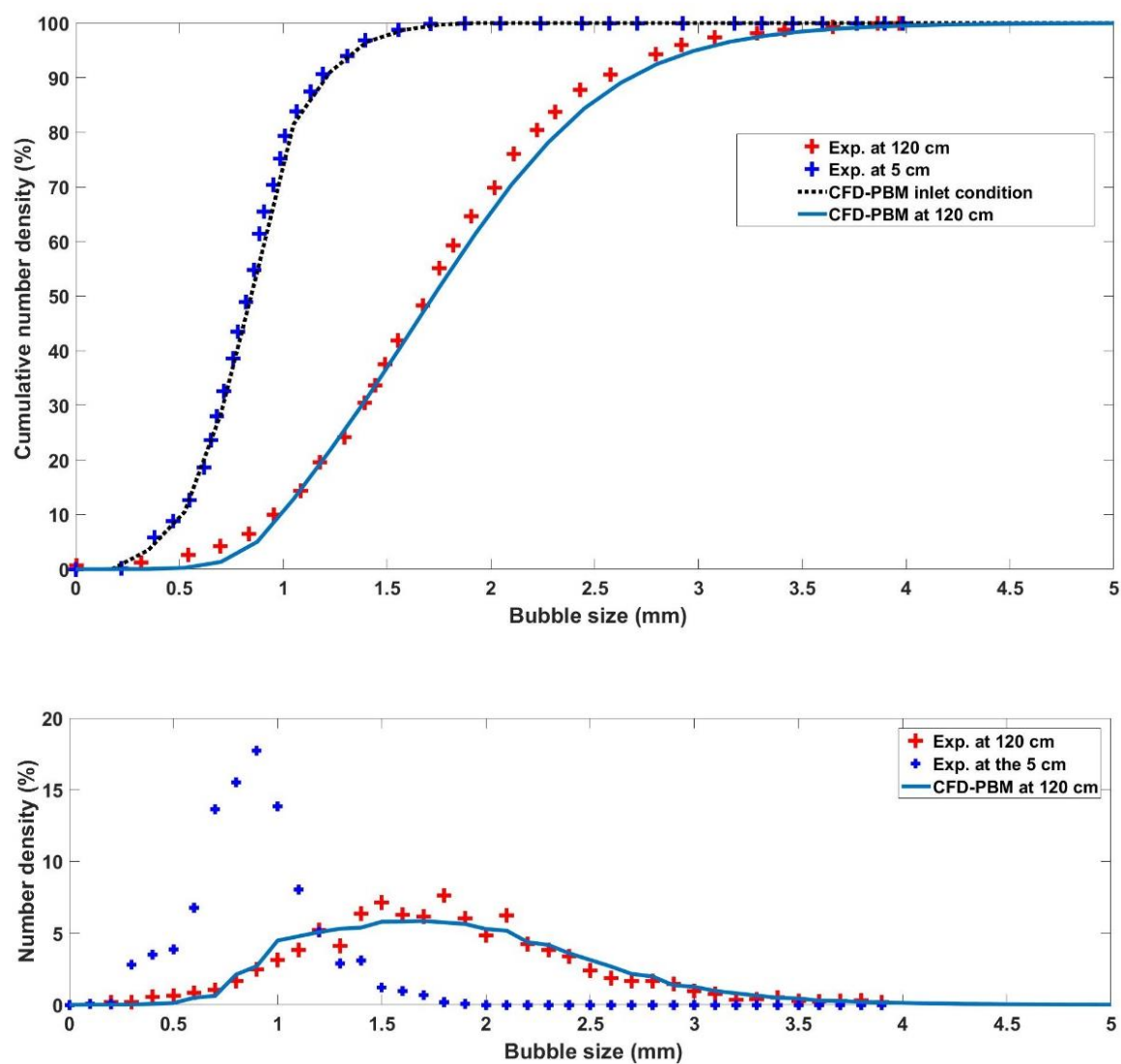


**Figure 2-6: Cumulative BSD (top) and BSD (bottom) for the validation of  $8 \text{ L} \cdot \text{min}^{-1}$  simulation**

### 2.4.2.2 Effect of Diffuser Boundary Conditions

The inlet boundary conditions corresponding to the air diffuser may produce an error if not treated carefully. To the best of our knowledge, no clear guideline is presented in the literature to define the inlet conditions. Mudde and Simonin (1999) developed a 2D model for the simulation of a bubble column where the air velocity at the sparger is presumed and the gas fractions are computed using the measured air flow rate. However, the uncertainty due to the assumption of the gas velocity at the inlet was not studied. Another approach adopted by Liang et al. (2016) is that inlet openings of the gas phase in the diffuser are constructed in the discretized computational domain such that only gas phase flows through the openings (gas fraction is unity). However, this method is not applicable for all cases since it requires a specific mesh refinement at the inlet to the column, which may increase the computational requirements dramatically. Moreover, this method can only be applied for the discrete openings of the gas phase (Deen et al., 2001 and Rzehak et al., 2017). For the case of flexible membrane, porous, and heavily ruptured diffusers, this method is not applicable.

The flow rate reported in Amaral et al. (2018) must be translated in terms of the boundary conditions that can be specified in the numerical simulation. For two-phase flow, the air flow rate at the inlet boundary is the product of the inlet area (the diffuser inner diameter),  $A_d$ , air velocity in the vertical direction,  $U_{g,y}$ , and volume fraction of air at the inlet boundary,  $Q = U_{g,y} A_d \alpha_g$ . The volume fraction of the air phase at the boundary is not usually defined due to the change in the free membrane when applying the pressurized air from the blower. Therefore, in this study the effect of different assumptions for the volume fractions and the corresponding air phase velocity are studied and compared to exclude the uncertainty that accompanies the unknown active surface area of the diffuser. The  $8 \text{ L} \cdot \text{min}^{-1}$  simulation is performed using three air phase volume fractions at the inlet; 0.5, 0.8, and 0.9. The time-averaged water phase velocity at 1.2 m above the air diffuser is compared in Fig. 2-7. In addition, the computed cumulative BSD and BSD profiles, respectively, are presented in Fig. 2-8 to show the influence of the presumed air volume fraction at the inlet on the performance of the PBM. The figures show that all of the profiles for the three different presumed air phase volume fractions are collapsing upon

each other. Therefore, the simulation results are not observed to be particularly sensitive to the air volume fraction at the inlet. Because the pores on the free surface membrane are dense, the volume fractions of 0.8 and 0.9 result in closer matching to the experimental BSD. Therefore, for the rest of the simulations herein, the volume fraction of 0.9 is used.

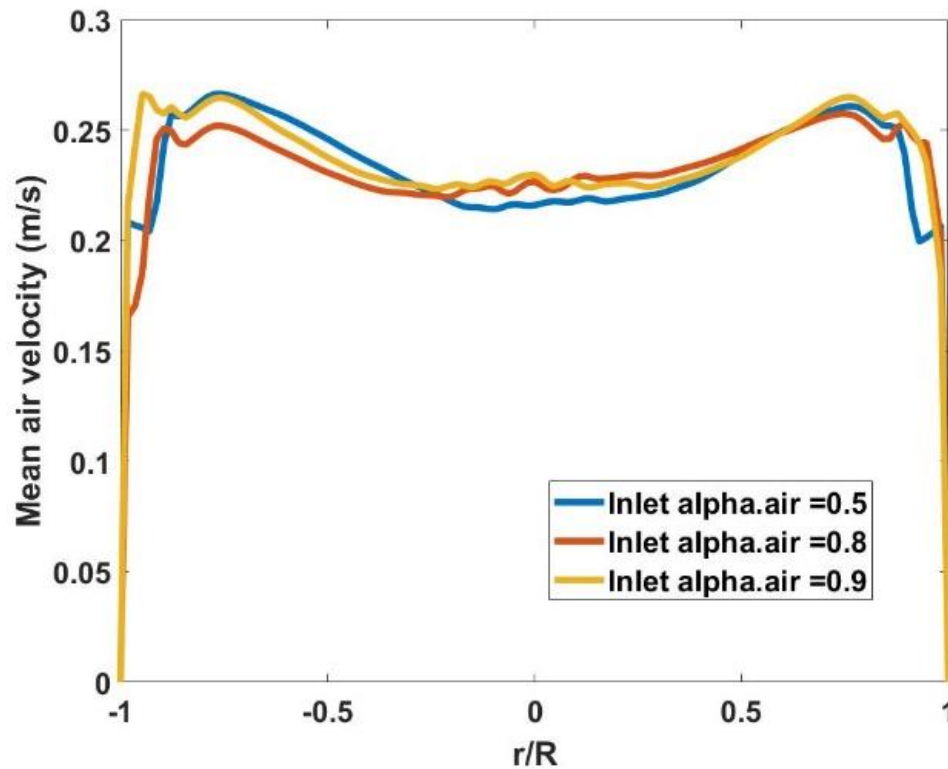


**Figure 2-7: Time-averaged air velocity at 1.2 m above the air diffuser using three different volume fractions at the inlet; 0.5, 0.8, and 0.9**

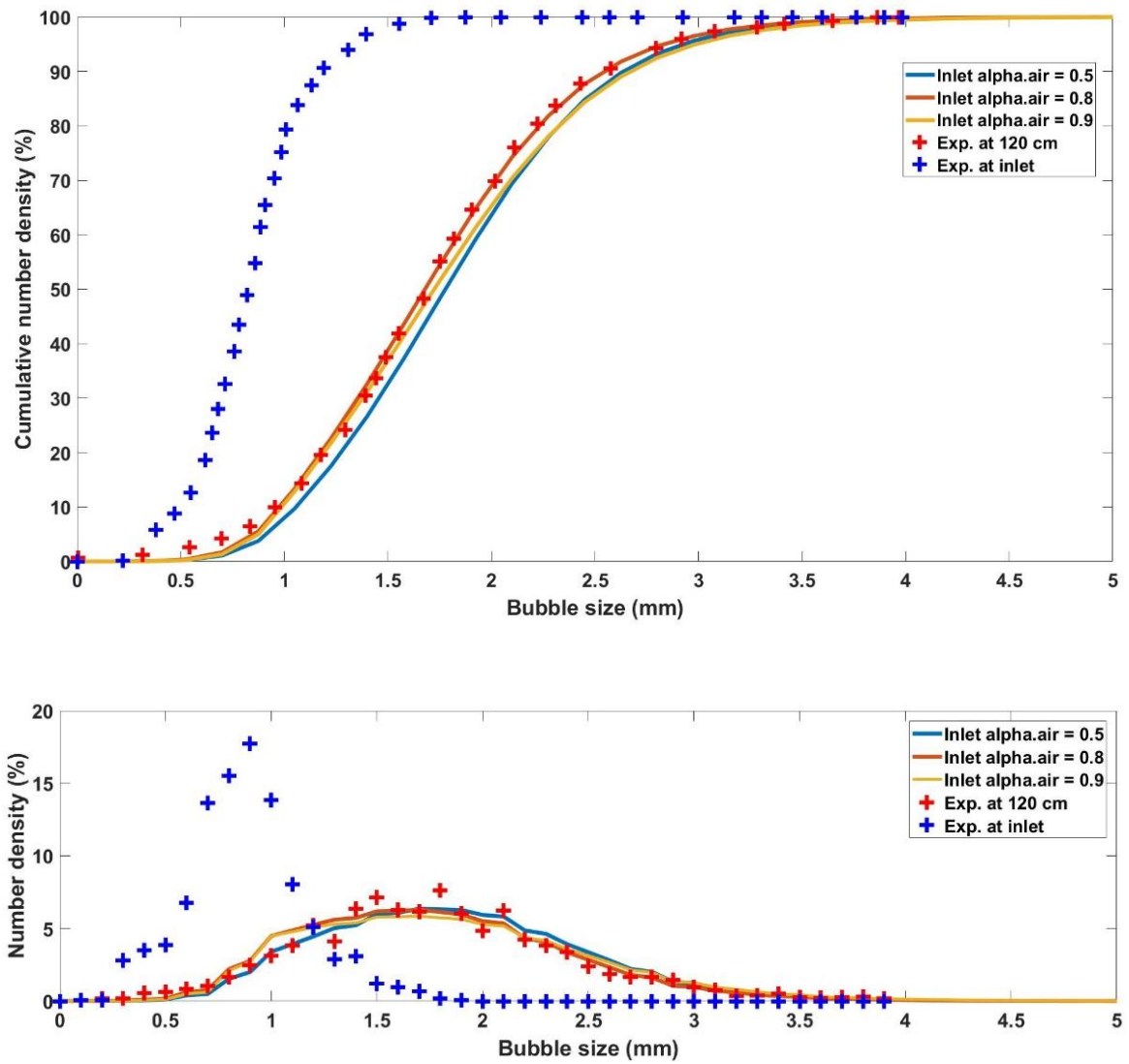


**Figure 2-8: Cumulative BSD (top) and BSD (bottom) for the boundary conditions tested with different values of air volume fraction at the diffuser**

### 2.4.2.3 Effect of Number of Bubble Size Bins

Since the bubble size is discretized into a number of discrete classes to be incorporated in the CFD framework, the uncertainty of the numerical solution regarding the resolution of the bubble size distribution discretization should be studied. Wang et al. (2006) studied the effect of the refinement of the bubble size coordinate with a maximum size of 80 mm. The results showed that the number classes greater than 30 had no pronounced influence on the simulation results. Herein, the BSD is discretized into 12, 22, and 32 classes to determine at what level the increase of the number of bubble class would only increase the computational cost without any further improvement in the results. Figure 2-9 shows the cumulative BSD and BSD, respectively, obtained by employing the three numbers of bubble classes. It is clear that increasing the number of bubble classes from 12 to 22 classes improves the matching with the experimental data, however, no further improvement is observed when 32 classes are implemented. Therefore, 22 bubble classes are used for the rest of the presented simulations.

### 2.4.2.4 Effect of Breakup Models

The breakup of rising bubbles reverses the effect of bubble coalescence on the average bubble size along the column. It is important to study the influence of the breakup model as it relates to the balance of the coalescence rate and the equilibrium BSD. For the previous sections, Lehr's bubble breakup model is used to compute the bubble breakup rate. In this section, Lehr's model is compared with Luo's model on the BSD and cumulative BSD. In addition, the breakup model is disabled to illustrate the balancing impact of the breakup model on the BSD.

As shown in Fig. 2-10, the BSD obtained by the different breakup models and without including the breakup effect is depicted. The figure shows the influence of the bubble breakup on the shape of the BSD. It is clear from the BSD that the breakup limits the production of the bubbles larger than 3.5 mm hence squeezes the BSD around the mean bubble size observed in the experimental data. Luo's and Lehr's models predict a very similar profiles for the BSD. A possible explanation is that both of the models are dependent on the turbulence level of the water phase which is low in the case of bubbly

(homogeneous) flow. A possible further study might be required to study the effect of the turbulence source terms in bubbly flow on the breakup models.

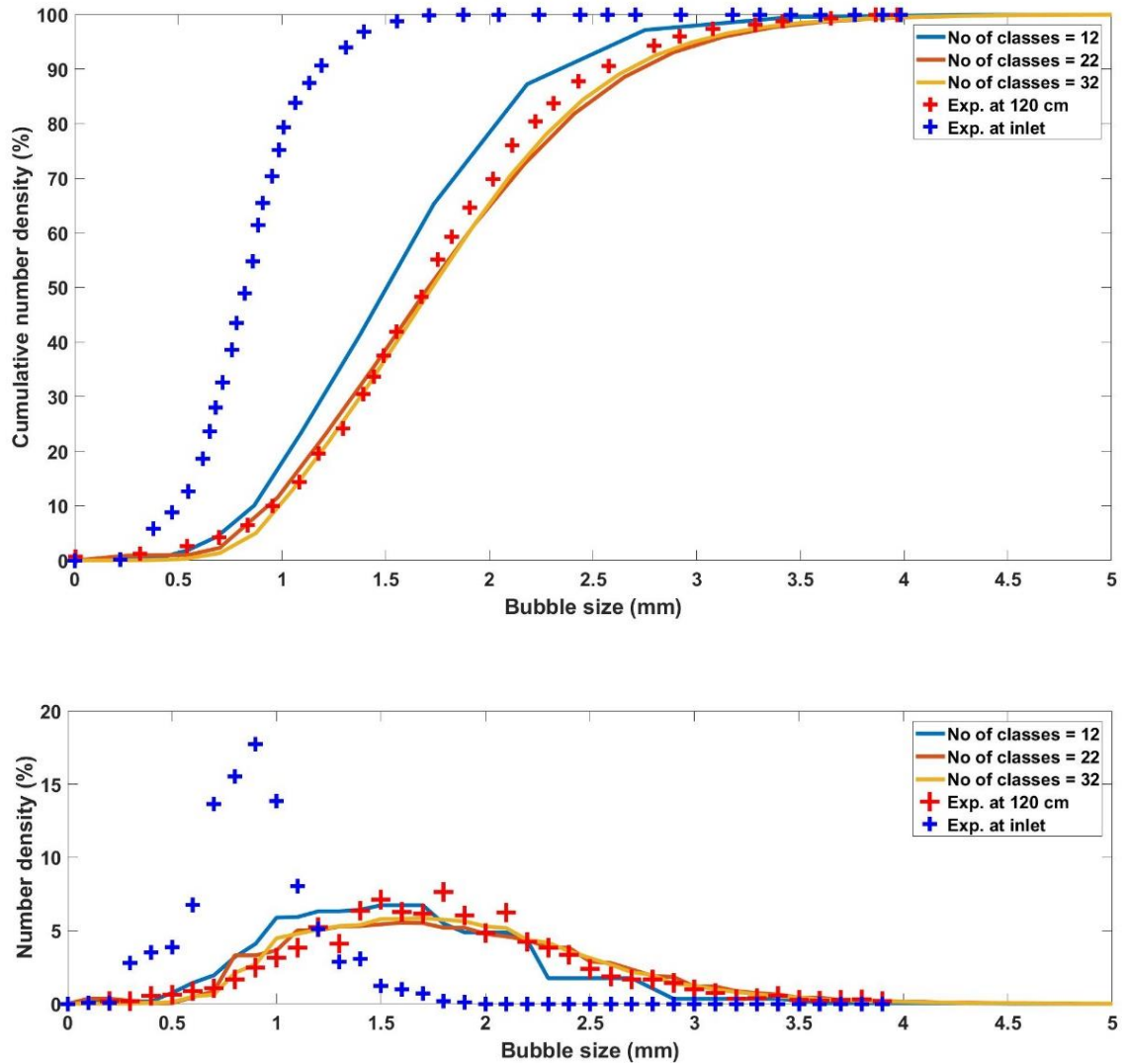


**Figure 2-9: Cumulative BSD (top) and BSD (bottom) for different numbers of bubble size classes**



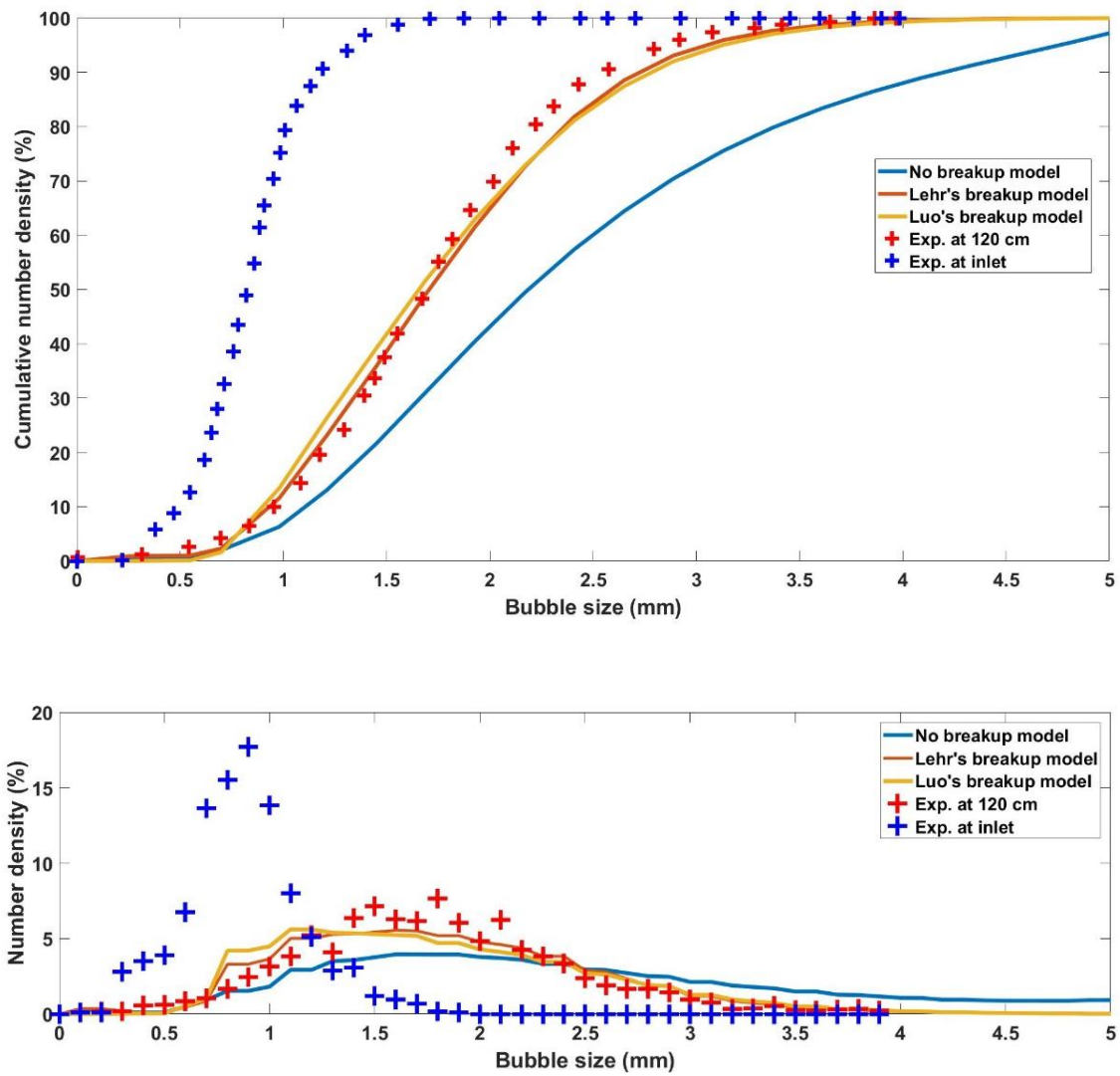


**Figure 2-10: Cumulative BSD (top) and BSD (bottom) using different bubble breakup model**

#### 2.4.2.5 Effect of Prince and Blanch Model Coalescence Terms

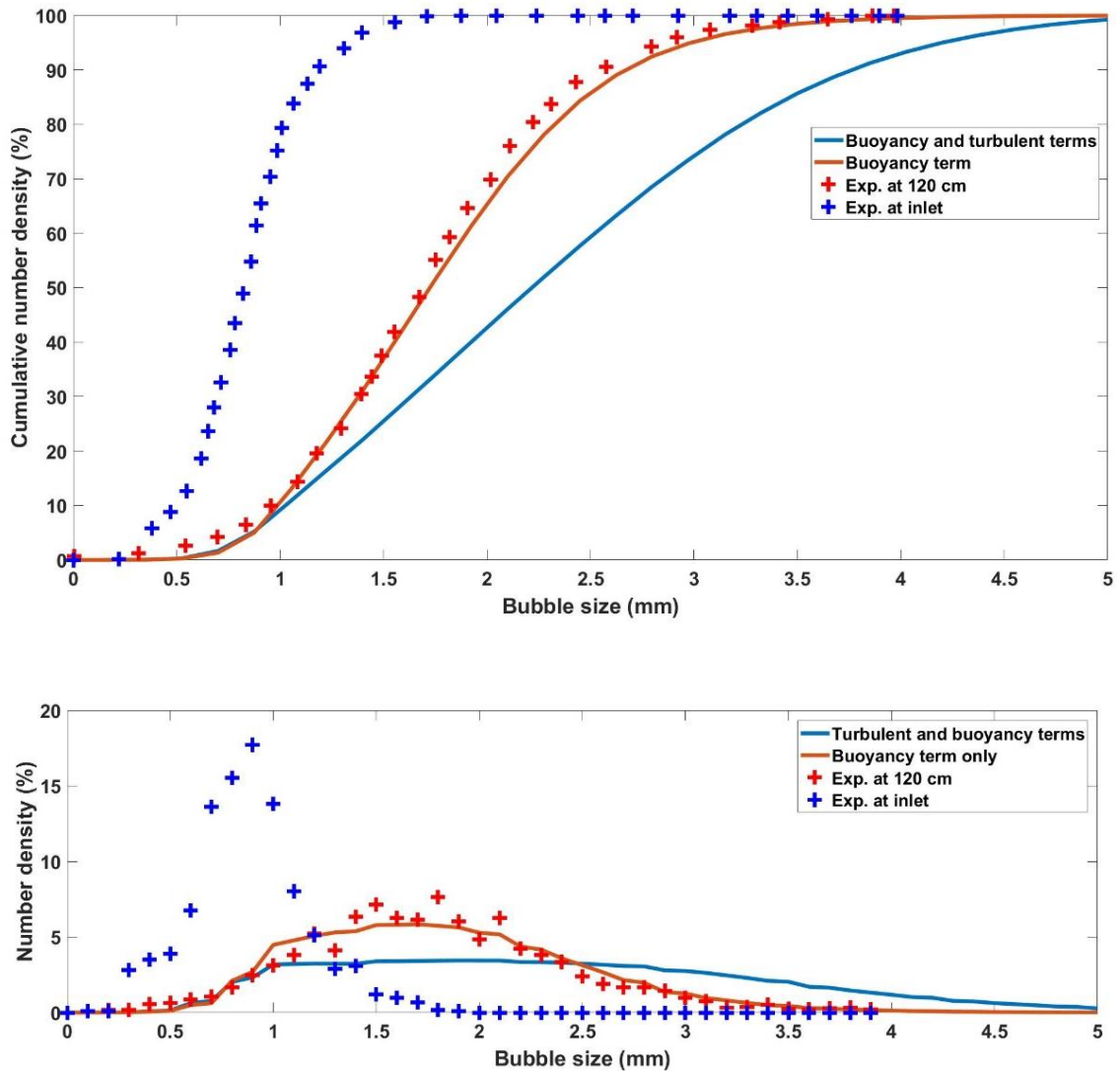
Prince and Blanch's bubble coalescence model includes two terms that can be enabled in the OpenFOAM implementation of the PBM. These terms are the coalescence due to the difference of bubbles' rising velocities (buoyancy) and due to the turbulent collisions. A comparison is made between two cases: first when both terms are enabled, and second when only the coalescence is due to different rising velocities.

Figure 2-11 shows the influence of including the coalescence due to turbulent collision on the BSD. This term leads to an overestimation of bubble coalescence, resulting in poor matching with the experimental data. In contrary to the breakup models, Prince and Blanch's coalescence model is sensitive to the turbulence. However, this conclusion needs further study to understand the interaction between turbulence and the breakup and coalescence rate in the PBM. Based on the current result, it appears that coalescence due to buoyancy is clearly dominant and that the coalescence due to turbulence is not well-described by the Prince and Blanch model for this flow condition.

#### 2.4.2.6 Effect of Drag Model

As illustrated in the following section, the drag model of Schiller and Naumann overpredicts the global gas holdup. Therefore, another widely used drag force model, Ishii and Zuber's model, is used to explore the effect of the drag model on the flow field, gas holdup, and BSD evolution. The first observation that can be made about the simulation result is the lack of the free surface "waving" as illustrated in Fig. 2-12. Referring to the grid independence test presented earlier, it is noted that the same behaviour is noticed when using the coarse grid. Furthermore, as will be shown in the gas holdup results, the drag model proposed by Ishii and Zuber predicts lower drag, and consequently, lower gas holdup is obtained. When the bubbles are subjected to lower drag force, higher rising velocity is expected. This could be the reason for the overestimation of the coalescence model as depicted in Fig. 2-13 where adopting Ishii and Zuber's model produces poor agreement in the BSD when compared with the experimental data. These results reveal the complexity of the multiphase modelling

integrated with BSD models. Selecting the drag model is critical to correctly predict the flow fields and the BSD.



**Figure 2-11: Cumulative BSD (top) and BSD (bottom) for simulation employing the bubble coalescence due to turbulence and different rising velocity**

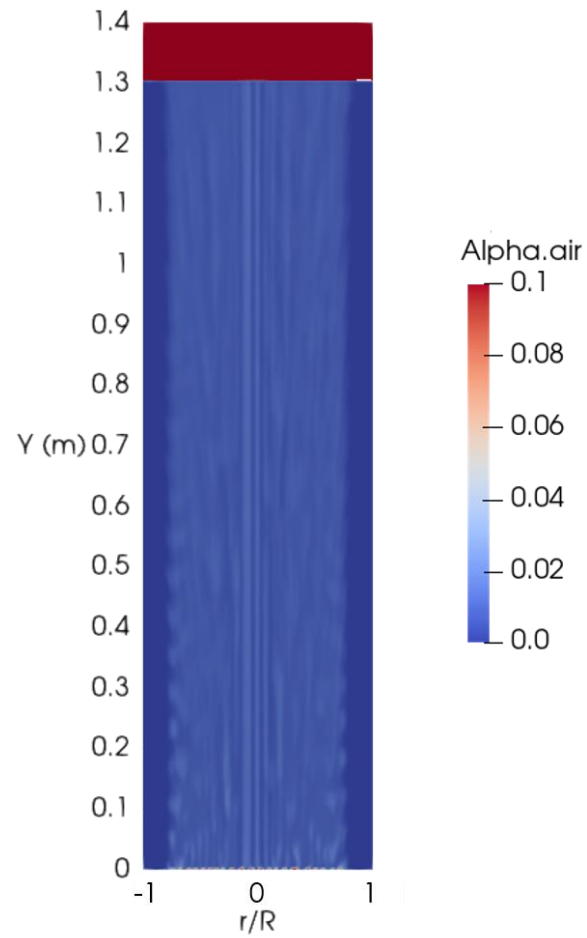


**Figure 2-12: Air volume fraction contours from the simulation adopting Ishii and Zuber's drag model**

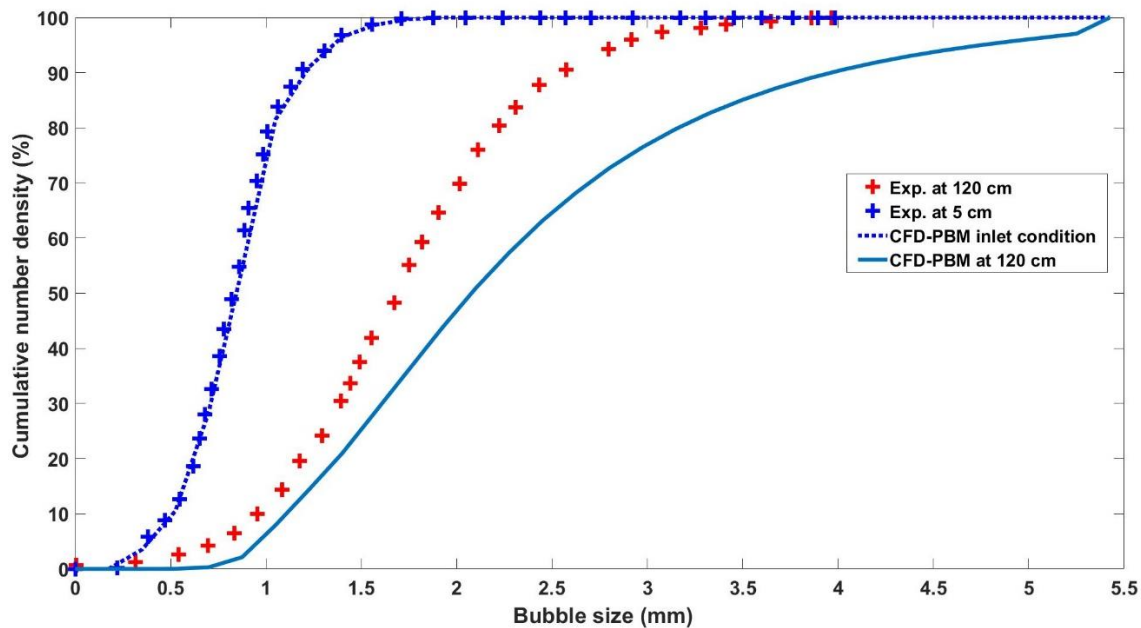


**Figure 2-13: Cumulative BSD for the simulation using Ishii's and Zuber's drag model**

#### 2.4.3 2 L·min<sup>-1</sup> Flow Rate

To examine the applicability of the current model over different gas flow rates, the experimental measurement in Amaral et al. (2018) for the gas flow rate of 2 L·min<sup>-1</sup> is simulated as well. The model shows a good performance to simulate the low flow rates. As depicted in Fig. 2-14, a reasonable matching is obtained when using the model with 2 L·min<sup>-1</sup> gas flow rate. The model captures the cumulative BSD and BSD at 120 cm above the air diffuser fairly well with average bubble size around 1.25 mm. Moreover, the contours of the gas phase volume fraction (Fig. 2-15) show that, for such low flow rate, the free surface does not experience strong waving. This indicates that the water phase circulation is weak hence the mass transfer and the breakup of the near the free surface are low as will be discussed while presenting the predicted mass transfer coefficient herein.

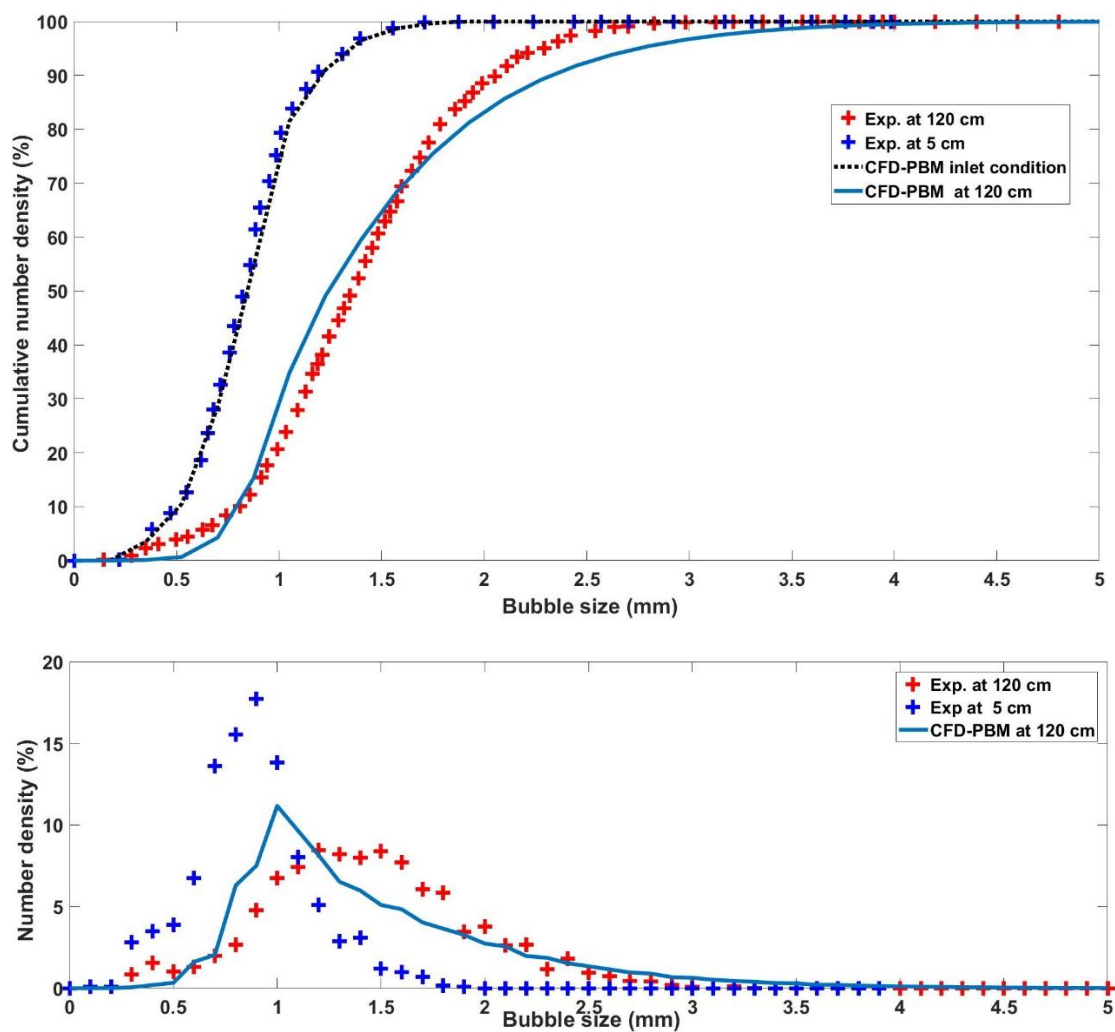
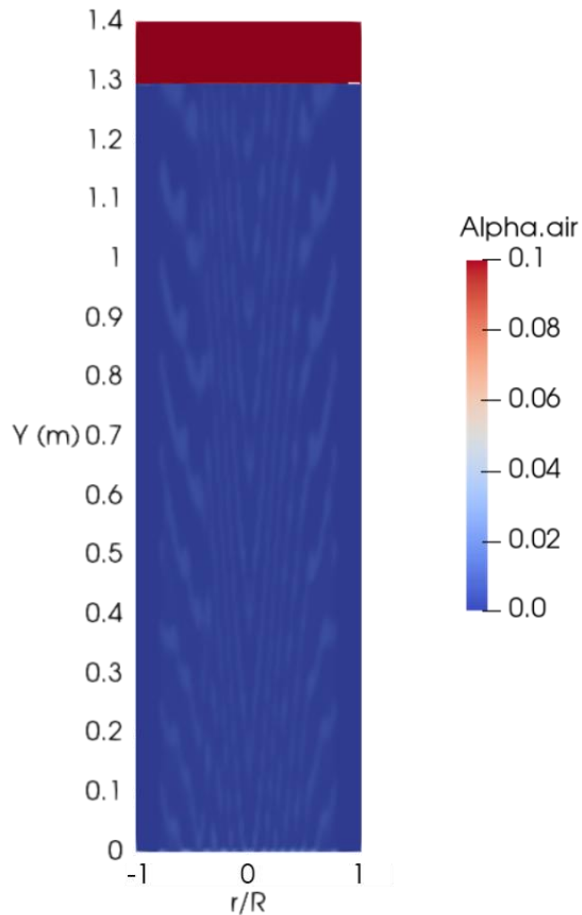


Figure 2-14: Cumulative BSD (top) and BSD (bottom) for gas flow rate of  $2 \text{ L} \cdot \text{min}^{-1}$



**Figure 2-15: Instantaneous contours of air volume fraction for the gas flow rate of 2  $\text{L}\cdot\text{min}^{-1}$**

#### 2.4.4 Gas Holdup

The gas holdup predicted by the numerical model is compared to the experimentally measured values. The measurement of the gas holdup in the experimental study was conducted by measuring the rise in the free surface of water in the bubble column using a graded ruler (Amaral et al., 2018). Therefore, high uncertainty was observed by the authors which was up to 20% for the highest air flow rate. This is due to the formation of the froth on the free surface of water in the bubble column. Simulations of the four air flow rates considered by Amaral et al. (2018) were conducted and the global gas holdup was calculated. Figure 2-16 depicts a comparison between the numerical model results using two different drag models and the measurement data. Additional simulations using

the constant bubble size (CBS) assumption were also performed to assess the importance of using PBM. These results are also included in Fig. 2-16. The comparison shows that both drag models used in the numerical model overestimate the gas holdup. However, it is noticed that the drag force computed by Ishii-Zuber's model is lower than that computed by Schiller-Naumann's model. This is reflected in the global gas holdup since the drag force controls the rising velocity of the bubbles in the bubble column hence the global gas holdup. Ishii-Zuber's model predicts closer gas holdup values to the experimental data. It is noted, however, that the CFD model predicts the correct trend with similar slope to the experimental results. Given the small gas holdup values (i.e. less than 1%), the uncertainty is expected to be so high that quantitative comparisons are quite difficult. It is also noted that the CBS assumption gives similar results to PBM and may be considered as a suitable model for the prediction of global gas holdup.

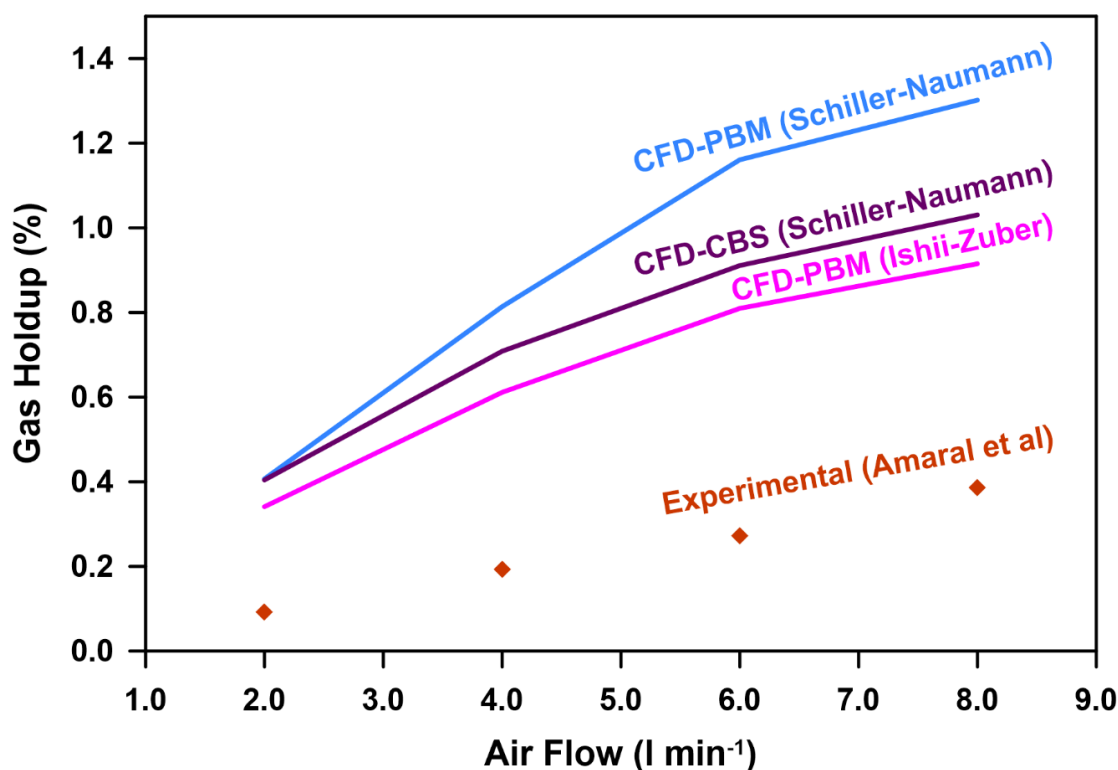


**Figure 2-16: Gas holdup vs gas flow rate for the simulation adopting Schiller-Naumann's and Ishii-Zuber's drag models in comparison to experimental data**



### 2.4.5 Oxygen Mass Transfer Rate

As the final objective of the current study is to investigate the effect of the evolution of the BSD and the flow field on the oxygen mass transfer from the gas phase (air bubbles) to the liquid phase (water), the mass transfer coefficient is computed based on the simulation result of the air flow rate of 8 and 2 L·min<sup>-1</sup>. The computed coefficient is compared to the results of the model developed in Amaral et al. (2018) and their assumptions are examined against the CFD-PBM simulation results. In addition, the mass transfer rate is computed from the result of the simulation of CBS and compared with the experimental data as well to evaluate the inaccuracy that accompanies this assumption.

The local oxygen transfer coefficient,  $K_L$ , is calculated using Higbie's model:

$$K_L = \sqrt{\frac{D_L U_{r,air}}{\pi d_g}} \quad (2.28)$$

where  $D_L$  is oxygen diffusion coefficient in water and assumed to be  $2.01 \times 10^{-9}$  m<sup>2</sup>/s, and  $d_g$  is the local Sauter diameter for the gas phase based on the computed BSD (in case of PBM used) or the defined diameter for the gas phase (in case of CBS assumption). The interfacial area density is given by:

$$a = \frac{6\alpha_a}{d_g} \quad (2.29)$$

The oxygen mass transfer characteristics are computed using the mean values of the flow field over the measurement windows illustrated in Fig. 2-1. In an attempt to understand the mutual influence between the flow field and BSD evolution and their effect on the oxygen mass transfer rate, the variables used in the calculation of  $K_L a$  are plotted along the vertical distance above the air diffuser in Fig. 2-17.

A comparison between the current work and the modelling results from Amaral et al., 2018 is illustrated in Fig.2-17a. The comparison shows that the  $K_L a$  coefficient estimated by the current model is lower for most of the distance above the air diffuser

except near the free surface. Furthermore, the  $K_L a$  estimated by Amaral et al. (2018) is more uniform along the bubble column. This can be explained as it was assumed that the global gas holdup is uniformly distributed over the column height in addition to the water phase which was assumed to be quiescent, and terminal bubble velocity was used as the relative velocity between the two phases.

An interesting observation is noticed in the CFD-PBM model result; a jump in the  $K_L a$  is observed near the free surface. This is can be explained by Fig. 2-17b and 17c , as the  $K_L a$  equals the product of the  $K_L$  and  $a$  . The increase in  $a$  is due to the decrease in the Sauter diameter near the free surface, as seen in Fig. 2-17d. One possible explanation is that the high circulation of the water phase at the free surface of such a small tank results in high turbulence and hence promotes more bubble breakup to occur. This may not happen at a large, full-scale plant where wall effects can be considered negligible, unlike in small research reactors. The higher air volume fractions at the surface are shown in Fig2-17e. Moreover, the increase in the  $K_L$  value is noticed as a result of the decrease in the Sauter diameter and high relative velocity observed in this region, as seen in Fig. 2-17f. This increase in the relative velocity could also be explained by the circulation in the water phase.

Therefore, computing the oxygen mass transfer rate based on the global gas holdup and the expressions of the terminal bubble rising velocity without considering the water phase motion due to the interaction between the phases might lead to higher uncertainty in the model results. The circulation of the water phase shows a strong influence on all the variables in the model, hence the final estimated oxygen mass transfer coefficient.

Similarly, for the flow rate of  $2 \text{ L} \cdot \text{min}^{-1}$ , the characteristics of the oxygen mass transfer are plotted along the bubble column and a comparison of  $K_L a$  is shown in Fig. 2-18. In this case, however, the waving of the free surface does not present itself for such a low flow rate. Therefore, monotonic behaviour of the mass transfer characteristics is observed and there is less departure between the vertical profiles in Fig. 2-18a.

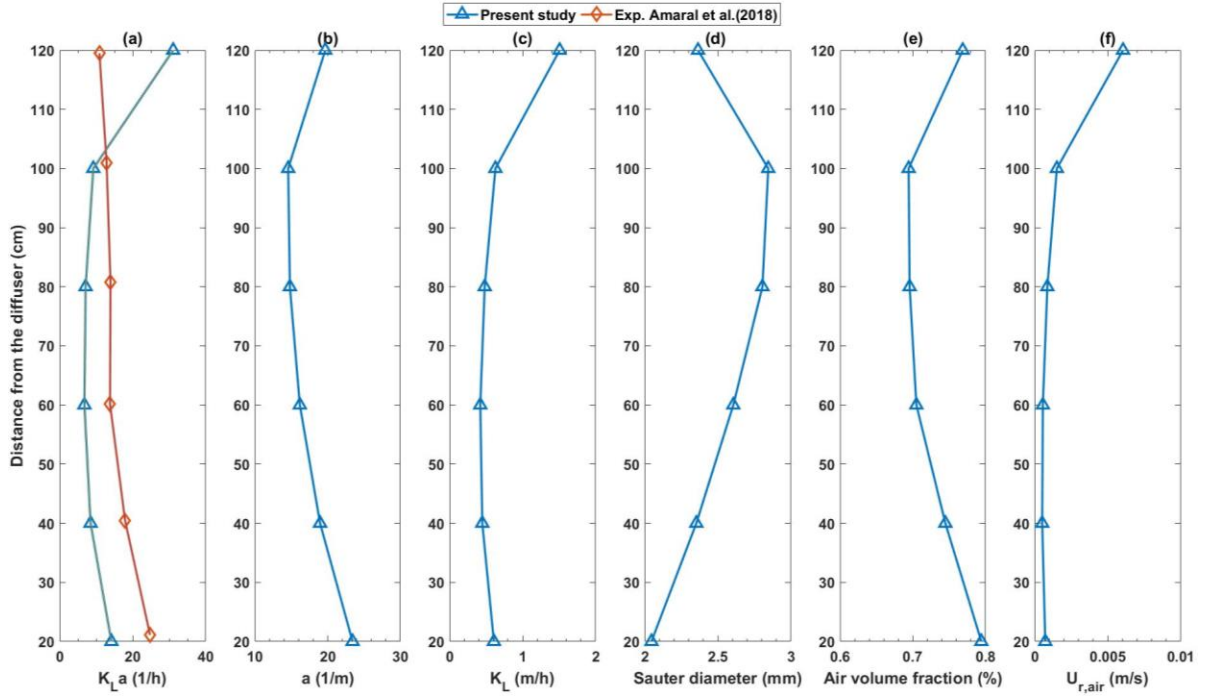


**Figure 2-17: Profiles of averaged (a)  $K_La$ ; (b) interfacial area density,  $a$ ; (c)  $K_L$ ; (d) Sauter diameter; (e) air volume fraction; and (f) air relative velocity along the bubble column height for air flow rate of  $8 \text{ L} \cdot \text{min}^{-1}$**

he overall oxygen mass transfer coefficient,  $K_La$ , is considered to be a comprehensive parameter that comprises the gas and liquid flow fields, BSD, and the mass transfer process. Thus, it is considered as the key point that the comparison between the simulation results and the experimental data should be based on. The predicted global  $K_La$  from the CFD-PBM simulation is computed as the average value over the entire computational domain, which in practical terms corresponds to the cumulative oxygen transfer over the entire column. The predicted global  $K_La$  is compared against the experimental data at different gas flow rates, as seen in Fig 2-19. Good agreement between the measured and predicted is obtained with only a slight overestimation of the experimental results. This overestimation can be largely attributed to the uncertainty in the measurement and the numerical error. However, this matching between the numerical model results and the experimental measurements indicates that the model has excellent accuracy for simulating the different aspects of the bubble column dynamics of the

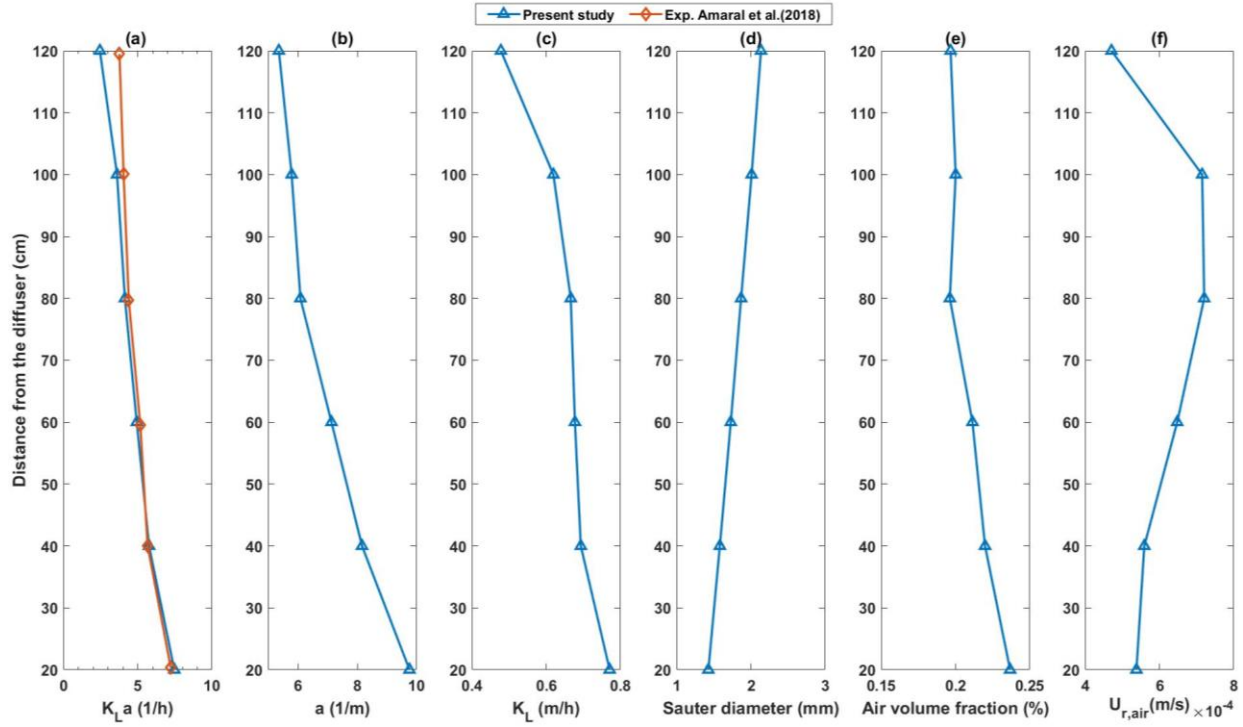


**Figure 2-18: Profiles of averaged (a)  $K_L a$ ; (b) interfacial area density,  $a$ ; (c)  $K_L$ ; (d) Sauter diameter; (e) air volume fraction; and (f) air relative velocity along the bubble column height for air flow rate of 2 L·min<sup>-1</sup>**

bubble column. On the other hand, the CBS assumption results in a significant overestimation of the oxygen mass transfer coefficient despite the good results obtained for the global gas holdup using CBS. This departure is enhanced by increasing gas flow rate and shows an overprediction of nearly 150% at a gas flow rate of 8 L·min<sup>-1</sup>. This indicates that the BSD plays a critical role in modelling mass transfer in multiphase flows and that the CBS assumption is unsuitable for such applications.

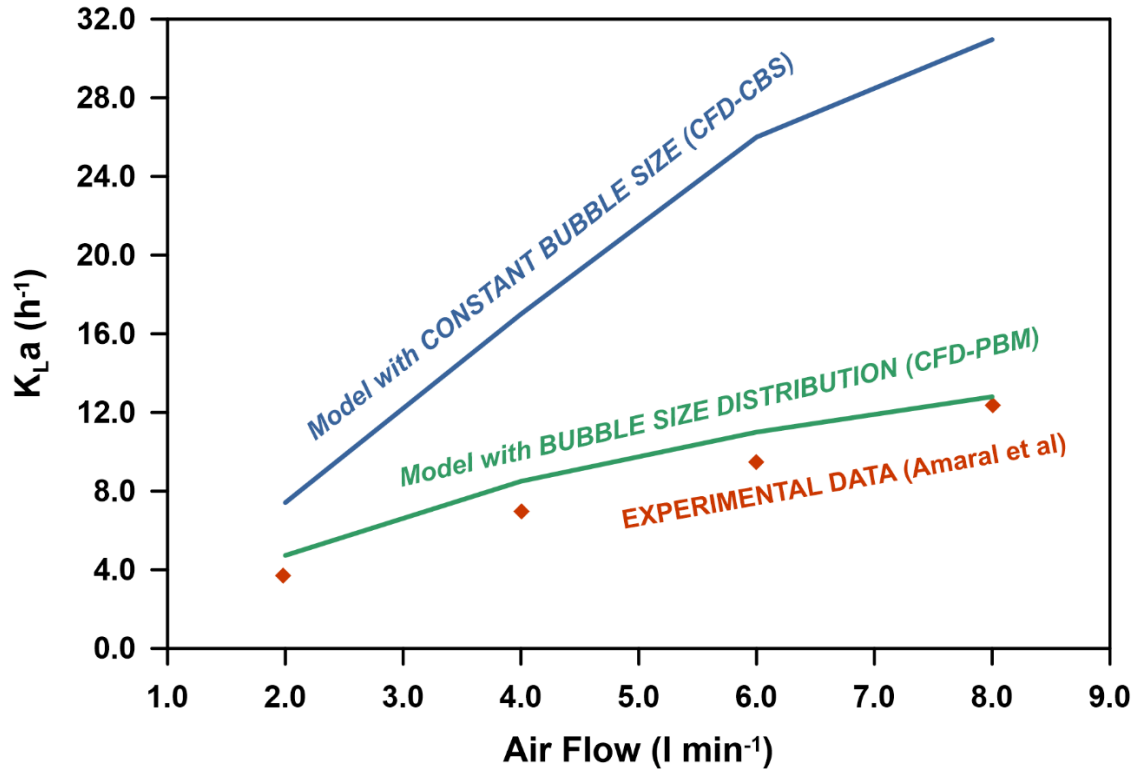


**Figure 2-19: Global oxygen mass transfer measurement against CFD-BPM simulation**

## 2.5 Conclusions

CFD coupled with PBM was used to model the dynamics in bubble columns operating within the bubbly regime. The simulations were performed using two flow rates. The CFD-PBM model was validated against the experimental data that includes bubble size distribution, global gas holdup, and global mass transfer coefficient with excellent agreement. The effect of different model parameters such as spatial grid refinement, specifying the boundary conditions for the gas phase, the number of classes used in the PBM class method, the different terms in Prince and Blanch's bubble coalescence model, breakup models, and drag models were studied and presented.

For the bubble size in range 0-5.5 mm, 22 bubble size classes were sufficient such that no improvement in the results was obtained with further refinement. Moreover, the results did not vary significantly with varying the gas volume fraction at the inlet boundary

conditions. It was shown that the coalescence due to difference in rising velocity of the bubbles that is implemented in Prince and Blanch's coalescence model was able to precisely capture the BSD over the two flow rates examined. The model showed sensitivity to the drag models used because lower estimated drag force and higher bubble rising velocity were obtained along with the overestimation of the bubble coalescence. Interestingly, it was shown how the circulating of the water phase near the free surface promotes the breakup of bubbles and, subsequently, increases the gas holdup and the mass transfer coefficient. This effect is expected to be much less relevant in full-scale deeper tanks. Furthermore, the importance of considering the variation of BSD is emphasized. The CBS assumption shows good performance regarding the prediction of the global gas holdup, but very poor performance in predicting the oxygen mass transfer coefficient.

## 2.6 References

- Askari, E., Proulx, P. & Passalacqua, A. (2019). Modelling of Bubbly Flow Using CFD-PBM Solver in OpenFOAM: Study of Local Population Balance Models and Extended Quadrature Method of Moments Applications. *Chem. Engineering*, 2(8), 1-23.
- Amaral, A. (2019) "Towards a detailed understanding of oxygen transfer in wastewater treatment: the effect of bubble size distribution", PhD Thesis, Department of Data Analysis and Mathematical Modelling, Ghent University, Ghent, Belgium, and Instituto Superior Tecnico, Universidade de Lisboa, Lisbon, Portugal.
- Amaral, A., Bellandi, G., Rehman, U., Neves, R., Amerlinck, Y., & Nopens, I. (2018). Towards improved accuracy in modeling aeration efficiency through understanding bubble size distribution dynamics. *Water Research*, 131, 346-355.
- Auton, T. R., Hunt, J. C. R., & Prud'Homme, M. (1988). The force exerted on a body in inviscid unsteady non-uniform rotational flow. *Journal of Fluid Mechanics*, 197, 241-257.
- Bannari, R., Kerdouss, F., Selma, B., Bannari, A., & Proulx, P. (2008). Three-dimensional mathematical modeling of dispersed two-phase flow using class method of population balance in bubble columns. *Computers & chemical engineering*, 32(12), 3224-3237.
- Bhole, M. R., Joshi, J. B., & Ramkrishna, D. (2008). CFD simulation of bubble columns incorporating population balance modeling. *Chemical Engineering Science*, 63(8), 2267-2282.
- Burns, A. D., Frank, T., Hamill, I., & Shi, J. M. (2004, May). The Favre averaged drag model for turbulent dispersion in Eulerian multi-phase flows. In *5th international conference on multiphase flow, ICMF* (Vol. 4, pp. 1-17). ICMF.
- Celik, I. B., Ghia, U., Roache, P. J., & Freitas, C. J. (2008). Procedure for estimation and reporting of uncertainty due to discretization in CFD applications. *Journal of fluids Engineering-Transactions of the ASME*, 130(7).
- Chen, P., Duduković, M. P., & Sanyal, J. (2005). Three-dimensional simulation of bubble column flows with bubble coalescence and breakup. *AIChE journal*, 51(3), 696-712.
- Chen, P., Sanyal, J., & Duduković, M. P. (2005). Numerical simulation of bubble columns flows: effect of different breakup and coalescence closures. *Chemical Engineering Science*, 60(4), 1085-1101.

- Darmana, D., Henket, R. L. B., Deen, N. G., & Kuipers, J. A. M. (2007). Detailed modelling of hydrodynamics, mass transfer and chemical reactions in a bubble column using a discrete bubble model: Chemisorption of CO<sub>2</sub> into NaOH solution, numerical and experimental study. *Chemical engineering science*, 62(9), 2556-2575.
- de Bertodano, M. A. L. (1998). Two fluid model for two-phase turbulent jets. *Nuclear engineering and design*, 179(1), 65-74.
- Deen, N. G., Solberg, T., & Hjertager, B. H. (2001). Large eddy simulation of the gas–liquid flow in a square cross-sectioned bubble column. *Chemical engineering science*, 56(21-22), 6341-6349.
- Delnoij, E., Lammers, F. A., Kuipers, J. A. M., & van Swaaij, W. P. M. (1997). Dynamic simulation of dispersed gas-liquid two-phase flow using a discrete bubble model. *Chemical engineering science*, 52(9), 1429-1458.
- Drew, D. A., & Lahey Jr, R. T. (1987). The virtual mass and lift force on a sphere in rotating and straining inviscid flow. *International Journal of Multiphase Flow*, 13(1), 113-121.
- Shah, Y. T., Kelkar, B. G., Godbole, S. P., & Deckwer, W. D. (1982). Design parameters estimations for bubble column reactors. *AIChE Journal*, 28(3), 353-379.
- Gemello, L., Cappello, V., Augier, F., Marchisio, D., & Plais, C. (2018). CFD-based scale-up of hydrodynamics and mixing in bubble columns. *Chemical Engineering Research and Design*, 136, 846-858.
- Gosman, A. D., Lekakou, C., Politis, S., Issa, R. I., & Looney, M. K. (1992). Multidimensional modeling of turbulent two-phase flows in stirred vessels. *AIChE Journal*, 38(12), 1946-1956.
- Grace, J. R., & TH, N. (1976). Shapes and velocities of single drops and bubbles moving freely through immiscible liquids. *Transactions of the Institute of Chemical Engineers*, 54(3), 167-173.
- Hasanen, A., Orivuori, P., & Aittamaa, J. (2006). Measurements of local bubble size distributions from various flexible membrane diffusers. *Chemical Engineering and Processing: Process Intensification*, 45(4), 291-302.
- Hounslow, M. J., Ryall, R. L., & Marshall, V. R. (1988). A discretized population balance for nucleation, growth, and aggregation. *AIChE journal*, 34(11), 1821-1832.



- Hulburt, H. M., & Katz, S. (1964). Some problems in particle technology: A statistical mechanical formulation. *Chemical engineering science*, 19(8), 555-574.
- Ishii, M., & Hibiki, T. (2010). *Thermo-fluid dynamics of two-phase flow*. Springer Science & Business Media.
- Ishii, M., & Zuber, N. (1979). Drag coefficient and relative velocity in bubbly, droplet or particulate flows. *AIChE journal*, 25(5), 843-855.
- Jakobsen, H. A., Lindborg, H., & Dorao, C. A. (2005). Modeling of bubble column reactors: progress and limitations. *Industrial & engineering chemistry research*, 44(14), 5107-5151.
- Jakobsen, H. A., Sannæs, B. H., Grevskott, S., & Svendsen, H. F. (1997). Modeling of vertical bubble-driven flows. *Industrial & Engineering Chemistry Research*, 36(10), 4052-4074.
- Kantarci, N., Borak, F., & Ulgen, K. O. (2005). Bubble column reactors. *Process biochemistry*, 40(7), 2263-2283.
- Krishna, R., Van Baten, J. M., & Urseanu, M. I. (2000). Three-phase Eulerian simulations of bubble column reactors operating in the churn-turbulent regime: a scale up strategy. *Chemical Engineering Science*, 55(16), 3275-3286.
- Krishna, R., & Ellenberger, J. (1996). Gas holdup in bubble column reactors operating in the churn-turbulent flow regime. *AIChE journal*, 42(9), 2627-2634.
- Kumar, S., & Ramkrishna, D. (1996). On the solution of population balance equations by discretization—I. A fixed pivot technique. *Chemical Engineering Science*, 51(8), 1311-1332.
- Lahey Jr, R. T. (2005). The simulation of multidimensional multiphase flows. *Nuclear Engineering and Design*, 235(10-12), 1043-1060.
- Lehr, F., Millies, M., & Mewes, D. (2002). Bubble-size distributions and flow fields in bubble columns. *AIChE Journal*, 48(11), 2426-2443.
- Lehr, F., Millies, M., & Mewes, D. (2002). Bubble-size distributions and flow fields in bubble columns. *AIChE Journal*, 48(11), 2426-2443.
- Liang, X. F., Pan, H., Su, Y. H., & Luo, Z. H. (2016). CFD-PBM approach with modified drag model for the gas–liquid flow in a bubble column. *Chemical Engineering Research and Design*, 112, 88-102.

- Liao, Y., Rzehak, R., Lucas, D., & Krepper, E. (2015). Baseline closure model for dispersed bubbly flow: Bubble coalescence and breakup. *Chemical Engineering Science*, 122, 336-349.
- Lubchenko, N., Magolan, B., Sugrue, R., & Baglietto, E. (2018). A more fundamental wall lubrication force from turbulent dispersion regularization for multiphase CFD applications. *International Journal of Multiphase Flow*, 98, 36-44.
- Lucas, D., Krepper, E., & Prasser, H. M. (2007). Use of models for lift, wall and turbulent dispersion forces acting on bubbles for poly-disperse flows. *Chemical Engineering Science*, 62(15), 4146-4157.
- Lucas, D., & Tomiyama, A. (2011). On the role of the lateral lift force in poly-dispersed bubbly flows. *International Journal of Multiphase Flow*, 37(9), 1178-1190.
- Luo, H., & Svendsen, H. F. (1996). Theoretical model for drop and bubble breakup in turbulent dispersions. *AIChE Journal*, 42(5), 1225-1233.
- Marchisio, D. L., & Fox, R. O. (2005). Solution of population balance equations using the direct quadrature method of moments. *Journal of Aerosol Science*, 36(1), 43-73.
- Marschall, H. (2011). *Towards the numerical simulation of multi-scale two-phase flows* (Doctoral dissertation, Technische Universität München).
- Masood, R. M. A., & Delgado, A. (2014). Numerical investigation of the interphase forces and turbulence closure in 3D square bubble columns. *Chemical Engineering Science*, 108, 154-168.
- Mudde, R. F., Groen, J. S., & Van Den Akker, H. E. A. (1997). Liquid velocity field in a bubble column: LDA experiments. *Chemical Engineering Science*, 52(21-22), 4217-4224.
- Mudde, R. F., & Simonin, O. (1999). Two-and three-dimensional simulations of a bubble plume using a two-fluid model. *Chemical Engineering Science*, 54(21), 5061-5069.
- Naumann, Z., & Schiller, L. (1935). A drag coefficient correlation. *Z. Ver. Deutsch. Ing.*, 77(318), e323.
- Oey, R. S., Mudde, R. F., & Van den Akker, H. E. A. (2003). Sensitivity study on interfacial closure laws in two-fluid bubbly flow simulations. *AIChE journal*, 49(7), 1621-1636.

- Pjontek, D., Parisien, V., & Macchi, A. (2014). Bubble characteristics measured using a monofibre optical probe in a bubble column and freeboard region under high gas holdup conditions. *Chemical Engineering Science*, 111, 153-169.
- Politano, M. S., Carrica, P. M., & Converti, J. (2003). A model for turbulent polydisperse two-phase flow in vertical channels. *International Journal of Multiphase Flow*, 29(7), 1153-1182.
- Prince, M. J., & Blanch, H. W. (1990). Bubble coalescence and break-up in air-sparged bubble columns. *AIChE journal*, 36(10), 1485-1499.
- Rafique, M., Chen, P., & Duduković, M. P. (2004). Computational modeling of gas-liquid flow in bubble columns. *Reviews in Chemical Engineering*, 20(3-4), 225-375.
- Randolph, A. (2012). *Theory of particulate processes: analysis and techniques of continuous crystallization*. Elsevier.
- Rosso, D. (2019). *Aeration, Mixing, and Energy: Bubbles and Sparks*. IWA Publishing, London.
- Rusche, H. (2002). *Computational fluid dynamics of dispersed two-phase flows at high phase fractions* (Doctoral dissertation, University of London).
- Rzehak, R., Krauß, M., Kováts, P., & Zähringer, K. (2017). Fluid dynamics in a bubble column: New experiments and simulations. *International Journal of Multiphase Flow*, 89, 299-312.
- Sato, Y., Sadatomi, M., & Sekoguchi, K. (1981). Momentum and heat transfer in two-phase bubble flow—II. A comparison between experimental data and theoretical calculations. *International Journal of Multiphase Flow*, 7(2), 179-190.
- Simonnet, M., Gentric, C., Olmos, E., & Midoux, N. (2008). CFD simulation of the flow field in a bubble column reactor: Importance of the drag force formulation to describe regime transitions. *Chemical Engineering and Processing: Process Intensification*, 47(9-10), 1726-1737.
- Sokolichin, A., Eigenberger, G., Lapin, A., & Lübert, A. (1997). Dynamic numerical simulation of gas-liquid two-phase flows Euler/Euler versus Euler/Lagrange. *Chemical engineering science*, 52(4), 611-626.
- Svendsen, H. F., Jakobsen, H. A., & Torvik, R. (1992). Local flow structures in internal loop and bubble column reactors. *Chemical Engineering Science*, 47(13-14), 3297-3304.

- Tchobanoglous, G, Stensel, D., Tsuchihashi, R, Burton, F, Abo-Orf, M., Bowden, G., Pfrang, W. (2014). *Wastewater Engineering – Treatment and Resource Recovery*, 5<sup>th</sup> ed., McGraw-Hill, New York.
- Terashima, M., So, M., Goel, R., & Yasui, H. (2016). Determination of diffuser bubble size in computational fluid dynamics models to predict oxygen transfer in spiral roll aeration tanks. *Journal of Water Process Engineering*, 12, 120-126.
- Tomiyama, A. (1998). Struggle with computational bubble dynamics. *Multiphase Science and Technology*, 10(4), 369-405.
- Tomiyama, A. (1995). Effects of Eotvos number and dimensionless liquid volumetric flux on lateral motion of a bubble in a laminar duct flow. In *2nd Int. Conf. on Multiphase Flow* (Vol. 3).
- Tomiyama, A., Kataoka, I., Zun, I., & Sakaguchi, T. (1998). Drag coefficients of single bubbles under normal and micro gravity conditions. *JSME International Journal Series B Fluids and Thermal Engineering*, 41(2), 472-479.
- Tomiyama, A., Tamai, H., Zun, I., & Hosokawa, S. (2002). Transverse migration of single bubbles in simple shear flows. *Chemical Engineering Science*, 57(11), 1849-1858.
- Troshko, A. A., & Hassan, Y. A. (2001). A two-equation turbulence model of turbulent bubbly flows. *International Journal of Multiphase Flow*, 27(11), 1965-2000.
- Vik, C. B., Solsvik, J., Hillestad, M., & Jakobsen, H. A. (2018). A multifluid-PBE model for simulation of mass transfer limited processes operated in bubble columns. *Computers & Chemical Engineering*, 110, 115-139.
- Wang, T., Wang, J., & Jin, Y. (2005). Population balance model for gas– liquid flows: Influence of bubble coalescence and breakup models. *Industrial & engineering chemistry research*, 44(19), 7540-7549.
- Wang, T., Wang, J., & Jin, Y. (2005). Population balance model for gas– liquid flows: Influence of bubble coalescence and breakup models. *Industrial & engineering chemistry research*, 44(19), 7540-7549.
- Wang, T., Wang, J., & Jin, Y. (2006). A CFD–PBM coupled model for gas–liquid flows. *AIChE Journal*, 52(1), 125-140.

- Yang, G., Guo, K., & Wang, T. (2017). Numerical simulation of the bubble column at elevated pressure with a CFD-PBM coupled model. *Chemical Engineering Science*, 170, 251-262.
- Zhang, D., Deen, N. G., & Kuipers, J. A. M. (2006). Numerical simulation of the dynamic flow behavior in a bubble column: a study of closures for turbulence and interface forces. *Chemical Engineering Science*, 61(23), 7593-7608.
- Zhang, D. Z., & VanderHeyden, W. B. (2002). The effects of mesoscale structures on the macroscopic momentum equations for two-phase flows. *International Journal of Multiphase Flow*, 28(5), 805-822.
- Zlokarnik, M. (1980) Eignung und Leistungsfähigkeit von Volumenbelüftern. *Korrespondenz Abwasser*. 27(3), 194-209.
- Zun, I. (1980). The transverse migration of bubbles influenced by walls in vertical bubbly flow.

## Chapter 3

### 3 Uncertainty analysis of rising sewer models with respect to input parameters and model structure using Monte Carlo simulations and computational fluid dynamics

Modelling conversion processes in sewers can help minimize odour and pipe corrosion issues, but model uncertainties and errors must be understood. In this chapter, the Wastewater Aerobic/Anaerobic Transformation in Sewers (WATS) model is implemented in two different frameworks; 1-D (CSTR-in-series) and computational fluid dynamics (CFD) to study the uncertainties due to model parameters and its mathematical form. The 1-D model is used to conduct uncertainty/sensitivity analysis using Monte Carlo simulations. Time-averaged outputs were represented using a general linearized model to quantify the importance of specific parameters. The sulfide formation rate per unit area of the biofilm is the most influential parameter. Parameters controlling anaerobic hydrolysis and fermentation are also significant. Uncertainty due to model structure is studied using CFD to explore the influences of non-homogeneous surface reactions and solids settling. These showed that the 1-D model provides a reasonable characterisation of the process for simple flows in pressure mains.

#### 3.1 Introduction

There are a number of potential problems that can arise from the biological and chemical reactions that occur in sewer systems, most commonly odour nuisance and corrosion (Carrera et al. 2016). The build-up of hydrogen sulfide and volatile organic compounds is the major cause of odour, while formation of hydrogen sulfide and its subsequent oxidation to sulfuric acid on the moist walls of the sewer pipes leads to pipe corrosion. The cost of replacement and maintenance due to corrosion is significant for municipalities (Rootsey and Yuan 2005). Production of methane by methanogens in the sewer can cause explosion risk in confined spaces. Furthermore, methane is a potent

greenhouse gas that is responsible for almost 20% of forcing in climate change models (Minami and Takata, 1991). Guisasola et al. (2013) reports that methane discharge from sewers contributes significantly to the overall greenhouse gas emissions that are associated with wastewater transport and treatment.

Developing a more complete understanding of the processes occurring in sewer networks has the potential to enable improvements in the performance of wastewater treatment plants (WWTPs). For example, removal of readily biodegradable chemical oxygen demand (COD) can be achieved in the sewer system through conversion to slowly biodegradable organic matter stored in biomass, which is more readily removed by mechanical treatment. In other words, the sewer is not only a collection system; it is also a pre-treatment stage that can be exploited in different ways to improve the performance of the WWTP (Guo et al., 2019). When considering such strategies, it is important to consider downstream processes where it may be necessary to preserve and produce readily biodegradable substrate, since this is beneficial for denitrification and biological phosphorus removal processes in advanced WWTP designs (Vollertsen and Matos, 2018). Furthermore, some microbial activities, such as methanogenesis, consume the available organic carbon which may be required for other downstream processes (Gutierrez et al., 2009). In light of these complex and coupled interactions, process modelling becomes increasingly important.

Moving from an empirical approach (Pomeroy and Parkhurst, 1978) to a conceptual understanding of the biological and chemical mechanisms of the in-sewer transformations allows for greater insight into the processes that occur. Microbial transformation processes in biological systems are, to a large extent, identical to the in-sewer transformations (Bjerre et al., 1998). Therefore, the mathematical model of the microbial processes described in the IWA Activated Sludge Model No. 1 (ASM1) (Henze et al., 1987) was adopted in the work of Bjerre et al. (1998) to model the aerobic processes in the wastewater collection system with two additional types of hydrolysis processes. Hvitved-Jacobsen et al. (1998) reported that certain modifications were necessary to adapt the ASM1 model to gravity sewer systems. First, the biomass decay rate was found to be unrealistic, so the biomass decay process was replaced by the energy maintenance

requirement rate as a reasonable alternative process. Further, the biofilm concentration was assumed to be constant and any growth of the biofilm was assumed to be released in the bulk water phase. Hvitved-Jacobsen et al. (1998) also included anaerobic processes in their model, based on the IWA Activated Sludge Model No. 2 (Gujer et al., 1995) where, even if aerobic conditions are assumed (as in gravity sewers), anaerobic regions could certainly exist within the sewer system (Carrera et al., 2016). The sulfur cycle was also included as it was necessary to describe sulfide formation and consumption (Hvitved-Jacobsen et al., 1999). The work of Hvitved-Jacobsen et al. (1999) is considered to be the foundation of the Wastewater Aerobic/Anaerobic Transformation in Sewers (WATS) model, which describes the aerobic and anaerobic transformation of carbon in the sewer, in addition to sulfide formation by the sulfate reduction process. Yongsiri et al. (2003) later improved upon the original WATS model by introducing the emission of the sulfide from the bulk water phase, which is considered as the first step toward incorporating physical processes alongside the biological and chemical transformations. The application and parameter estimation of the WATS model were reported by Tanaka and Hvitved-Jacobsen (2002). However, the uncertainty and sensitivity analysis of the WATS model is scarce in the literature.

Model-based design, operation, and development of control strategies for wastewater systems management is prone to risk of not meeting regulatory standards or operating a system inefficiently as a result of model uncertainties; therefore, uncertainty and sensitivity analysis is essential (Sin et al., 2009). Uncertainty analysis is concerned with the propagation uncertainty from different sources onto the global model output, while sensitivity analysis is concerned with the weight of each of the model inputs on the model output. According to Saltelli (2000), sensitivity analysis in wastewater applications can be categorized into three class: local methods, global methods, and screening methods. This work is focused on global sensitivity analysis, which is capable of providing information regarding the effect of model parameters on the model output over the space of all possible parameter values. Many global sensitivity analysis techniques have been applied in the literature, including regression-based methods, e.g. the Standard Regression Coefficient (SRC) method (Flores-Alsina et al., 2012; Sin et al., 2011), and



variance-based methods, e.g. the Fourier Amplitude Sensitivity Testing (FAST) and Extended-FAST methods (Chen et al., 2012; Cosenza et al., 2014).

Uncertainty analysis framing defines the sources of the uncertainty that are to be considered in the study, including the model assumptions and approximations, as well as the identification of the uncertainty range assigned for each of the model inputs. Sin et al. (2009) conducted uncertainty analysis under different model framings, concluding that the uncertainty of the different framings is almost additive if combined together. The main sources of uncertainty on model outputs, as described in Sin et al. (2009), arise from the uncertainty of the model inputs, the form (structure) of the mathematical model, and stochastic events. In the literature, sewers are modeled by coupling biochemical models with a hydraulic model, where the sewer pipe is commonly approximated as series of Continuous Stirred Tank Reactors (CSTRs) (Sharma et al., 2008). One downside of CSTR model is the spatial distribution of the species and their associated reactions cannot be taken into account, representing a model structure uncertainty. This can be particularly problematic for biofilm reactions, e.g. sulfide production by sulfate-reduction bacteria (Mohanakrishnan et al., 2009), which are highly localized at the biofilm accumulated on the sewer walls. Similarly, settling of particulate species can generate spatial non-uniformities that cannot easily be captured using existing modelling approaches. This study is intended to shed the light on the process model uncertainties that may arise from two common simplifications that are assumed in the such models: (i) the homogenization of surface reactions using the ratio of wall surface area to volume and (ii) the omission of particulate settling.

A computational fluid dynamics (CFD) approach for modelling sewer systems offers some potential improvements over a CSTR model, since it is able to resolve the spatial variations in species concentration and reaction rates along with the transport of the different species by advection and diffusion. CFD solvers are robustly capable of solving the hydrodynamics of the sewer system while the biological and chemical reactions embodied by the various kinetic models discussed previously that can be implemented as additional coupled advection-diffusion transport equations. Of course, CFD simulation of pressure mains is computationally expensive, but can be useful for examining the details

of the spatial distribution and the heterogeneity of the reactions in certain cross-sections of the pipes. As such, the uncertainties that accompany the usage of the CSTR model structure can be examined using CFD and can ultimately be used to further improve the lumped-parameter-based models. For gravity sewers, CFD could also play an important role in determining the mass transfer mechanisms (Teuber, 2020), thereby improving modelling of hydrogen sulfide emission.

The aim of this work is to determine the sources of uncertainty in the modelling of sewer systems using the WATS model. These sources are associated with the biochemical model parameters (input uncertainty) and with the mathematical form of the model (model structure). The input uncertainty related to the model parameters is examined using the SRC method. The structural uncertainties that will be considered are: (i) the representation of the sewer pipe as a series of tanks, (ii) the homogenization of biofilm surface reactions, and (iii) exclusion of the physical processes of solids settling. The structural uncertainties are assessed using a detailed CFD model which allows for each of these factors to be included and their effects examined.

## 3.2 Materials and Methods

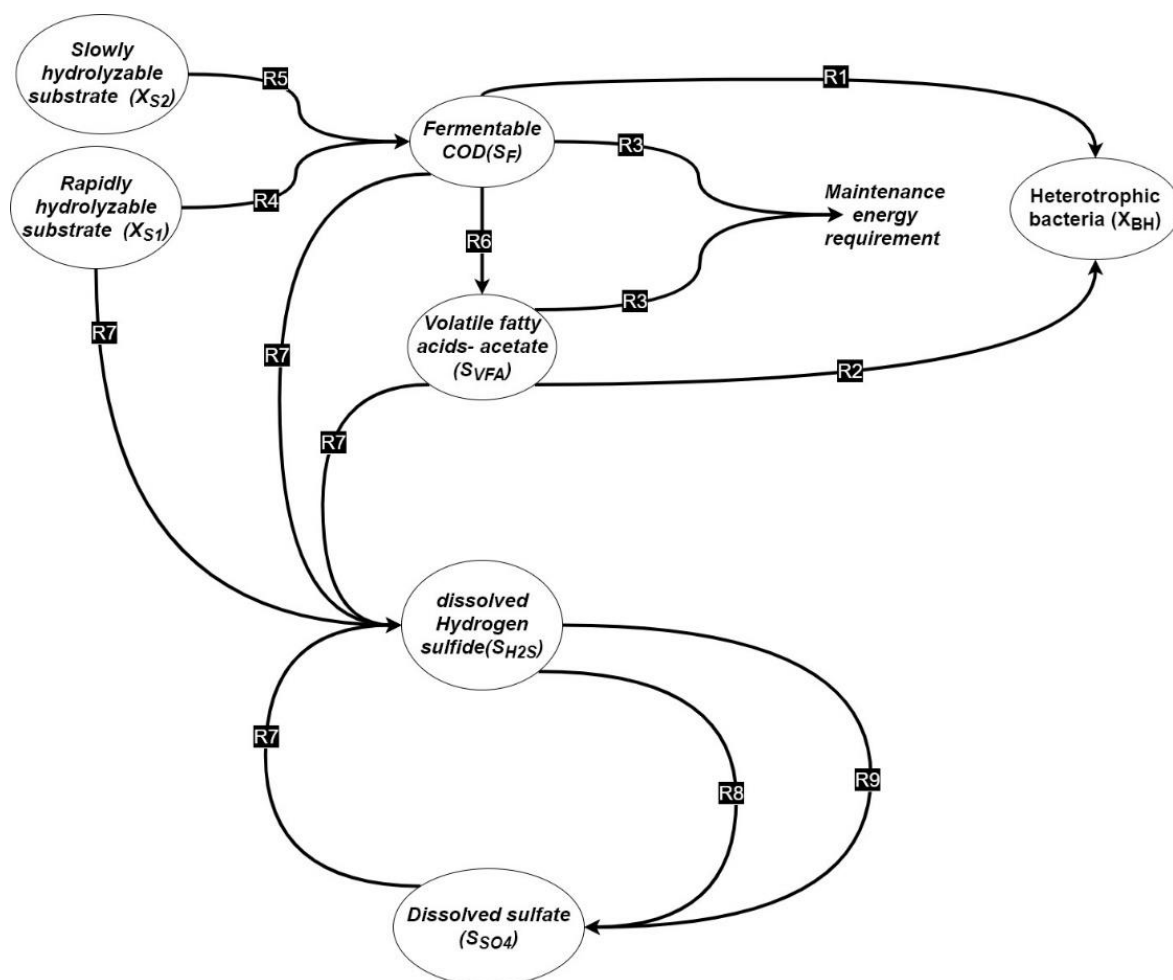
### 3.2.1 Measurement data

Measurement data provided in Guo et al. (2018) is used for the calibration of the models in the present study. A 24-hour on-site sampling and measurement campaign on a force main system in California, US was reported. The current study is concerned with one of three force mains that transport sewage from three different catchments to a WWTP. The main under consideration is 9.09 km in length and 40.64 cm in diameter. The flow rates and the water characteristics of the sewage were measured at the inlet and the outlet of the pipe during the sampling period. Soluble COD, VFA, and total sulfide measurements are the main characteristics that are used for the calibration and validation (see supplementary information).

### 3.2.2 Biochemical model

The WATS model is the basis of most of the recently developed models (Sharma et al., 2008) to model the anaerobic processes that include fermentation, hydrolysis of particulate COD and sulfide production. Therefore, WATS biochemical model reported by Yongsiri et al. (2003) and Nielsen et al. (2005) is adapted in this work to model the biological and chemical conversions in the sewer. These conversions include main processes in the carbon and the sulfur cycles. Modifications of the original model are made by adding the chemical and biological oxidation reactions of sulfide (Carrera et al. 2016). The kinetics of the biological and chemical oxidation of sulfide in the water phase and biofilm are adopted from Nielsen et al. (2003) and Nielsen et al. (2006). The diagram in Fig. 3-1 describes the key processes in the implemented biochemical model showing the main state variables in the model. The resulting model is in the form of a system of ordinary differential equations (ODEs) that describe the production and consumption rates of the modelled species.

Integration of the biokinetics with the hydrodynamics can either be carried out using a conventional CSTR-in-series approach or by solving the complete advection-diffusion equation for each of the species using CFD method. Both of these are considered in the present work, where the CSTR model is used for calibration and sensitivity/uncertainty analysis of the model to its input parameters, while the CFD model is used to assess uncertainty with respect to the influence of solids settling and non-homogeneous reactions in the biofilm on the walls.



Code	Reaction	Remarks	location
R1	Het. Biomass growth (aerobic and anoxic conditions)	by fermentable COD	Bulk and biofilm
R2	Het. Biomass growth (aerobic and anoxic conditions)	by VFA	Bulk and biofilm
R3	Energy maintenance requirement (aerobic and anoxic conditions)	by fermentable COD and VFA	Bulk
R4	Hydrolysis of $X_{S1}$ (aerobic and anoxic conditions)		Bulk and biofilm
R5	Hydrolysis of $X_{S2}$ (aerobic and anoxic conditions)		Bulk and biofilm
R6	Fermentation		Bulk
R7	Sulfate reduction to sulfide		Biofilm
R8	Chemical sulfide oxidation to sulfate		Bulk
R9	Biological sulfide oxidation to sulfate		Biofilm and bulk

**Figure 3-1: Key processes in the WATS model implemented in the current study**

### 3.2.3 CSTR-in-series process model

The process model is developed in MATLAB/Simulink, where the sewer pipe is represented as a series of Continuous Stirred-Tank Reactors (CSTRs). Sensitivity analysis for the number of the CSTRs was conducted as a preliminary step. It was found that including more than 80 CSTRs resulted in no noticeable change in the concentration profiles, which indicated that this is an adequate representation of the plug flow behaviour. Therefore, all subsequent results implement 80 CSTRs. As the sewage flow rate and characteristics largely vary along day- and night-time, dynamic inlet conditions are necessary to be considered for better prediction of the dynamic and peak concentration of the species. Species concentrations at the outlet of the series of the CSTR are monitored for the calibration and sensitivity analysis of the model.

### 3.2.4 Calibration and uncertainty/sensitivity analysis

Studies on the uncertainty/sensitivity of the sewer biochemical models is scarce in the literature. Therefore, most of the initial values for the biochemical model parameters used herein are adopted from Calabrò et al. (2009) and Hvitved-Jacobsen et al. (2013) as an initial parameter state. Using 24-hr dynamic measurement data, the key parameters of the model are calibrated to obtain a reasonable match between the model prediction and the dynamic measurement data for total COD, soluble COD (sCOD), VFA, and total sulfide. For further quantification of the significance of the role of each of the key parameters in calibrating the model and potential source of model output variance, uncertainty/sensitivity analysis is conducted. Following the work of Sin et al. (2011), the analysis is conducted into two steps. First, Monte Carlo method is used to explore the propagation of uncertainty from the model input to the output. Then, the Monte Carlo results are used for analysis by graphical representation and by fitting to multivariate linear functions of the model input using the Standardized Regression Coefficient (SRC) method. This study is concerned with identifying the most influential parameters in the model. However, SRCs could be used to determine the non-influential parameters as well, if the coefficient of determination ( $R^2$ ) is higher than 0.7, as in the case of our study (section 3.2.2) (Cosenza et al., 2013). Further study could be conducted using one of the

variance-based sensitivity analysis methods such as Extended-FAST method (Cosenza et al., 2013) to explore the higher order effect of the model parameters.

Monte Carlo simulations are performed for the uncertainty/sensitivity analysis of the model parameters using 1000 simulations in a randomly sampled parameter space. A pre-defined variational range for each parameter, except the parameters pertaining to the anoxic processes, as illustrated in Table 3-1, was determined. A guideline for specifying the variational range and default values are provided by Brun et al. (2002). Parameters are classified into three uncertainty classes (Table 3-1) with variations of 5%, 25% and 50%, around the preliminary calibrated parameter values, where these values correspond to classes 1, 2, and 3, respectively. A parameter sampling matrix,  $S$ , is created using the Latin Hypercube Sampling (LHS) technique to ensure full coverage of the range for each parameter variation (Sin et al. 2009; Helton and Davis, 2003). The calibrated parameter values are used as the mean values of the variation range and reference values.

The influence of variations in each of the model parameters is isolated using both graphical and SRC methods. In the SRC approach, Monte Carlo output time series of sCOD, VFA and total sulfide are time-averaged and represented by linear multivariate functions of model inputs,  $\theta_i$ , in the form:

$$y_{reg} = a + \sum_i b_i \theta_i \quad (3.1)$$

The regression coefficients,  $b_i$ , are obtained and scaled to calculate the Standardized Regression Coefficients,  $\beta_i$ , using the standard deviation of the model output,  $\sigma_y$ , and input,  $\sigma_{\theta_i}$ , as:

$$\beta_i = \frac{\sigma_{\theta_i}}{\sigma_y} b_i \quad (3.2)$$

The values of  $\beta_i$  should be in the range of -1 to 1. For the values of  $\beta_i$  to be valid, the coefficient of determination of the linear regression should be high enough, i.e.  $R^2 > 0.7$ , to ensure that the model is adequately linear. The absolute values of  $\beta_i$  are used to

determine the sensitivity of the model output to the corresponding input and, consequently, the contribution of that model input to the output variance.

A graphical representation of the influence of each of the parameters on the simulation output is conducted by plotting the simulation results of the highest and lowest values of this parameter of interest against the Monte Carlo simulation output bands. In order to quantify the model uncertainty with respect to a specific parameter,  $\theta_j$ , an average measure for the output sensitivity,  $\gamma_j$ , is defined as:

$$\gamma_j = \frac{Y(\theta_j)_{i,ub} - Y(\theta_j)_{i,lb}}{Y_{i,ub} - Y_{i,lb}} \quad (3.3)$$

where  $Y(\theta_j)_{i,ub}$  and  $Y(\theta_j)_{i,lb}$  are the upper and lower bounds, respectively, of simulation outputs that correspond to the range limit values of parameter  $\theta_j$ . This sensitivity parameter represents the maximum change in a specific output parameter that occurs with a variation in  $\theta_j$ , normalized by the difference between the upper and lower band of the outputs of Monte Carlo,  $Y_{i,ub}$  and  $Y_{i,lb}$ , respectively.

**Table 3-1: Model parameters default values and variation range**

Parameter	Symbol	Unit	Calibrated Value	Uncertainty Class
<i>Biomass growth in bulk water parameters</i>				
Maximum aerobic specific growth rate	$\mu_{H,O2}$	$[d^{-1}]$	7	3
Yield constant for heterotrophic biomass in water phase	$Y_{hw}$	$[gCOD/gCOD]$	0.55	1
Maintenance energy requirement rate constant	$q_m$	$[d^{-1}]$	1	3
Saturation constant for readily biodegradable substrate	$K_{sw}$	$[gCOD/m^3]$	1	3
Saturation constant for dissolved oxygen	$K_O$	$[gO_2/m^3]$	0.05	3
<i>Biomass growth in biofilm parameters</i>				
Half-order aerobic reaction rate constant per unit area for biofilm surface	$K_{1/2}$	$[gO_2^{0.5}m^{-0.5}d^{-1}]$	4	3
Yield constant for heterotrophic biomass in biofilm	$Y_{hf}$	$[gCOD/gCOD]$	0.55	1
Saturation constant for readily biodegradable substrate in biofilm	$K_{sf}$	$[gCOD/m^3]$	5	3
Saturation constant for dissolved oxygen	$K_O$	$[gO_2/m^3]$	0.05	3
<i>Particulate hydrolysis parameters</i>				
Rapidly hydrolysis rate constant	$K_{h1}$	$[d^{-1}]$	12	3
Saturation constant for the rapidly hydrolyzable substrate	$K_{X1}$	$[gCOD/gCOD]$	1.5	3
Slowly hydrolysis rate constant	$K_{h2}$	$[d^{-1}]$	5	3
Saturation constant for the slowly hydrolyzable substrate	$K_{X2}$	$[gCOD/gCOD]$	0.5	3
Efficiency constant for anaerobic hydrolysis	$\eta_{h,ana}$	—	0.18	2
Relative efficiency constant for the biomass in the biofilm	$\varepsilon$	—	0.15	2
Biomass concentration in the biofilm	$X_{bf}$	$[gCOD/m^2]$	10	3
<i>Fermentation parameters</i>				
Fermentation rate constant	$q_{ferm}$	$[d^{-1}]$	2	3
Saturation constant for fermentation	$k_{ferm}$	$[gCOD/m^3]$	20	3
<i>Hydrogen sulfide formation parameters</i>				
Rate constant for sulfide formation	$a$	$[gS^{0.5}m^{-0.5}h^{-1}]$	0.003 2	3
Sulfate saturation constant	$K_{so4}$	$[gS/m^3]$	2	3
<i>Hydrogen sulfide oxidation parameters</i>				
Rate constant for sulfide oxidation in biofilm	$K_{s(II)ox,f}$	$[gS^{0.5}gO_2^{-0.5}md^{-1}]$	12	3
Chemical oxidation reaction order	$n_1$	—	0.9	2
Chemical oxidation reaction order	$n_2$	—	0.15	2
Rate constant for chemical sulfide oxidation of molecular sulfide	$K_{H2S,c}$	$[(gSm^{-3})^{1-n_1}(gO_2m^{-3})^{n_2}d^{-1}]$	0.96	3
Rate constant for chemical sulfide oxidation of ionic sulfide	$K_{HS,c}$	$[(gSm^{-3})^{1-n_1}(gO_2m^{-3})^{n_2}d^{-1}]$	12	3
Maximum rate constant for biological sulfide oxidation at the $pH_{opt}$ value	$K_{s(II),b,pH,opt}$	$[(gSm^{-3})^{1-n_1}(gO_2m^{-3})^{n_2}d^{-1}]$	19.92	3
Constant for sulfide oxidation rate function of pH level	$\Omega_{s(II)b}$	—	25.00	2



### 3.2.5 Distributed parameter CFD model

While the process model divides the geometry of pipe into a number of CSTRs, assuming homogeneity in each CSTR, the geometry is discretized into a number of computational cells in the CFD model. In each of these cells, the governing conservation equations are integrated using the finite volume method to arrive at a coupled set of algebraic equations. The geometry of the computational domain is based on that described in Section 2.1, where the domain is discretized using ANSYS ICEM meshing software to produce a structured-like mesh with an O-grid profile at the cross section. Due to the length of the domain, the computational cells are created with high aspect ratio to reduce the number of the cells hence the computational cost. Therefore, it is necessary to produce cell faces perpendicular to the flow direction to reduce the error coming from the interpolation of the different variables at the face centroids. A grid independence test was done on three different meshes containing 1.82, 3.17, and 5.88 million cells. The velocity profiles at different sections were compared and it was determined that the difference in the velocity values between the intermediate the finest mesh is less than 5%. Therefore, the intermediate mesh was used as a compromise between the accuracy and the computational cost.

ANSYS FLUENT CFD software was used for the simulation of the hydrodynamics of the flow in the pipe in addition to the settling behaviour of the solids in the flow. Due to the dynamic nature of the sewer system, a transient simulation was performed to simulate the dynamic behaviour of the flow and species concentration at the domain inlet. A transient table of the inlet conditions was defined for the CFD case providing the variation of the inlet flow rate and the concentrations of the simulated species. The biological and chemical reactions in the sewage were simulated along with the transport of each species in the sewage. The simulated species in the sewage were defined based on the integrated biochemical model. In the following sections, the governing equations for the hydrodynamics, modelling of the solids settling and surface reactions in the biofilm model development and the integration between the CFD and the biochemical model are presented.

### 3.2.5.1 Governing equations

The pressure-based solver in the ANSYS FLUENT software was used for simulating the flow field. The general momentum and continuity equations for incompressible, turbulent flow were solved. In addition, turbulent kinetic energy and turbulent energy dissipation rate equations were solved to compute the turbulent viscosity for the momentum equation. The continuity equation is given by:

$$\frac{\partial \rho \bar{v}_i}{\partial y} = 0 \quad (3.4)$$

where  $\rho$  is the water density,  $\bar{v}_i$  is the mean velocity in the  $i$  direction. Momentum conservation equation for turbulent flow is described as:

$$\frac{\partial \rho \bar{v}_i}{\partial t} + \frac{\partial}{\partial x_j} (\rho \bar{v}_i \bar{v}_j) = -\frac{\partial \bar{p}}{\partial x_i} + \frac{\partial}{\partial x_j} \left[ \mu \left( \frac{\partial \bar{v}_i}{\partial x_j} + \frac{\partial \bar{v}_j}{\partial x_i} - \frac{2}{3} \delta_{ji} \frac{\partial \bar{v}_l}{\partial x_l} \right) \right] + \frac{\partial}{\partial x_j} (-\rho \overline{v'_i v'_j}) \quad (3.5)$$

Here,  $\bar{p}$  is the mean pressure,  $\mu$  is the dynamic viscosity,  $\overline{\rho v'_i v'_j}$  is Reynolds stress tensor, and  $v'$  is the velocity fluctuation. The Reynolds stress tensor, the final term in Eq. 3.5, is closed using the realizable k- $\epsilon$  turbulence model.

### 3.2.5.2 Biochemical model integration with CFD

In order to couple the hydrodynamic simulation with the biochemical model, a general advection-diffusion transport equation in the liquid phase was solved for each species of the biochemical model. The transport equation defined for each species describes the spatial distribution for each species based on the liquid flow. The general transport equation solved in ANSYS FLUENT is defined as:

$$\frac{\partial \rho \phi_k}{\partial t} + \frac{\partial}{\partial x_i} (\rho v_i \phi_k - \Gamma_k \frac{\partial \phi_k}{\partial x_i}) = S_{\phi_k} \quad (3.6)$$

Here  $\phi_k$  is the concentration of the  $k^{th}$  species,  $\Gamma_k$  is the diffusivity of the scalar in water, and  $S_{\phi_k}$  is the source term of the  $k^{th}$  species. The turbulent diffusivity is included in  $\Gamma_k$  and is defined using the computed turbulent viscosity assuming a turbulent Schmidt number of 0.7.

### 3.2.5.2.1 Production/consumption rate of the wastewater constituents

The source terms,  $S_{\phi_k}$ , for the different species is defined by the corresponding conversion rates in the biochemical model and is implemented using user-defined functions. The source term describes the production and consumption rates of each species. These rates were computed using the local values of the dependent species concentrations in each computational cell, thereby accounting for the heterogeneity.

### 3.2.5.2.2 Surface reaction modelling

A technique is developed for the surface reactions in the biofilm such that these reactions are modelled as a superficial flux from the wall faces. A user-defined function is used to identify wall faces and, for all cells adjacent to a wall, the flux from the wall face is defined with direction defined based on the net generation/consumption of the corresponding species and magnitude defined by the biochemical model. More details and verification of the technique used for the simulation of the surface reactions are provided in the supplementary information.

It is hypothesised that one of the most influential parameters in the biochemical model is the sulfide production rate per unit area,  $a$ . Special attention is drawn to this parameter since it is directly affected by the homogenization of the surface reactions model as described in the sulfide formation rate:

$$r_{HS} = a \sqrt{S_F + S_A + X_{S1}} \frac{K_O}{K_O + S_O} \frac{A}{V} \quad (3.7)$$

Here,  $S_F$ ,  $S_A$ ,  $S_O$ , and  $X_{S1}$  are the concentrations of fermentable COD, VFA, soluble oxygen, and rapidly hydrolysable substrate, respectively.  $K_O$  is the oxygen saturation

constant and the factor  $\frac{A}{V}$  is the homogenization factor that converts the areal sulfide formation rate to volumetric form in the process model structure. In the CFD model, this homogenization factor is not required, such that the model uncertainty resulting from the introduction of this parameter can be assessed through the CFD results.

### 3.2.5.2.3 Solids settling

Particulate species settle due to gravity. A multi-phase approach that includes solids as a separate phase is incompatible with the scalar approach taken for soluble substrates, and does not represent dilute hindered settling well. Therefore, settling is incorporated in the scalar system by subjecting settling species additional advection flux at the computational cell faces that is normal to the gravity direction. This method was implemented in Lakehal et al. (1999) to model the setting of the solids in a secondary clarifier. The settling velocity of the solids is a function of the solids concentration, which is evaluated as a sum of the particulate species in each computation cell. The settling velocity is then calculated using the double exponential model (Takacs and Nolasco, 1991) which is defined as:

$$v_s = v_o (e^{-r_h(X_s - X_{min})} - e^{-r_p(X_s - X_{min})}) \quad (3.8)$$

where  $v_o$  is a reference settling velocity,  $X_{min}$  is the non-settleable concentration, and  $r_h$  and  $r_p$  are model parameters. The model parameters for this model are highly dependent on the nature of the solids in the wastewater. For approximation, the data from Patziger and Kiss (2015) measured for primary sludge is used to determine the model parameters for this study. Takacs's model is originally was proposed for the activated sludge. However, it was adapted in the work of Patziger and Kiss (2015) to model the settling of solids in the primary clarifier. The maximal settling velocity in the primary clarifier is much higher than that of activated sludge. This is due to the relative higher density of the primary sludge and larger particle size that varies in the range of 0.01-0.5 mm (Patziger and Kiss, 2015) which results in settling velocity of 10-11 cm/s at concentration of 100-200 mg/L suspended solids.

### 3.3 Results and Discussion

#### 3.3.1 Monte Carlo Simulations

The global uncertainty of the model is assessed using Monte Carlo simulations without assuming any correlation between the input parameters. Time series of the concentrations of sCOD, VFA and sulfide at the pipe outlet were monitored for each simulation. The upper and lower bands, along with the 10<sup>th</sup> and 90<sup>th</sup> percentiles, of the Monte Carlo simulation outputs are shown in Fig. 3-2. Higher band represents the largest difference between an instance of the Monte Carlo simulation output and the mean profile of the all simulations in the positive direction. On the other hand, the lower band represent the largest difference in the negative direction. These give an overall indication of the uncertainty level of the model, where a larger difference between the Monte Carlo bands and the mean indicates a higher uncertainty.

#### 3.3.2 Uncertainty/Sensitivity Analysis

##### 3.3.2.1 Graphical Representation

Figures 3-3 to 3-5 show the influence of the key parameters of the model (as defined in Table 3-1) on the model outputs, with respect to the uncertainty envelope of the Monte Carlo simulations output. The parameters related to the biomass growth in the bulk water, which describe the suspended biomass growth kinetics on the sCOD, show no effect on the model outputs. This can be explained on the basis that the present study involves a pressure main where the dissolved oxygen concentration is low enough that anaerobic conditions prevail. The same conclusion can be made for the biomass growth in the biofilm parameters as well. The hydrolysis processes are more impactful on the model output. The anaerobic hydrolysis rate constant,  $k_{h1}$ , and efficiency,  $\eta_{h,ana}$ , show no direct effect on the sulfide and VFA levels. However, they have a significant effect on the sCOD, since these parameters control the rate of conversion of particulate COD to fermentable substrate. Therefore, by increasing  $k_{h1}$  and  $\eta_{h,ana}$ , the concentration of the sCOD increases. However,  $k_{h1}$  and  $\eta_{h,ana}$  are not the predominant parameters for sulfide concentration output of the model. In general, the hydrolysis process parameters are the most influential parameters on the sCOD output.

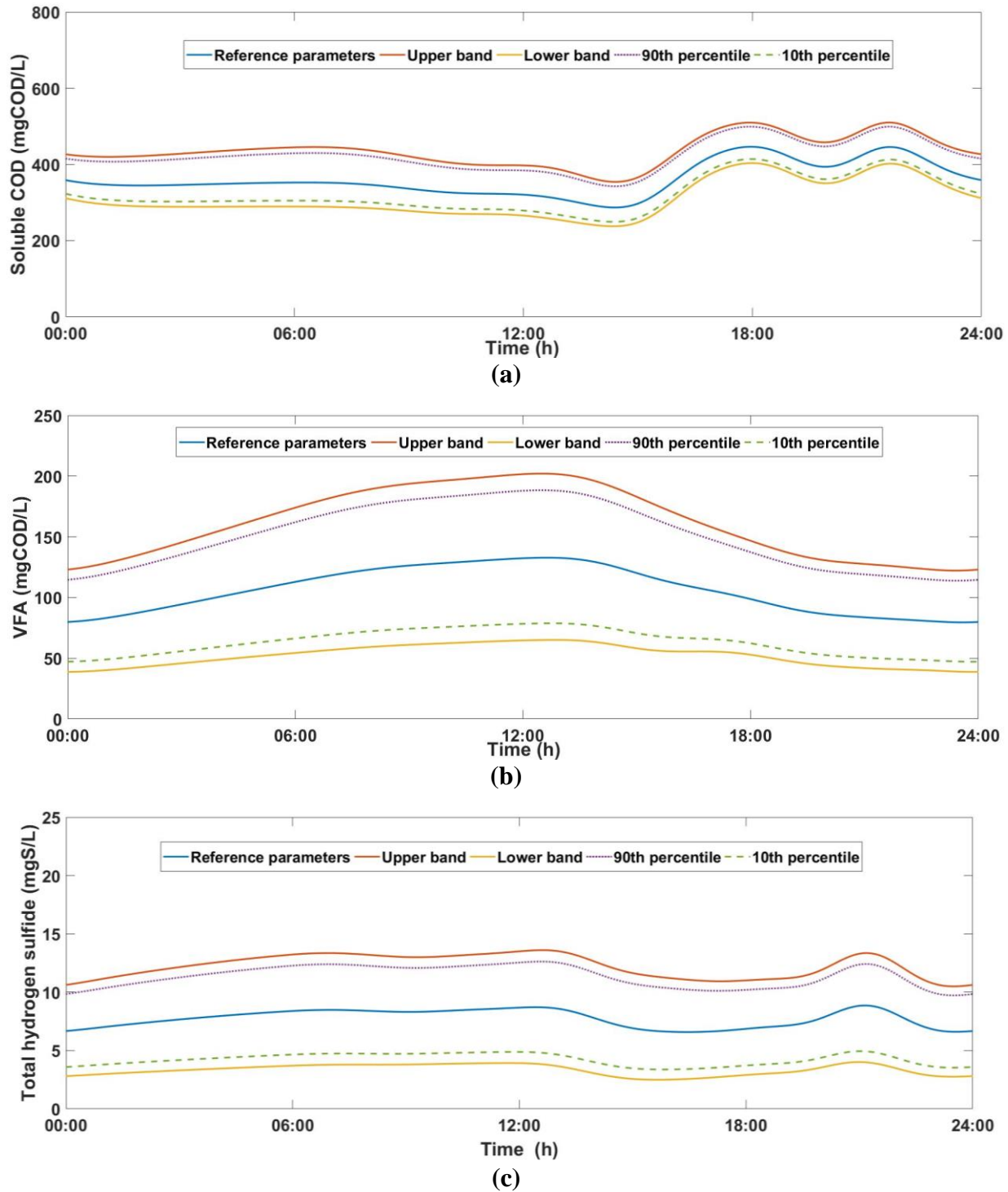


**Figure 3-2: Model uncertainties for (a) soluble COD, (b) VFA, (c) total sulfide, represented using mean, 10th and 90th percentiles, and upper and lower band values from the Monte Carlo simulations**

determining the variation in the sCOD. This can be concluded by comparing with the upper and lower bands of Monte Carlo simulations. Sulfide formation rate,  $a$ , and saturation constant of rapidly hydrolysable substrate,  $k_{x1}$ , play a significant role in determining the correct sCOD level as well.

The average sensitivity measure,  $\gamma_j$ , of  $k_{h1}$  and  $\eta_{h,ana}$  on sCOD are 53.8% and 25.4%, respectively. The saturation constant for the rapidly hydrolysable substrate shows a high influence on the sCOD with relative sensitivity of 19.8%. Fermentation rate,  $q_{ferm}$ , is another key parameter in calibrating the model where its effect is clear on the VFA levels only (Fig. 3-4). The sensitivity measure of the fermentation rate constant on the VFA concentrations is 67.6%, whereas the other parameters do not exceed 13.3% with respect to VFA. The sulfide formation constant,  $a$ , is a key parameter that has large influence on all of the model outputs. This is clear in Figs. 3-3 to 3-5, where its value has a significant impact on the concentration of sCOD and VFA, and it is the major parameter that controls the sulfide concentration output as shown in Fig. 3-5. The sensitivity measure of the sulfide formation rate constant on the sCOD, VFA, and sulfide are 23.3%, 13.3% and 81.6%, respectively.

From the data presented, it is concluded that the sulfide formation rate constant shows a significant influence on all of the monitored species. It is the predominant parameter affecting the predicted sulfide. On the other hand, the fermentation rate constant is the main parameter controlling the concentration of VFA, but it has almost no effect on the other species. This can be explained by the fact that the fermentation process is responsible for converting the fermentable substrate to acetate, which is another form of sCOD. As a result, the overall sCOD does not change as a result of fermentation. In addition, the sulfide formation expression is a function of sCOD, thereby the concentration of the sulfide is not determined by the fermentation process rate. The anaerobic hydrolysis efficiency and hydrolysis rate constant of the rapidly hydrolysable substrate have a predominant influence on sCOD since anaerobic conditions prevail in pressure mains. For sulfide formation, the colloidal COD is considered as rapidly hydrolysable substrate and is added to sCOD in the sulfide formation rate expression. Therefore, the effect of the anaerobic hydrolysis efficiency does not propagate to the

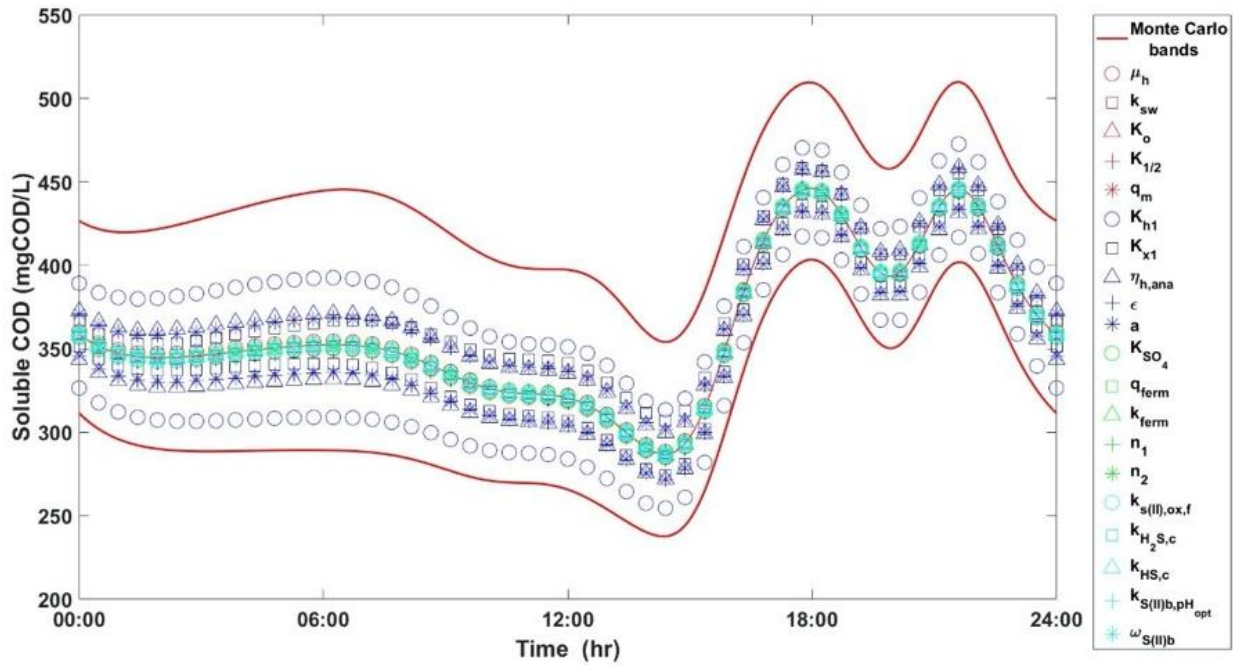


**Figure 3-3: Graphical representation of the sensitivity of the predicted time-series of soluble COD concentration at the outlet for selected model parameters**

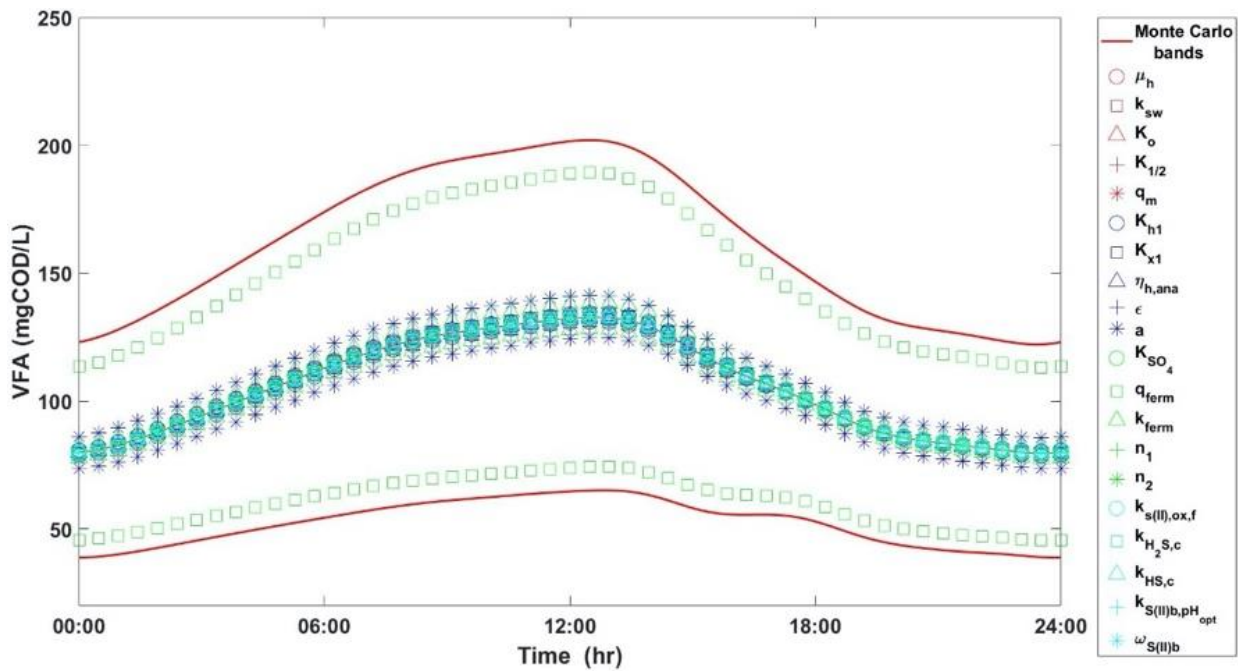
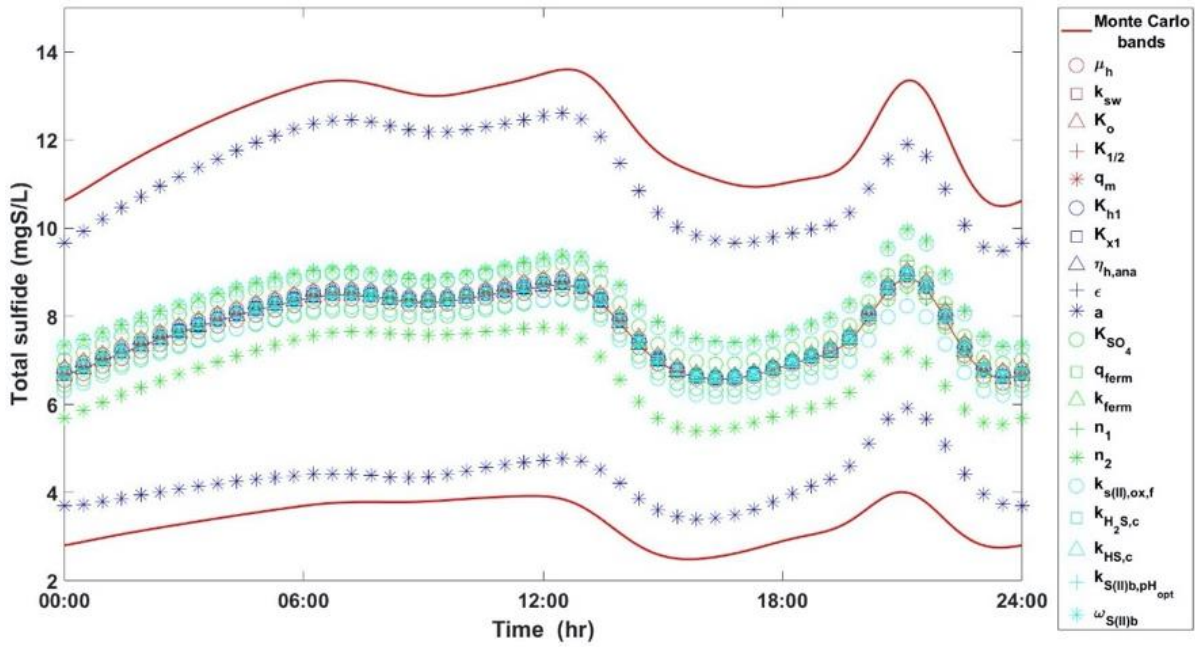


**Figure 3-4: Graphical representation of the sensitivity of the predicted time-series of VFA concentration at the outlet for selected model parameters**





(c)

**Figure 3-5: Graphical representation of the sensitivity of the predicted time-series of total sulfide concentration at the outlet for selected model parameters**

### 3.3.2.2 Standardized linear regression (SRC)

Three multivariate linear models are fitted using linear regression (implemented in MATLAB) for the averaged concentrations of sCOD, VFA, and total sulfide at the sewer outlet. The fitted models can reasonably reproduce the time-averaged output of the Monte Carlo simulations as depicted in Figs. 3-6 to 3-8. The figures show a comparison between the probability distribution of the Monte Carlo simulations and the fitted model outputs where clear overlap is obtained except some differences (blue and orange part of the bars illustrate higher probability by the Monte Carlo simulations and by the fitted models, respectively). This is illustrated by the determination coefficient reported in Table 3-2 for each of the model outputs where  $R^2 > 0.9$  for all the outputs. This indicates that linear effect of parameter variability could account for the majority of average output variation. The regression coefficients,  $\beta_i$ , can be used to evaluate the contribution of each of the model parameters on the overall variance. Furthermore, the condition of the standardized

regression coefficients  $\sum_i (\beta_i)^2 \approx 1$  is generally satisfied, as shown in the last row of Table 3-2. The parameters that show the greatest influence ( $|\beta_i| > 0.1$ ) on the model output hence highest sensitivity and contribution in the overall variance can be deduced from Table 3-2. The SRC results support the results obtained from the graphical representation, where the parameters that have the most important influence on the results of the model are the same, namely,  $k_{hl}$ ,  $k_{xl}$ ,  $\eta_{h,ana}$ ,  $q_{ferm}$ , and  $a$  are the most influential parameters in the model. Further to this, the sign of the standardized regression coefficients indicates the direction of the influence of the parameter on the model output while the magnitude reflects the strength of the parameter effect.

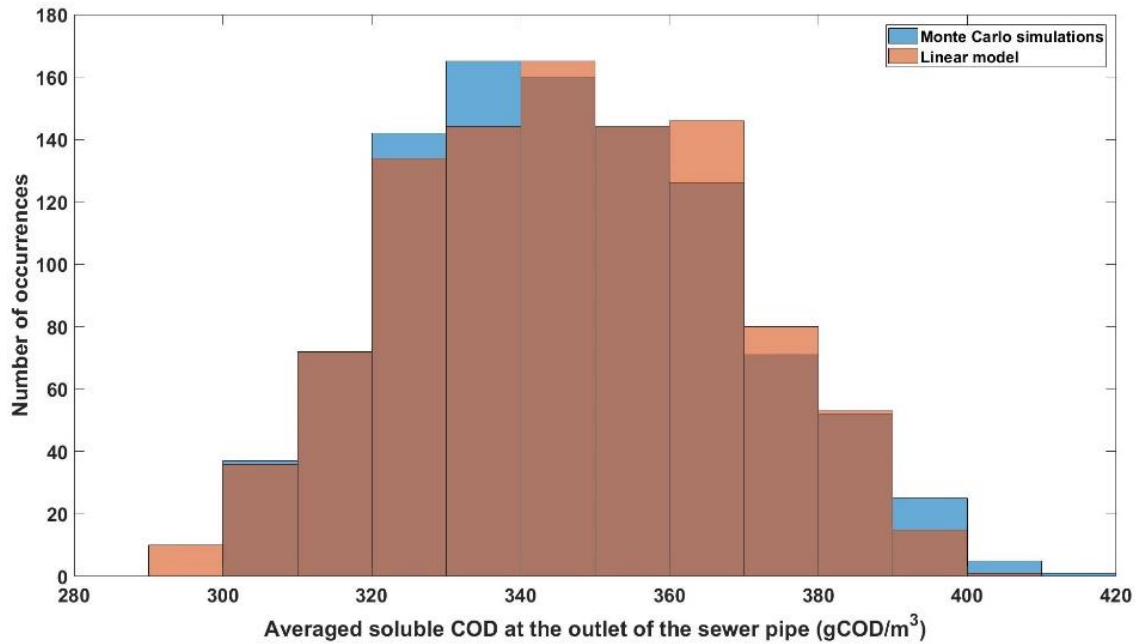


**Figure 3-6: Histogram for the time-averaged Monte Carlo output compared with the fitted linear multivariate model for soluble COD**

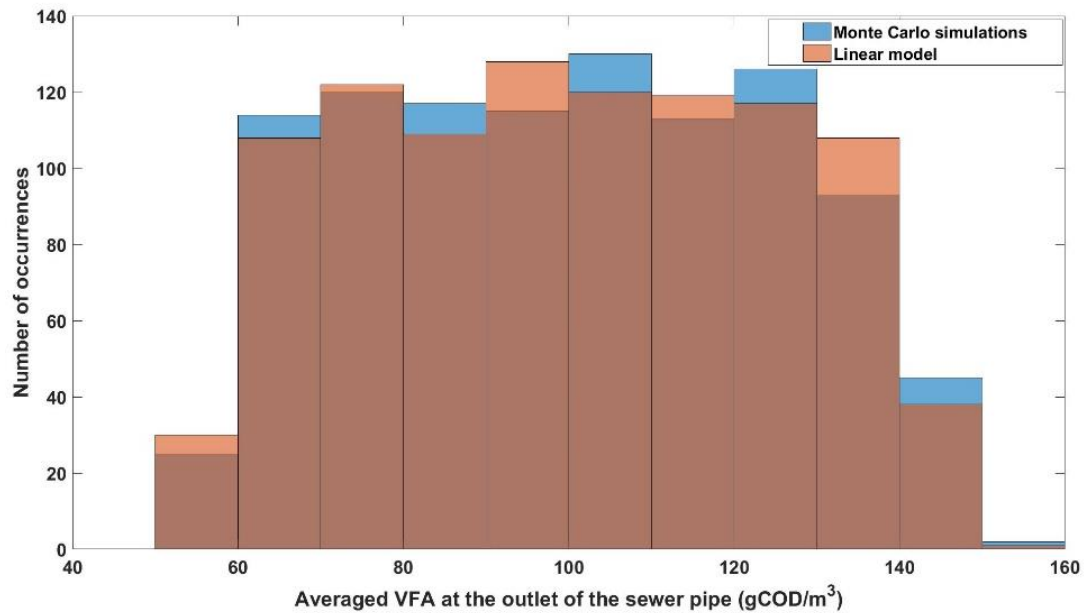


**Figure 3-7: Histogram for the time-averaged Monte Carlo output compared with the fitted linear multivariate model for VFA**

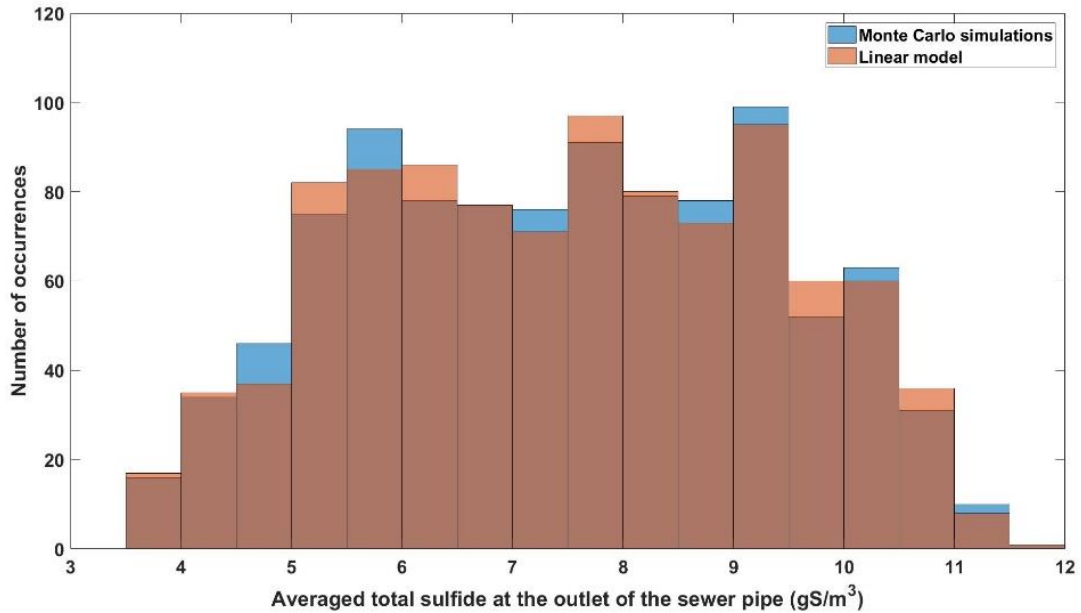


**Figure 3-8: Histogram for the time-averaged Monte Carlo output compared with the fitted linear multivariate model for total sulfide**

**Table 3-2: Standardized regression coefficients for linear models of soluble COD, VFA, and total sulfide with the determination coefficients (R<sup>2</sup>) for each model. The values in bold are those with the most significant effects on the model outputs**

Parameter	Soluble COD		VFA		Total sulfide	
R <sup>2</sup>	<b>0.974</b>		<b>0.981</b>		<b>0.981</b>	
	Estimate	p-Value	Estimate	p-Value	Estimate	p-Value
$\mu_H$	-0.050	0.000	-0.023	0.000	0.035	0.000
$K_{sw}$	-0.001	0.859	0.000	0.913	-0.003	0.086
$K_o$	0.002	0.678	-0.006	0.148	-0.015	0.000
$K_{sf}$	-0.012	0.018	-0.005	0.234	-0.001	0.672
$K_{1/2}$	-0.007	0.176	0.001	0.739	0.004	0.025
$q_m$	-0.004	0.470	-0.005	0.266	0.005	0.003
$K_{h1}$	<b>0.773</b>	<b>0.000</b>	0.038	0.000	-0.001	0.578
$K_{x1}$	<b>-0.299</b>	<b>0.000</b>	-0.013	0.003	0.000	0.968
$\eta_{h,ana}$	<b>0.361</b>	<b>0.000</b>	0.000	0.929	-0.002	0.269
$\varepsilon$	0.045	0.000	0.063	0.000	-0.001	0.740
$a$	<b>-0.340</b>	<b>0.000</b>	<b>-0.161</b>	<b>0.000</b>	<b>0.953</b>	<b>0.000</b>
$K_{so4}$	0.035	0.000	0.019	0.000	-0.091	0.000
$q_{ferm}$	0.005	0.323	<b>0.970</b>	<b>0.000</b>	0.001	0.726
$K_{ferm}$	0.006	0.274	-0.067	0.000	0.001	0.446
$n_1$	0.003	0.565	0.002	0.729	-0.035	0.000
$n_2$	0.002	0.642	-0.003	0.447	<b>0.240</b>	<b>0.000</b>
$K_{S(II)ox}$	-0.003	0.587	-0.002	0.629	<b>-0.151</b>	<b>0.000</b>
$K_{H2S,c}$	0.002	0.746	-0.002	0.612	0.001	0.627
$K_{HS,c}$	0.001	0.920	0.003	0.481	-0.001	0.494
$K_{S(II),b,pH,opt}$	0.002	0.690	-0.002	0.612	-0.026	0.000
$\Omega_{S(II)b}$	-0.001	0.804	0.007	0.109	0.000	0.973
$\sum \beta_i^2$	0.977		0.977		1.001	

Improvement of the model accuracy can be obtained by reducing the uncertainty of these parameter values. The uncertainty reduction required for the model parameters, in order to achieve a specific reduction in variance in the model outputs, can be quantified (Sin et al. 2011). Therefore, the most influential parameters should be studied in more detail, with more lab experiments being conducted to reduce the uncertainty of the overall model. For instance, the sulfide production rate constant,  $a$ , is emphasized to be the most influential parameter on the model as it significantly affects all the outputs of the model

as illustrated from the graphical and analytical results. Thus, special attention should be drawn to get an accurate value of this parameter.

### 3.3.3 CFD Model Results

First, the influence of the homogenization of the surface reactions in the biofilm is studied using the CFD model. Three simulations of the biochemical conversions along with the flow field in the sewer pipe were conducted using different values of  $a$ . The upper and lower limits of the  $a$  variation range used in the Monte Carlo simulation are used along with best fit value obtained from the calibration using Weighted Sum of Squared Errors (WSSE) criteria, which is  $a = 0.0032 \text{ gS}^{0.5} \text{ m}^{-0.5} \text{ h}^{-1}$ . The mass-weighted average of the concentrations of the simulated species are monitored at the outlet of pipe and plotted in Figs. 3-9 to 3-11. The 1-D model simulations for the same parameter set are plotted on the same figures to compare between the outputs of the two models. The comparison shows that similar variation of the results of the CFD model is obtained as that of the 1-D CSTR-in-series model structure. It is obvious that CSTR-in-series model tends to smear out the high dynamic variation in the inlet concentration. This is could be explained by the fact that the CFD model is, in general, better in modelling the advection and diffusion influence than the 1-D CSTR-in-series model. However, the mean values of the different concentrations predicted by the CFD model and 1-D CSTR-in-series model are similar. Thus, the detailed modelling of the surface reactions in the case of pipe flow shows that the approximation used in the process model of the homogenization of the surface reactions is acceptable in this case. However, this cannot be generalized for all segments of the sewer network and other surface reactions in the biological treatment stages in WWTP. The CFD model demonstrated herein could be used in such cases to determine whether or not the heterogeneous nature of the reactions is important to take into account or whether a homogenized CSTR-in-series model is acceptable. Moreover, the dynamic response of the 1-D CSTR-in-model could be examined using the CFD model to ensure that the variation is in the design limit of the chemical treatment dosing of sewer systems.

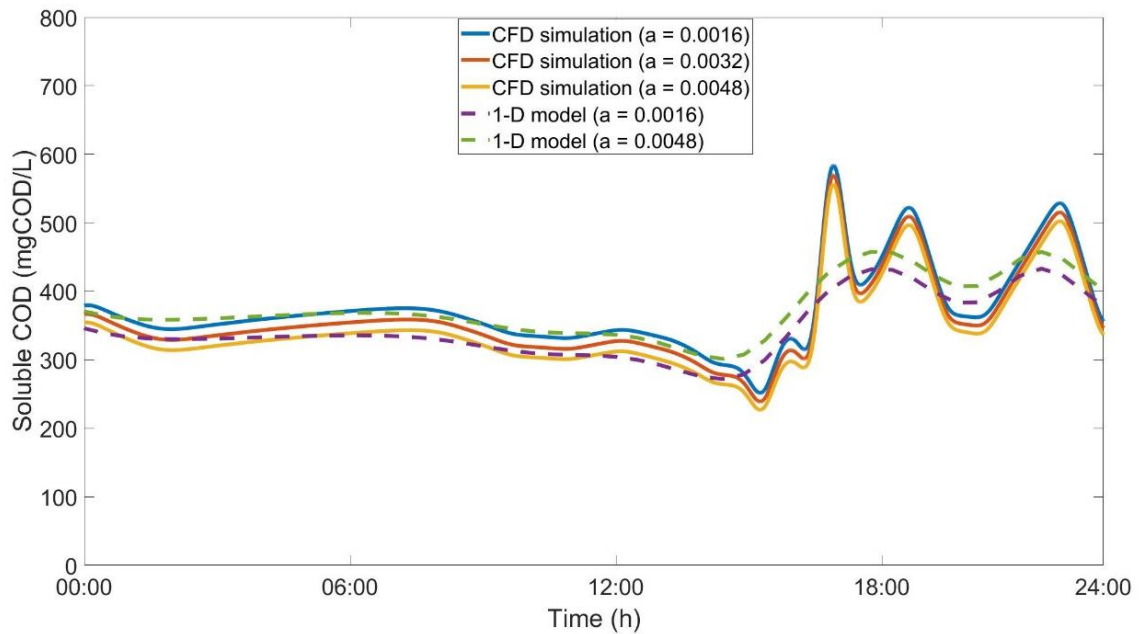


**Figure 3-9: Plots of mass-weighted average at pipe outlet of the CFD model vs 1-D model of soluble COD concentration at the outlet**

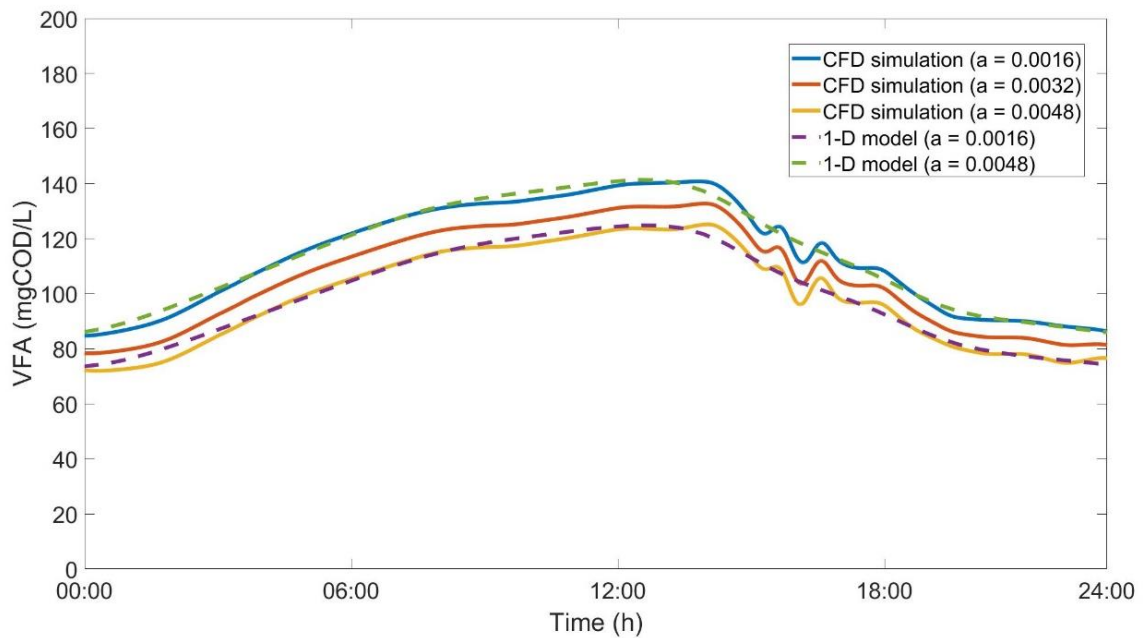


**Figure 3-10: Plots of mass-weighted average at pipe outlet of the CFD model vs 1-D model of VFA concentration at the outlet**

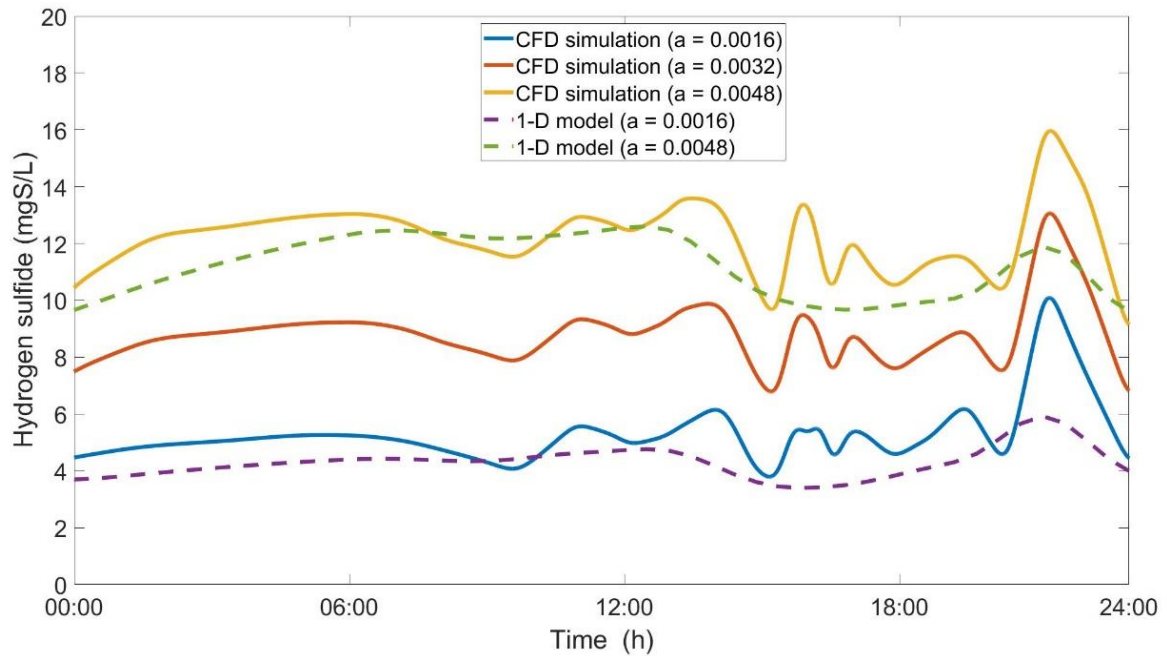


**Figure 3-11: Plots of mass-weighted average at pipe outlet of the CFD model vs 1-D model of total sulfide concentration at the outlet**

Figure 3-12a shows the spatial distribution of the total COD at a pipe cross section at the middle of the simulated pipe. It is clear that because of the settling of the particulate COD, higher concentration is noticed at the bottom of the pipe. However, the variation of the total COD is not significant across the cross section of the pipe, such that the completely mixed assumption of the 1-D CSTR-in-series model is deemed to be acceptable. The same can be observed from the sCOD contours where in Fig. 3-12b, due to the utilization of the sCOD by the sulfate reduction bacteria (SRB) in the biofilm, higher utilization rate is observed near the wall. Therefore, lower concentration of the sCOD is near the wall. However, the variation of the sCOD concentration across the cross section of the pipe is negligible this due to the diffusion of the soluble matters and the hydrolysis process which compensates for the sCOD consumption by the SRB. Since the production of sulfide is mainly at the wall, slightly higher sulfide concentration was noticed near the wall. However, due to diffusion, this difference between the sulfide concentration at wall and in the bulk water is negligible.

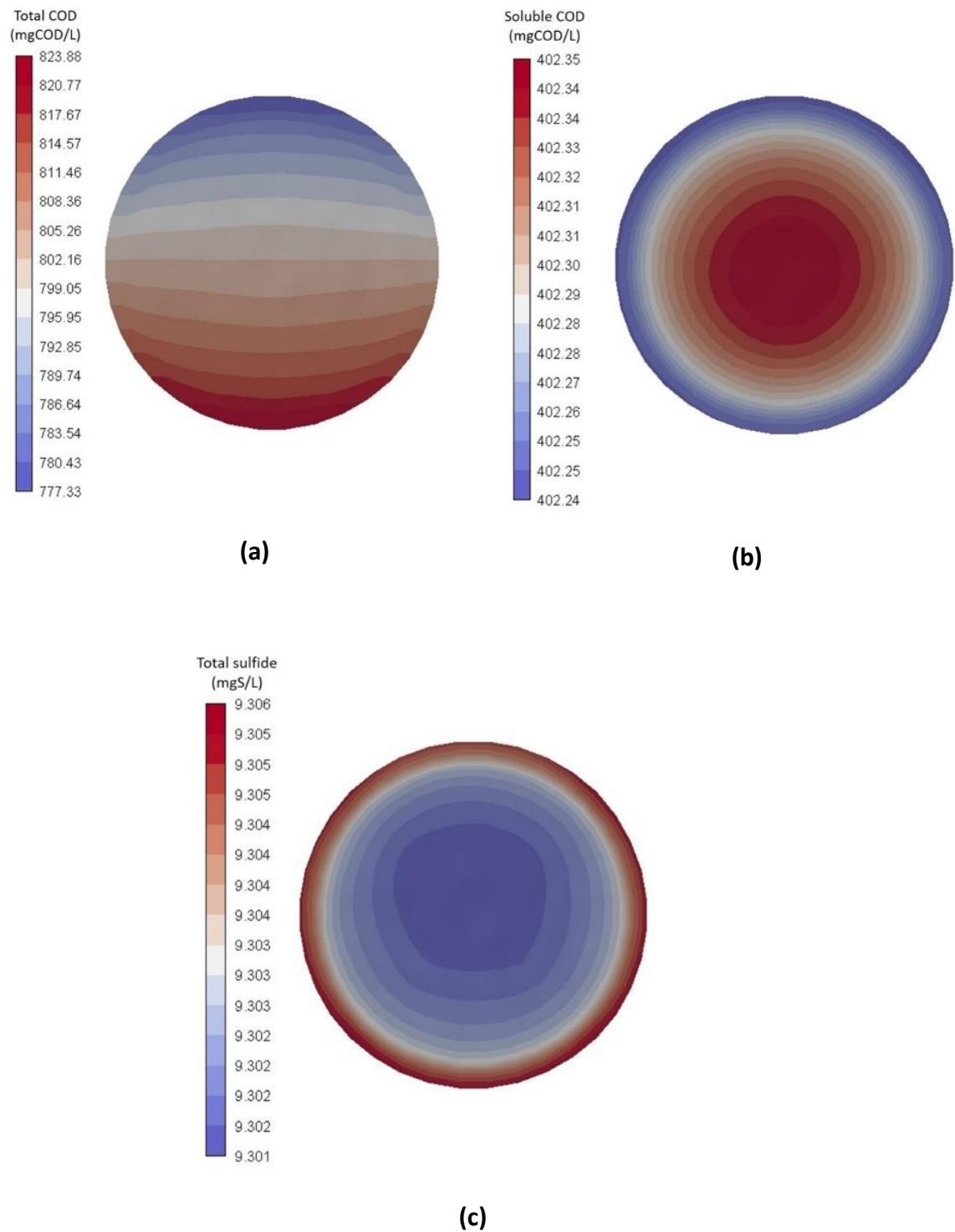


**Figure 3-12: Contour plots of the concentrations of (a) total COD (mgCOD/L), (b) soluble COD (mgCOD/L), and (c) total sulfide (mgS/L) for a cross-section of the pipe halfway between the inlet and outlet**



To assess the impact of solids settling on the model outputs, two simulations were performed: one with the solids settling term included in the CFD model and the other without considering this term. Settling of the solids does have noticeable influence on the mass-weighted average of the species concentrations if compared with the simulations that disregards the solids settling (results not shown). This indicates that the solids settling for the low solids concentration in the sewer may not have a significant influence on the overall simulation outputs in straight pipes. Again, this conclusion should not be generalized to all sewers, and this methodology can be considered as a useful tool in assessing the influence of settling for other operating conditions as well. For example, the case of intermittent flow is not considered in this work and could result in solids settling being important.

For illustration of the effect of the solids settling on the profiles of the particulate species along the pipe length, the particulate COD profiles at different distance from the inlet are plotted in Fig. 3-13. From the figure, the concentration gradients in the radial direction are evolved from the uniform distribution assumed at the inlet (zero gradient) to more noticeable values based on the solids concentration. However, due to transient concentration of the solids at the inflow of the sewer pipe, the concentration gradient of the particulate COD is not uniform in the longitudinal direction. It is noticeable that the radial concentration gradient increases with the level of the solids concentration as described in Eq. 3.8.

In conclusion, the influence of the detailed modelling of the solids settling and chemical and biological reactions heterogeneity has a marginal in the case of straight pressure sewer pipes. This could be explained by the fact that the gradients of the different species due to solids setting and heterogeneous model of the sulfide formation are low since the convection of the species in the flow direction is predominant on the distribution of the species concentrations.

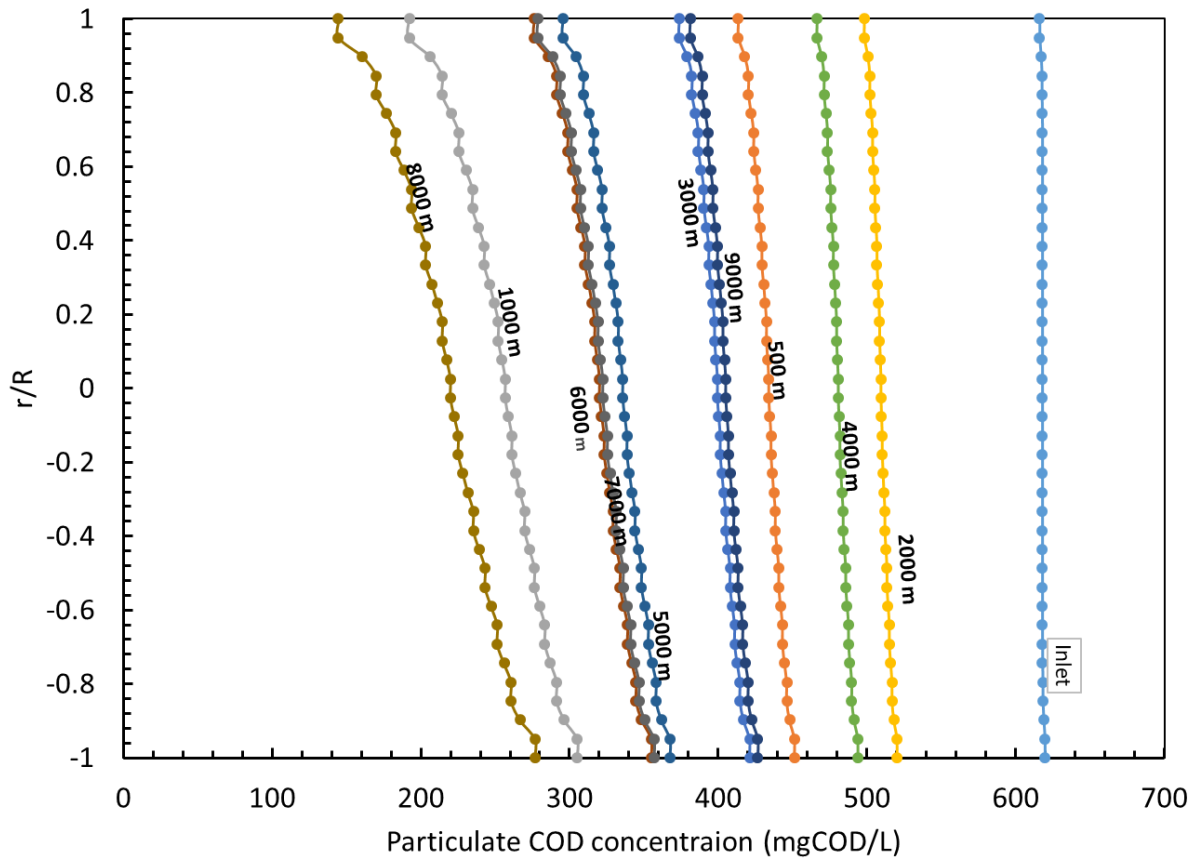


**Figure 3-13: Plot of the radial concentration profiles of particulate COD at different locations along the length of the sewer pipe**

### 3.4 Conclusions

SRC analysis of outcomes from time averaged outputs from the biochemical WATS model demonstrated that parameters could account for >90% of the output variance observed in sCOD, VFA, and total sulfides. Parameters pertaining hydrolysis, efficiency of the anaerobic processes, and sulfide production rate constant per unit area of biofilm area were the most significant predictors of these outputs. Comparison of 1-D biochemical and multidimensional CFD analysis, including settling, turbulent flow, and biochemical reactions indicated that the 1-D model was an adequate representation of the multi-dimensional model, with increased short-term time dependent behaviour in the multi-dimensional model. Further study should be conducted in more complex segments in the sewer system that could be hot spots for hydrogen sulfide production. In such

locations, it would be beneficial to assess the accuracy of the process models in predicting the hydrogen sulfide levels in light of the highly heterogeneous reactions. While CFD is not justified by improved predictive capability in output values for the case considered, it provides mechanistic analysis into the way that sedimentation, reaction, and hydraulic processes can interact.

### 3.5 References

- Bjerre, H. L., Hvitved-Jacobsen, T., Teichgräber, B., & Schlegel, S. (1998). Modeling of aerobic wastewater transformations under sewer conditions in the Emscher River, Germany. *Water environment research*, 70(6), 1151-1160.
- Brun, R., Kühni, M., Siegrist, H., Gujer, W., & Reichert, P. (2002). Practical identifiability of ASM2d parameters—systematic selection and tuning of parameter subsets. *Water research*, 36(16), 4113-4127.
- Calabro, P. S., Mannina, G., & Viviani, G. (2009). In sewer processes: mathematical model development and sensitivity analysis. *Water science and technology*, 60(1), 107-115.
- Carrera, L., Springer, F., Lipeme-Kouyi, G., & Buffiere, P. (2016). A review of sulfide emissions in sewer networks: overall approach and systemic modelling. *Water Science and Technology*, 73(6), 1231-1242.
- Cosenza, A., Mannina, G., Vanrolleghem, P. A., & Neumann, M. B. (2013). Global sensitivity analysis in wastewater applications: A comprehensive comparison of different methods. *Environmental modelling & software*, 49, 40-52.
- Cosenza, A., Mannina, G., Vanrolleghem, P. A., & Neumann, M. B. (2014). Variance-based sensitivity analysis for wastewater treatment plant modelling. *Science of the Total Environment*, 470, 1068-1077.
- Flores-Alsina, X., Corominas, L., Neumann, M. B., & Vanrolleghem, P. A. (2012). Assessing the use of activated sludge process design guidelines in wastewater treatment plant projects: A methodology based on global sensitivity analysis. *Environmental Modelling & Software*, 38, 50-58.
- Guisasola, A., Sharma, K. R., Keller, J., & Yuan, Z. (2009). Development of a model for assessing methane formation in rising main sewers. *Water Research*, 43(11), 2874-2884.

- Gujer, W et al. 1995. “The Activated Sludge Model No. 2: Biological Phosphorus Removal.” *Water science and technology* 31(2): 1–11.
- Guo, Lisha et al. 2018. “Model-Based Management and Control of the Bioreactions in a Collection System.” *Proceedings of the Water Environment Federation* 2018(13): 2700–2708.
- Guo, L., Tik, S., Ledergerber, J. M., Santoro, D., Elbeshbishy, E., & Vanrolleghem, P. A. (2019). Conceptualizing the sewage collection system for integrated sewer-WWTP modelling and optimization. *Journal of hydrology*, 573, 710-716.
- Gutierrez, O., Park, D., Sharma, K. R., & Yuan, Z. (2009). Effects of long-term pH elevation on the sulfate-reducing and methanogenic activities of anaerobic sewer biofilms. *Water research*, 43(9), 2549-2557.
- Helton, J. C., and F. J. Davis. 2003. “Latin Hypercube Sampling and the Propagation of Uncertainty in Analyses of Complex Systems.” *Reliability Engineering and System Safety* 81(1): 23–69.
- Henze, M et al. 1987. “Activated Sludge Model No. 1. Scientific and Technical Report No. 1.” *London, UK: IAWPRC*.
- Hvitved-Jacobsen, T., Vollertsen, J., & Nielsen, P. H. (1998). A process and model concept for microbial wastewater transformations in gravity sewers. *Water Science and Technology*, 37(1), 233-241.
- Hvitved-Jacobsen, T., Vollertsen, J., & Tanaka, N. (1999). Wastewater quality changes during transport in sewers—an integrated aerobic and anaerobic model concept for carbon and sulfur microbial transformations. *Water science and technology*, 39(2), 233-249
- Hvitved-Jacobsen, T., Vollertsen, J., & Nielsen, A. H. (2013). *Sewer processes: microbial and chemical process engineering of sewer networks*. CRC press.
- Lakehal, D., Krebs, P., Krijgsman, J., & Rodi, W. (1999). Computing shear flow and

- sludge blanket in secondary clarifiers. *Journal of Hydraulic Engineering*, 125(3), 253-262.
- Minami, K., & Takata, K. (1997). Atmospheric methane: sources, sinks, and strategies for reducing agricultural emissions. *Water Science and Technology*, 36(6-7), 509-516.
- Mohanakrishnan, J., Gutierrez, O., Sharma, K. R., Guisasola, A., Werner, U., Meyer, R. L., ... & Yuan, Z. (2009). Impact of nitrate addition on biofilm properties and activities in rising main sewers. *Water research*, 43(17), 4225-4237.
- Nielsen, A. H., Vollertsen, J., & Hvitved-Jacobsen, T. (2003). Determination of kinetics and stoichiometry of chemical sulfide oxidation in wastewater of sewer networks. *Environmental science & technology*, 37(17), 3853-3858.
- Nielsen, A. H., Hvitved-Jacobsen, T., & Vollertsen, J. (2005). Kinetics and stoichiometry of sulfide oxidation by sewer biofilms. *Water Research*, 39(17), 4119-4125.
- Nielsen, A. H., Vollertsen, J., & Hvitved-Jacobsen, T. (2006). Kinetics and stoichiometry of aerobic sulfide oxidation in wastewater from sewers—Effects of pH and temperature. *Water environment research*, 78(3), 275-283.
- Patziger, M., & Kiss, K. (2015). Analysis of suspended solids transport processes in primary settling tanks. *Water Science and Technology*, 72(1), 1-9.
- Pomeroy, R. D., & Parkhurst, J. D. (1978, January). The forecasting of sulfide build-up rates in sewers. In *Eighth International Conference on Water Pollution Research* (pp. 621-628). Pergamon.
- Rootsey, R., & Yuan, Z. (1989). SEWER CORROSION & ODOUR RESEARCH (SCORE) PROJECT—DELIVERING OUTCOMES TO THE WATER INDUSTRY. *Development*.
- Saltelli, A., Ratto, M., Andres, T., Campolongo, F., Cariboni, J., Gatelli, D., ... & Tarantola, S. (2008). *Global sensitivity analysis: the primer*. John Wiley & Sons.

- Sharma, K. R., Yuan, Z., de Haas, D., Hamilton, G., Corrie, S., & Keller, J. (2008). Dynamics and dynamic modelling of H<sub>2</sub>S production in sewer systems. *Water Research*, 42(10-11), 2527-2538.
- Sin, G., Gernaey, K. V., Neumann, M. B., van Loosdrecht, M. C., & Gujer, W. (2009). Uncertainty analysis in WWTP model applications: a critical discussion using an example from design. *Water Research*, 43(11), 2894-2906.
- Sin, G., Gernaey, K. V., Neumann, M. B., van Loosdrecht, M. C., & Gujer, W. (2011). Global sensitivity analysis in wastewater treatment plant model applications: prioritizing sources of uncertainty. *Water research*, 45(2), 639-651.
- Sin, G., De Pauw, D. J., Weijers, S., & Vanrolleghem, P. A. (2008). An efficient approach to automate the manual trial and error calibration of activated sludge models. *Biotechnology and bioengineering*, 100(3), 516-528.
- Takács, I., Patry, G. G., & Nolasco, D. (1991). A dynamic model of the clarification-thickening process. *Water research*, 25(10), 1263-1271.
- Tanaka, N., & Hvitved-Jacobsen, T. (2002). Anaerobic transformations of wastewater organic matter and sulfide production—investigations in a pilot plant pressure sewer. *Water science and technology*, 45(3), 71-79.
- Teuber, K. (2020). A three-dimensional two-phase model for flow, transport and mass transfer processes in sewers (Doctoral dissertation, TU Berlin University, Berlin, Germany).
- Hvitved-Jacobsen, T., Vollertsen, J., & Matos, J. S. (2002). The sewer as a bioreactor—a dry weather approach. *Water Science and technology*, 45(3), 11-24.
- Yongsiri, C., T. Hvitved-Jacobsen, J. Vollertsen, and N. Tanaka. 2003. “Introducing the Emission Process of Hydrogen Sulfide to a Sewer Process Model (WATS).” *Water Science and Technology* 47(4): 85–92.

## Chapter 4

### 4 Numerical study of the nitrate dosing in lab-scale experiment of sewer system

Hydrogen sulfide and methane production in sewer systems is a serious problem that has various negative consequences. Nitrate dosing is one of the most common methods that is used to alleviate the sulfide levels in sewers. The optimal Nitrate dosing rate and location is investigated in a lab-scale experiment at the Greenway wastewater treatment plant (WWTP), in London, Ontario. This plant treats the wastewater for nearly 50% of the city. This chapter is directed towards developing a simple mathematical model that can be used in developing experimental plans for the lab-scale reactor by testing scenarios using the model prior to experimentation. The mathematical model is calibrated and validated using measurement data from the experiment without and with nitrate dosing. Then, the model was used to investigate several possibilities of the dosing position and rate. Recommendations for the current dosing strategy were drawn and possible modifications were proposed.

#### 4.1 Introduction

The sewer system is an essential infrastructure component in urban environments, primarily tasked with collecting and conveying produced sewage waste to wastewater treatment plants (WWTP). Sewer networks suffer from a common problem of hydrogen sulfide and methane formation, each by different microorganism populations, since the formation of both species is favorable in the same redox potential levels. Since the retention time is relatively short for biomass growth in the bulk water phase, biofilm developed on the inner walls as well as sediments formed at the bottom of the pipes are the most common environments for bacteria to accumulate and develop. Hydrogen sulfide is produced by sulfate-reducing bacteria (SRB) accumulated in the biofilm developed in pressure mains (Sharma et al., 2008) and solids sediments in gravity mains (Liu et al., 2015). SRB use sulfate as the electron acceptor through the anaerobic respiration process. Emission of hydrogen sulfide from the liquid phase and oxidization to sulfuric acid on the inner walls of the sewer pipes leads to pipes corrosion which



requires expensive maintenance. In addition, hydrogen sulfide released to the environment causes odor nuisance and has a harmful effect on human health because of its toxicity (Carrera et al., 2016). Meanwhile, methane is produced as a product of the methanogenic archaea (MA) metabolism (Guisasola et al., 2009). Methane contributes significantly to the overall greenhouse gas emissions from wastewater management (Liu et al., 2015). Furthermore, it is an explosive gas if mixed with air even at low concentration (Guisasola et al., 2009).

Several strategies have been developed to overcome the problem of hydrogen sulfide formation. These strategies range from simple mechanical cleaning of the biofilm and sediments to prevent the accumulation of the SRB (Saracevic et al., 2007) to strategies involving dosing of chemicals at certain points in the sewer network (Ganigue et al., 2011). For example, injecting alkalis to elevate the pH level in the sewer reduces the mass transfer of hydrogen sulfide from the liquid to gas phase, thereby reducing the oxidation to sulfuric acid and the subsequent corrosion (Ganigue et al., 2011). Another strategy is to dose metal salts, such as iron salts, which react with sulfide and remove it by precipitation (Zhang et al., 2009). The most common chemicals used are nitrate and oxygen to oxidize the produced sulfide and methane. However, the high solubility of nitrate salts gives an advantage to the use of nitrate over oxygen as the oxidant (Gutierrez et al., 2010). This advantage makes the optimization of the oxidant dosing more flexible in terms of solution concentration, rate, and position of dosing in the sewer system.

Oxidation of sulfide in the presence of oxygen is mainly a biological process. It was indicated in the work of Mora et al. (2016) that chemical oxidation by oxygen is negligible if compared with the biological oxidation rates. Moreover, it was reported that thiosulfate is main product of the aerobic chemical sulfide oxidation. On the other hand, thiosulfate and elemental sulfur are intermediate products of the biological oxidation by oxygen before further oxidation to sulfate. Nielsen et al. (2006) reported that 95% of the sulfide oxidation by oxygen is biological.

Biochemical conversions in nitrate-receiving wastewater has been studied in several works in the literature. Deep investigation on how nitrate prevents the accumulation of

sulfide in the sewer system was conducted by Mohanakrishnan et al. (2009) and Liu et al. (2015). Biological oxidation of sulfide was attributed to the activity of the biomass in the biofilm (Mohanakrishnan et al., 2009). It was concluded that the nitrate-reducing sulfide-oxidizing bacteria (NR-SOB) are responsible for oxidizing the produced sulfide in the biofilm. Another mechanism that was suggested is that the development of heterotrophic nitrate reducing bacteria (hNRB) in the biofilm compete with the SRB for the available organic carbon (Ganigue et al., 2011; Zhang et al., 2008). Moreover, nitrate was found not to have long-term inhibitory influence on the sulfide formation, even after long exposure time.

Sulfide oxidation steps were studied in the work of Jiang et al. (2009). It was illustrated that the sulfide oxidation by nitrate takes place over two steps. First, oxidation of sulfide to elemental sulfur occurs. Then, elemental sulfur is further oxidized to sulfate at slower rate. Accumulated elemental sulfur in the biofilm could be a source of sulfide if reduced in the anaerobic regions of the biofilm or the depletion of nitrate in the bulk liquid phase (Auguet et al. 2015). However, the measured rates of sulfide oxidation were 20-30 times the reduction rate of sulfate and elemental sulfur back to sulfide. This difference in oxidation and reduction rates is favorable for controlling the sulfide concentration in the sewer system by nitrate dosing. Jiang et al. (2013) suggested that after a short adaptation period for the microorganisms in the biofilm, four different processes take place simultaneously in three distinct stratified layers in the biofilm. These processes include sulfide oxidation, nitrate reduction, sulfate production, and methane production. The competition between the different microorganisms for the soluble COD (sCOD) determines the depth of the existence for each species.

Several dosing concentrations and strategies have been studied in literature (Bentzen et al., 1995; Rodríguez-Gómez et al., 2005; Saracevic et al., 2007). Gutierrez et al. (2010) tested seven scenarios of nitrate dosing in a lab-scale sewer system. The study revealed the importance of choosing an effective nitrate dosing strategy to control the sulfide levels at the system discharge. Two principal parameters were emphasized to control the nitrate dosing. These parameters are the dosing position and the rate of nitrate dosing. It was recommended that nitrate dosing to be in proportion to the hydraulic retention time

(HRT) of the sewage. Moreover, dosing should be in a position near to the discharge point (or the sulfide-controlled point in the system) such that sulfate oxidizing bacteria have adequate time to consume all the sulfide formed upstream. Due to the intermittent flow rate in the sewer systems, anaerobic and anoxic conditions could alternate based on the retention time of the sewage and the sulfide concentration levels (Jiang et al., 2009). Therefore, synchronizing nitrate dosing with the HRT of the sewage in the system is crucial to avoid excess dosing of nitrate, which would consequently reach the WWTP at high concentration.

Modelling of biochemical conversions in sewer systems is beneficial in predicting the “hot spots” of hydrogen sulfide production and planning for treatment location and strategies (Vollertsen et al., 2011). In the early stages of modelling sulfide formation in sewer systems, several empirical models have been proposed to predict sulfide concentration as a function of the organic strength of the wastewater, sewer pipe characteristics, flow rate, and temperature (Boon, 1975; Pomeroy and Parkhurst, 1978). Hvitved-Jacobsen et al. (2000) developed the Wastewater Aerobic/Anaerobic Transformations in Sewer (WATS) model that considers the carbon and sulfur cycles in more detail. Further improvement on the WATS model have been proposed to model the oxygen concentration (Gudjonsson et al., 2002), anoxic processes (Abdul-Talib et al., 2005), sulfide emission from the liquid to gas phase (Yongsiri et al., 2003) and sulfide oxidation by oxygen (Nielsen et al., 2005; Nielsen et al., 2006). More recently, the SeweX model was developed by (Sharma et al., 2008) to model the dynamic conversions of carbon, nitrogen, and sulfur in the sewer environment under aerobic, anaerobic, and anoxic conditions, resulting in good predictions of the sulfide concentration. This model was extended by Guisasola et al. (2009) to include the production of methane by modelling the competition between SRB and MA in the biofilm. Moreover, in order to include the long-term influence on the production rate of sulfide and methane, Sun et al. (2018) proposed an empirical relation, using a detailed and validated model, to predict the sulfide and methane production rates as function of sCOD and sulfate.

In the current work, a mathematical model based on the WATS model is developed by considering sulfide oxidation by nitrate in addition to methane production. The model is

calibrated and validated by data collected from a lab-scale system that is composed of four reactors in series that are intended to mimic the HRT of a real pressurized sewer pipe. Then, the model was used to study the strategy of nitrate dosing in the reactors in order to achieve complete oxidation of sulfide with minimal nitrate residual in the effluent flow from the last reactor.

## 4.2 Material and methods

### 4.2.1 Experiment setup

A lab-scale system was used to mimic the biochemical conversions in the sewer system as illustrated in Fig. 4-1. The system consists of four air-sealed reactors designated as R1 to R4 that are connected in series. The volume of each reactor is 1.5 L with an internal diameter of 110 mm. Internal biofilm carriers were inserted from the lid of each reactor to increase the area available for the biofilm growth. The total biofilm area in the reactor, including the reactor internal wall and surface area of the carriers, is 0.085 m<sup>2</sup> (area to volume ratio,  $A/V = 56.7 \text{ m}^2/\text{m}^3$ ). Magnetic stirrers and recirculating pumps were installed as well to ensure that the content is homogeneous with minimum settling of solids. The reactors were totally covered by aluminum foil to prevent exposing the biofilm and sewage to light. This design was first proposed by (Guisasola et al., 2008). However, the system has some limitations to perfectly mimic the biochemical conversions in a real pipe. These limitations are due to differences from the real system such as shear stress applied on the developed biofilm on the walls, higher A/V, settling of some solids in the first reactors due to imperfect mixing and insufficient number of reactors to mimic the plug flow in the real sewer pipe.

The system was running in Greenway wastewater facility located in London, Ontario, Canada. Raw wastewater was weekly collected from the Oxford pollution pant, London, Ontario wastewater treatment plant because it has a low concentration of iron, as compared to the Greenway plant. This is to ensure the experiments are not significantly affected by other treatments applied by the plants. Raw wastewater was stored in a cold room at 4 °C to minimize the microbial activities. A feeding tank to the reactors with a mixing pump was installed to ensure complete mixing of the solids and to prevent

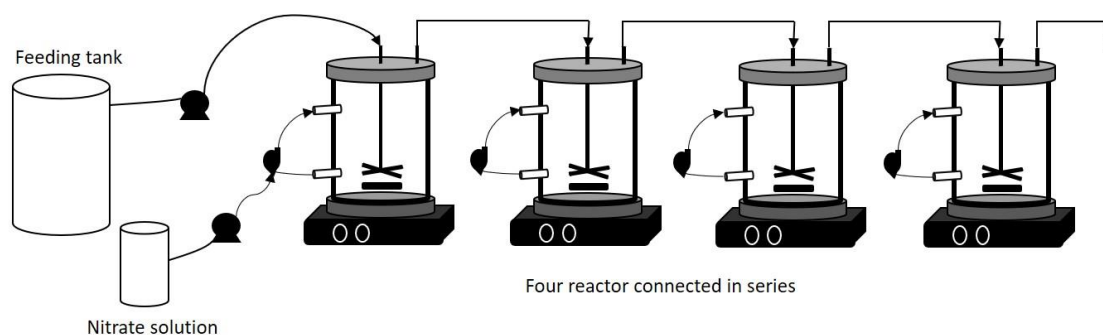


**Figure 4-1: Schematic of the lab-scale system**

settling. Influent and effluent samples were characterized using HACH methods and kits: chemical oxygen demand (total COD and sCOD), total nitrogen (TN), soluble nitrogen (SN), ammonia-N ( $\text{NH}_4\text{-N}$ ), and volatile fatty acids (VFA) (HACH Odyssey DR/2500 spectrophotometer manual). Total sulfide, sulfate, and ferrous/ferric iron were measured using (DR900 multiparameter portable colorimeter).  $1.2\ \mu\text{m}$  filter papers were used for VSS and TSS analysis (APHA 2005). Soluble parameters were determined by filtration through  $0.45\ \mu\text{m}$  filter papers (VWR International, Mississauga Ontario, Canada).

A Peristaltic pump was used to feed the system with sewage intermittently (average of 30 minutes per hour in the daytime and 20 minutes per hour at nighttime, for a total of 10 hours per day) following the typical pumping system in real sewers. HRT variation of the sewage in the system varies with the pumping events. The pump is programmed to run at the top of the hour for a duration that varies from 16 to 31 minutes, where the short running durations were scheduled after midnight to 6:00 am.

#### 4.2.2 Developing biofilm and nitrate dosing

The system was running for several months to develop the biofilm on the walls and carriers until the quasi steady-state performance was reached. The average concentration of sulfide produced was  $10.4 \pm 1.4\ \text{mgS/L}$ . After reaching steady state, dosing of nitrate at a concentration of  $1500\ \text{mgNO}_3\text{/L}$  was commenced in the first reactor in the line for three months.

### 4.2.3 System hydrodynamics

Two tracer tests were conducted using sodium chloride (NaCl) as a tracer. Two tracer tests were conducted using two different concentrations of sodium chloride in raw sewage. The two concentrations correspond to conductivity of 12 and 6.2 mS/cm of the sewage that were fed to the system during the test as a step input. The peristaltic pump was running on the programmed schedule for the system feeding. The conductivity of the feeding sewage and background conductivity of the sewage without sodium chloride were measured. Then, the conductivity probe was installed at the effluent of the system to measure and store the data continuously. Each test was run for 24 hours with the continuous conductivity measurement using Hach HQ40d portable conductivity meter.

### 4.2.4 Data for the mathematical model calibration/validation

For the calibration and validation of the biochemical model, samples from the effluent were collected every 10 minutes for 2 hours during the normal operation without nitrate dosing. These data were used for the calibration of the anaerobic processes in the model. Then, batch tests were conducted in the last reactor by turning off the feeding pump and isolating the reactor from the system. The recirculating pumping and the magnetic stirrer provided gentle mixing to the content of the reactor during the batch test. A nitrate solution was dosed in the reactor to have initial concentration of 50 mgNO<sub>3</sub>-N/L. Samples were drawn from the reactor for 2 hours and were analysed for sulfide and nitrate. Sulfide oxidation and nitrate reduction processes in the biochemical model were calibrated using the collected data.

### 4.2.5 Biochemical mathematical model

A mathematical model was developed based on the WATS model framework, with additional processes added to better predict the consumption of the sCOD and the anoxic oxidation of sulfide. Figure 4-2 depicts a diagram of the biochemical reactions included in the model (details of the model reactions are illustrated in Tables (4-2 and 4-3). Methane production kinetics were adopted from the work of Guisasola et al., 2009 and Sun et al., 2018 to consider the competition with the SRB, hence better modelling the sCOD concentration. The kinetics parameter values reported in the literature are used in

the current model. Moreover, the anoxic oxidation mechanism and the associated kinetic parameters are adopted from the work of Jiang et al. (2009). The key processes added to the basic WATS model are illustrated in Table (4-1). The reaction rates (first term in each expression) are denoted  $K$  with subscript according to the processes listed in the leftmost column. Moreover,  $K_O$ ,  $K_{NO3}$ ,  $K_{VFA,MB}$ ,  $K_{SRB}$ ,  $K_{H2}$ ,  $K_{SO4}$ ,  $K_{S0}$  and  $K_{S2-}$  are the saturation constants of the Monod kinetics defined for the added processes. The state variables in the expressions are summarized in Table (4-3). The biochemical model is implemented using Matlab/Simulink for the ease of manipulation of the system configuration.

**Table 4-1: Kinetics added to the WATS model**

Process	Conditions	Kinetics
Methanogenesis using VFA	Anaerobic	$K_{CH4,acid,f} \frac{S_{VFA}}{K_{VFA,MB} + S_{VFA}} \frac{K_O}{K_O + S_O} \frac{K_{NO3}}{K_{NO3} + S_{NO3}} \left(\frac{A}{V}\right) \alpha_s^{(T-20)}$
Methanogenesis using hydrogen	Anaerobic	$K_{CH4,Hyd,f} \frac{S_{H2}}{K_{H2} + S_{H2}} \frac{K_O}{K_O + S_O} \frac{K_{NO3}}{K_{NO3} + S_{NO3}} \left(\frac{A}{V}\right) \alpha_s^{(T-20)}$
Sulfide production by sulfate reduction	Anaerobic	$K_{H2S,VFA,f} \frac{S_{VFA}}{K_{SRB} + S_{VFA}} \frac{S_{SO4}}{K_{SO4} + S_{SO4}} \frac{K_O}{K_O + S_O} \left(\frac{A}{V}\right) \alpha_s^{(T-20)}$
Sulfide production by elemental sulfur reduction	Anaerobic	$K_{S0,VFA,f} \frac{S_{VFA}}{K_{SRB} + S_{VFA}} \frac{X_{S(0)}}{K_{S0} + X_{S(0)}} \frac{K_O}{K_O + S_O} \left(\frac{A}{V}\right) \alpha_s^{(T-20)}$
Sulfide biological oxidation by nitrate to elemental sulfur	Anoxic	$K_{S(2-),anox,f} \frac{S_{S(2-)}}{K_{S2-} + S_{S(2-)}} \frac{S_{NO3}}{K_{NO3} + S_{NO3}} \left(\frac{A}{V}\right) \alpha_s^{(T-20)}$
Elemental sulfur biological oxidation by nitrate to sulfate	Anoxic	$K_{S(0),anox,f} \frac{X_{S(0)}}{K_{S0} + X_{S(0)}} \frac{S_{NO3}}{K_{NO3} + S_{NO3}} \left(\frac{A}{V}\right) \alpha_s^{(T-20)}$

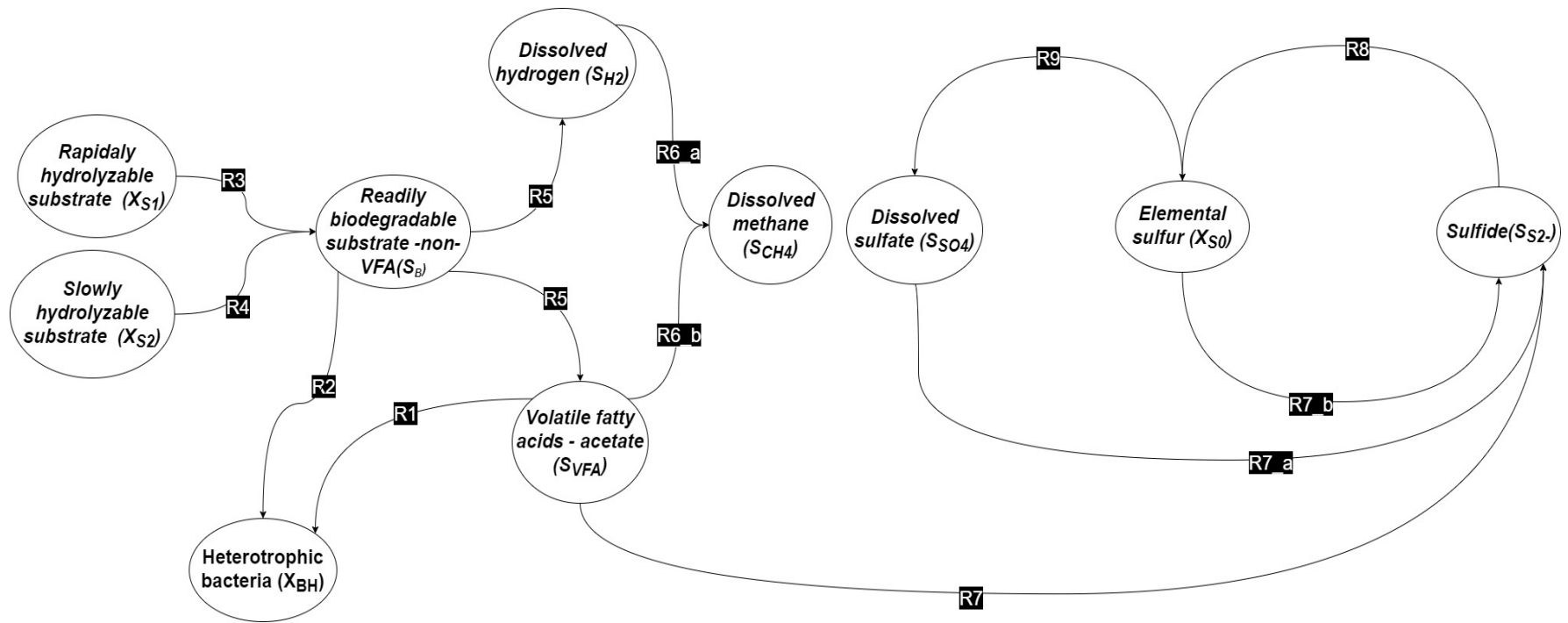


**Figure 4-2: Mathematical model biochemical processes included**



**Table 4-2: Mathematical model process definitions**

Code	Process	Conditions	Remarks
<b>R1</b>	Growth of heterotrophs on $S_{VFA}$	Aerobic/anoxic	bulk/biofilm
<b>R2</b>	Growth of heterotrophs on $S_B$	Aerobic/anoxic	bulk/biofilm
<b>R3</b>	Hydrolysis, fast	Aerobic/anaerobic/anoxic	bulk/biofilm
<b>R4</b>	Hydrolysis, slow	Aerobic/anaerobic/anoxic	bulk/biofilm
<b>R5</b>	$S_B$ fermentation, acetogenesis and acidogenesis	Anaerobic	bulk/biofilm
<b>R6</b>	Methanogenesis using hydrogen (a) and VFA(b)	Anaerobic	Biofilm
<b>R7</b>	Sulfide production by sulfate (a) and elemental sulfur reduction (b)	Anaerobic	Biofilm
<b>R8</b>	Sulfide biological oxidation by nitrate to elemental sulfur	Anoxic	Biofilm
<b>R9</b>	Elemental sulfur biological oxidation by nitrate to sulfate	Anoxic	Biofilm

**Table 4-3: Mathematical model state variable definitions**

Symbol	Variable
$S_B$	Readily biodegradable substrate (non-VFA)
$S_{VFA}$	Volatile fatty acids (acetate)
$X_{Het}$	Heterotrophic bacteria
$X_{S1}$	Rapidly hydrolysable particulate COD
$X_{S2}$	Slowly hydrolysable particulate COD
$S_{NO3}$	Dissolved nitrate and nitrite
$S_{S2-}$	Sulfide in molecular and ionic form
$X_S$	Elemental sulfide
$S_{SO4}$	Dissolved sulfate
$S_{CH4}$	Methane
$S_{H2}$	Dissolved hydrogen

### 4.3 Results and Discussion

The system is modelled as four continuously stirred-tank reactors (CSTRs) in series. Dynamic inlet flow was specified according to the pumping events scheduled. The model shows a reasonable fit with the tracer test measurements, indicated that the hydrodynamics are reasonably well modelled. This can be illustrated in the cumulative residence time distribution,  $F(t)$ , that is shown in Fig. 4-3. It is observed that the numerical model indicates that the actual volume of the reactor is different from that of the calculated cylindrical volume. The effective volume was determined to be 75% of the calculated volume (based on the internal dimensions of the reactor). This agreed with the calculations of the effective volume by deducting the occupied volume of the biofilm carriers and the inlet tube. The effective volume was confirmed with the measurement of the initial concentration of nitrate during the batch test. Moreover, the  $F(t)$  curve indicated that time required for the 10, 50, and 90% of the feeding sewage to pass the systems was 2.8, 7.1 and 18 h, respectively. The mean residence time was computed as 10.44 h. The hydrodynamic configuration with the effective volume that was verified by the tracer test was used for the following modelling of the biochemical conversions.

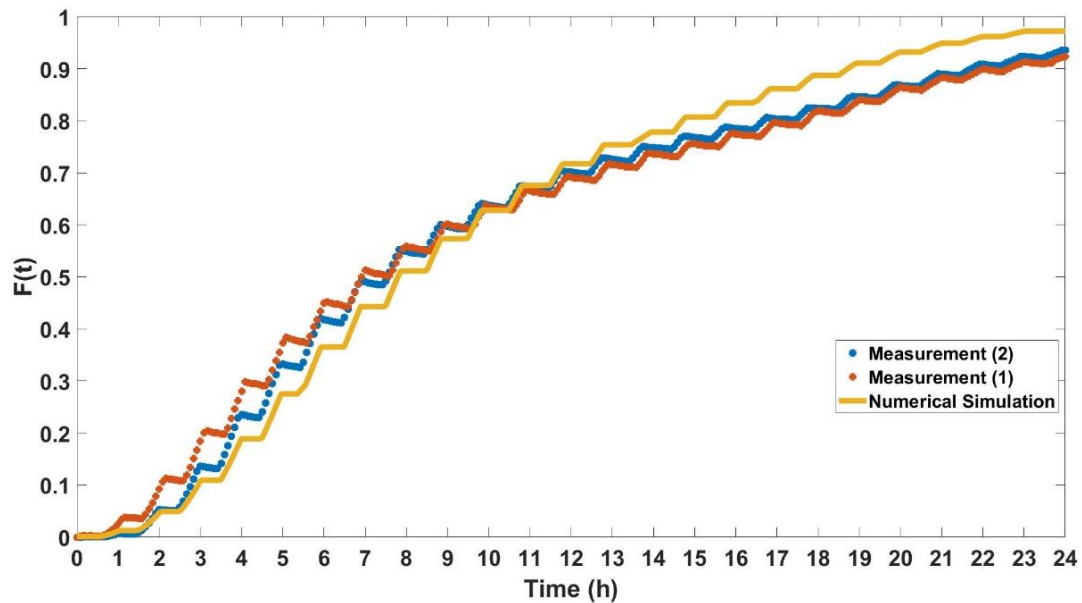


**Figure 4-3: Cumulative residence time distribution ( $F(t)$ ) of the tracer test against the numerical model results**

#### 4.3.1 Numerical model calibration/validation without nitrate dosing

Data collected from the system effluent during normal operation of the system without dosing was used to calibrate the model. Parameter estimation was initiated from the default values reported in Calabrò et al. (2009) and Guisasola et al. (2009) for the anaerobic processes and methane production, respectively. Sulfate reduction rate was the only parameter that was adjusted to get a good fit with the experimental measurements for the effluent measurements as compared with R4 concentrations (Fig. 4-4 and 4-5). Since the variation of the wastewater characteristics as a function of time were mild, the time average and the standard deviation are illustrated in Fig. 4-4. The model showed a reasonable agreement with the measurements, with all model predictions being within one standard deviation of the observed values. There is a gradual increase in the sulfide concentration from R1 through R4 due to sulfate reduction, as indicated by the sulfate concentration reduction through the reactors. It should be noted that sulfide production using hydrogen in the wastewater was neglected based on the estimation provided in the work of Guisasola et al. (2009). Therefore, only VFA was used by SRB to reduce sulfate to sulfide. However, the increase of VFA indicated that the fermentation of more complex soluble carbon compounds ( $S_B$ ) to VFA is higher. Since both VFA and  $S_B$  are part of the sCOD measurement, the decrease of sCOD is due to the sulfide formation process.

Figure 4-5 shows the variation of the sulfide in the effluent with time for the measurements and the model predictions. The sulfide production rate was found to be  $1.46 \text{ gS/m}^2\text{-day}$ , which is comparable to the empirical values reported in Hvitved-Jacobsen (2002), which range from  $0.48$  to  $2.4 \text{ gS/m}^2\text{-d}$ . The variation of sulfide was due to the dilution of the contents of the last reactor (R4) with the flow coming from R3 during the pumping events. However, the concentration of sulfide in R3 was comparable to that in R4. Therefore, the variation of sulfide with respect to time was mild. In the no-flow conditions, SRB had more time to reduce the sulfate in the reactor and produce sulfide.

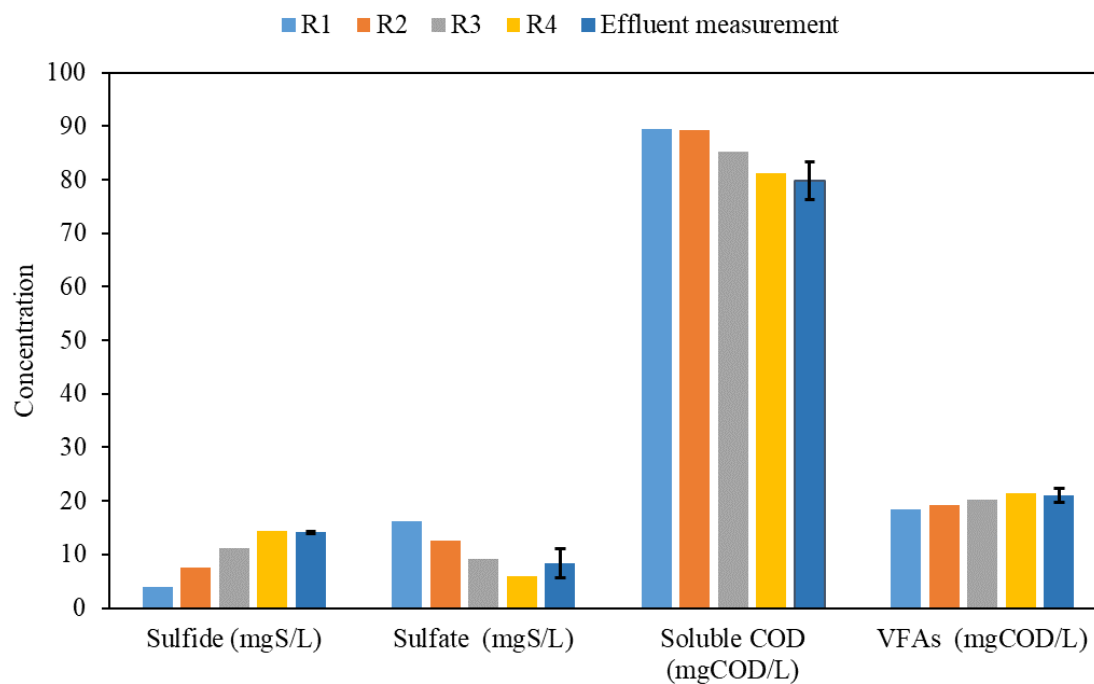


**Figure 4-4: Model calibration: average concentration measurements at the effluent (blue columns) and model predictions effluent of each reactor in the system for sulfide, sulfate, soluble COD and VFA (R1-R4)**

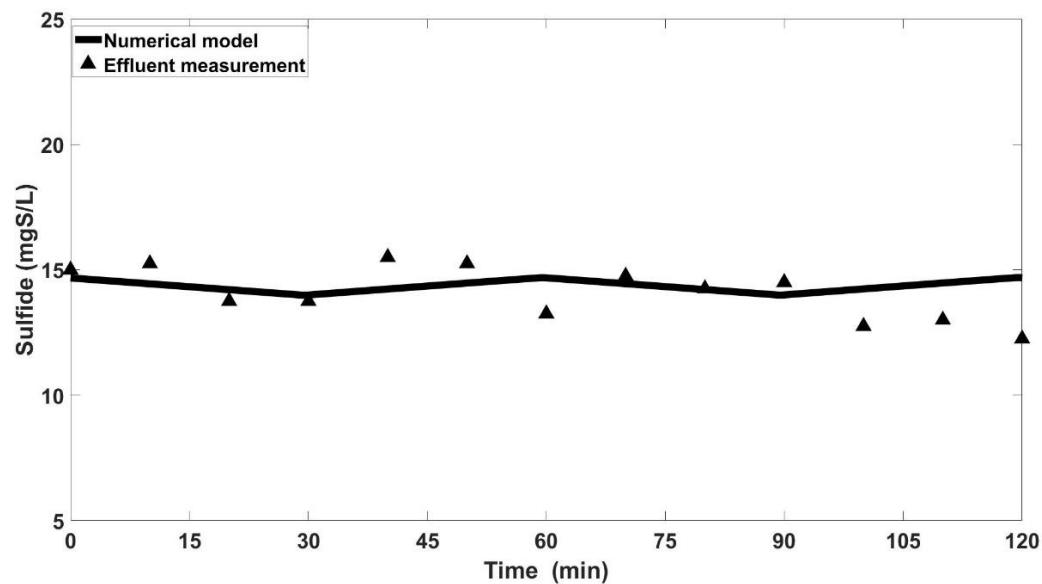


**Figure 4-5: Calibrated sulfide production: measurement and model prediction of sulfide concentration at the system effluent**

Validation of the model was then performed using the second 2-h data set collected during normal operations. The model was able to reasonably capture the mean concentration of wastewater characteristics (Fig. 4-6 and 4-7). At this point only the anaerobic processes were activated due to the absence of the nitrate. The next step is to calibrate the anoxic processes that involve the sulfide and elemental sulfur oxidation.

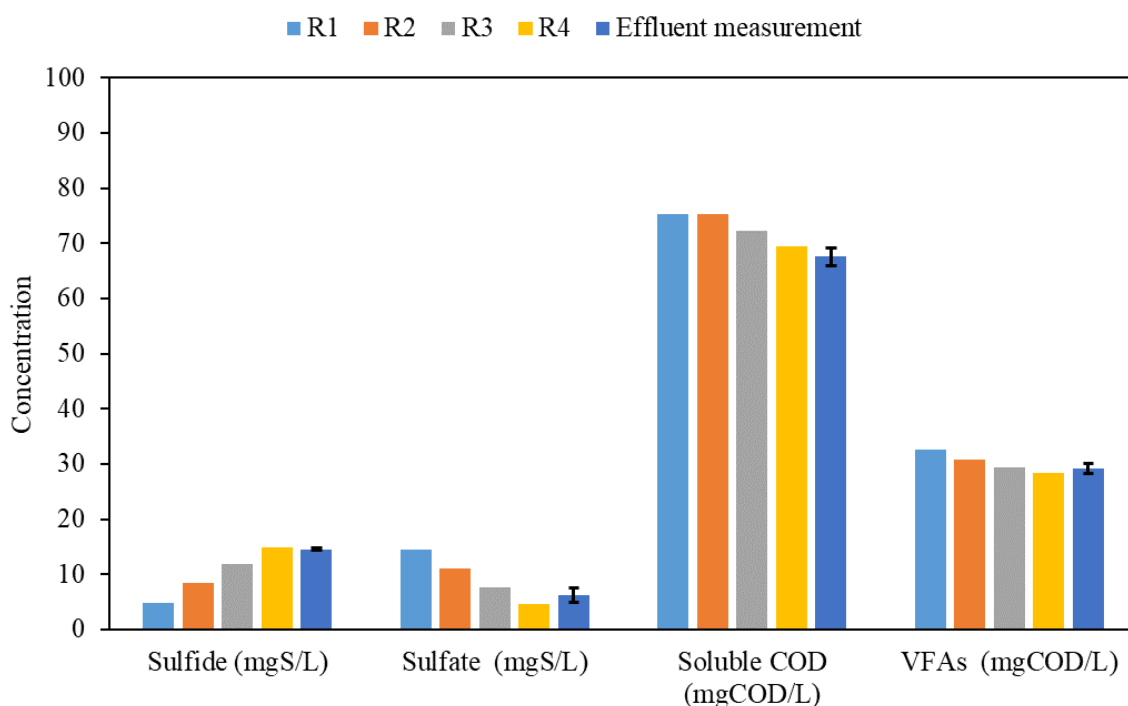


**Figure 4-6: Model validation: average concentration measurements at the effluent and model predictions effluent of each reactor in the system for sulfide, sulfate, soluble COD and VFA**

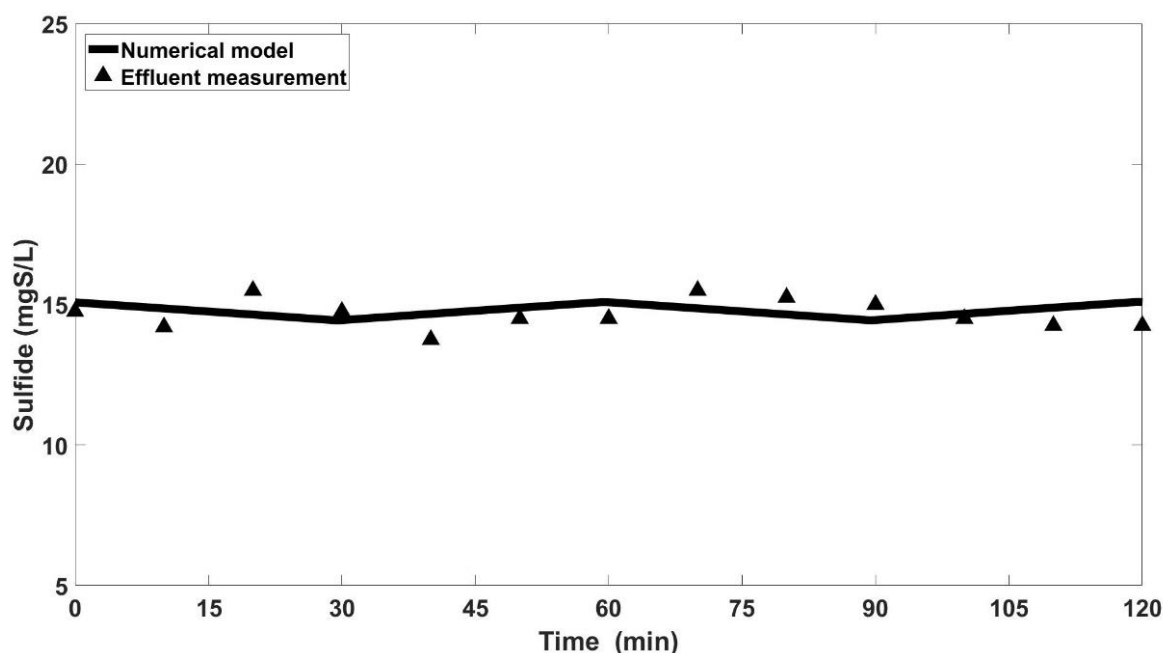


**Figure 4-7: Validated sulfide production: measurement and model prediction of sulfide concentration at the system effluent**

#### 4.3.2 Numerical model calibration for nitrate dosing

The data collected from the 2-h batch test with nitrate were used to calibrate the model for the oxidation of sulfide by nitrate and elemental sulfur as an intermediate species. Two reaction expressions were compared for the sulfide oxidation in the biofilm, namely half-order and Monod-type kinetics. The results showed that both expressions captured the reaction rate of sulfide and nitrate with good agreement, therefore Monod type kinetics was used herein (Fig. 4-8 and 4-9). The anoxic oxidation rates that were measured by Jiang et al. (2009) were used as the reference values for the calibration. It was concluded that the oxidation rate of the elemental sulfur was about  $2.2 \text{ mgS/m}^2\text{-d}$  which was used in the current model. On the other hand, the rate of anoxic oxidation of sulfide was estimated as  $12.1 \text{ mgS/m}^2\text{-d}$  by the current model. This value is lower than the anoxic oxidation rate reported ( $17.1 \pm 2.3 \text{ mgS/m}^2\text{-d}$ ). From Fig. 8, it is shown that only 35 min was needed for the complete biological oxidation of sulfide. This similar behaviour to what was observed by Jiang et al. (2009).

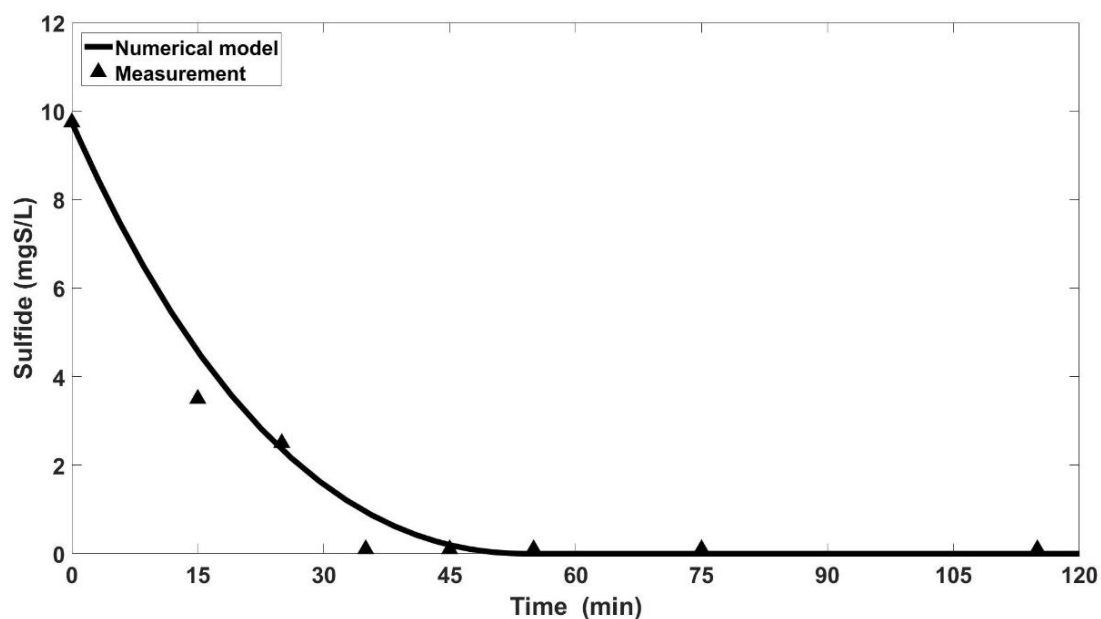


**Figure 4-8: Calibrated profile of sulfide oxidation: measurement and model prediction of sulfide concentration at the system effluent**

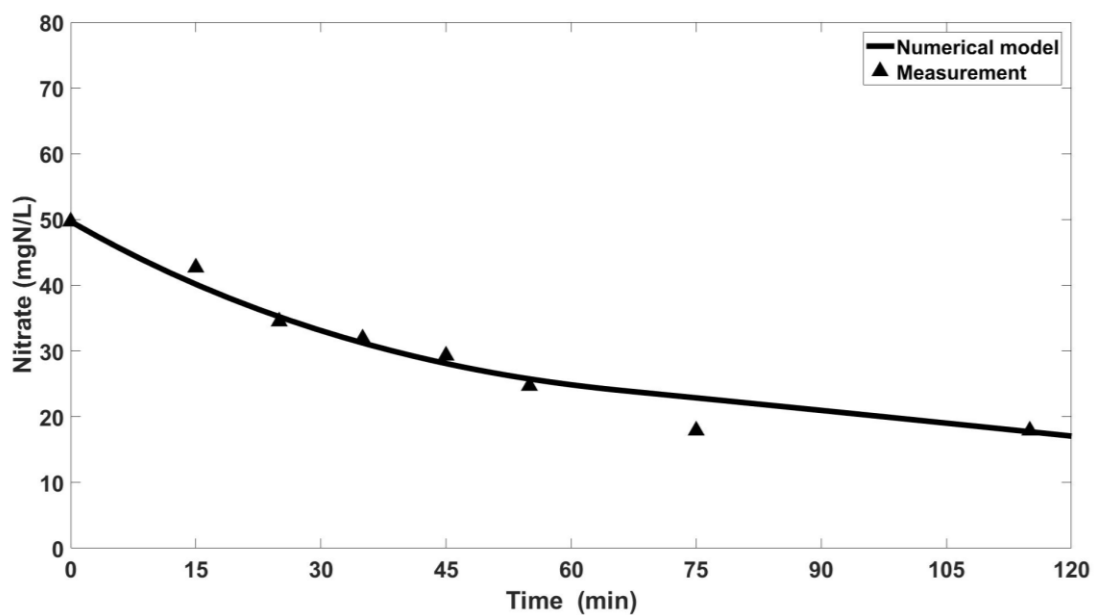


**Figure 4-9: Calibrated profile of nitrate reduction: measurement and model prediction of nitrate concentration at the system effluent**

### 4.3.3 Nitrate dosing rate and location study

The calibrated model was used to develop a strategy for nitrate dosing in the system to help with planning the experiments that will be done in the future. The dosing strategy of nitrate in the system was studied to optimize the nitrate dosing effectiveness. The study was based on the same nitrate stock solution concentration of 2600 mg  $\text{NO}_3/\text{L}$ . The pumping events of the nitrate solution were based on the schedule of the fresh sewage pumping in the system. Thus, the nitrate pumping started with the sewage feeding and stopped once the feeding event was completed. The studied optimization parameters were the nitrate flow rate and the position of the dosing. Dosing was tested in one reactor at a time while varying the reactor that was receiving the nitrate. The flow rates tested in this study were chosen to determine the flow rates that achieve 0.5 mgS/L sulfide and 0.5mg $\text{NO}_3\text{-N/L}$  nitrate average concentrations at the effluent when certain reactor was dosed with nitrate. These goals were used to measure the effectiveness of the nitrate dosing rate to oxidize the sulfide and having no negative influence on the subsequent treatment stage. The total volume of nitrate solution dosed per day is computed and used for the comparison between the different cases. The average concentrations of sulfide and nitrate at the effluent were used to judge the influence of the optimization parameters.

### 4.3.4 Dosing in the 1<sup>st</sup> reactor

Dosing in the first reactor was examined at four flow rates (0.2, 0.3, 0.41 and 0.445 L/d). Nitrate flow rates resulting in sulfide and nitrate average concentrations lower than 0.5 mgS/L and 0.5 mg $\text{NO}_3\text{-N/L}$ , respectively, at the effluent were determined. It was found that 0.41 L/d achieved sulfide concentration at the effluent of the system lower than 0.5 mgS/L while a slightly higher dosing rate (0.445 L/d) was required for the nitrate concentration of the outlet to be 0.5 mg $\text{NO}_3\text{-N/L}$  and complete elimination of sulfide as shown in Fig. 4-10. Since the nitrate was dosed in R1 and flowed to the following reactors, the sulfide was noticed to be completely oxidized in all the reactors.



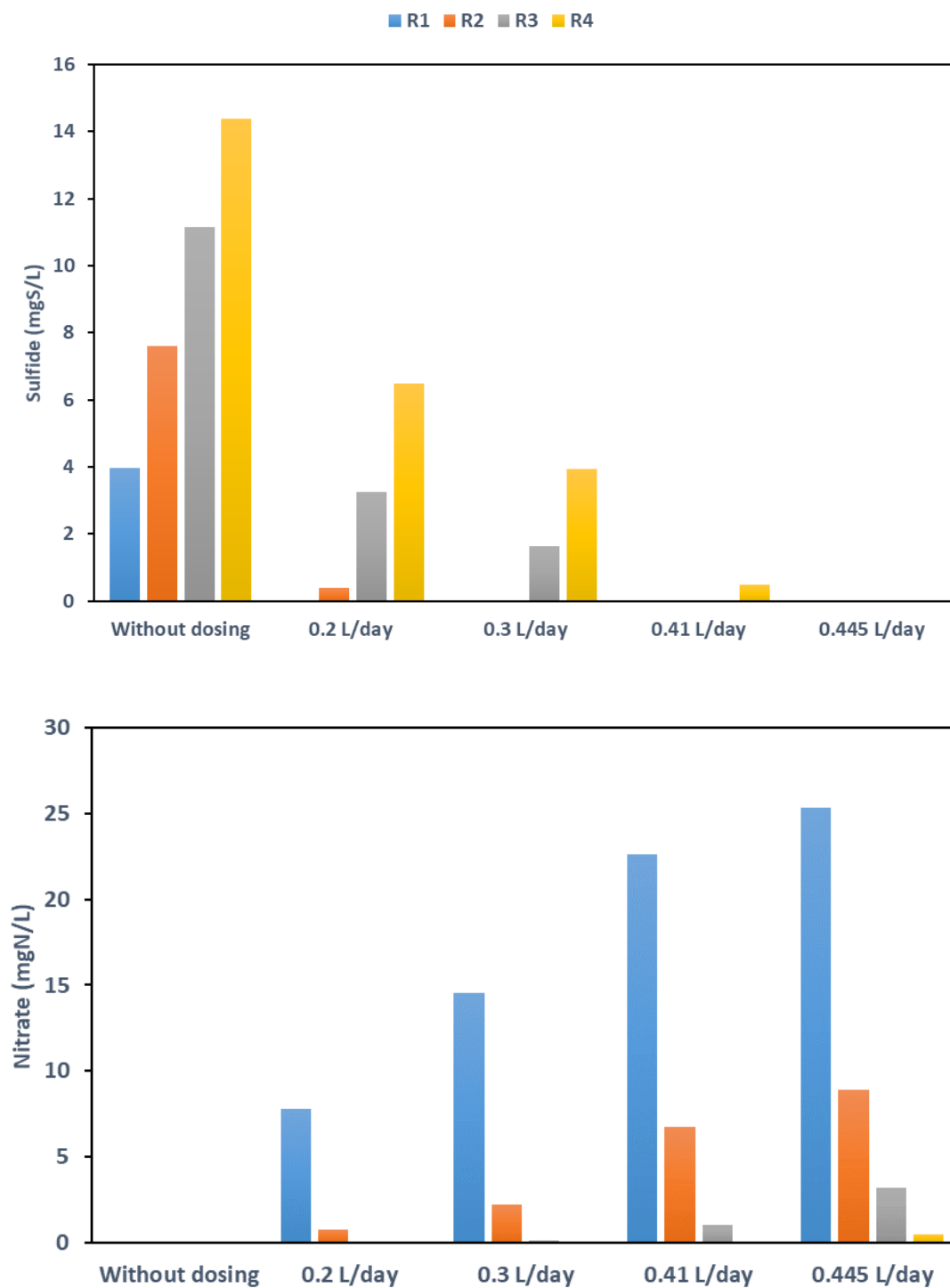


**Figure 4-10: Sulfide (top) and nitrate (bottom) concentrations in the effluent of the reactors (R1-R4) when dosing in R1**

It was observed that the average nitrate concentration in R3 and R4 was the main parameter to determine the sulfide concentration in the effluent. Since the dosing was carried out in R1, a gradient of the nitrate concentration was obtained. However, a sufficient nitrate concentration was needed to suppress the sulfide in these reactors. This is clear in the case of dosing flow rate of 0.3 L/d. Nitrate concentration in R3 was around 2 mgNO<sub>3</sub>-N/L leading to 2 and 4 mgS/L in R3 and R4, respectively.

#### 4.3.5 Dosing in the 2<sup>nd</sup> reactor

For dosing in the second reactor, nitrate solution flow rates of 0.3, 0.387, 0.4 and 0.418 were examined. It was illustrated that lower nitrate solution flow rate (0.387 L/d) was required to achieve 0.5 mgS/L sulfide at the effluent than in the case of dosing in R1. However, the average sulfide level in the R1 was around 4 mgS/L (Fig. 4-11). Sulfide produced in the first reactor is transported to the following reactors when the feeding pump is on. For the complete elimination of sulfide and 0.5 mgNO<sub>3</sub>-N/L in the effluent, higher dosing rate was needed (0.481 L/d).

Nitrate was dosed in R1 and R2 and then transported with the flow to R3 and R4. This resulted in lower nitrate concentration in the last two reactors. Therefore, high dosing rate was needed as illustrated in the next two cases. The dilution of the nitrate solution dosing over a larger volume of sewage negatively affects the effectiveness of the dosing.

#### 4.3.6 Dosing in the 3<sup>rd</sup> reactor

In case of dosing in the third reactor, dosing flow rate resulting in 0.5 mgS/L sulfide in the effluent was 0.282 L/d which is lower than the dosing rates in the previous two cases. However, using this flow rate lead the average nitrate concentration in the effluent to be 0.9 mgNO<sub>3</sub>-N/L. This is due to inadequate time available for the nitrate to oxidize the sulfide. Therefore, higher dosing is needed to get higher nitrate concentration and higher oxidation rate. This was illustrated by the dosing rate (0.223 L/d) that resulting 0.5 mgNO<sub>3</sub>-N/L in the effluent. Moreover, the higher concentration of sulfide in R2 (7.8 mgS/L) that was transported to R3 made the sulfide amount to be oxidized higher (Fig. 4-12). However, still the dosing rate needed for the full oxidation of sulfide is lower than the dosing rates required when dosing in R1 or R2.

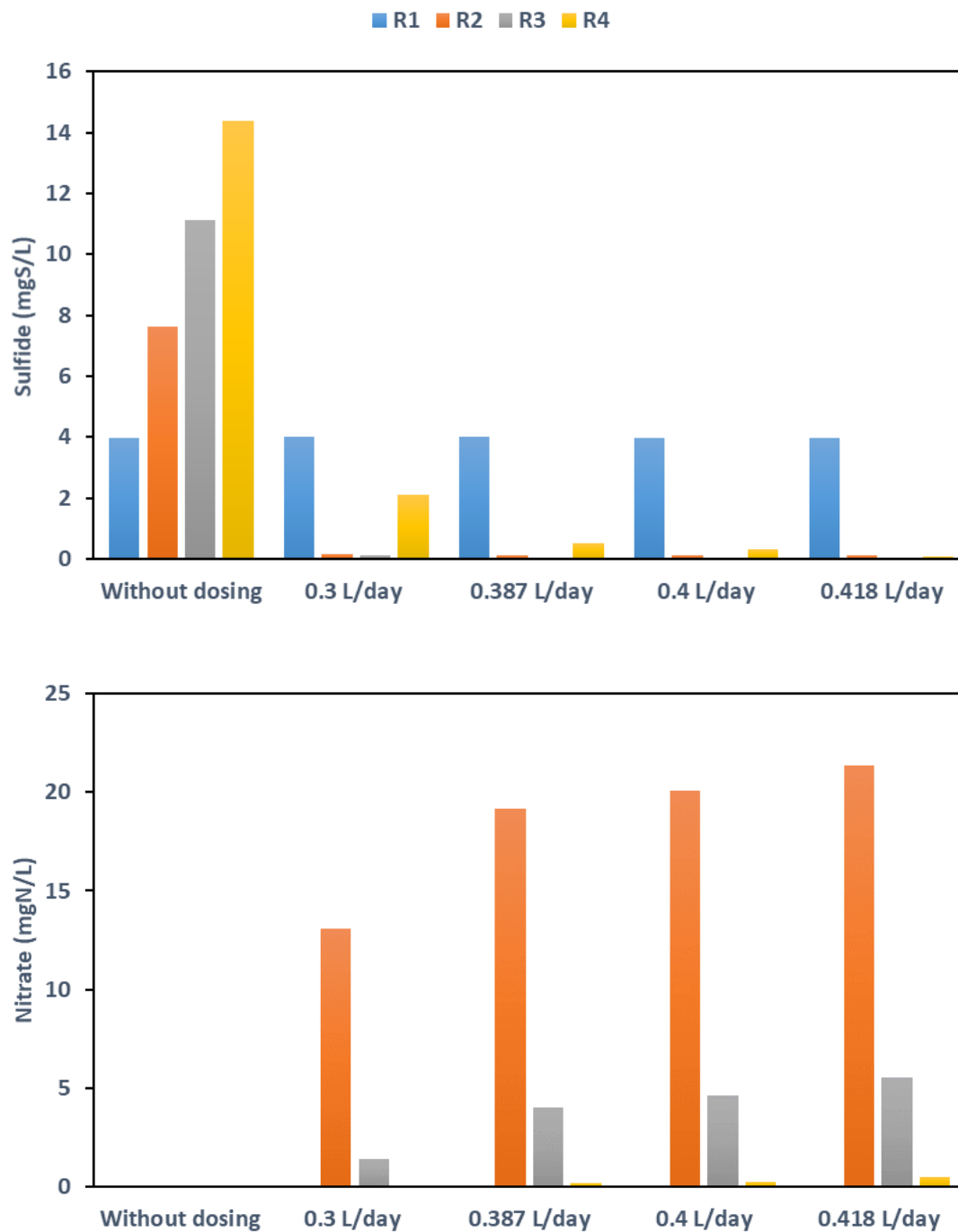


**Figure 4-11: Sulfide (top) and nitrate (bottom) concentrations in the effluent of**

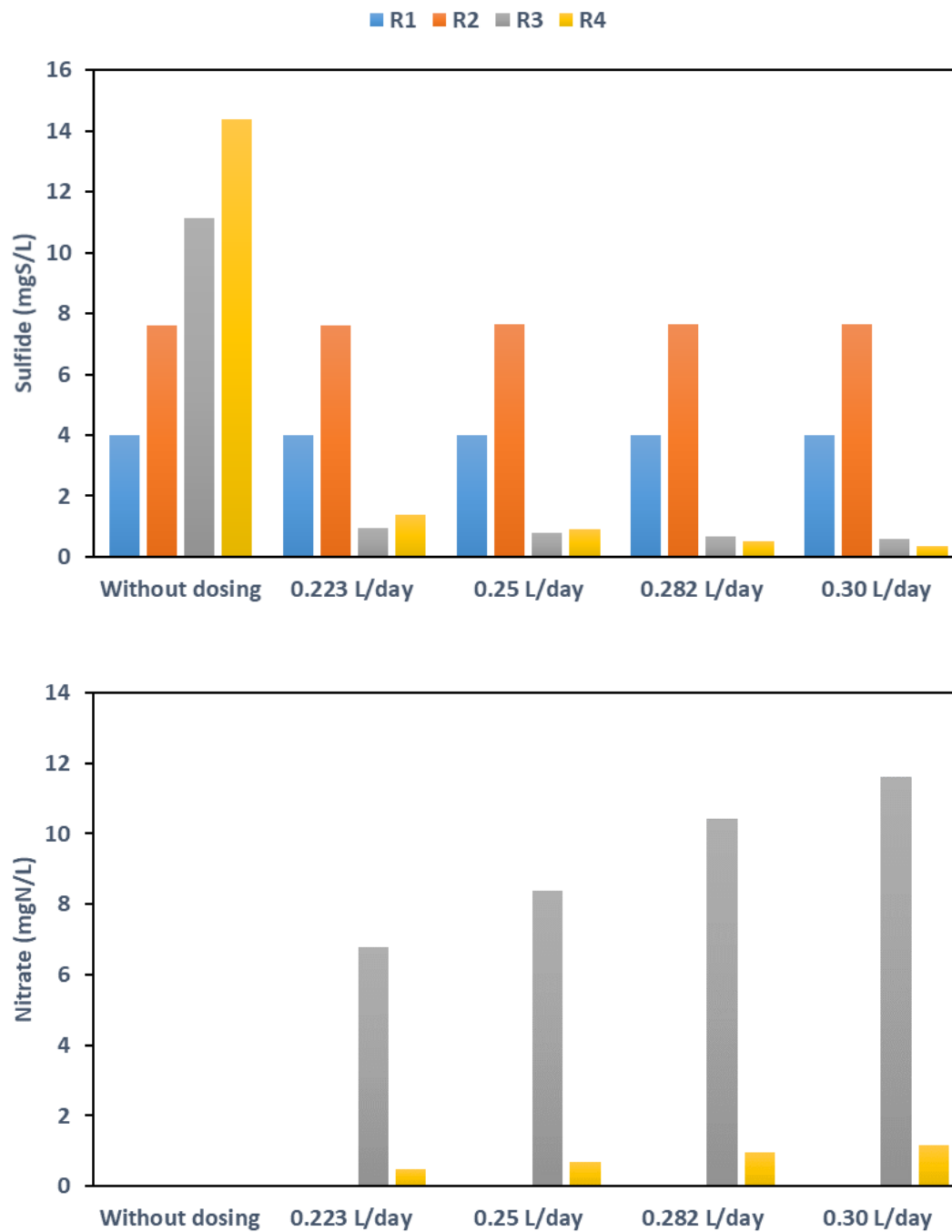


**Figure 4-12: Sulfide (top) and nitrate (bottom) concentrations in the effluent of the reactors (R1-R4) when dosing in R3**

### 4.3.7 Dosing in the 4<sup>th</sup> reactor

Dosing in the last reactor (R4) seems to be attractive to reduce the nitrate amount needed, but this was not observed in the current study. The simulation showed that a very high dosing rate is needed to achieve 0.5 mgS/L in the effluent. This may be explained by the fact that the sulfide concentration coming from R3 is much higher than the other cases. Moreover, since the dosing was scheduled during the feeding duration, a significant amount of nitrate was flushed with the effluent of the system, leading to higher dosing rate being required to achieve a higher concentration of nitrate to be adequate for rapid oxidation of sulfide. The simulations showed that 0.53 L/d was required to get 0.5 mgS/L in the effluent (Fig. 4-13) which is much higher than if the dosing was in R1, R2 or R3. Moreover, the nitrate concentration in the effluent in this case is high (27 mgNO<sub>3</sub>-N/L) which may have a negative impact on the treatment processes. More information can be obtained by examining the dosing rate that achieves 0.5 mgNO<sub>3</sub>-N/L nitrate concentration at the effluent. On the other hand, only 0.06 L/d could result in 0.5 mgNO<sub>3</sub>-N/L of nitrate in the effluent.

### 4.3.8 HRT versus nitrate concentration

The total HRT of 10.44 h was assumed to be uniformly distributed among the four reactors. Thus, the sewage slug stayed the same amount of time in each reactor. Based on this assumption, four HRTs for the nitrate dosing are computed. The applied nitrate concentration is the resultant concentration of the dilution of the stock solution in the sewage flow during pumping event. Figure 4-14 shows the effective dosing rate to have 0.5 mgS/L sulfide in the effluent, as a function of HRT. It was clear that the lowest HRT (2.11 h), which corresponds to the dosing in R4, has the highest applied nitrate concentration. This was explained above was due to the short time available for the nitrate to oxidize the sulfide accompanying with high sulfide concentration that was produced in R1 to R3 hence higher nitrate was needed. Moreover, almost no difference is observed between the applied nitrate concentrations when dosing R1 and R2. On the other hand, dosing in R3 shows the lowest value. Therefore, dosing in R3 is the most efficient way in this dosing strategies even with nitrate concentration in the effluent of 0.9 mgNO<sub>3</sub>-N/L that could be neglected. Figure 4-15 showed the applied nitrate

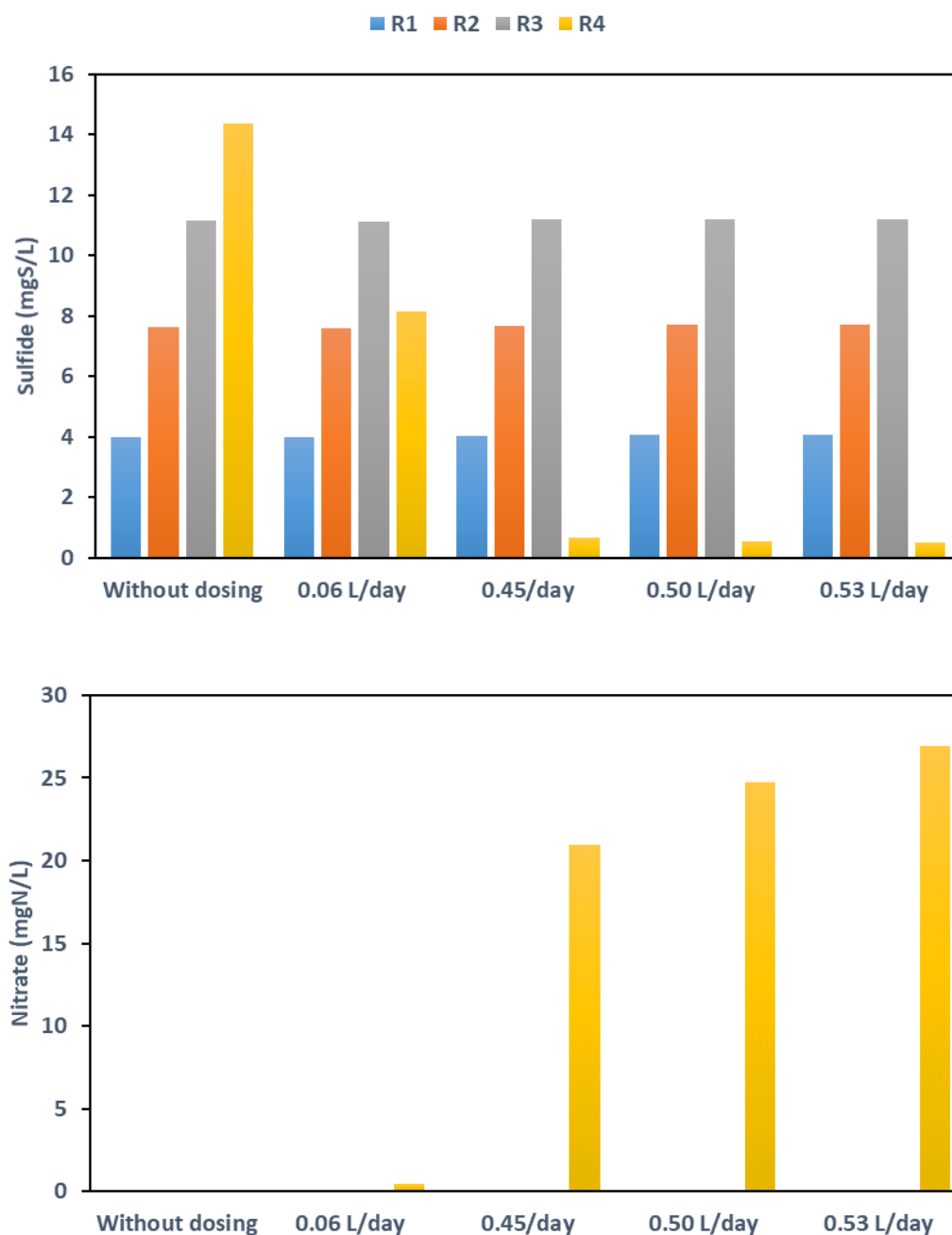


**Figure 4-13: Sulfide (top) and nitrate (bottom) concentrations in the effluent of the reactors (R1-R4) when dosing in R4**

concentration for dosing flow rates that results in 0.5 mgNO<sub>3</sub>-N/L in the effluent against the HRT. Since this criterion does not necessarily result in complete depletion of sulfide, it cannot be used as a measure of the effectiveness of the nitrate dosing. However, it

illustrates the maximum applied nitrate that can be used at each HRT without affecting the subsequent treatment process.

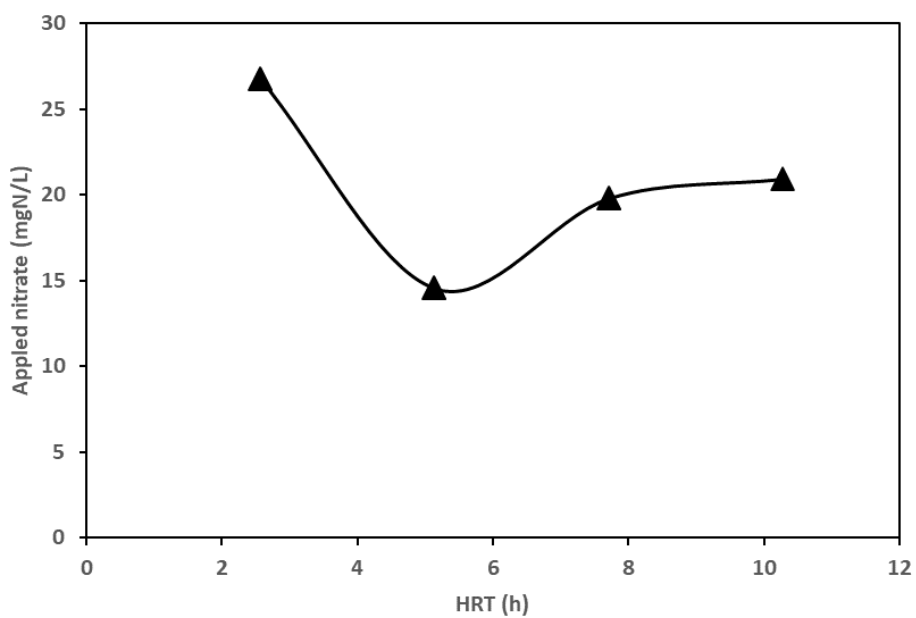


**Figure 4-14: Effective nitrate dosing to achieve 0.5 mgS/L sulfide in the effluent**

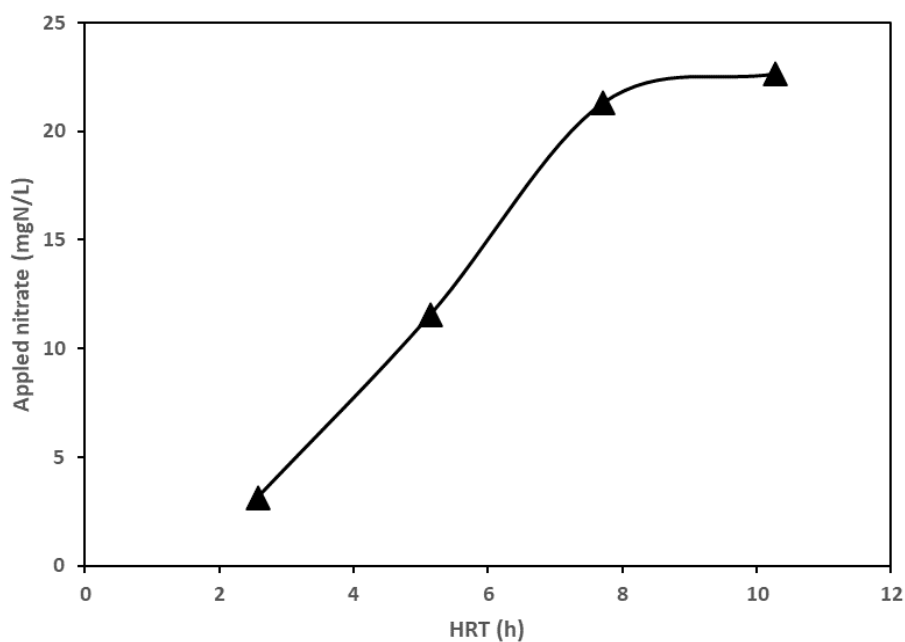


**Figure 4-15: Effective nitrate dosing to achieve 0.5 mgNO<sub>3</sub>-N/L sulfide in the effluent**

## 4.4 Conclusions

The model proposed herein, based on the WATS model, reasonably described the kinetics of the anaerobic biochemical conversions in the sewer system. Moreover, sulfide oxidation rate by nitrate was well-captured. However, more data should be collected for more precise calibration and validation. Batch tests at different concentrations of nitrate and sulfide are needed to ensure the good performance of the model. In addition, sensitivity/uncertainty analysis of the model should be conducted to determine the key parameters and uncertainty of the model predictions.

The modelling results showed that the optimal dosing was found to be carried out in R3 while dosing in the last reactor results in the worst effectiveness. The same effectiveness was noticed when dosing in R1 and R2.

Synchronizing the dosing pump with the feeding pump may not be the best strategy to follow, especially when dosing in the last reactor since nitrate could be flushed thus effectiveness was significantly reduced. Moreover, dosing in multiple reactors at the same time should be studied. In addition, increasing the number of the reactors in the model could be performed to investigate the optimal location of nitrate dosing where this cannot be feasible to be done in the current experiment setup.



## 4.5 References

- Abdul-Talib, S., Ujang, Z., Vollertsen, J., & Hvitved-Jacobsen, T. (2005). Model concept for nitrate and nitrite utilization during anoxic transformation in the bulk water phase of municipal wastewater under sewer conditions. *Water science and technology*, 52(3), 181-189.
- Auguet, O., Pijuan, M., Guasch-Balcells, H., Borrego, C. M., & Gutierrez, O. (2015). Implications of downstream nitrate dosage in anaerobic sewers to control sulfide and methane emissions. *Water research*, 68, 522-532.
- Bentzen, G., Smit, A. T., Bennett, D., Webster, N. J., Reinholt, F., Sletholt, E., & Hobsont, J. (1995). Controlled dosing of nitrate for prevention of H<sub>2</sub>S in a sewer network and the effects on the subsequent treatment processes. *Water Science and Technology*, 31(7), 293-302.
- Boon, A. G. (1975). Formation of sulphide in rising main sewers and its prevention by injection of oxygen. *Prog. Wat. Tech.*
- Calabro, P. S., Mannina, G., & Viviani, G. (2009). In sewer processes: mathematical model development and sensitivity analysis. *Water science and technology*, 60(1), 107-115.
- Carrera, L., Springer, F., Lipeme-Kouyi, G., & Buffiere, P. (2016). A review of sulfide emissions in sewer networks: overall approach and systemic modelling. *Water Science and Technology*, 73(6), 1231-1242.
- Ganigue, R., Gutierrez, O., Rootsey, R., & Yuan, Z. (2011). Chemical dosing for sulfide control in Australia: an industry survey. *Water research*, 45(19), 6564-6574.
- Gudjonsson, G., Vollertsen, J., & Hvitved-Jacobsen, T. (2002). Dissolved oxygen in gravity sewers—measurement and simulation. *Water science and technology*, 45(3), 35-44.
- Guisasola, A., de Haas, D., Keller, J., & Yuan, Z. (2008). Methane formation in sewer

- systems. *Water Research*, 42(6-7), 1421-1430.
- Guisasola, A., Sharma, K. R., Keller, J., & Yuan, Z. (2009). Development of a model for assessing methane formation in rising main sewers. *Water Research*, 43(11), 2874-2884.
- Gutierrez, O., Sutherland-Stacey, L., & Yuan, Z. (2010). Simultaneous online measurement of sulfide and nitrate in sewers for nitrate dosage optimisation. *Water Science and Technology*, 61(3), 651-658.
- Hvitved-Jacobsen, T., Vollertsen, J., & Nielsen, A. H. (2013). *Sewer processes: microbial and chemical process engineering of sewer networks*. CRC press.
- Jiang, G., Sharma, K. R., Guisasola, A., Keller, J., & Yuan, Z. (2009). Sulfur transformation in rising main sewers receiving nitrate dosage. *Water Research*, 43(17), 4430-4440.
- Jiang, G., Sharma, K. R., & Yuan, Z. (2013). Effects of nitrate dosing on methanogenic activity in a sulfide-producing sewer biofilm reactor. *Water research*, 47(5), 1783-1792.
- Liu, Y., Ni, B. J., Ganigué, R., Werner, U., Sharma, K. R., & Yuan, Z. (2015). Sulfide and methane production in sewer sediments. *Water Research*, 70, 350-359.
- Liu, Y., Sharma, K. R., Ni, B. J., Fan, L., Murthy, S., Tyson, G. Q., & Yuan, Z. (2015). Effects of nitrate dosing on sulfidogenic and methanogenic activities in sewer sediment. *water research*, 74, 155-165.
- Mohanakrishnan, J., Gutierrez, O., Sharma, K. R., Guisasola, A., Werner, U., Meyer, R. L., ... & Yuan, Z. (2009). Impact of nitrate addition on biofilm properties and activities in rising main sewers. *Water research*, 43(17), 4225-4237.
- Mora, M., López, L. R., Lafuente, J., Pérez, J., Kleerebezem, R., van Loosdrecht, M. C., ... & Gabriel, D. (2016). Respirometric characterization of aerobic sulfide, thiosulfate and elemental sulfur oxidation by S-oxidizing biomass. *Water*

*research*, 89, 282-292.

- Nielsen, A. H., Hvitved-Jacobsen, T., & Vollertsen, J. (2005). Kinetics and stoichiometry of sulfide oxidation by sewer biofilms. *Water Research*, 39(17), 4119-4125.
- Nielsen, A. H., Vollertsen, J., & Hvitved-Jacobsen, T. (2006). Kinetics and stoichiometry of aerobic sulfide oxidation in wastewater from sewers—Effects of pH and temperature. *Water environment research*, 78(3), 275-283.
- Pomeroy, R. D., & Parkhurst, J. D. (1978, January). The forecasting of sulfide build-up rates in sewers. In *Eighth International Conference on Water Pollution Research* (pp. 621-628). Pergamon.
- Rodríguez-Gómez, L. E., Delgado, S., Álvarez, M., & Elmaleh, S. (2005). Inhibition of sulfide generation in a reclaimed wastewater pipe by nitrate dosage and denitrification kinetics. *Water Environment Research*, 77(2), 193-198.
- Saracevic, E., Bertrán de Lis, F., & Matsché, N. (2007). Odour and corrosion problems in pressure sewers. *Water Practice and Technology*, 2(1).
- Sharma, K. R., Yuan, Z., de Haas, D., Hamilton, G., Corrie, S., & Keller, J. (2008). Dynamics and dynamic modelling of H<sub>2</sub>S production in sewer systems. *Water Research*, 42(10-11), 2527-2538.
- Sun, J., Ni, B. J., Sharma, K. R., Wang, Q., Hu, S., & Yuan, Z. (2018). Modelling the long-term effect of wastewater compositions on maximum sulfide and methane production rates of sewer biofilm. *Water research*, 129, 58-65.
- Hvitved-Jacobsen, T., Vollertsen, J., & Tanaka, N. (2000). An integrated aerobic/anaerobic approach for prediction of sulfide formation in sewers. *Water science and technology*, 41(6), 107-115.
- Vollertsen, J., Nielsen, L., Blicher, T. D., Hvitved-Jacobsen, T., & Nielsen, A. H. (2011). A sewer process model as planning and management tool—hydrogen sulfide simulation at catchment scale. *Water Science and Technology*, 64(2), 348-354.

- Yongsiri, C., Hvitved-Jacobsen, T., Vollertsen, J., & Tanaka, N. (2003). Introducing the emission process of hydrogen sulfide to a sewer process model (WATS). *Water Science and Technology*, 47(4), 85-92.
- Zhang, L., De Schryver, P., De Gussemé, B., De Muynck, W., Boon, N., & Verstraete, W. (2008). Chemical and biological technologies for hydrogen sulfide emission control in sewer systems: a review. *Water research*, 42(1-2), 1-12.
- Zhang, L., Keller, J., & Yuan, Z. (2009). Inhibition of sulfate-reducing and methanogenic activities of anaerobic sewer biofilms by ferric iron dosing. *Water research*, 43(17), 4123-4132.

## Chapter 5

### 5 Summary and recommendations for future work

In this chapter, a summary of the work in this thesis is presented along with the major conclusions for each chapter. This is followed by recommendations for future work.

#### 5.1 Summary

In this work, the uncertainty of the most common approximations used in modelling the biochemical processes occurring in wastewater management systems were evaluated using a CFD framework. Two major subjects were of concern in this work: the aeration of activated sludge reactors and sulfide formation in sewer systems. For the aeration model, a CFD-PBM approach was adopted to investigate the influence of the constant bubble size approximation. For the sewer modelling, the WATS model was implemented in 1-D and CFD frameworks for comparison and for studying the uncertainty of the 1-D model mathematical form. A novel technique is developed to simulate the biofilm reactions in the biofilm using a CFD model. Moreover, the settling of the solids in sewers is considered to include its influence on the homogeneity of the reactions. Then, the 1-D model structure was selected to implement an extension of the WATS model to simulate the anoxic sulfide biological oxidation.

In chapter 2, CFD model integrated with PBM was used to simulate air bubbles flowing in a bubble column reactor operating within the homogeneous regime. The CFD-PBM model was validated using the experimental measurement of bubble size distribution at different levels, global gas holdup in the column and global oxygen mass transfer coefficient at two air flow rates. Different closure models for bubble breakup and coalescence rates, along with drag force models, were examined to determine the suitable combination that can predict the evolution of the bubble size distribution in the reactor effectively. The applied boundary conditions (gas volume fraction at the air diffuser surface) were investigated as well to provide the best practices for using such model. The discretization of the bubble size distribution was studied to determine the dependency of the model results on the number of the bubble classes.

The CFD-PBM model showed excellent performance in terms of capturing the evolution of the bubble size distribution and oxygen mass transfer parameters. Specifying the gas volume fraction at the inlet did not affect the accuracy of the results as long as the same gas flow rate is applied at the inlet. Moreover, 22 bubble size classes of the PBM was sufficient to obtain a good agreement with the experimental data with no further improvement with increasing the number of classes. Prince and Blanch's coalescence model with only buoyancy activated showed the most precise performance for the two gas flow rates examined. However, the drag model used has a critical role on the accuracy of the results. Nevertheless, analysis of the flow fields and the BSD along the bubble column height showed a significant influence of the water phase recirculation near the free surface on the bubble size distribution and oxygen mass transfer. Finally, the constant bubble size approximation was examined using the mean diameters observed in the experimental data at each flow rate. The results showed that this approximation has similar prediction of the global gas holdup as the CFD-PBM model. However, adopting this approximation resulted in poor prediction of the oxygen mass transfer.

In chapter 3, uncertainty/sensitivity analysis of the WATS biochemical model implemented in the 1-D framework was conducted to determine the key parameters that influence the performance of the model. It was demonstrated using the computed standardized regression coefficients that the parameters of the hydrolysis processes, efficiency of the anaerobic processes, and sulfide formation rate per unit area of the biofilm are the main parameters that determine the accuracy of the model. Therefore, it was concluded that special attention should be taken while estimating these parameters. On the other hand, the WATS model was integrated in CFD with developed models to consider the settling of particulate matter and reactions in the biofilm. The implementation of the surface reactions in the CFD model was verified using a very simple domain (results shown in appendix A). The analysis of the CFD results showed that the influence of the heterogeneity of the reactions in the biofilm and due to the settling of solids does not have a significant influence on the results. Therefore, the 1-D model could be used for simple domains such as pressure mains.

In chapter 4, the WATS model implemented in the 1-D framework was used with an extension added to consider the biological oxidation of sulfide with nitrate. A lab-scale experiment, which consists of four well-mixed tanks connected in series, was used to generate data to calibrate and validate the model. First, the model was calibrated and validated for the anaerobic processes that include hydrolysis, fermentation, and sulfate reduction to produce sulfide. Then, the anoxic processes of sulfide and elemental sulfur oxidation were included. Calibration and validation of the anoxic processes were conducted using data of batch tests performed. Finally, the validated 1-D model was used to test a number of strategies for nitrate dosing. The study was based on determining the nitrate concentration that is required to get 0.5 mgNO<sub>3</sub>-N/L of nitrate and 0.5 mgS/L sulfide at the outlet. The study showed that dosing near the outlet is beneficial in terms of the amount of nitrate needed. However, the nitrate dosing location should not be too close to the outlet in order to avoid flushing the nitrate solution from the system without sufficient time being available for the microorganisms to oxidize the sulfide. Moreover, it was recommended not to use simultaneous nitrate dosing and fresh sewage feeding to the system.

## 5.2 Recommendations for future work

- For CFD-PBM, further study is needed to understand the interaction between the turbulence model and the bubble breakup/coalescence models to gain more insight into the physics of the bubble evolution along the bubble column. This study requires more experimental data that includes bubble size distribution at different levels of the bubble column and at different levels of turbulence. Turbulence in this system could be generated either by high gas flow rate or using any other means that generate eddies that physically interact with the bubbles. The bubble size distribution could be measured using photographic techniques or using an optical probe. The turbulence intensity should be measured as well to quantitatively evaluate the CFD model.
- For CFD-PBM modelling of the bubble size evolution and mass transfer in bubble columns and activated sludge reactors, the breakup/coalescence models should be studied in the case of various contaminants being present in the water as well as

the effects of foam accumulation at the free surface. The suggested study should focus on developing breakup and coalescence models that can capture the effect of suspended solids in the water phase. Moreover, soluble matters that have an influence on the bubble size distribution and oxygen mass transfer (such as surface-active agents) should be examined, along with suspended solids concentrations that vary in size and concentration. An interesting study that could be beneficial to the modelling of the aeration of activated sludge reactors is to investigate the concentration of alpha-cellulose on oxygen mass transfer. The biodegradation of alpha-cellulose in activated sludge reactor was recently studied. Therefore, the influence of alpha-cellulose could be incorporated in the modelling of dynamic  $\alpha$ -factor.

- Simulation of a bubble column operating within the heterogeneous regime using CFD-PBM model could be examined. Measurement data in the heterogeneous flow regime would be beneficial for examining the capability of the CFD-PBM model to capture the BSD evolution, flow field, and mass transfer coefficient in such cases. Developing new models of bubble breakup and coalescence or modifying the existing ones should be conducted to capture the evolution of the bubble size distribution and consequent mass/heat transfer parameters.
- Further study on the detailed modelling of biofilm reactions in membrane bioreactors using the developed CFD model of heterogeneous reactions, would be an interesting extension of the current work. The numerical technique developed in this study to simulate the heterogeneous reactions could be further applied on membrane bioreactors to explore the uncertainties within current models. Moreover, detailed modelling of such reactors could be crucial for further development of new designs.
- Modelling of sewer system ventilation and more robust particulate settling would be a valuable further extension of the proposed CFD model integrated with the biochemical model. The model could be extended to simulate the ventilation of sewer systems where the formed hydrogen sulfide produced in the liquid phase transfers to the sewer environment. Moreover, different segments of sewer system could be prone to high emission of hydrogen sulfide in the gas phase due to



higher turbulence and air velocity at the free surface of the water phase. In addition, settling of solids could be imperative in some segments of the sewer system. Therefore, more robust settling function of solids in sewers should be developed.

- Modelling of nitrate dosing in sewer systems through experimental investigation should be performed to test nitrate dosing at different concentrations and rates. This experimental data could be used to develop more robust nitrate model. Moreover, to ensure the dynamic behaviour of the sewer system could be captured by the model, more dynamic flow or concentration of the sewage constituents should be generated and used in testing the model.

## Appendices

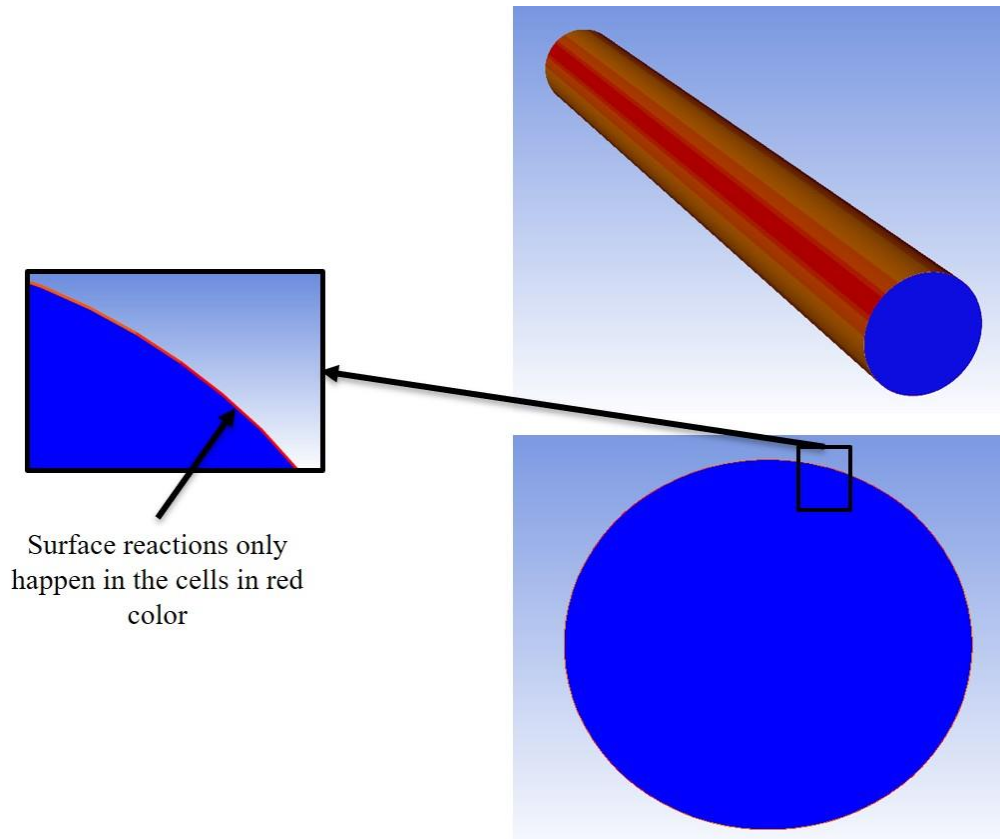
### Appendix A: Supplementary information for Chapter 3

#### **Biochemical surface reactions implementation in CFD model**

ANSYS FLUENT CFD commercial software was used for the simulation of the flow field along with the biochemical conversions. The biochemical reactions that happen in the water phase are modelled using the technique described in the paper. However, a technique was developed for the reactions happen in the biofilm that is accumulated on the inner wall of the sewer pipes (surface reactions). User-Defined Scalars (UDS) in ANSYS FLUENT has a capability that enables us to define a general transport equation and to customize the different terms in the equations. This includes volumetric source term (as was done for the integration of the consumption/generation of different species in water phase) and the flux at the computational cell faces. User-defined flux was developed for the integration of the solids settling and the surface biofilm reactions. The advection term in the general transport equation is described as:

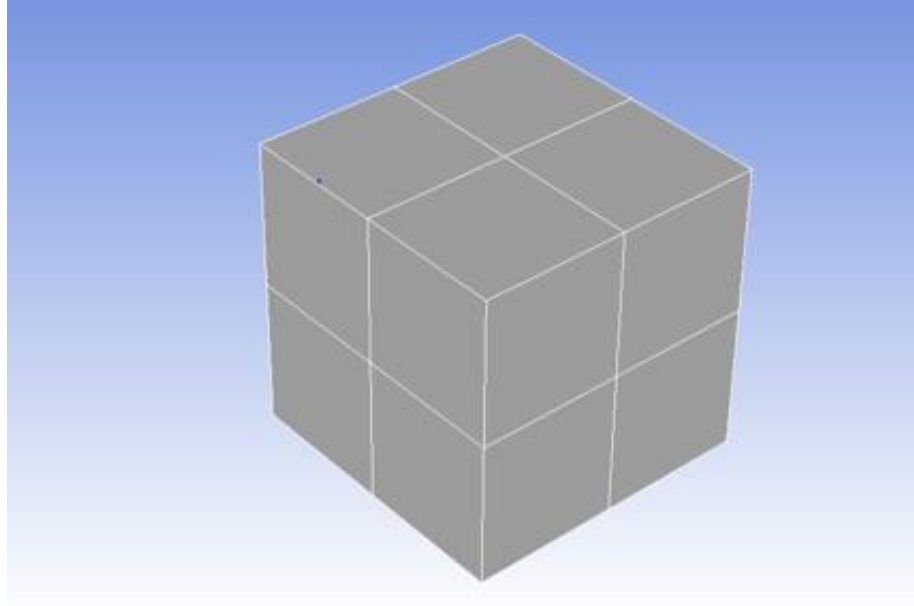
$$\nabla \cdot \bar{\psi} \phi \quad (\text{A.1})$$

where  $\bar{\psi}$  is a vector field that has a default of the multiplication of the velocity vector field and the density of the medium. However, it was customized to adopt the surface reactions. First, identification of the computational cell on the wall was carried out using a built-in macro in the software (shown in Fig. A.1). Then, artificial flux for each of the species that is involved in the surface reactions is defined with direction based on if this species is consumed or produced in reactions. The sign of the flux is assigned as positive in case of species consumption and vice versa.



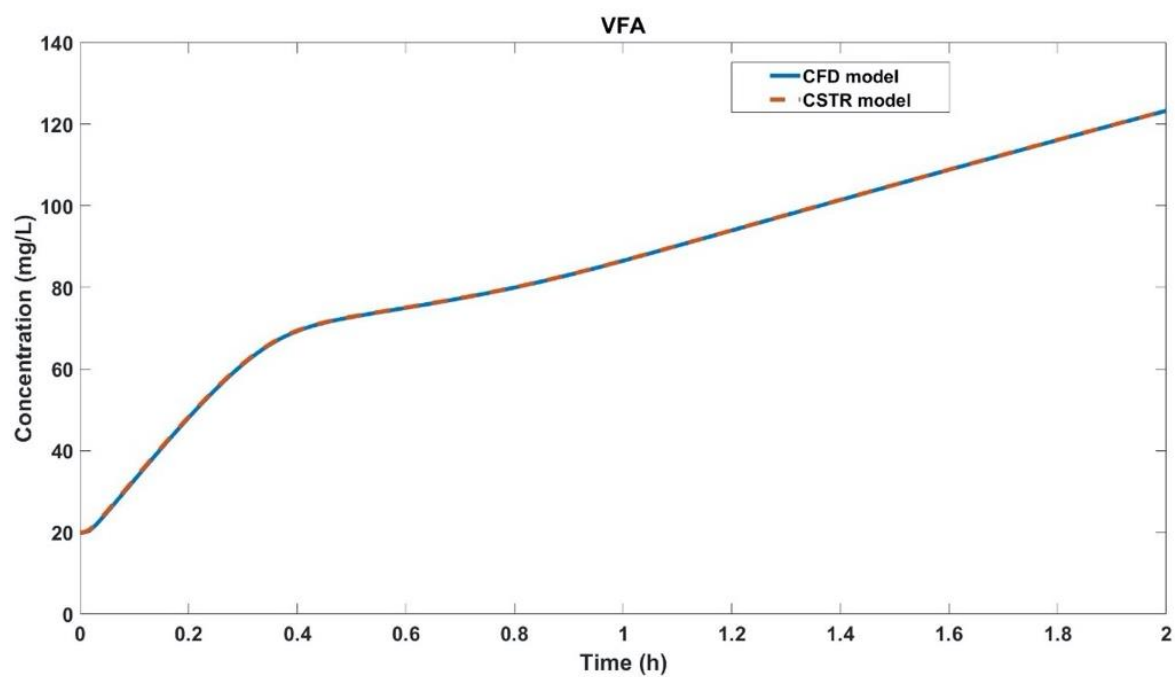
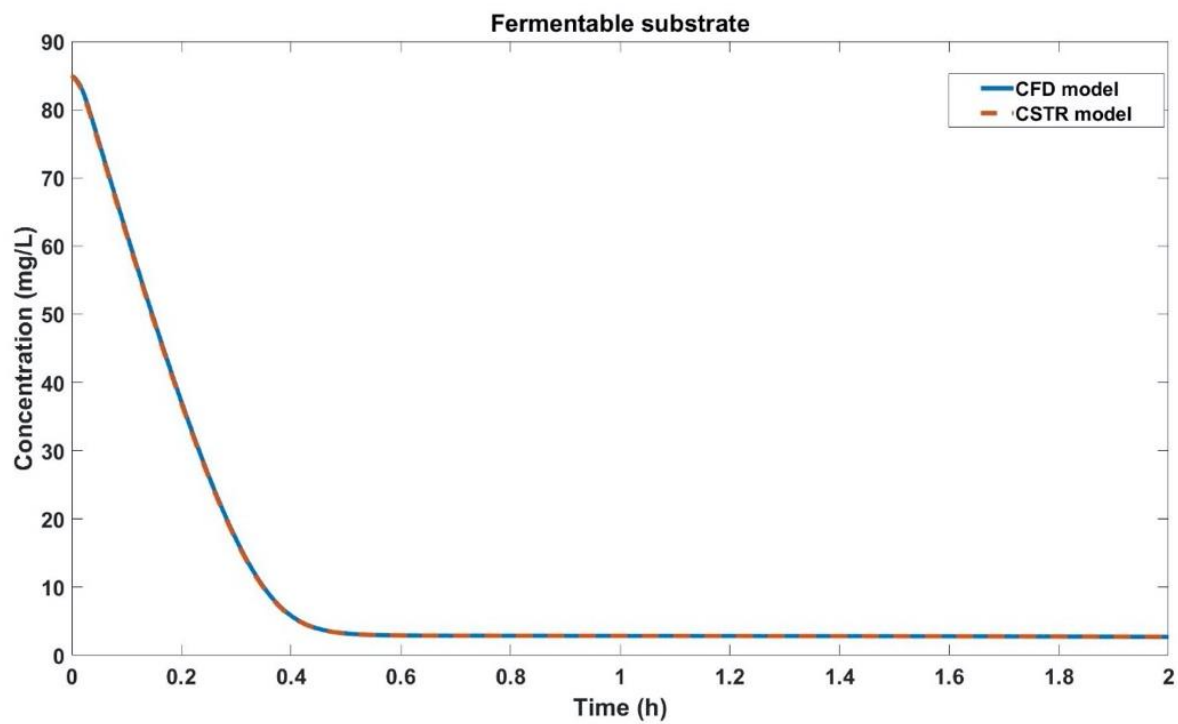
***Fig. A.1: Identification of the computational cells where surface reactions occur.***

Verification of this technique is conducted by comparing the results of the MATLAB/Simulink model for one CSTR with the CFD model with no-flow conditions and fictitious initial concentrations. A simple computational domain is created in the form a cube with six faces and volume of  $1 \text{ m}^3$  (shown in Fig. A.2). This results in area-to-volume ratio of 6. Therefore, the area-to-volume ratio of the CSTR model is set to 6 as well.



***Fig. A.2: The computational domain for the CFD model***

The time series of the different concentration resulting from the two models are plotted in Fig. A.3. An essentially perfect match is obtained since only the biochemical reactions are responsible for the species change in the two models (no flow conditions). The figure shows the predicted concentration of the fermentable substrate, VFA, sulphide and sulphate. The matching proves the correct coding of the customized source terms and fluxes (surface reactions).



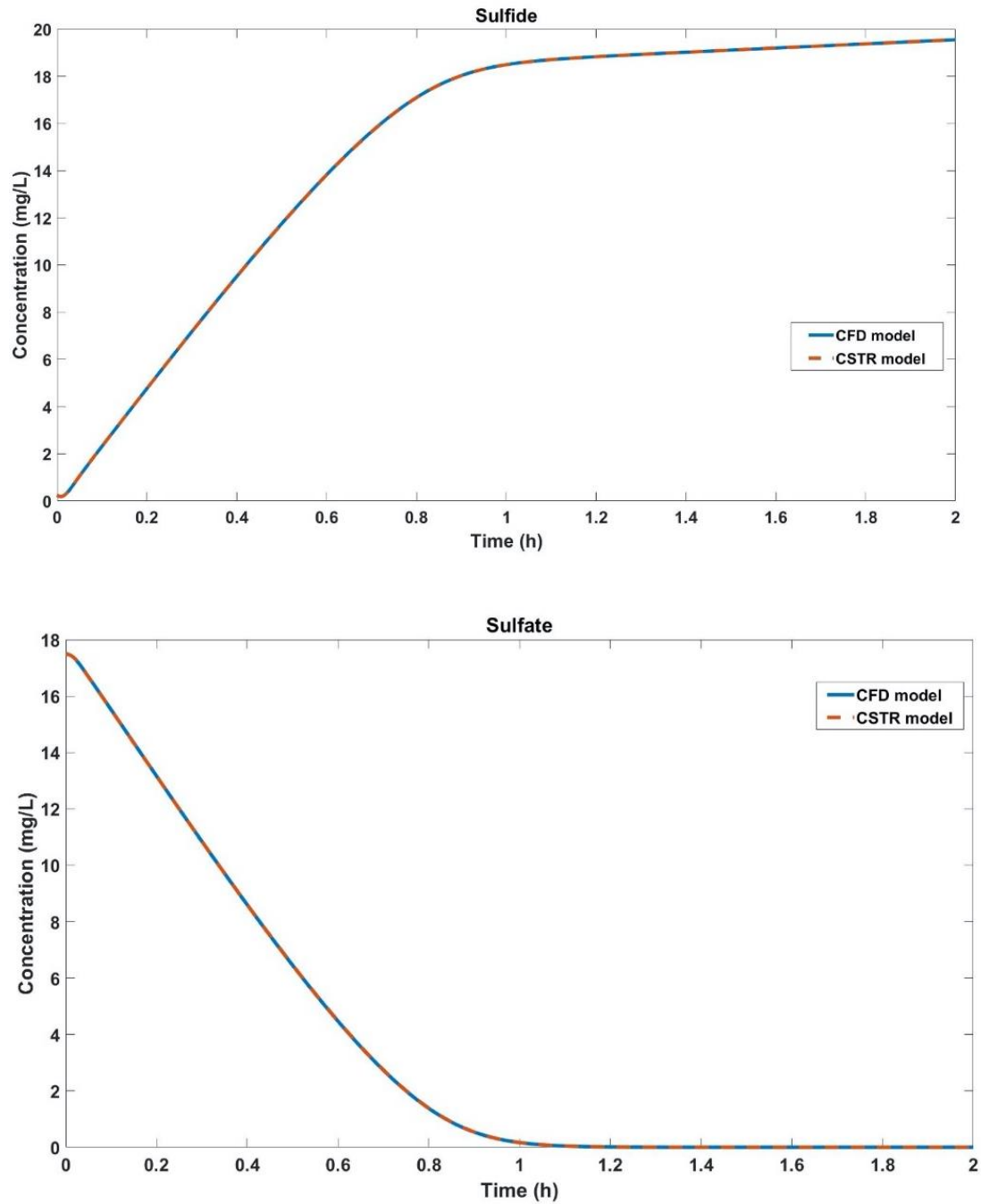
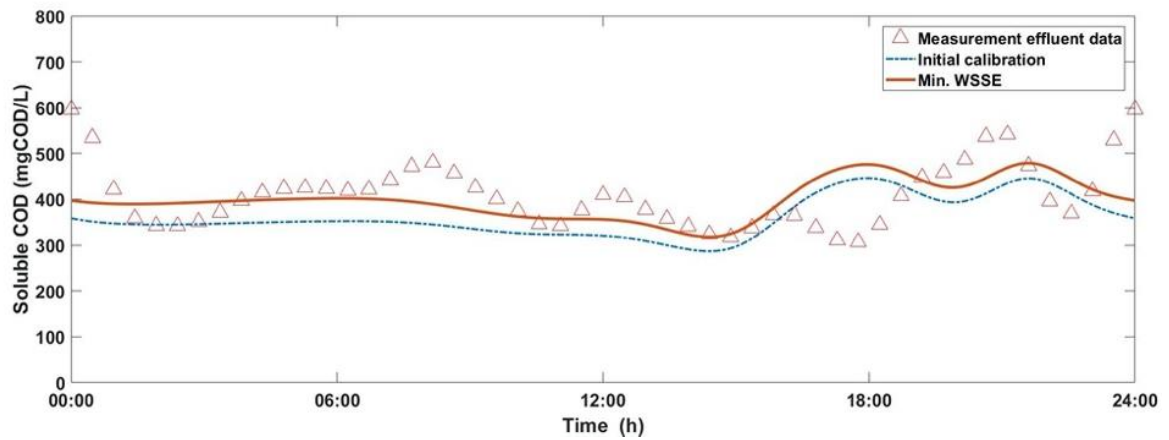


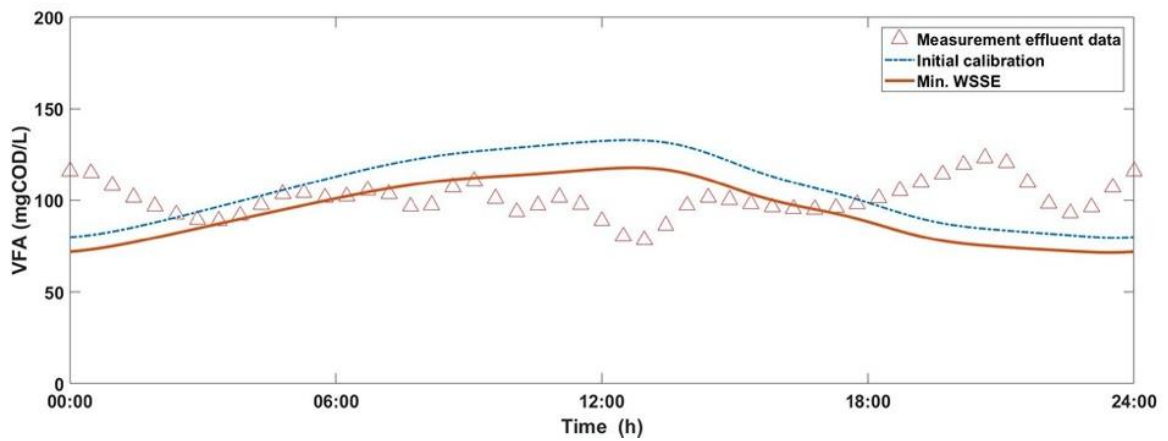
***Fig. A.3: Comparison between the results of the CFD model and the CSTR model with test case for verification of the biochemical model implementation in the water phase and biofilm.***

### Comparison between experimental and model results

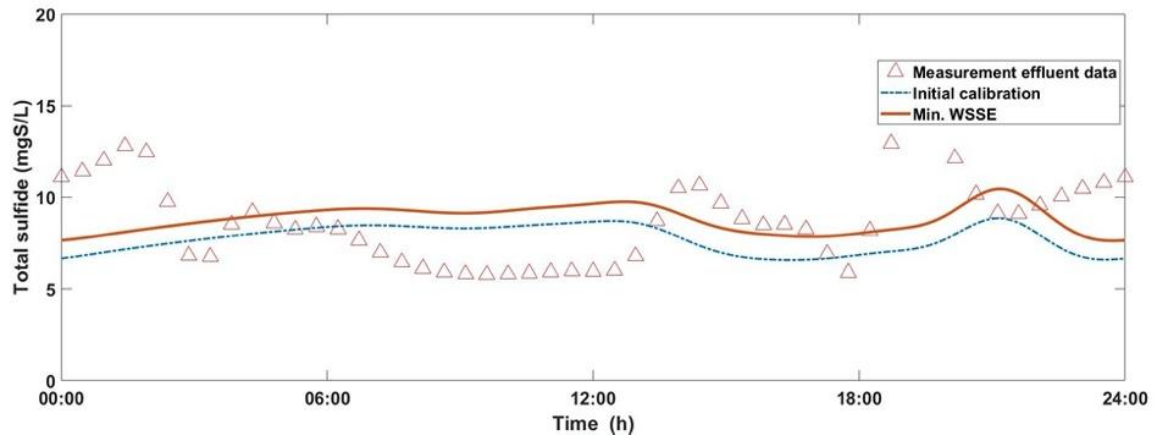
The experimental data is compared against the model predictions (using the two different calibrations used in this work) in Fig. A.4. These show good agreement for sCOD both in terms of the magnitude and the trend. The agreement for VFA and total sulfide is acceptable, showing the correct magnitude, but missing some aspects of the dynamic response.



(a)



(b)



(c)

**Fig. A.4: Comparison between the experimental results and the model results with the preliminary calibration and the minimum WSSE calibration results for (a) soluble COD, (b) VFA, and (c) total sulfide**



## Curriculum Vitae

**Name:** Ahmed Khalil

**Post-secondary  
Education and  
Degrees:** Cairo University  
Cairo, Egypt  
2007-2012 B.A.

Cairo University  
Cairo, Egypt  
2012-2016 M.A.

The University of Western Ontario  
London, Ontario, Canada  
2017-2021 Ph.D.

**Honours and  
Awards:** Mitacs  
Accelerate  
May 2020 -August 2020

CHI University Grant Program Notice of Award  
March 2020- March 2021

**Related Work  
Experience** Teaching and Research Assistant  
The University of Western Ontario  
2017-2020

### Journal Publications:

Khalil, A., Kayed, H., Hanafi, A., Nemitallah, M., & Habib, M. (2019). Numerical Predictions of Three-Dimensional Unsteady Turbulent Film-Cooling for Trailing Edge of Gas-Turbine Blade Using Large Eddy Simulation. *Journal of Energy Resources Technology*, 141(4).

Ahmed, A. S., Khalil, A., Ito, Y., van Loosdrecht, M. C., Santoro, D., Rosso, D., & Nakhla, G. (2020). Dynamic impact of cellulose and readily biodegradable substrate on oxygen transfer efficiency in sequencing batch reactors. *Water Research*, 190, 116724.

Khalil, A., Santoro, D., Batstone, D. J., & DeGroot, C. T. (2021). Uncertainty analysis of rising sewer models with respect to input parameters and model structure using Monte Carlo simulations and computational fluid dynamics. *Water Science and Technology*.

Khalil, A., Santoro, D., Batstone, D. J., & DeGroot, C. T. Effects of flow velocity and bubble size distribution on oxygen mass transfer in bubble column reactors – A critical evaluation of the CFD-PBM model. submitted to Water Environmental Research.

**Conference Proceedings:**

Khalil, A., DeGroot, C. T. (2018). CFD-PBM study of bubble column reactor integrated with mass transfer calculations. Proceedings of The Joint Canadian Society for Mechanical Engineering and CFD Society of Canada International Congress 2019, London, On, Canada, June 2–5.

Khalil, A., Santoro, D., DeGroot, C. T. (2018). Understanding Sewer Bioprocesses Using Computational Fluid Dynamics. 55th CENTRAL Canadian Symposium on Water Quality Research, Ryerson University, Toronto, Ontario: February 20, 2020